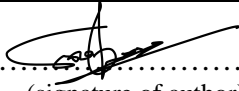




Universitetet
i Stavanger

FACULTY OF SCIENCE AND TECHNOLOGY

MASTER'S THESIS

Study program/Specialization: Industrial Asset Management (Technical and Operational Integrity)	Spring semester, 2019 Open/ Confidential
Author: Jesse Ebubechukwu Inoma	 (signature of author)
Programme coordinator: Professor Jayantha Prasanna Liyanage Supervisor(s): Professor Dimitrious Pavlou , Professor Jayantha Prasanna Liyanage External Supervisor : Mr. Julian Zec (National Oilwell Varco)	
Title of master's thesis: Review and Optimization of Current Fatigue Analysis Models	
Credits: 30 ECTS	
Keywords: Multiaxial Fatigue Rainflow Counting Palmgren-Miners rule Manson's double linear damage rule Bi-linear S-N Curve Subramanyan's non-linear damage rule Mean stress correction	Number of pages: 126 + supplemental material/other: 81 Stavanger, 15th June 2019

Abstract

The offshore oil and gas industry have been exposed to major challenges over the last decade, particularly demanding cost cuts and more effective technical solutions. Predictive systems and remaining life assessments for both machine and structural components are known to be one of the core areas that has gathered much attention lately. This thesis focuses on multiaxial fatigue that is a problem in a number of engineering structures and equipment. The ability to properly assess and quantify multiaxial fatigue of offshore equipment and structures has major benefits for owners of engineering assets both in terms of technical safety and integrity. Traditionally, Palmgren-Miner's damage rule is used for life estimation involving multiaxial fatigue due to its ease of use. There are however some known shortcomings with Palmgren-Miner's rule namely: it does not take into account the loading sequences. This for instance can result in overestimation of fatigue life in scenarios where stress amplitudes are decreasing, and moreover underestimation of fatigue life in scenarios where stress amplitudes increase.

This research work thus involves closely studying the application of Palmgren-Miner's linear damage rule, Manson's double linear damage rule, and Subramanyan's non-linear damage rule for the purpose of enhancing the predictability of damage as well as accuracy of fatigue life assessments. Each of these techniques were applied on tie-rods of an offshore drilling top-drive having a known stress history. The loading histories were provided by a drilling company. The torque and axial force values are transformed to stress components for the corresponding critical spots. The "rainflow" counting technique is applied to the obtained stress histories and the mean stress effect is considered for the damage accumulation calculations. The fatigue life prediction of the three models are justified and discussed.

This research work is aimed at contributing towards the utilization of more robust fatigue life estimation techniques such as Manson's double linear damage rule and simplified non-linear damage rules which capture the true nature of the fatigue that equipment's are subjected to, and thus to improve the reliability of the fatigue life predictions.

Acknowledgements

All glory to my Lord Jesus Christ for his grace and divine guidance throughout this thesis.

My heartfelt gratitude goes to Professor Jayantha Prasanna Liyanage for his guidance in this thesis as well as providing me with the platform through the close co-operation between the Cluster of Industrial Asset Management (CIAM) and the industry to get and work on this topic with National Oilwell Varco. Thanks for the important foundational lectures about engineering processes and human factors, I look forward to applying the knowledge you transferred to me in the industry.

I express my deepest appreciation to my supervisor Professor Dimitrious Pavlou for guiding me in this research work. Professor Pavlou gave me an excellent introduction into this subject area of multiaxial fatigue by providing me with deeper insight to aid my understanding of this topic. Thanks for steering me on the right path to becoming an independent researcher.

My sincere appreciation goes to Mr. Julian Zec my external supervisor at National Oilwell Varco for the regular appraisals to ensure that the thesis was going smoothly and that deadlines were being kept. Thanks for providing me with deeper insights in the field of data analytics and ensuring I had access to all the tools and data I needed to complete this thesis.

My appreciation goes to National Oilwell Varco for providing me with a working space and all the resources that made this thesis a success.

My gratitude goes to Kristen Rege Ph.D. for helping me understand key concepts about the various fatigue damage models, this enabled me to finish this thesis on time.

I also express my gratitude to my close friend, Gilberto Cervantes Ochoa his help in proofreading this thesis and providing constructive criticism to ensure my final work was top-notch.

My special thanks to my family for their prayers and support throughout this thesis. You provided me with the extra motivation to drive on and complete this thesis.

Finally, I will like to dedicate this thesis to my late father Obi Inoma, who always believed in me and encouraged me to strive for excellence, thanks for setting me on the right path.

Contents

Abstract	i
Acknowledgements	ii
List of Figures	vii
List of Tables	xv
Abbreviations	xviii
1 Introduction.....	1
1.1 Background and Challenge Description	1
1.2 Objective	4
1.3 Scope.....	4
1.4 Methodology	5
1.5 Limitations	7
1.6 Thesis Outline.....	9
2. Literature Survey.....	10
2.1 Introduction	10
2.2 What is Fatigue.....	10
2.3 Mechanism of Fatigue.....	14
2.4 Factors Influencing Fatigue.....	15
2.5 Classification of Fatigue	22
2.6 Fatigue Modelling and Analysis.....	25
2.6.1 Stress-Life (S-N)- approach.....	26
2.6.2 Strain-Life (EN) and Energy based approach.....	31
2.6.3 Fracture Mechanics approach	34
2.6.4 Critical Plane Approach.....	35
2.7 Mean Stress Correction Theories	36

2.7.1 Stress-Life Mean Stress Correction Methods	38
2.8 Rain Flow Cycle Counting	44
3 Review of Selected Fatigue Damage Models	49
3.1 Palmgren-Miner’s Linear Damage Model	49
3.2 Manson’s Double Linear Damage Model	51
3.3 Subramanyan’s Non-Linear Damage Model.....	55
4 Data Quality and Diagnostics	59
4.1 Importance of Data Quality and Diagnostics	59
4.2 Data Acquisition and Storage In-house	61
4.3 Data Quality Assessment	63
4.4 Data Quality Parameters and Tools	65
5. Analysis Methods and Tools.....	67
5.1 Description of the HPS-03 1000T Top Drive	67
5.2 Fatigue Damage Model Tests.....	73
5.2 Palmgren Miner’s Linear Damage Model.....	76
5.2.1 Parameter Calculation and Model Evaluation	76
5.3 Manson’s Double Linear Damage Model	77
5.3.1 Parameter Calculation and Model Evaluation	77
5.4 Subramanyan’s Non-linear Damage Model.....	77
5.4.1 Parameter Calculation and Model Evaluation	77
5.5 Modelling Probability of Failure of HPS-03 1000T Tie Rods.....	78
5.5.1 Fatigue resistance modelling.....	78
5.5.2 Load modelling	80
5.5.3 Variables and parameters data:	81
6 Results and Discussion	86

6.1 Finite Element Method Results	86
6.1.1 General.....	86
6.1.2 Model.....	86
6.1.2.1 Geometry	86
6.1.3 Structural Results	87
6.1.4 ANSYS FEM Plots.....	88
6.2 Data Diagnosis Results.....	94
6.3 Comparison Results for Miner’s linear damage rule, Manson’s double linear damage rule and Subramanyan’s non-linear damage rule models.....	99
6.3.1 Comparison of Fatigue Damage Results	100
6.3.3 Comparison of the number of loading blocks until failure results for Miners linear damage rule and Manson’s double linear damage rule models.....	105
7 Conclusion and Recommendations	122
7.1 Conclusion.....	122
7.2 Recommndations.....	124
8 References	126
9 Appendices	-1-
Appendix A: Wohler Curve	-1-
Appendix B: Data Quality Checks	-3-
Appendix C: Outlier Diagnosis	-15-
Appendix D: Stress Time-Series Graphs	-29-
Appendix E: Rainflow Matrixes	-42-
Appendix F: Comparison of Fatigue Damage Results for Miner’s linear damage rule, Manson’s double linear damage rule and Subramanyan’s non-linear damage rule models.....	-51-

Appendix G: Comparison of the number of loading blocks until failure results for Miners linear damage rule, Manson’s double linear damage rule and Subramanyan’s non-linear damage models -61-

Appendix H: R and Python Codes..... -71-

List of Figures

Figure 1-1: Thesis Methodology.....	6
Figure 1-2: Schematic showing project limitations and the possibilities for further research (Zec, 2018).....	8
Figure 2-1 (a) Alexander Kielland Accident(OOTW, 2013, Raabe, 1980) (b) De Havilland comet accident (Wanhill, 2002, Archives, 1954) (c) Versailles train crash (Wikipedia, 2019).....	13
Figure 2-2: Illustration showing the mechanism of fatigue (Anaee and Hameed, 2016)	15
Figure 2-3: Illustration showing a constant amplitude loading stress history(Eurocode, 1993) ...	17
Figure 2-4 : Illustration showing a variable amplitude loading stress history(Eurocode, 1993)...	18
Figure 2-5: Illustration showing principal stress variation (a) in-phase and (b) out-of-phase loading(Maddox and Razmjoo, 2001).....	19
Figure 2-6: Types of shaft/ pipe specimens (Laboratory et al., 2019)	20
Figure 2-8: Boxbeam specimen details(Gustafsson and Saarinen, 2007).....	21
Figure 2-9 Graph showing fatigue failure as a function of strain amplitude(Courtney, 1990)	23
Figure 2-10: Illustration of a metal cube undergoing (a) uniaxial stress and (b) multiaxial strain.....	24
Figure 2-11: Illustration showing the multiaxial stresses acting on a Crank shaft(Fatemi, 2018).....	25
Figure 2-12 Illustration showing a typical S-N- curve (Irvine, 2013)	26
Figure 2-13 : Illustration showing parameters of a cyclic loading (UIS, 2016).....	37
Figure 2 -14: Comparison of mean stress correction equations	43
Figure 2-15 : Rainwater flowing down the roof of a Pagoda (Irvine, 2013).....	44
Figure 2-16: Removal of cycles smaller than amplitude range from load history (Hiatt, 2016) ..	45
Figure 2-17: Peak-Valley Filtering retaining loading data points (black dots) which represent reversals (Hiatt, 2016).....	46
Figure 2-18: Binning of data points. Black dots amplitudes are adjusted to the centre of the bins. Data points whose amplitude is affected by binning are circled in purple.(Hiatt, 2016).....	47
Figure 2-19: Illustration showing complete and incomplete cycles using the four point counting method (Hiatt, 2016).....	48
Figure 3-1: Sinusoidal loading spectra that is assumed to apply Miner’s rule.....	50

Figure 3-2: Schematic showing the application of Miner’s rule in this case D exceeds 1 so failure will occur (Hiatt, 2016).....	51
Figure 3-3: Double linear damage accumulation occurring in the two phases for a material (Lee et al., 2004).....	54
Figure 3-4: Linear damage rules for Phase I and Phase II (Lee et al., 2004).....	54
Figure 3-5: Comparison between Subramanyan’s model of iso-damage lines to Miner’s approach for estimating the number of cycles until failure (Subramanyan, 1976).....	56
Figure 4-1: The Rise of Big Data and Industry 4.0.....	60
Figure 4-2: Illustration showing the process flow of data from Rigs to the data collection centre at NOV (Zec, 2018).....	62
Figure 4-3: (a) The outcome of a data quality check (ISO, 2015) (b) Filtering of bad data from good quality data (Zec, 2018).....	64
Figure 4-4: The Data quality process (DNV-GL, 2017).....	65
Figure 5-4: S-N curve according to F.E.M section 4.1.3.5 used in this thesis (F.E.M, 1998).....	76
Figure 6-1: Mesh Geometry.....	88
Figure 6-2: Environment Geometry.....	89
Figure 6-3: Equivalent Stress Contours(a).....	89
Figure 6-4: Equivalent Stress Contours(b).....	90
Figure 6-5: Equivalent Stress Contours (c).....	91
Figure 6-6: Equivalent Stress Contours (d).....	91
Figure 6-7: Equivalent Stress Contours (d).....	92
Figure 6-8: Equivalent Stress Contours (e).....	92
Figure 6-9: Maximum Principal Stress Contours.....	93
Figure 6-10 : Total Deformation Contours.....	93
Figure 6-11: Outlier Diagnosis Results for Rig 1 Main Well Datasets from January -July 2014.....	97
Figure 6-12: Outlier Diagnosis Results for Rig 1 Main Well Datasets from July - December 2014.....	98
Figure 6-13: Non-conservative estimates of damage versus the number of remaining cycles until failure from the selected fatigue damage models for Rig 1 Main Well in 2014.....	100

Figure 6-14: Conservative estimates of damage versus the number of remaining cycles until failure from the selected fatigue damage models for Rig 1 Auxiliary Well in 2014	100
Figure 6-15: Conservative estimates of damage versus the number of remaining cycles until failure from the selected fatigue damage models for Rig 2 Main Well in 2014	102
Figure 6-16: Non-conservative estimates of damage versus the number of remaining cycles until failure from the selected fatigue damage models for Rig 2 Auxiliary Well in 2014	103
Figure 6-17: Conservative estimates of damage versus the number of remaining cycles until failure from the selected fatigue damage models for Rig 3 Main Well in 2014	104
Figure 6-18: Conservative estimates of damage versus the number of remaining cycles until failure from the selected fatigue damage models for Rig 3 Auxiliary Well in 2014	104
Figure 6-19: Non-conservative estimates of the number of loading blocks until failure from the selected fatigue damage models for Rig 1 Main Well	106
Figure 6-20: Non-conservative estimates of the number of loading blocks until failure from the selected fatigue damage models for Rig 1 Auxiliary Well	108
Figure 6-21: Non-conservative estimates of the number of loading blocks until failure from the selected fatigue damage models for Rig 2 Main Well	110
Figure 6-22: Non-conservative estimates of the number of loading blocks until failure from the selected fatigue damage models for Rig 2 Auxiliary Well	111
Figure 6-23: Non-conservative estimates of the number of loading blocks until failure from the selected fatigue damage models for Rig 3 Main Well	113
Figure 6-24: Non-conservative estimates of the number of loading blocks until failure from the selected fatigue damage models for Rig 3 Auxiliary Well	113
Figure 6-25: Conservative estimates of the number of loading blocks until failure from the selected fatigue damage models for Rig 1 Main Well	115
Figure 6-26: Conservative estimates of the number of loading blocks until failure from the selected fatigue damage models for Rig 1 Auxiliary Well	116
Figure 6-27: Conservative estimates of the number of loading blocks until failure from the selected fatigue damage models for Rig 2 Main Well	117
Figure 6-28: Conservative estimates of the number of loading blocks until failure from the selected fatigue damage models for Rig 2 Auxiliary Well	118

Figure 6-29: Conservative estimates of the number of loading blocks until failure from the selected fatigue damage models for Rig 3 Main Well.....	119
Figure 6-30: Conservative estimates of the number of loading blocks until failure from the selected fatigue damage models for Rig 3 Auxiliary Well.....	120
Figure 9-1: S-N curve according to F.E.M section 4.1.3.5 (F.E.M, 1998)	2
Figure 9-2: S-N curve according to F.E.M section 4.1.3.5 reproduced and used in this thesis (F.E.M, 1998).....	3
Figure 9-3 : Outlier Diagnosis Results for Rig 1 Main Well Datasets from January 2014 (a)-December 2014 (b).....	15
Figure 9-4 : Outlier Diagnosis Results for Rig 1 Main Well Datasets from January 2015 (a)-December 2015 (b).....	16
Figure 9-5 : Outlier Diagnosis Results for Rig 1 Main Well Datasets from January-July 2016...	17
Figure 9-6 : Outlier Diagnosis Results for Rig 1 Auxiliary Well Datasets from January 2014 (a)-December 2014 (b).....	18
Figure 9-7 : Outlier Diagnosis Results for Rig 1 Auxiliary Well Datasets from January 2015 (a)-December 2015 (b).....	19
Figure 9-8 : Outlier Diagnosis Results for Rig 1 Auxiliary Well Dataset from January-July 2016.....	20
Figure 9-9 : Outlier Diagnosis Results for Rig 2 Main Well Datasets from July 2014 (a)-July 2015 (b).....	21
Figure 9-10 : Outlier Diagnosis Results for Rig 2 Main Well Datasets from July 2015 (a)-July 2016 (b).....	22
Figure 9-11: Outlier Diagnosis Results for Rig 2 Auxiliary Well Datasets from July 2014 (a) -July 2015 (b).....	23
Figure 9-12: Outlier Diagnosis Results for Rig 2 Auxiliary Well Datasets from July 2015 (a) -July 2016 (b).....	24
Outlier Diagnosis Results for Rig 3 Main Well Datasets from July 2014 (a) - July 2015 (b)	25
Figure 9-13 : Outlier Diagnosis Results for Rig 3 Main Well Datasets from July 2014 (a) - July 2015 (b).....	25
Figure 9-14 : Outlier Diagnosis Results for Rig 3 Main Well Datasets from July 2015 (a) - July 2016 (b).....	26

Figure 9-15: Outlier Diagnosis Results for Rig 3 Auxiliary Well Datasets from July 2014 (a) - July 2015 (b).....	27
Figure 9-16 : Outlier Diagnosis Results for Rig 3 Auxiliary Well Datasets from July 2015 (a) - July 2016 (b).....	28
Figure 9-17: Equivalent Stress Time Series Rig 1 Main Well January – July 2014	29
Figure 9-18 : Equivalent Stress Time Series Rig 1 Main Well July 2014- January 2015	29
Figure 9-19 : Equivalent Stress Time Series Rig 1 Main Well January - July 2015	30
Figure 9-20 : Equivalent Stress Time Series Rig 1 Main Well July 2015- January 2016	30
Figure 9-21 : Equivalent Stress Time Series Rig 1 Main Well January - July 2016	31
Figure 9-22 : Equivalent Stress Time Series Rig 1 Auxiliary Well January - July 2014	31
Figure 9-23 : Equivalent Stress Time Series Rig 1 Auxiliary Well July 2014 - January 2015	32
Figure 9-24 : Equivalent Stress Time Series Rig 1 Auxiliary Well January - July 2015	32
Figure 9-25 : Equivalent Stress Time Series Rig 1 Auxiliary Well July 2015 - January 2016.....	33
Figure 9-26 : Equivalent Stress Time Series Rig 1 Auxiliary Well January - July 2016	33
Figure 9-27 : Equivalent Stress Time Series Rig 2 Main Well July 2014 – January 2015.....	34
Figure 9-28 : Equivalent Stress Time Series Rig 2 Main Well January- July 2015	34
Figure 9-29 : Equivalent Stress Time Series Rig 2 Main Well July 2015 – January 2016.....	35
Figure 9-30 : Equivalent Stress Time Series Rig 2 Main Well January - July 2016	35
Figure 9-31 : Equivalent Stress Time Series Rig 2 Auxiliary Well July 2014 – January 2015	36
Figure 9-32 : Equivalent Stress Time Series Rig 2 Auxiliary Well January-July 2015	36
Figure 9-33 : Equivalent Stress Time Series Rig 2 Auxiliary Well July 2015 – January 2016	37
Figure 9-34 : Equivalent Stress Time Series Rig 2 Auxiliary Well January-July 2016	37
Figure 9-35 : Equivalent Stress Time Series Rig 3 Main Well July 2014 – January 2015.....	38
Figure 9-36 : Equivalent Stress Time Series Rig 3 Main Well January - July 2015	38
Figure 9-37 : Equivalent Stress Time Series Rig 3 Main Well July 2015 – January 2016.....	39
Figure 9-38 : Equivalent Stress Time Series Rig 3 Main Well January -July 2016	39
Figure 9-39 : Equivalent Stress Time Series Rig 3 Auxiliary Well July 2014 – January 2015	40
Figure 9-40 : Equivalent Stress Time Series Rig 3 Auxiliary Well January - July 2015	40
Figure 9-41 : Equivalent Stress Time Series Rig 3 Auxiliary Well July 2015 – January 2016	41
Figure 9-42 : Equivalent Stress Time Series Rig 3 Auxiliary Well January - July 2016	41
Figure 9-43 : Rainflow Matrix Histogram Rig 1 Main Well 2014	42

Figure 9-44 : Rainflow Matrix Histogram Rig 1 Main Well 2015	42
Figure 9-45 : Rainflow Matrix Histogram Rig 1 Main Well 2016	43
Figure 9-46 : Rainflow Matrix Histogram Rig 1 Auxiliary Well 2014	43
Figure 9-47 : Rainflow Matrix Histogram Rig 1 Auxiliary Well 2015	44
Figure 9-48 : Rainflow Matrix Histogram Rig 1 Auxiliary Well 2016	44
Figure 9-49 : Rainflow Matrix Histogram Rig 2 Main Well 2014	45
Figure 9-50 : Rainflow Matrix Histogram Rig 2 Main Well 2015	45
Figure 9-51 : Rainflow Matrix Histogram Rig 2 Main Well 2016	46
Figure 9-52 : Rainflow Matrix Histogram Rig 2 Auxiliary Well 2014	46
Figure 9-53 : Rainflow Matrix Histogram Rig 3 Auxiliary Well 2015	47
Figure 9-54 : Rainflow Matrix Histogram Rig 3 Auxiliary Well 2016	47
Figure 9-55 : Rainflow Matrix Histogram Rig 3 Main Well 2014	48
Figure 9-56 : Rainflow Matrix Histogram Rig 3 Main Well 2015	48
Figure 9-57 : Rainflow Matrix Histogram Rig 3 Main Well 2016	49
Figure 9-58 : Rainflow Matrix Histogram Rig 3 Auxiliary Well 2014	49
Figure 9-59 : Rainflow Matrix Histogram Rig 3 Auxiliary Well 2015	50
Figure 9-60 : Rainflow Matrix Histogram Rig 3 Auxiliary Well 2016	50
Figure 9-61: Non-conservative estimates of damage versus the number of remaining cycles until failure from the selected fatigue damage models for Rig 1 Main Well in 2014	51
Figure 9-62: Non-conservative estimates of damage versus the number of remaining cycles until failure from the selected fatigue damage models for Rig 1 Main Well in 2016	52
Figure 9-63: Non-conservative estimates of damage versus the number of remaining cycles until failure from the selected fatigue damage models for Rig 1 Auxiliary Well in 2016	52
Figure 9-64: Non-conservative estimates of damage versus the number of remaining cycles until failure from the selected fatigue damage models for Rig 2 Auxiliary Well in 2014	53
Figure 9-65: Non-conservative estimates of damage versus the number of remaining cycles until failure from the selected fatigue damage models for Rig 2 Auxiliary Well in 2015	53
Figure 9-66: Non-conservative estimates of damage versus the number of remaining cycles until failure from the selected fatigue damage models for Rig 2 Auxiliary Well in 2016	54
Figure 9-67: Conservative estimates of damage versus the number of remaining cycles until failure from the selected fatigue damage models for Rig 1 Main Well in 2015	54

Figure 9-68: Conservative estimates of damage versus the number of remaining cycles until failure from the selected fatigue damage models for Rig 1 Auxiliary Well in 201455

Figure 9-69: Conservative estimates of damage versus the number of remaining cycles until failure from the selected fatigue damage models for Rig 1 Auxiliary Well in 201555

Figure 9-70: Conservative estimates of damage versus the number of remaining cycles until failure from the selected fatigue damage models for Rig 2 Main Well in 201456

Figure 9-71: Conservative estimates of damage versus the number of remaining cycles until failure from the selected fatigue damage models for Rig 2 Main Well in 201556

Figure 9-72: Conservative estimates of damage versus the number of remaining cycles until failure from the selected fatigue damage models for Rig 2 Main Well in 2016.....57

Figure 9-73: Conservative estimates of damage versus the number of remaining cycles until failure from the selected fatigue damage models for Rig 3 Main Well in 201457

Figure 9-74: Conservative estimates of damage versus the number of remaining cycles until failure from the selected fatigue damage models for Rig 3 Main Well in 201558

Figure 9-75: Conservative estimates of damage versus the number of remaining cycles until failure from the selected fatigue damage models for Rig 3 Main Well in 201658

Figure 9-76: Conservative estimates of damage versus the number of remaining cycles until failure from the selected fatigue damage models for Rig 3 Auxiliary Well in 201459

Figure 9-77: Conservative estimates of damage versus the number of remaining cycles until failure from the selected fatigue damage models for Rig 3 Auxiliary Well in 201559

Figure 9-78: Conservative estimates of damage versus the number of remaining cycles until failure from the selected fatigue damage models for Rig 3 Auxiliary Well in 2016.....60

Figure 9-79: Non-conservative estimates of the number of loading blocks until failure from the selected fatigue damage models for Rig 1 Main Well61

Figure 9-80: Non-conservative estimates of the number of loading blocks until failure from the selected fatigue damage models for Rig 1 Auxiliary Well62

Figure 9-81: Non-conservative estimates of the number of loading blocks until failure from the selected fatigue damage models for Rig 2 Main Well62

Figure 9-82: Non-conservative estimates of the number of loading blocks until failure from the selected fatigue damage models for Rig 2 Auxiliary Well63

Figure 9-83: Non-conservative estimates of the number of loading blocks until failure from the selected fatigue damage models for Rig 3 Main Well63

Figure 9-84: Non-conservative estimates of the number of loading blocks until failure from the selected fatigue damage models for Rig 3 Auxiliary Well64

Figure 9-85: Conservative estimates of the number of loading blocks until failure from the selected fatigue damage models for Rig 1 Main Well.65

Figure 9-86: Conservative estimates of the number of loading blocks until failure from the selected fatigue damage models for Rig 1 Auxiliary Well.....66

Figure 9-87: Conservative estimates of the number of loading blocks until failure from the selected fatigue damage models for Rig 2 Main Well.67

Figure 9-88: Conservative estimates of the number of loading blocks until failure from the selected fatigue damage models for Rig 2 Auxiliary Well.....68

Figure 9-89: Conservative estimates of the number of loading blocks until failure from the selected fatigue damage models for Rig 3 Main Well69

Figure 9-90: Conservative estimates of the number of loading blocks until failure from the selected fatigue damage models for Rig 3 Auxiliary Well.....70

List of Tables

Table 1-1: Thesis Outline.....	9
Table 5-1: Probability of fatigue failure for the inspection intervals.....	85
Table 6-1: Data Description for Rig 1 Main Well Datasets between January-December 2014....	94
Table 6-2: Non-conservative estimates of the number of loading blocks until failure from the selected fatigue damage models for Rig 1 Main Well	109
Table 6-3: Non-conservative estimates of the number of loading blocks until failure from the selected fatigue damage models for Rig 1 Auxiliary Well	109
Table 6-4: Non-conservative estimates of the number of loading blocks until failure from the selected fatigue damage models for Rig 2 Main Well	112
Table 6-5: Non-conservative estimates of the number of loading blocks until failure from the selected fatigue damage models for Rig 2 Auxiliary Well	112
Table 6-6: Non-conservative estimates of the number of loading blocks until failure from the selected fatigue damage models for Rig 3 Main Well	114
Table 6-7: Non-conservative estimates of the number of loading blocks until failure from the selected fatigue damage models for Rig 3 Auxiliary Well	114
Table 6-8: Conservative estimates of the number of loading blocks until failure from the selected fatigue damage models for Rig 1 Main Well	115
Table 6-9: Conservative estimates of the number of loading blocks until failure from the selected fatigue damage models for Rig 1 Auxiliary Well.....	116
Table 6-10: Conservative estimates of the number of loading blocks until failure from the selected fatigue damage models for Rig 2 Main Well.....	117
Table 6-11: Conservative estimates of the number of loading blocks until failure from the selected fatigue damage models for Rig 2 Auxiliary Well.....	118
Table 6-12: Conservative estimates of the number of loading blocks until failure from the selected fatigue damage models for Rig 3 Main Well.	119
Table 6-13: Conservative estimates of the number of loading blocks until failure from the selected fatigue damage models for Rig 3 Auxiliary Well.....	120
Table 9-1: Data Description for Rig 1 Main Well Datasets between January-December 2014.....	4
Table 9-2: Data Description for Rig 1 Main Well Datasets between January-December 2015.....	4

Table 9-3: Data Description for Rig 1 Main Well Dataset between January-July 2016	5
Table 9-4: Data Description for Rig 1 Auxiliary Well Datasets between January-December 2014.....	6
Table 9-5: Data Description for Rig 1 Auxiliary Well Datasets between January-December 2015.....	6
Table 9-6: Data Description for Rig 1 Auxiliary Well Dataset between January-July 2016.....	7
Table 9-7: Data Description for Rig 2 Main Well Dataset between July-December 2014.....	7
Table 9-8: Data Description for Rig 2 Main Well Datasets between January-December 2015.....	8
Table 9-9: Data Description for Rig 2 Main Well Dataset between January-July 2016	9
Table 9-10: Data Description for Rig 2 Auxiliary Well Dataset between July-December 2014	9
Table 9-11 : Data Description for Rig 2 Auxiliary Well Datasets between January-December 2015.....	10
Table 9-12 : Data Description for Rig 2 Auxiliary Well Dataset between January-July 2016.....	10
Table 9-13 : Data Description for Rig 3 Main Well Dataset between July-December 2014.....	11
Table 9-14 : Data Description for Rig 3 Main Well Datasets between January-December 2015.....	12
Table 9-15 : Data Description for Rig 3 Main Well Dataset between July-December 2016.....	12
Table 9-16: Data Description for Rig 3 Auxiliary Well Datasets between January-December 2014.....	13
Table 9-17 : Data Description for Rig 3 Auxiliary Well Datasets between January-December 2015.....	13
Table 9-18 : Data Description for Rig 3 Auxiliary Well Datasets between January-July 2016 ...	14
Table 9-19: Conservative estimates of the number of loading blocks until failure from the selected fatigue damage models for Rig 1 Main Well.....	65
Table 9-20: Conservative estimates of the number of loading blocks until failure from the selected fatigue damage models for Rig 1 Auxiliary Well.....	66
Table 9-21: Conservative estimates of the number of loading blocks until failure from the selected fatigue damage models for Rig 2 Main Well.....	67
Table 9-22: Conservative estimates of the number of loading blocks until failure from the selected fatigue damage models for Rig 2 Auxiliary Well.....	68

Table 9-23: Conservative estimates of the number of loading blocks until failure from the selected fatigue damage models for Rig 3 Main Well.....69

Table 9-24: Conservative estimates of the number of loading blocks until failure from the selected fatigue damage models for Rig 3 Auxiliary Well.....70

Abbreviations

TPM	Total Productive Maintenance
OEM	Original Equipment Manufacturers
MTTF	Mean time to failure
HSE	Health, safety & environment.
PSA	Petroleum Safety Authority
NCS	Norwegian Continental Shelf
NOV	National Oilwell Varco
NDT	Non-Destructive Testing
AI	Artificial Intelligence
IP	Intellectual Property
QA	Quality Assurance
KPI	Key Performance Indicator
API	American Petroleum Institute
F.E.M	Federation Europeenne De La Manutention
HPS	Hydralift Power Swivel
ASTM	American Society for Testing and Materials
DNV-GL	Det Norske Veritas (Norway) and Germanischer Lloyd (Germany).
WAFO	Wave Analysis for Fatigue and Oceanography
BOP	Blow-out Preventer
ISO	International Organization for Standardization
MTTR	Mean Time to Repair

MTBF	Mean Time Before Failure
SAE	Society of Automotive Engineers
DLDR	Double Linear Damage Rule

1 Introduction

1.1 Background and Challenge Description

Condition monitoring and equipment maintenance are essential activities which must be carried out by managers of modern engineering assets, equipment and infrastructure. These activities are important to ensure that the structural integrity of an asset is maintained as well as to ensure an asset performs its function and at the same time can maintain resilience when it is exposed to sudden shocks or changes. There has been an evolution in the industry from a reactionary philosophy of maintenance through to preventive maintenance and finally to a condition monitoring based philosophy of equipment maintenance. The reactionary philosophy of maintenance was geared towards the principle that equipment was operated until it failed, this is a 'run-to failure' approach. In this scenario it was only after an equipment failed that maintenance was carried out on it, the result of this approach was a significant loss in productivity, increased downtimes and increased costs to get back to an operational state. To eliminate the problems associated with the reactionary style of maintenance there was a shift towards a preventive maintenance philosophy which was heavily influenced by the TPM principles that were posited by Toyota in the 90's. The preventive maintenance philosophy was based on the use of statistical data and expected life statistics that were supplied by manufacturers or providers of an equipment. One of the drawbacks of this approach is that most original equipment manufacturer (OEM) were quite conservative in their assessments of the mean time to failure (MTTF) of their equipment irrespective of the functions of the equipment, for example the replacement time for a drilling top-drive exposed to low cycle fatigue versus one exposed to high cycle fatigue. This led to unnecessary repairs or replacements being carried out on equipment which could have continued in an operational state for a much longer time. To overcome these inefficiencies, there was a shift to a condition monitoring based philosophy where the operating conditions of critical equipment are monitored and logged, this data is then used to schedule maintenance for this critical equipment. This approach has helped in reducing the occurrence of equipment downtimes thus reducing the life cycle cost of an equipment as well as ensuring its useful life is extended significantly.

In a nutshell, condition monitoring of critical equipment is essential for companies to stay competitive and meet the strict HSE regulations set by the Petroleum Safety Authority (PSA) and

other regulators for operating on the Norwegian Continental Shelf (NCS). To fully harness the advantages of condition monitoring, correct models need to be used to determine the structural integrity of equipment and infrastructure that are being utilised for operations. This is so important because using wrong models and assumptions will result in scheduled maintenance or replacement being initiated for equipment which could have been used for many more years without failure.

At NOV, optimization of condition-based maintenance is one of their key priorities to remain competitive and maximize profits in the drilling industry. At the Q4 NOV Investor meeting in 2018, NOV CEO Clay Williams stated, “Drilling automation, optimization of condition-based maintenance and continuous certifications driven by key data are development priorities in NOV”(NOV, 2019).

Structural integrity of assets is an important issue of concern and a key cost factor for NOV. Several time-scheduled non-destructive testing (NDT) techniques are used to inspect integrity (fatigue, wear, corrosion) of structural members (e.g every 5 years for a lot of NOV equipment), this has some significant drawbacks such as: it is time consuming, requiring often full disassembly of equipment, while few failures are found in structures. There is a great need for competence outside the crew to carry out this analysis – which drive high costs and results in significant downtime for structural engineers to access these equipment’s.

It has been observed that these periodical inspections usually add more failures to the system (due to coupling errors). It is because of this reason that the industry has moved into transferring inspection scheduling from ‘time-based’ inspections to ‘condition-based monitoring’ of equipment usage by applying ‘physics based’ fatigue or wear mathematical condition focused (machine learning & AI) data driven models. The challenge with such models especially physics and statistics based) are as follows:

- These involve high level of intellectual property (IP) and this is seldomly shared/ given insight into.
- These are often hard-coded and difficult to evolve, when data contradicts conservative model assumptions.
- It is difficult to document such model changes and foundation for improvements.

- It is difficult to get consensus on what to improve, when and by using what QA process, involving who.
- Access to results require access to special systems, without direct coaction to what these data are used for.
- Relation between data/results is manually compared and translated to value, KPI or certification process.
- Physics based models require a lot of infrastructure / hardware power to be utilized (several layers of differential equations, hard coded according to system taxonomy).
- On other hand data driven approaches require equality of configurations, data quality and data sets to achieve complete validation.

This thesis therefore provides insight on the current approach of using (API 8C "*Specification of Drilling and Production Hoisting Equipment*" and F.E.M. "*Rules for the Design of Hoisting Appliances*") standard by NOV to assess fatigue damage and the structural integrity of their top-drive members with special focus on the tie rods of the HPS-03 1000T top-drive. The current approach being used by NOV to assess fatigue damage will be compared to two other models (Manson's Double Linear Damage model and Subramanyan's Non-Linear Damage model). The F.E.M 1.001 standard is based on the use of Palmgren-Miner's model and S-N curves when calculating fatigue damage on equipment. Generally, Miner's rule is widely accepted as the method to assess the fatigue damage due to its simplicity and ease of use in design of equipment where loading history is not available. This drawback of using this method is that it does not take into account the load sequence for example an equipment might be exposed to a higher loading cycle of let's say 900 MPa followed by 600 MPa or vice versa but the Miner approach will still generate the same damage even if the smaller load cycle comes before the higher cycle. The result of this is that the life of a structure or equipment will be overestimated when the cycles are reversed low load - high load sequence and underestimated in a high load - low load sequence. This is one of the main reasons why a lot of times when scheduled maintenance is carried out on the top drives at NOV no faults are discovered due to the conservative nature of Palmgren Miner's rule.

This thesis will utilise the same approach adopted by NOV as prescribed by the F.E.M 1.001 standard when reviewing the Palmgren Miner approach to fatigue damage. The results of this

approach will be compared to those obtained by using Manson's Double Linear Damage model and Subramanyan's Non-linear damage model and conclusions will be drawn from these approaches to estimating fatigue damage.

1.2 Objective

The focus of the thesis is centred on improving process of control and validation of structural integrity of NOV's top-drive tie-rods. This will be achieved by applying Palmgren Miner's rule, Manson's double linear damage rule and Subramanyan's non-linear damage rule to improve damage predictions and fatigue life assessments. The results from these tests using the selected fatigue damage models will serve as a basis for optimizing the current methodology of fatigue analysis employed at NOV.

These models will be built and coded in Python to attain a shift from physics dominated differential equation-based component models to hybrid models adapted from linear algebra and vector calculus. The aim of this approach is to reduce internal IT infrastructure capacity dependence (now in cloud or big data centres, depending again on good connectivity), speed up calculations and implement machine learning techniques to improve results. Such simplification will enable execution on edge devices or within control devices.

1.3 Scope

This thesis will seek to compare the fatigue calculation results when using the Palmgren-Miner's model for fatigue analysis with Manson's double linear damage model and Subramanyan's non-linear damage model. The Von-Mises equivalent stress approach will be used for transforming torque and axial forces into an equivalent stress. In this equivalent stress approach, the Von-Mises equivalent stress equation for static loading is utilised by replacing the stresses with an alternating stress (Juvinal and Marshek, 2006) . This approach is commonly used for a variety of multiaxial fatigue problems and it is suitable for materials that exhibit ductile behaviour as is the case in this research work.

Manson and Subramanyan's models will be used to take into account the various mechanisms of fatigue which are neglected in the Palmgren Miner approach. It is hoped that the results from this investigation will serve as decision support for the company. Focus will be placed on building these models in a way that it is user-friendly and easily adaptable to other equipment apart from

the tie-rods on the top drives. This will be necessary to ensure that calculations are quick and allow for the use of machine learning techniques to further optimize the results from this model.

1.4 Methodology

The following steps will be taken to achieve the objectives of this thesis:

- Obtaining load and torque signal data.
- Carrying out data quality checks on the load and torque signal data as prescribed by DNV-RP- 0497.
- Obtaining Von-Mises equivalent stresses from the stress in the x-direction and shear stress combinations at the various load levels.
- Applying rainflow counting as prescribed in ASTM- E-1049 by using the WAFO fatigue toolbox in Python.
- Applying Goodman's mean stress correction to the rainflow counted stress cycles to get fully reversible stresses.
- Investigation and testing of the Palmgren-Miner's model to calculate fatigue damage on the tie rods on the HPS-03 1000T top-drive as prescribed by DNV-RP C203.
- Investigation and testing of Manson's double linear damage model to calculate fatigue damage on the tie rods of the HPS-03 1000T top-drive.
- Investigation and testing of Subramanyan's non-linear damage model to calculate fatigue damage on the tie rods of the HPS-03 1000T top-drive.
- Evaluation of results obtained from the selected models.

The summary of these steps can be seen in the figure below

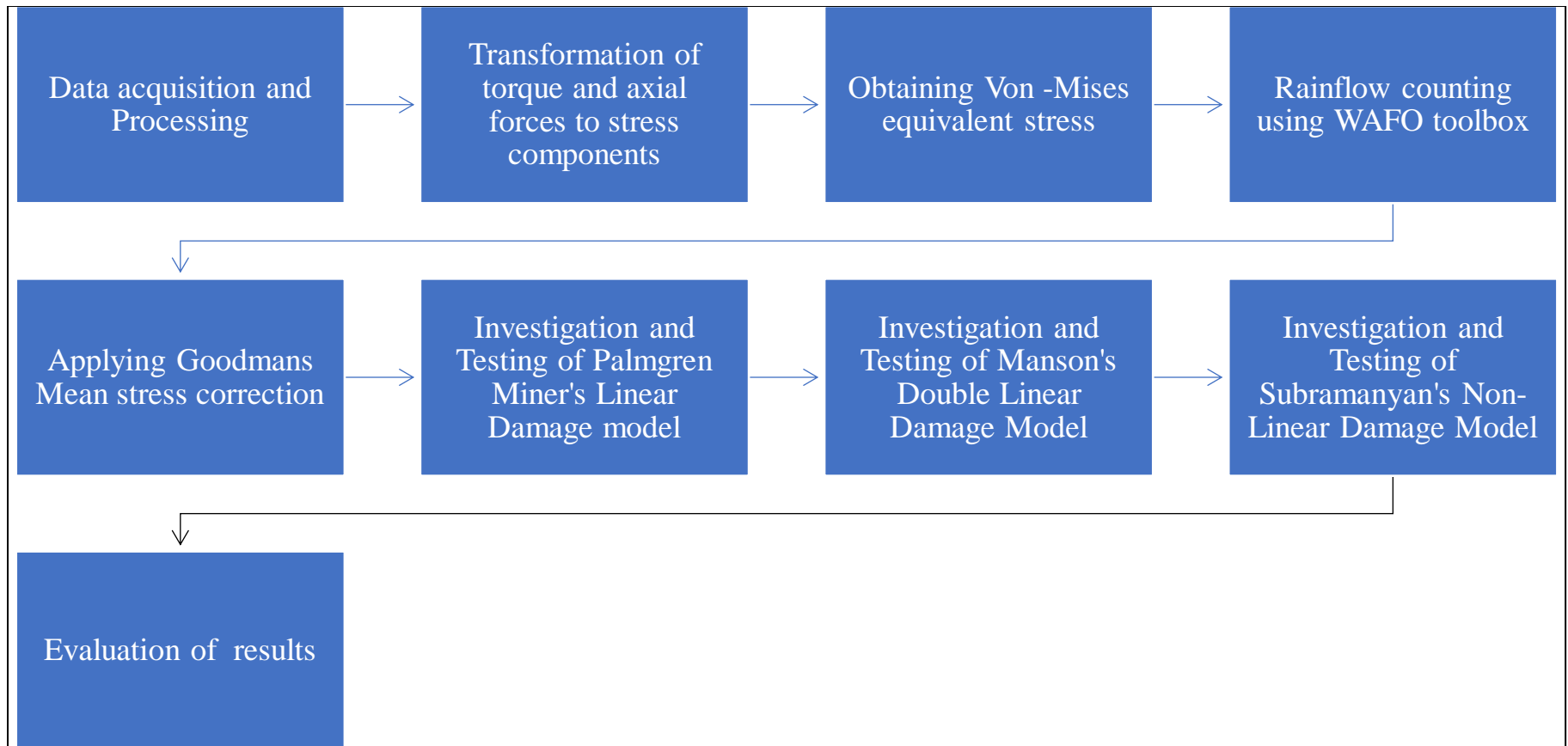


Figure 1-1: Thesis Methodology

1.5 Limitations

This thesis is limited to analysing fatigue damage of the HPS-03 1000T tie rods of the top-drives being used at NOV. It is hoped that the results of this analysis will provide decision support for the choice of a robust and user-friendly model which can be applied to other equipment based on their geometry, loading characteristics and stress history. Further research should be geared towards integrating the model obtained from this thesis into a blockchain database for easy validation of structural integrity of various equipment by validators such as DNV-GL and suppliers or users of these equipment's. A schematic is provided below to show the goal of this research and the possibilities for future research.

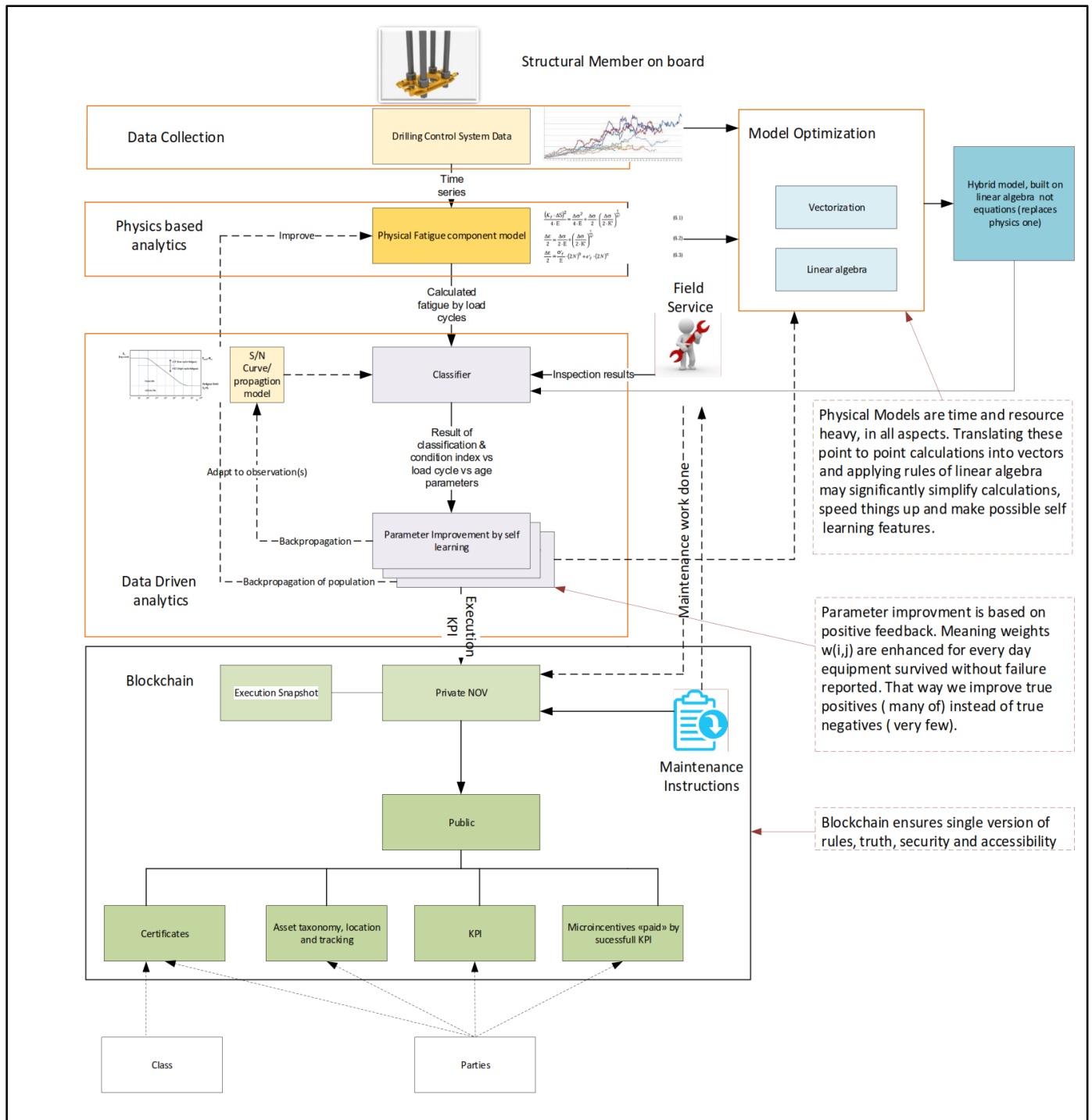


Figure 1-2: Schematic showing project limitations and the possibilities for further research (Zec, 2018)

1.6 Thesis Outline

To achieve the objective of this thesis the following outline presented in this table will be utilized after this introductory chapter.

Chapter	Purpose
2	An extensive literature survey to show the mechanism of fatigue, classes of fatigue and the applications of fatigue analysis.
3	An evaluation of the selected fatigue damage models that will be evaluated in this thesis. The advantages and drawbacks from utilising these models will be also be discussed.
4	Presentation of how torque signals and hook loads data is acquired, processed and analysed before being used for fatigue calculation's
5	Presentation of the HPS-03 1000T top drive as well as the tie rods being analysed in this thesis. Presentation of methods and tools used to carry out the fatigue analysis
6	Presentation of results obtained from using Palmgren-Miner's model, Manson's Double Linear model and Subramanyan's Non-Linear model. Evaluation and discussion of the results obtained from the tests
7	Presentation of conclusions from the results obtained and recommendations for further research

Table 1-1: Thesis Outline

2. Literature Survey

2.1 Introduction

In this section of the thesis the basic concepts of fatigue analysis will be explained. This will focus mainly on structural fatigue analysis of materials with a base metal and steel alloys.

Uniaxial fatigue analysis approaches will be introduced first to serve as a basis before the methods for multiaxial fatigue analysis will be introduced.

The final sections of this chapter will focus on mean stress correction theories and cycle counting techniques as recommended in the ASTM E-1049 standard.

2.2 What is Fatigue

Fatigue can be defined simply as the wearing out of a material, when this process occurs continuously eventually the material will fail and fracture. The term fatigue of materials was coined by Frederick Braithwaite in 1854, in his words “there are reasons for believing that many of the appalling and apparently uncountable accidents on railways and elsewhere are to be ascribed to that progressive action which may be termed ‘fatigue of metals’. This fatigue may arise from a variety of causes such as repeated strain, blows, concussions, jerks, torsion, or tension etc”. According to the International Organisation of Standardization “Fatigue applies to changes in properties which can occur in a metallic material due to repeated application of stresses or strains, although usually this term applies specially to those changes which lead to cracking or failure”.

From the above definitions, fatigue can occur below the elastic limit of a material and in most cases the mechanism of fatigue can go undetected from initiation through to propagation and it is at the instantaneous phase of fracture that the effects are finally seen. This is due to the short time interval that exists between the process of crack initiation through to propagation in a material.

Historically, the issue of fatigue has been one of the foremost engineering challenges from the transportation industry to the aviation industry and the oil and gas industry. This issue is quite problematic because it can occur within the elastic limit of a material if it occurs for a great number of cycles. There is still limited knowledge on aspects of fatigue, one of the more understood areas of fatigue is uniaxial fatigue which occurs in one direction or principal plane. This is due to the robust life prediction models available as well as the vast amounts of experimental data that has

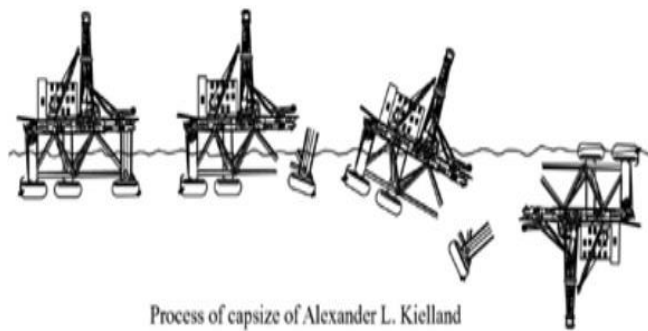
been obtained on materials undergoing this type of fatigue. Meanwhile, the area of multiaxial fatigue is actively undergoing research. Engineering equipment and components are subjected to multiaxial fatigue most of the time in comparison uniaxial fatigue hence why a better understanding of this field is needed. It is a standard practice to solve cases of multiaxial fatigue by adopting a Von Mises stress equivalent or strain equivalent approach as recommended by standard organisations such as DNV-GL, F.E.M and API. In adopting this approach, multiaxial stresses are simplified using stress or strain equivalent to uniaxial stresses or strains which are then read off an S-N or ϵ -N curves to estimate fatigue damage and remaining life left. There are significant drawbacks from using this generalisation such as this tends to result in overly conservative decisions being taken in the design of components. This can be seen in the DNV-GL-RP-C-203 standard where they utilise simplified S-N curves and the Palmgren-Miner rule to estimate fatigue damage and remaining life left for an equipment or component. By adopting these criteria, a multiaxial fatigue problem will be estimated using data obtained from uniaxial fatigue tests, which will result in overdesign of these equipment's or components because of the high level of conservativeness in this standard.

There has been more notable research in this area of multiaxial fatigue with methods looking to develop a model that incorporates equivalent stress, equivalent strain, fracture mechanics and the critical planes. These methods were presented by Gustafsson and Saarinen in their dissertation (Gustafsson and Saarinen, 2007) showing the advantages and disadvantages of each approach.

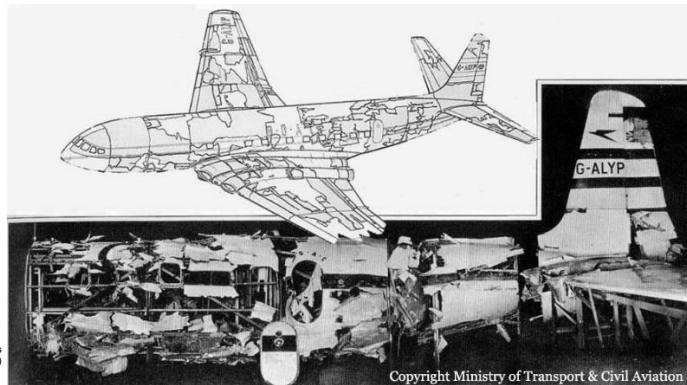
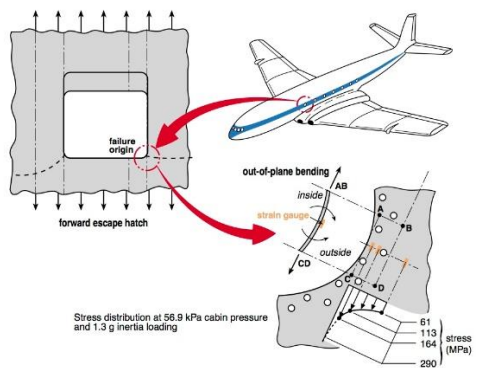
In this thesis the Von Mises equivalent stress approach has been used, this method is used to ascertain if a material will fracture or yield when it is subjected to multiaxial stresses. This approach states that “if the von Mises stress of a material under load is equal or greater than the yield limit of the same material under simple tension — which is easy to determine experimentally —, then the material will yield” (Simscale, 2019). Due to its practicality and simplicity for application in engineering applications this approach has been used, more justification of this choice will be presented in the methodology section of this thesis.

From the early years of fatigue study to date there have been accidents that have occurred due to structural fatigue failure. Some notable examples to illustrate the case of fatigue failure can be seen

in the Versailles train crash, Alexander Kielland platform capsizing accident and the de Havilland comet.



(a)



(b)



(c)

Figure 2-1 (a) Alexander Kielland Accident(OOTW, 2013, Raabe, 1980) (b) De Havilland comet accident (Wanhill, 2002, Archives, 1954) (c) Versailles train crash (Wikipedia, 2019)

From the figures above it can be seen that the materials utilised in all the accidents were subjected to a period of exposure to cyclic stresses, which might have been below the endurance limit of the materials. However, when this exposure occurred over a time period fatigue damage was accumulated and the structures eventually experienced fracture and failure. In general, fatigue is a very localised occurrence whereby its effects can be observed on a material or structure over time. These localised plastic deformations due to cyclic stresses being applied to the material will lead to changes in the structure of the material and eventually compromise its integrity.

2.3 Mechanism of Fatigue

It has been shown so far that fatigue is a localized phenomenon which occurs when a material is exposed to cyclic loading which might be proportional or non-proportional. There are three phases that occur during the mechanism of fatigue namely: crack initiation, crack propagation and fracture.

i. Crack initiation

In this phase, cracks are created in a material in a specific zone or shear plane, as cyclic loading is applied to a material. This process occurs at both microscopic and macroscopic levels. At the microscopic level there is accumulation of plastic strain over each load cycles which will increase damage in the material as the cycles continue. Meanwhile, at the macroscopic level there is plastic deformation and the effects of these deformations will reach a certain degree of equivalence and negate each other. In general, the initiation phase will start off at the surface of a material, it is only in special cases of strengthened steel alloys such as high strength steel that the process will occur interiorly in the material (Almar-Næss, 1985)

ii. Crack propagation

This phase is a result of continuous cyclic loading being applied to a material, which causes cracks to grow along the maximum shear stress plane and within the materials grain boundaries. There are two stages in this phase: a short crack growth stage and a long crack growth stage.

Short crack growth is the initial crack growth stage, and in this stage, there is propagation of cracks over a limited number of the grains in the maximum shear stress plane. The plasticity of the cracks in this phase is mainly affected by the grain size, orientation, slip characteristics, stress level, since the size of the cracks is equivalent to the microstructure of the material.

Long crack growth stage is associated with the propagation of long cracks along the global principal plane of the material and in the local maximum shear stress plane. Since the zone of plasticity for the tips of the cracks is larger than those in the short crack growth phase, the effects of the materials microstructure are not so significant. (Lee et al., 2004).

iii. Final fracture

In this phase the cracks that have been propagating in the crack growth stage will finally grow so big that there will eventually be a fracture or failure of the material. This fracture of the material is usually termed the end of fatigue life of a material and it is maximum size of crack that a material can tolerate before it fails. In this fatigue phase there exist three additional mechanisms namely: brittle fracture, plastic collapse and ductile fracture. These mechanisms depends on the characteristics of the material, loading and environmental conditions (Almar-Næss, 1985). An illustration is given below to further expand on the mechanism of fatigue.

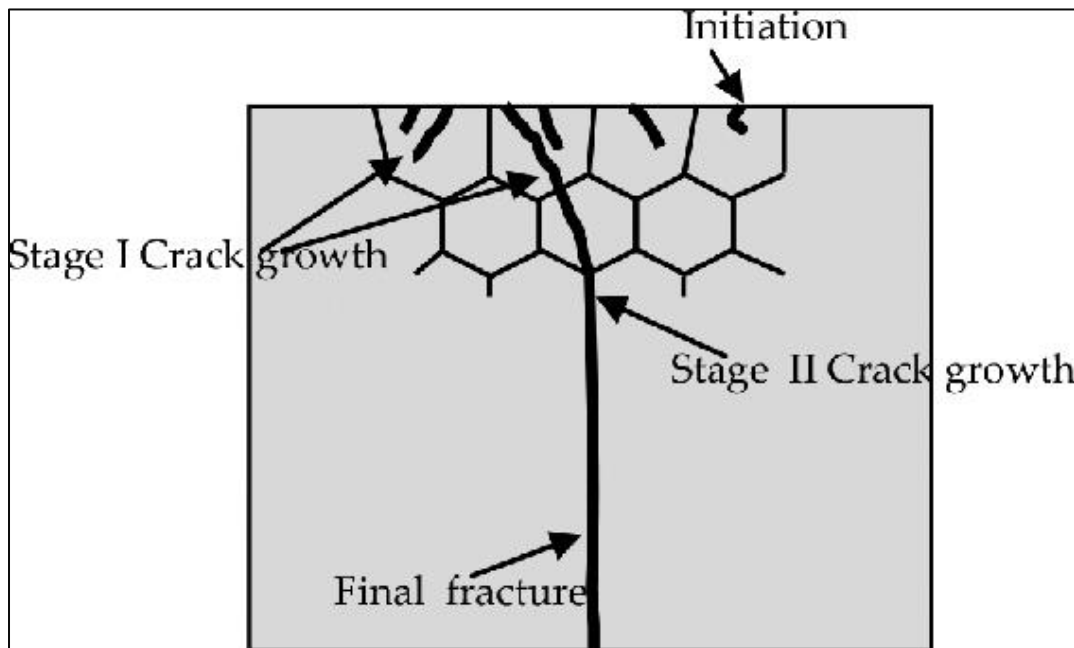


Figure 2-2: Illustration showing the mechanism of fatigue (Aanae and Hameed, 2016)

2.4 Factors Influencing Fatigue

It has been shown from the previous section the nature of fatigue and the mechanisms that are involved in this process. Prior to the initiation of the fatigue process there are some factors that will influence how fatigue will occur namely: loading type, geometry of the material, properties

of the material and environmental conditions such as corrosion. These factors shall be expounded on in this section:

1. Loading type

This factor has the largest influence on fatigue and how it occurs in a material. According to (Kusssmaul K. F., 1991) “ To determine the resulting fatigue strength of a material under complex loading, the effects of time –dependence of the stress wave form the frequency, and the phase-difference between stress components should be considered in addition to the various mean and alternating stress components and the number of cycles”. This is a useful guideline when trying to determine the influence of the loading type on resulting fatigue of a material. There are three main classification of loading types that a material can be subjected to: constant amplitude & variable amplitude loading, proportional & non-proportional loading and in-phase & out- of- phase loading.

i. Constant amplitude and Variable amplitude loading

Constant amplitude loading occurs when amplitude of the applied load is constant as the mean of the applied load varies continually with time. A good example of constant amplitude loading can be seen with a sinusoidal signal where there is a constant maximum and minimum value for the applied load in each cycle. In principle it is quite straight forward to design an equipment or structure that will undergo constant amplitude loading and in cases where the loads are also proportional no cycle counting and cumulative damage calculations will need to be done. In this special case of constant amplitude proportional loading, finite element model software’s such as Ansys can be used to identify the critical fatigue locations of the material and this single set of finite element results will be enough for the analysis.

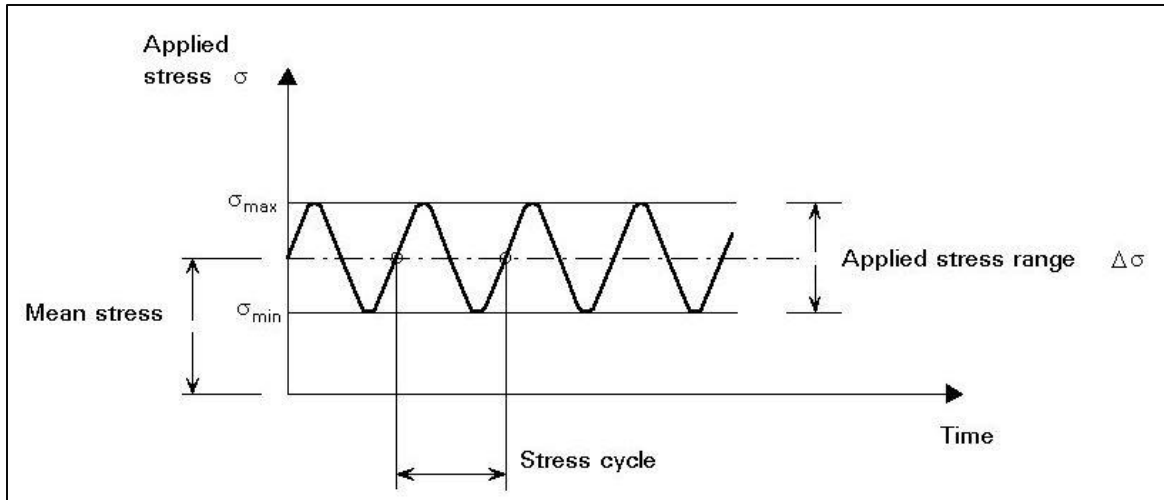


Figure 2-3: Illustration showing a constant amplitude loading stress history(Eurocode, 1993)

Meanwhile, variable amplitude loading occurs when the amplitude of the applied load and the mean of the applied load vary in each cycle with time. This typically occurs in most real-world engineering cases and it is solved by making use of cycle counting techniques such as the rainflow counting technique to convert the variable amplitude loads to a constant amplitude load case scenario which can be then assessed using the cumulative damage calculation models such as Palmgren-Miner's cumulative damage rule. In variable amplitude loading a lot of importance is placed on stress amplitudes which are above the endurance limit of the material as well as the variations in the mean stresses since these will result in an increment or decline in the fatigue life of a material.

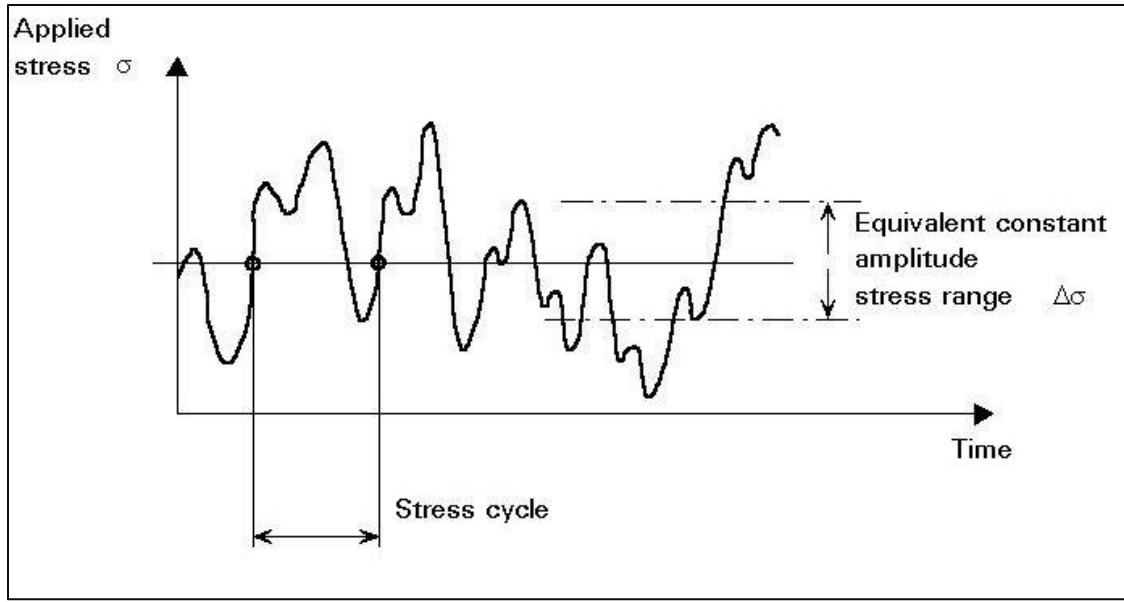


Figure 2-4 : Illustration showing a variable amplitude loading stress history(Eurocode, 1993)

ii. Proportional and Non-proportional loading

Proportional loading occurs when the principal stresses maintain a constant ratio and direction with time in this loading scenario even though the Mohr's circle experiences changes in its size as the cyclic loads are applied the orientation or the principal axes will remain fixed (Fatemi, 2018).

Meanwhile, non-proportional loading occurs when the principal stresses do not have the same ratio or maintain the same direction with time. In this loading scenario the orientation of the principal stresses will change. This scenario is important in the design of components where it is necessary to have a good understanding how the contributions from torsion, bending can combine to form normal or shear stresses.

iii. In-phase and Out- of- phase loading

In-phase loading occurs when the sinusoidal loads that are applied to a material attain their highest peaks simultaneously. Generally, in-phase loads produce proportional load histories which contribute less fatigue damage in comparison to out-of-phase

non/proportional loading. Figure 2-5 (a) below illustrates this scenario where the applied loads are in-phase.

Meanwhile, out-of-phase loading occurs when the sinusoidal loads that are applied to a material does not reach the same peaks simultaneously, rather there is a delay that is experienced. Out-of-phase loads may generate non-proportional load histories which are more damaging in comparison to in-phase and proportional loads. Cases where the normal and shear stresses are out-of-phase will produce non-proportional load histories. This is shown in Figure 2-5 (b) below where the delay in the applied loads attaining their maxima can be seen.

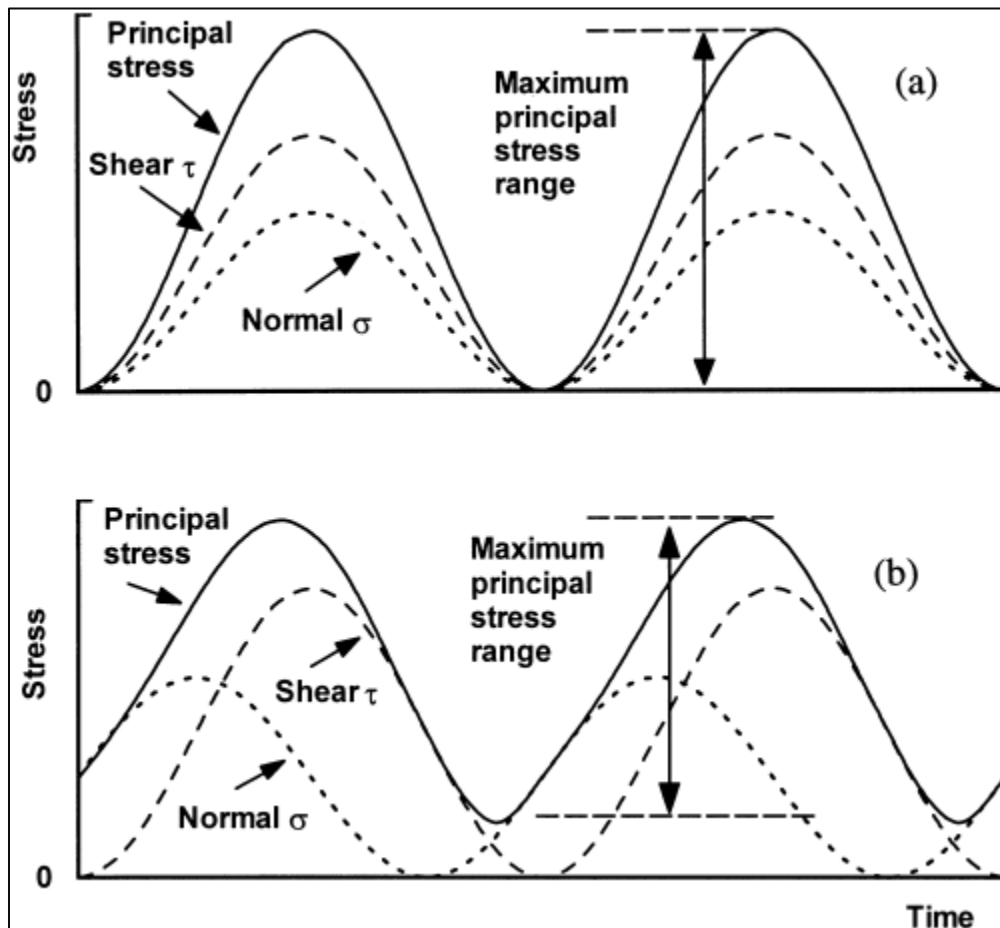


Figure 2-5: Illustration showing principal stress variation (a) in-phase and (b) out-of-phase loading(Maddox and Razmjoo, 2001)

2. Material Geometry

The geometry of a material has a significant influence on the fatigue life of the component. As a material undergoes changes in its geometry it will experience changes in the distribution of stresses and in some cases, there will be concentration of stress dependent on the material shape.

There are various test specimens that can be used to investigate the multiaxial stress combinations a material is exposed to these are namely: shafts/pipe specimen, cruciform specimen and box-beam specimen

Shaft/pipe specimen is the most popular approach utilised where round or rectangular shafts welded to steel plates are exposed to torsion in combination of normal loading.

The other notable tests that can be carried out involve the use of torsion, bending and directional change during shape testing. These tests can involve the use of a cruciform specimen or a box-beam specimen.

Cruciform specimens are used to investigate if the constant principal stress directions should be handled in a different way in comparison to those with variable directions.

Box-beam specimens are used to investigate the effect of bending and torsional loading on the material.

The tests can also account for loading by making use of the following specimens: Welded/seamless specimen, notched/un-notched specimen, slotted/un-slotted specimen. An illustration is given below to provide more clarity on these types of specimens.



Figure 2-6: Types of shaft/ pipe specimens (Laboratory et al., 2019)

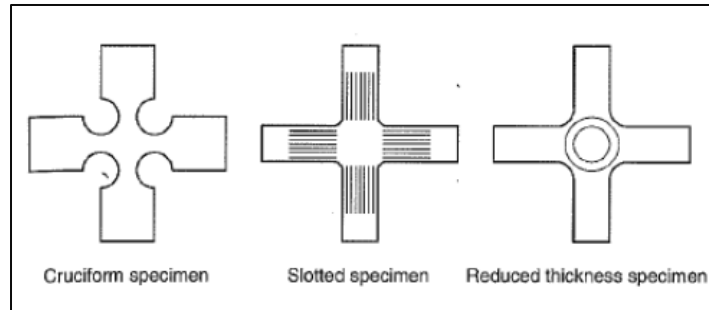


Figure 2-7: Types of Cruciform specimen(Leese G. E. and Socie D., 1989)

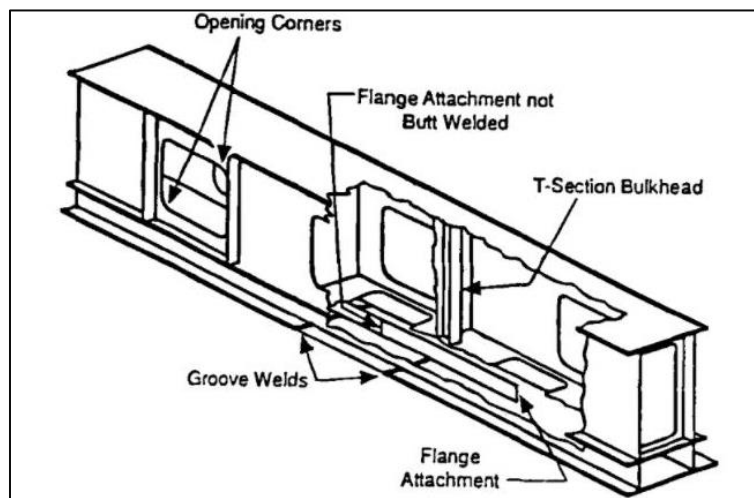


Figure 2-8: Boxbeam specimen details(Gustafsson and Saarinen, 2007)

3. Material Properties

The properties of a material have a significant effect on its fatigue life. When a material undergoes structural changes due to fatigue the properties of the material will also undergo changes. This factor is significantly amplified in the scenario of multiaxial fatigue where the structural changes of the material significantly distorts the properties of the material.

4. Environmental Conditions

Environmental conditions such as corrosion and erosion significantly affect the life of a component that is subjected to fatigue from applied loads.

2.5 Classification of Fatigue

There are two main characteristics that can be used to classify fatigue namely:

1. Number of cycles to failure
2. Stress state

The kinds of fatigue based on these characteristics will be expanded on as this topic is discussed further below.

1. **Number of cycles to failure:** There are two types of fatigue when considering this fatigue characteristic which are: High cycle fatigue and Low cycle fatigue.
 - i. **High Cycle Fatigue:** In high cycle fatigue there is a high loading frequency, stress amplitudes are relatively low and elastic. The number of cycles experienced in high cycle fatigue is usually greater than 10^4 cycles. In this thesis it is assumed that the tie-rod material exhibits elastic behaviour and because of this stresses that are above the yield stress of the tie rods will result in a fracture.
 - ii. **Low Cycle Fatigue:** In low cycle fatigue there are high stress amplitudes but with fewer number of cycles less than 10^4 cycles. Here there is little emphasis on accounting the loading frequency in terms of stress since there are so few cycles, instead the strain in the material provides a simpler approach to measure fatigue. Low cycle fatigue can be characterised by making use of the Coffin-Manson relation which was developed by S.S. Manson and L.F. Coffin separately in 1953 and 1954 (Coffin, 1954, Manson, 1953). This is illustrated in equation 2-1 below.

$$\frac{\Delta \xi_p}{2} = \xi'_f (2N)^c \quad \text{Eqn. 2-1}$$

Where:

- $\frac{\Delta\xi_p}{2}$ is the plastic strain amplitude
- ξ'_f is the fatigue ductility coefficient which is the failure strain for a single reversal
- $2N$ is the number of cycles to failure
- c is fatigue ductility exponent within the range of -0.5 to -0.7 for metals in time independent fatigue. The slopes can be steeper in cases of creep

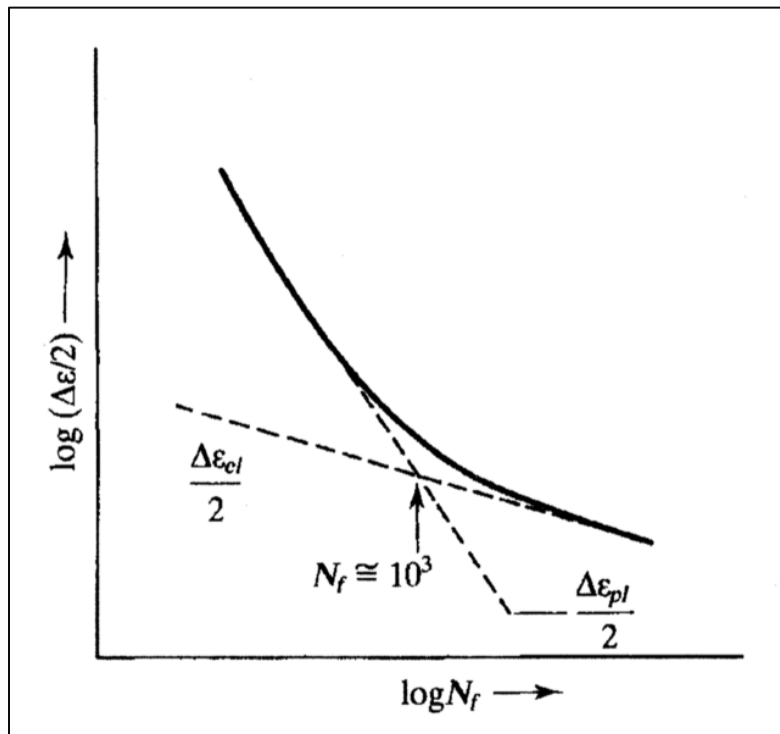


Figure 2-9 Graph showing fatigue failure as a function of strain amplitude(Courtney, 1990)

2. **Stress state:** By referring to the orthogonal planes in a Cartesian coordinate system, states of stress and strain can be easily expressed. For stress normal stress will occur in the (X, Y, Z) planes while shear stresses will occur in the (XY, YZ and ZX) planes. These 6 states also exist for normal strain and shear strain.

When considering the stress states of a material as a fatigue characteristic there are namely two kinds of fatigue that will arise: uniaxial fatigue and multiaxial fatigue.

- i. **Uniaxial fatigue:** Simply put, in this type of fatigue the cyclic stresses that a material is subjected to, act on the material in only one principal plane or direction. It should be noted that although stress might occur in an exactly one direction or pane resulting in uniaxial stress the corresponding strain will be multiaxial. For example, if we have a solid metal cube where cyclic stress is acting on the metal cube in just the y-direction, the corresponding strain will be triaxial. This occurrence can be illustrated by the figure below.

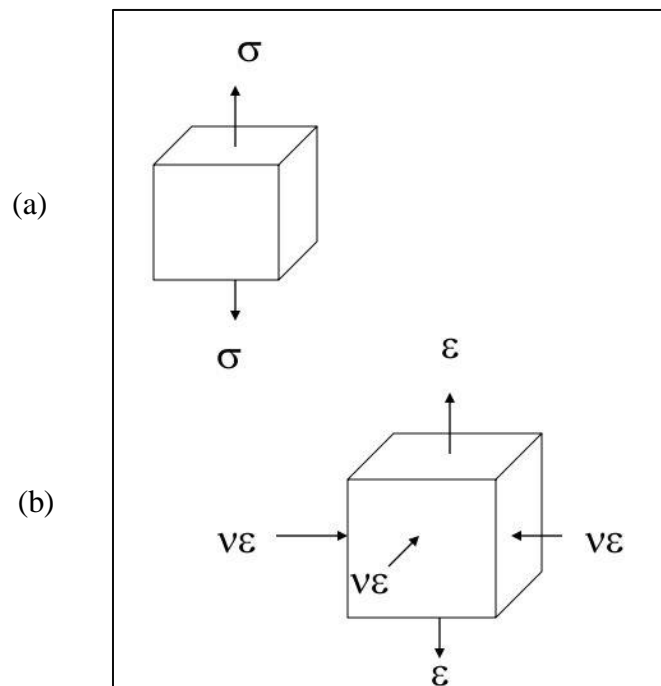


Figure 2-10: Illustration of a metal cube undergoing (a) uniaxial stress and (b) multiaxial strain

- ii. **Multiaxial fatigue:** Meanwhile, in multiaxial fatigue the cyclic stresses that a material is subjected to, act on the material in two or more principal planes or directions. For example, in a crankshaft there is presence of both torsion and bending making it to undergo multiaxial stresses. This can also be shown in the illustration below.

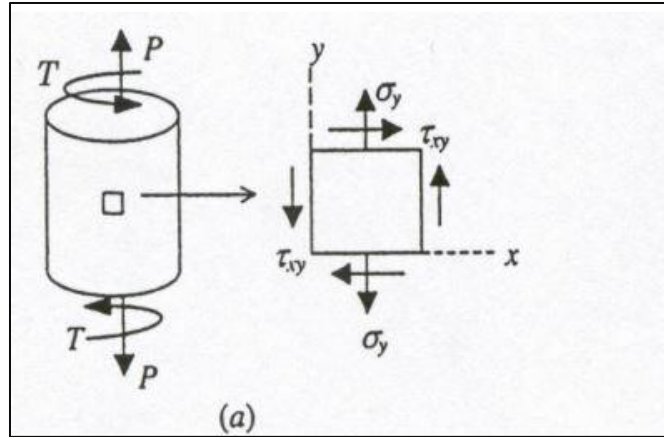


Figure 2-11: Illustration showing the multiaxial stresses acting on a Crank shaft(Fatemi, 2018)

2.6 Fatigue Modelling and Analysis

In the previous sections we have established a definition for fatigue, the mechanism of fatigue has also been shown as well as the classification of fatigue based on stress states or number of cycles. In this section the approaches used in multiaxial fatigue modelling will be treated. Due to the undesirable consequences that arise when a material or component fractures, the regulatory bodies such as DNV-GL and API have put out standards that emphasise a relative degree of conservativeness and safety in the design of components. This is to increase the robustness and resilience of designed components so that they will be able to maintain operation while they are being subjected to damage from fatigue.

According to Fatemi(Fatemi, 2018) there are four main approaches used in fatigue modelling and analysis for estimating the fatigue damage of a component and the useful life left. These are namely:

- i. Stress-life approaches
- ii. Strain-life & energy-based approaches
- iii. Fracture mechanics approach
- iv. Critical plane approach

Some of the more popular approaches within these four main approaches will be presented and reviewed in the preceding sections, a more detailed presentation of multiaxial fatigue models can

be seen in the work done by Gustafsson and Saarinen (Gustafsson and Saarinen, 2007) where they reviewed extensively the approaches to multiaxial fatigue analysis. The various approaches to multiaxial fatigue analysis that will be presented have their advantages and disadvantages which will be shown as we proceed. In this thesis the stress-life approach has been adopted whereby Von-Mises equivalent stress relation has been used for stress calculations in conjunction with S-N-curves from the F.E.M 1.001 standard.

2.6.1 Stress-Life (S-N)- approach

This approach is the most commonly used method for analysing high cycle fatigue due to the amount of data available from experiments and material testing. In this approach emphasis is placed on the number of cyclic stress cycles a material or component tolerate before it experiences a fracture or failure. Extensive testing is carried out on materials to extract data on the various properties of the materials, this information is then used to develop Wohler curves (S-N-curves) which have stress ranges for various materials. These S-N-curves contain the stress ranges and the corresponding number of cycles that a material or component can endure before it fractures (SolidWorks, 2009).

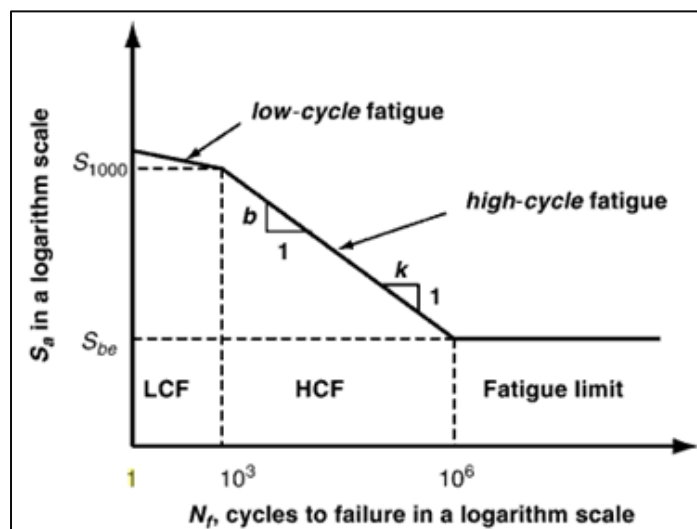


Figure 2-12 Illustration showing a typical S-N- curve (Irvine, 2013)

According to Gustafsson and Saarinen the models utilised for the Stress-Life (S-N)- approach can be broken into four additional classes namely:

- i. Empirical equivalent stress models
- ii. Stress invariants models
- iii. Average stress models
- iv. Critical plane stress models

The empirical equivalent stress model is the most widely used and accepted approach to multiaxial fatigue problems is comparison to the other stress-life models. The Sine's method is also a commonly used stress-based approach more clarity will be given on the various empirical equivalent stress models that are being used in practice as well as the Sine's method in the preceding sections of this review.

2.6.1.1 Equivalent Stress Approaches

According to Fatemi, the methods adopted in the equivalent stress approach are extensions of the static yield criteria to fatigue. There are three commonly used equivalent stress approaches for analysing fatigue these are: Von-Mises octahedral shear stress theory, Tresca's maximum shear stress theory and the Maximum principal shear stress theory. In these three approaches a stress equivalent based on the nominal stress amplitude can be calculated according to the principles underlining each approach (Fatemi, 2018). This will be demonstrated below with the supporting equations.

i. Von-Mises octahedral shear stress theory

In this equivalent stress approach, the Von-Mises equivalent stress equation for static loading is utilised by replacing the stresses with alternating stress. This approach is commonly used for a variety of multiaxial fatigue problems and it is suitable for materials that exhibit ductile behaviour.

$$\sigma_{Eq.a} = \frac{1}{\sqrt{2}} \sqrt{[\sigma_x - \sigma_y]^2 + [\sigma_y - \sigma_z]^2 + [\sigma_z - \sigma_x]^2 + 6(\tau_{xy}^2 + \tau_{yz}^2 + \tau_{zx}^2)}$$

Eqn. 2-2

Where:

- $\sigma_{Eq.a}$ is the equivalent nominal stresses amplitude

- σ_x , σ_y and σ_z are the principal nominal stresses acting on the material
and ($\sigma_x > \sigma_y > \sigma_z$)

Mean stresses can also be taken care of in this model by utilising Von-Mises effective stress equation to obtain the equivalent mean nominal stress $\sigma_{Eq.m}$. This is shown in equation 2-3 below.

$$\sigma_{Eq.m} = \frac{1}{\sqrt{2}} \sqrt{[\sigma_{m1} - \sigma_{m2}]^2 + [\sigma_{m2} - \sigma_{m3}]^2 + [\sigma_{m3} - \sigma_{m1}]^2} \quad \text{Eqn. 2-3}$$

Where:

- $\sigma_{Eq.m}$ is the equivalent nominal stresses amplitude
- σ_{m1} , σ_{m2} and σ_{m3} are the principal mean nominal stresses acting on the material

This equivalent mean stress can also be represented as a sum of the normal mean stresses

$$\sigma_{Eq.m} = \sigma_{m1} + \sigma_{m2} + \sigma_{m3} = \sigma_{mx} + \sigma_{my} + \sigma_{mz} \quad \text{Eqn. 2-4}$$

The summation of the principal mean-nominal stresses σ_{m1} , σ_{m2} and σ_{m3} presents a stress invariant which is independent of the principal axes used, this is the justification for the second equality. The main difference between Eqn. 2-3 and Eqn. 2-4 is that in Eqn-2-3 compared results will always be a positive equivalent stress while in Eqn. 2-4 the equivalent stress obtained can be positive or negative. This scenario means positive effects of compressive mean stresses versus tensile mean stresses are better represented with Eqn. 2-4 (Fatemi, 2018).

ii. Tresca's maximum shear stress theory

In this equivalent stress approach, the nominal equivalent stress amplitude is equal to the differences between the principal nominal alternating stresses.

$$\sigma_{Eq.a} = \sigma_{a1} - \sigma_{a3} \quad \text{Eqn. 2-5}$$

Where:

- $\sigma_{Eq.a}$ is the equivalent nominal stresses amplitude
- σ_{a1} and σ_{a3} are the principal nominal stresses acting on the material and ($\sigma_{a1} > \sigma_{a3}$)

iii. Maximum principal shear stress theory

This approach is good for estimating multiaxial fatigue of material or components which are brittle. In this equivalent stress approach, the equivalent stress amplitude is equal to the principal stresses.

$$\sigma_{Eq.a} = \sigma_{a1} \quad \text{Eqn. 2-6}$$

In summary, by applying the above mentioned approaches the equivalent stress amplitude $\sigma_{Eq.a}$ and the equivalent mean stress of a material can be computed thus resolving this multiaxial stress state to an equivalent uniaxial stress state. Therefore, the multiaxial fatigue problem can then be solved using the S-N- approach whereby the equivalent stress amplitudes is equated to the uniaxial stress amplitude for of the reference curve. The simplicity of applying the equivalent stress approach is one of the main reasons why it is widely used although there are some limitations to its use. In general, the equivalent stress approaches can only be used when there is a case of proportional loading and the principal axes directions are fixed during the loading cycles (Fatemi, 2018).

2.6.1.2 Sines Method

This approach is utilises the octahedral shear stress for cyclic stresses and the hydrostatic stress for mean stresses (Fatemi, 2018). This is shown in the equation below.

$$\sigma_{Nf} = \frac{1}{\sqrt{2}} \sqrt{\left([\sigma_{a1} - \sigma_{a2}]^2 + [\sigma_{a2} - \sigma_{a3}]^2 + [\sigma_{a3} - \sigma_{a1}]^2 \right) + m(\sigma_{mx} + \sigma_{my} + \sigma_{mz})} \quad \text{Eqn.2-7}$$

Where:

- σ_{Nf} is the uniaxially fully reversed fatigue strength which is expected to give the same fatigue life on uniaxial smooth specimens as the multiaxial stress state.
- m is the coefficient to cater for mean stress effects (this can be determined experimentally by utilising a nonzero mean stress level to obtain the fatigue strength and the value of m is on the order of 0.5)

By expressing the above equation in terms of x, y and z axes a new expression is obtained as shown below:

$$\sigma_{Nf} = \frac{1}{\sqrt{2}} \sqrt{[\sigma_{ax} - \sigma_{ay}]^2 + [\sigma_{ay} - \sigma_{az}]^2 + [\sigma_{az} - \sigma_{ax}]^2 + 6(T^2_{axy} + T^2_{ayz} + T^2_{azx}) + m(\sigma_{mx} + \sigma_{my} + \sigma_{mz})}$$

Eqn. 2-8

Like in the empirical equivalent stress approaches the Sines method should also only be used in cases where there is proportional loading. when the loading is proportional the Sines method can adequately capture most observations with respect to long life fatigue and can be applied for strain-controlled low cycle fatigue(Fatemi, 2018). One disadvantage of this model is that it is not considered to be conservative enough as stated in the work by Gustafsson and Saarinen(Gustafsson and Saarinen, 2007).

Apart from the equivalent stress approaches and the Sines method there have been other notable stress-based models developed by Gough, Wang, You and Papadopoulos.

Gough was one of the first researchers in the field of fatigue to carry out various tests under stresses from torsion and bending. Gough et al presented an ellipse quadrant model to be used for ductile material and an ellipse arc to be used for brittle materials(Gustafsson and Saarinen, 2007).

Wang and Yao continued research on Gough's work and showed that the ellipse-based model cannot be used in cases where the loading is non-proportional. It was also shown by Wang and Yao, that Gough's model cannot be used for all engineering materials since the tests he carried out were on just a specific set of materials(Wang Y.Y. and W.X., 2003).

The model by Gough was optimised by You et al in their work where they improved the ellipse quadrant formula by adding a material constant, phase difference and an empirical constant to eliminate the challenges that arise from utilising Gough's model. You et al utilised Findley's model to optimise Gough's model to make it appropriate for both in-phase and out-of-phase loading (You B.R. and Lee S.B., 1995).

Finally, a model based on average shear stress acting on the critical plane was given by Papadopoulos et al (Papadopoulos I. V. et al., 1997, Papadopoulos I. V., 2001). In the approach suggested by Papadopoulos both proportional and non-proportional constant amplitude loads are catered for. According to Gustafsson and Saarinen this approach is quite challenging and complex to implement (Gustafsson and Saarinen, 2007)

In summary, it is important to should be realize that stress-based approaches to multiaxial fatigue analysis are more suited for fatigue cases that involve a long life where the strains that are applied to the material are majorly elastic (Fatemi, 2018).

2.6.2 Strain-Life (EN) and Energy based approach

This approach is used when a material mainly undergoes plastic deformations, plastic stresses that a material is subjected to are computed and it can be used for estimation of total life and location of cracks. To utilise this approach strain-life curves are used to obtain the strain amplitude and the corresponding number of cycles to failure analogous to the approach used in the stress-life method. Suresh(Suresh, 1992), states that mean stress effects are captured by means of corrective relationships

similar to those of the stress-life approach and notch effects are captured through the prediction of elastic-plastic deformation in response to stress concentrations based on rules such as Neuber's rule.

This method is commonly used in cases where there is low cycle fatigue in contrast to the stress-based approaches which are used for high cycle fatigue cases and deformation is elastic. One of the significant limitations in using this approach is the absence of material information (SolidWorks, 2009). It is quite demanding to use the strain-based approach for fatigue analysis due to the presence of many analysis phases. One of the main arguments put forward by proponents of this approach is that it better captures the nature of fatigue failure in materials because it takes into account the constrained nature of the deformation in real assemblies according to Quoc-Viet Le-The (Quoc-Viet L.T., 2016). According to Dowling, by utilising the strain-life approach it is possible to reduce stress-life approximations which are in the high-cycle region and he postulated that this approach can be a replacement for the stress-based approach (Dowling, 1993).

Yongming (Yongming L., 2006) states that there are two main methods which are based on the strain-life approach namely:

i. Critical plane approach

The critical plane approach can be further sub-divided into approaches based on shear failure and tensile failure.

In the shear failure approach, some of the notable models are: Lohr & Ellison 1980, Brown & Miller 1982, Fatemi & Socie 1988, Socie 1989, Pan 1999 and Farahani 2000. Meanwhile, in the tensile failure approach some of the notable models are: Smith 1970, and Socie 1987 (Yongming L., 2006).

ii. Characteristic approach

This approach has close similarities with the procedures adopted in the critical plane approach where the reference plane is established, and the strain components of this plain are then combined to determine the fatigue life of the material. According to Gustafsson and Saarinen the main difference between this approach and the critical plane approach is that the models utilised in this approach do not rely on physical observations of a crack but rather on dimension reduction (Gustafsson and Saarinen, 2007).

Similar to the stress-based approach where an equivalent stress approach is commonly used to resolve multiaxial fatigue problems an equivalent strain approach is also used to solve multiaxial fatigue problems in the strain-based approach. It should be noted that in order to use this simplification there must be proportional strain loading. The equivalent strain approaches are variants of the three most common equivalent stress models namely: maximum principal strain model, maximum shear strain model and octahedral shear strain model

- Maximum principal strain model:

$$\varepsilon_{Eq.a} = \varepsilon_{a1} \quad \text{Eqn. 2-9}$$

- Maximum shear strain model:

$$\varepsilon_{Eq.a} = \frac{\varepsilon_{a1} - \varepsilon_{a3}}{1 + \nu} \quad \text{Eqn. 2-10}$$

- Octahedral shear strain model:

$$\varepsilon_{Eq.a} = \frac{\sqrt{(\varepsilon_{a1} - \varepsilon_{a2})^2 + (\varepsilon_{a2} - \varepsilon_{a3})^2 + (\varepsilon_{a3} - \varepsilon_{a1})^2}}{\sqrt{2}(1 + \nu)} \quad \text{Eqn. 2-11}$$

Where:

- ε_{a1} , ε_{a2} , and ε_{a3} are the principal alternating strains and $\varepsilon_{a1} > \varepsilon_{a2} > \varepsilon_{a3}$

The energy-based approaches make use of a combination of stress and strain to analyse the fatigue damage on a material. Some of the common parameters that are used in this approach to quantify fatigue are: plastic work per cycle and total strain energy density per cycle.

Plastic work per cycle is obtained by integrating the product of stress times the increment of plastic strain i.e. the hysteresis loop area of the six components of stress. By summing the six integrals for each of the stress components the plastic work per cycle is then acquired. This factor is used to

determine the life to crack nucleation of a material, there are significant difficulties in using this parameter when there is a high cycle fatigue scenario since plastic strains are small in this scenario. Total strain energy density per cycle is obtained from the elastic and plastic energy density terms. One of the advantages of energy based approaches is that they can be used for fatigue scenarios where the loading is non-proportional. However, this approach has a significant drawback from the fact that energy is a scalar quantity and will not take into account fatigue damage growth and nucleation on specific planes (Fatemi, 2018).

A more in-depth analysis on the models used in both the critical plane approach and the characteristic plane approach can be seen in the work done by Gustafsson and Saarinen (Gustafsson and Saarinen, 2007) and will not be delved into in this thesis since this thesis is based on the stress-based models.

2.6.3 Fracture Mechanics approach

In this approach the growth rate of micro cracks in a material is calculated to ascertain fatigue, where the material eventually fails as these micro cracks form a principal crack. To obtain the crack growth, the stress intensity at the tip of a crack is analysed. This stress intensity is ascertained through Paris' law where the number of cycles is expressed in terms of the stress intensity parameter (Gustafsson and Saarinen, 2007). This relationship between crack growth and stress intensity can be seen from equation 2-12 below. The underlying assumption in the approach is that cracks already exist in the material being analysed, so its use is limited to situations where cracks exist in the material being studied (SolidWorks, 2009).

$$\frac{da}{dn} = C \cdot \Delta K^m \quad \text{Eqn. 2-12}$$

Where

- $\frac{da}{dn}$ is the crack growth rate
- C is the material constant

- ΔK is the stress intensity parameter which can be expressed by $K = \sigma\sqrt{\Pi \cdot a}$
- A is the crack length
- m is the material constant

2.6.4 Critical Plane Approach

In this approach the stresses and strains on the critical planes are analyzed to estimate the fatigue damage that a material accrues. From experimental results carried out by researchers it has been shown that cracks nucleate and grow on these critical planes and these planes can be maximum shear planes or maximum tensile stress planes as determined by the material properties and loading conditions. With this approach it is possible to predict the fatigue life of a material as well as the direction of the crack or failure plane (Fatemi, 2018). Some of the common models based on the critical plane approach are Findley, McDiarmid, Dang Van, Susmel & Lazzarin and Fatemi-Sofie.

The first critical plane model for fatigue estimation was developed by Findley in 1959. Findley's model is based analyzing the stress that are acting on a specific plane. Where both shear and normal stress exist in a biaxial stress field a Mohr's circle can be used to determine these variables (Findley W. N., 1959).

Fatemi-Socie proposed a critical pane model to capture the physical mechanisms of fatigue damage and this model utilizes the maximum shear strain amplitude and the maximum normal stress acting on the maximum shear strain amplitude plane as its principal parameters (Fatemi, 2018). Fatemi-Socie's model is based on equation 2-13 below and it was evaluated by Park and Nelson (Park and Nelson, 2000) under varying conditions of constant amplitude proportional loading and constant amplitude non-proportional loading for a variety of metal alloys.

$$\frac{\Delta\gamma_{max}}{2} \left(1 + k \frac{\sigma_{n,max}}{S_y} \right) = \frac{\tau'_f}{G} (2N_f)^{b_0} + \gamma'_f (2N_f)^{c_0} \quad \text{Eqn. 2-13}$$

Where:

- τ'_f is the shear fatigue strength coefficient
- G is the shear modulus
- γ'_f is the shear fatigue ductility coefficient

- b_o and c_o are shear fatigue strength and shear fatigue ductility exponents respectively. These properties can be estimated by making use of uniaxial strain-life properties as: $\tau'_f \approx \sigma'_f / \sqrt{3}$, $b_o \approx b$, $\gamma'_f \approx \sqrt{3}\epsilon'_f$ and $c_o \approx c$. (Fatemi, 2018)

In summary, the models based on the critical plane approach have been shown to have good agreement with experimental results. However, it has some drawbacks: the critical plane approach is that the critical plane cannot be defined when the stress amplitude tends to zero or equals to zero. It is also difficult to use this model when the material being studied has microstructures that are not similar with commonly used metals.

2.7 Mean Stress Correction Theories

So far, a background has been set to show the nature of fatigue, how it can be quantified and its effect on engineering equipment or structures. The various approaches to fatigue have also been looked at with focus on the fundamental aspects of each approach.

Fatigue data from S-N curves are essential requirements to carry out a fatigue assessment and these data are obtained experimentally in laboratories. In most cases these data are collected based on scenarios that the loads being applied in each are fully reversed

This condition of fully reversed loading makes analysing mean stress quite easy, fully reversed loading is met when the mean stress is equal to zero and the stress ratio (ratio of minimum stress to maximum stress in a loading cycle) is equal to -1. However, this is not the case in most engineering scenarios involving fatigue instead the applied loads tend to be complex with a non-zero mean stress. To be able to carry out a fatigue assessment in such a scenario the applied loads must be converted to equivalent fully reversed loads and this is done by using mean stress correction methods. This is necessary to account for the effects of mean stress in the fatigue life calculations. To give a better understanding of this concept definitions of the following terms with respect to a loading cycle will be given.

- Stress range is defined as the difference between the maximum and minimum stress in each loading cycle:

$$\Delta\sigma = \sigma_{\max} - \sigma_{\min} \quad \text{Eqn. 2-14}$$

- The stress amplitude is average of the stress range:

$$\sigma_a = \frac{\Delta\sigma}{2} = \frac{\sigma_{\max} - \sigma_{\min}}{2} \quad \text{Eqn. 2-15}$$

- Mean stress is defined as the average of the minimum and maximum stresses in each loading cycle:

$$\sigma_m = \frac{\Delta\sigma}{2} = \frac{\sigma_{\max} + \sigma_{\min}}{2} \quad \text{Eqn. 2-16}$$

An illustration is given below to show the loading cycle parameters that have been defined in this section

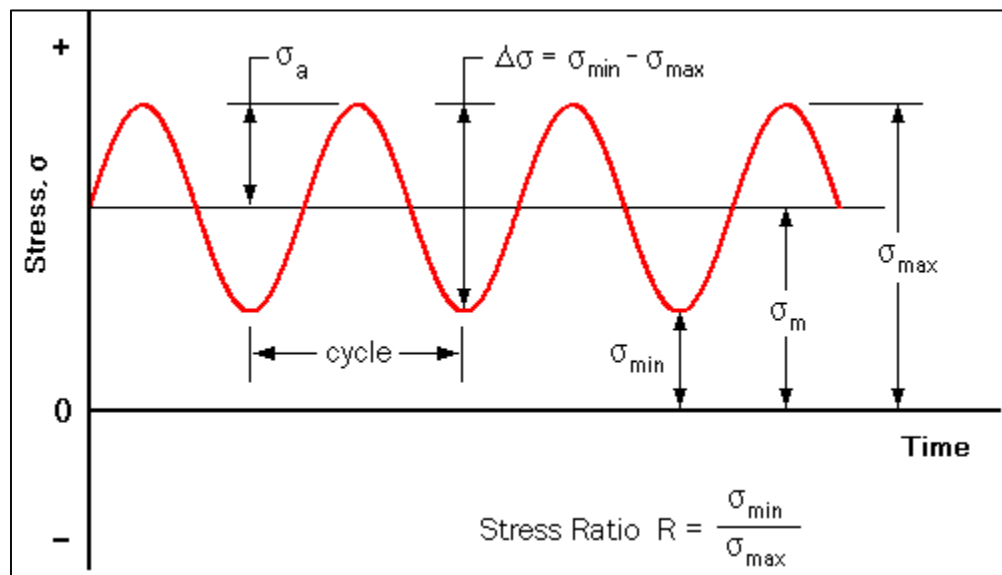


Figure 2-13 : Illustration showing parameters of a cyclic loading (UIS, 2016)

There are a couple of mean stress correction factors which are used in the stress-life approach to fatigue. The more popular methods for mean stress correction in the stress life approach include Goodman, Gerber, Soderberg and Morrow. The Smith Watson Topper is another mean stress correction method that has shown some promising results, but research is still ongoing on its suitability. These mean stress correction theories will be presented and the drawbacks from each method will be revealed.

2.7.1 Stress-Life Mean Stress Correction Methods

Goodman (1899), Gerber (1874) and Soderberg (1930) are the mean stress correction methods that will be briefly treated in this section.

1. **Goodman:** Goodman's mean stress correction relation is a linear correction that is used to correct non-zero mean stresses. According to the Dowling (Dowling, 2004) if we express the static strength of a material as the ultimate strength, a straight line will be obtained with the following equation:

$$\frac{\sigma_a}{\sigma_{ar}} + \frac{\sigma_m}{\sigma_u} = 1 \quad \text{Eqn. 2-17}$$

Solving for σ_{ar} the equivalent fully reversed stress amplitude can be obtained as follows:

$$\sigma_{ar} = \frac{\sigma_a}{\left(1 - \frac{\sigma_m}{\sigma_u}\right)} \quad \text{Eqn. 2-18}$$

Where:

- σ_{ar} is the fully reversed equivalent stress amplitude
- σ_a is the stress amplitude of the loading cycle

- σ_m is the mean stress of the loading cycle
- σ_u is the ultimate strength of the material

This equation is known as the modified Goodman equation which was presented by Smith (Smith, 1942) and can be used to obtain the equivalent fully reversed stress amplitude (σ_{ar}) that corresponds to the stress amplitude and mean stress combination in that loading cycle. This equivalent fully reversed stress amplitude will cause the same damage as the mean stress and stress amplitude combination in the calculated loading cycle (Dowling, 2004). The Goodman mean stress correction relationship is conservative and has shown good results for high-strength materials and low ductility materials as shown by the results obtained by Schijve in (Schijve J., 2009). This was one of the reasons why this method was chosen as the mean stress correction method for this thesis since the main material of construction for the tie-rods on the HPS-03 1000T top drive is high strength steel. Additional motivation for this choice will be given at the end of this section.

2. **Gerber:** Gerber's mean stress correction method is similar to the approach used by Goodman; the main difference is that in Gerber's method the ratio of the mean stress to the ultimate strength of the material is squared. By squaring the ratio of the mean stress to the ultimate strength of the material a parabola will be generated when the stress amplitudes and mean stresses are plotted on a Haigh diagram. This method is less Conservative in comparison to the Modified Goodman method and it is a good choice when the material of construction is ductile (Schijve J., 2009).

$$\frac{\sigma_a}{\sigma_{ar}} + \left(\frac{\sigma_m}{\sigma_u}\right)^2 = 1 \quad \text{Eqn. 2-19}$$

Solving for σ_{ar} the equivalent fully reversed stress amplitude can be obtained as follows:

$$\sigma_{ar} = \frac{\sigma_a}{\left(1 - \left(\frac{\sigma_m}{\sigma_u}\right)^2\right)} \quad \text{Eqn. 2-20}$$

Where:

- σ_{ar} is the fully reversed equivalent stress amplitude
- σ_a is the stress amplitude of the loading cycle
- σ_m is the mean stress of the loading cycle
- σ_u is the ultimate strength of the material

3. Soderberg: Soderberg's mean stress correction method utilises the yield strength and fatigue strength of a material. This is also a linear method and it was postulated by Soderberg that a straight line exists between the yield strength of a material and its fatigue strength. This method is the most conservative of the stress-life mean stress correction methods and it is mostly used in the aviation and aerospace industries where it is not expected for fatigue failure or yielding to occur (Suresh, 1992) .

$$\frac{\sigma_a}{\sigma_{ar}} + \frac{\sigma_m}{\sigma_y} = 1 \quad \text{Eqn. 2-21}$$

Solving for σ_{ar} the equivalent fully reversed stress amplitude can be obtained as follows:

$$\sigma_{ar} = \frac{\sigma_a}{\left(1 - \frac{\sigma_m}{\sigma_y}\right)} \quad \text{Eqn. 2-22}$$

Where:

- σ_{ar} is the fully reversed equivalent stress amplitude
- σ_a is the stress amplitude of the loading cycle
- σ_m is the mean stress of the loading cycle
- σ_y is the yield strength of the material

4. Morrow: This mean stress correction method was postulated by Morrow where he modified the Goodman relationship by replacing the ultimate strength with the true fracture strength of the material. This true fracture strength is used as the intercept of the straight-line equation that is obtained. In this method the true fracture strength has to be estimated analytically from the stress-life curve (Dowling, 2004). This can be seen in the equation below:

$$\frac{\sigma_a}{\sigma_{ar}} + \frac{\sigma_m}{\sigma_f} = 1 \quad \text{Eqn. 2-23}$$

Solving for σ_{ar} the equivalent fully reversed stress amplitude can be obtained as follows:

$$\sigma_{ar} = \frac{\sigma_a}{\left(1 - \frac{\sigma_m}{\sigma_f}\right)} \quad \text{Eqn. 2-24}$$

Where:

- σ_{ar} is the fully reversed equivalent stress amplitude

- σ_a is the stress amplitude of the loading cycle
- σ_m is the mean stress of the loading cycle
- σ_f is the true fracture strength of the material

5. Smith-Watson-Topper: This is one of the new relationships that has been proposed to correct non-zero mean stresses by Smith, Watson and Topper in their work on a new stress strain function for the fatigue of materials (Smith et al., 1970). This method has three forms as can be seen in the equation below and it can be used in both stress -life and strain-life approaches.

$$\sigma_{ar} = \sqrt{\sigma_a \sigma_{max}} \quad \text{Eqn. 2-25}$$

$$\sigma_{ar} = \sigma_{max} \sqrt{\frac{1-R}{2}} \quad \text{Eqn.-2-26}$$

$$\sigma_{ar} = \sigma_a \sqrt{\frac{2}{1-R}} \quad \text{Eqn. 2-27}$$

Where:

- σ_{ar} is the fully reversed equivalent stress amplitude
- σ_a is the stress amplitude of the loading cycle
- σ_{max} is the maximum stress of the loading cycle
- R is the stress ratio between the minimum stress and the maximum stress of the loading cycle

In summary, most data from experimental tests fall between the curves for Goodman and Gerber. The Modified Goodman expression is mostly used due to its simplicity and its reasonable amount

of conservativeness hence why it was adopted in this thesis. Other important things to take note of with respect to the discussed methods are:

- Mean stress corrections methods should only be utilised in tensile cases for the tensile mean stresses.
- In cases where the stress ratio is small i.e. less than 1 there is little difference between the mean stress correction method that is used.
- As the stress ratio tends towards 1 the differences between the three methods discussed here are amplified
- In cases where the material is hard steel as the ultimate strength approaches the true fracture strength the Modified Goodman and Morrow relationships give equivalent results.
- The Morrow mean stress correction method shows less sensitivity to mean stress effects in cases where the fracture strength is greater than the ultimate strength of the material. This scenario occurs in ductile materials.

A graphical illustration is provided below to show how the mean stress correction methods compare to each other.

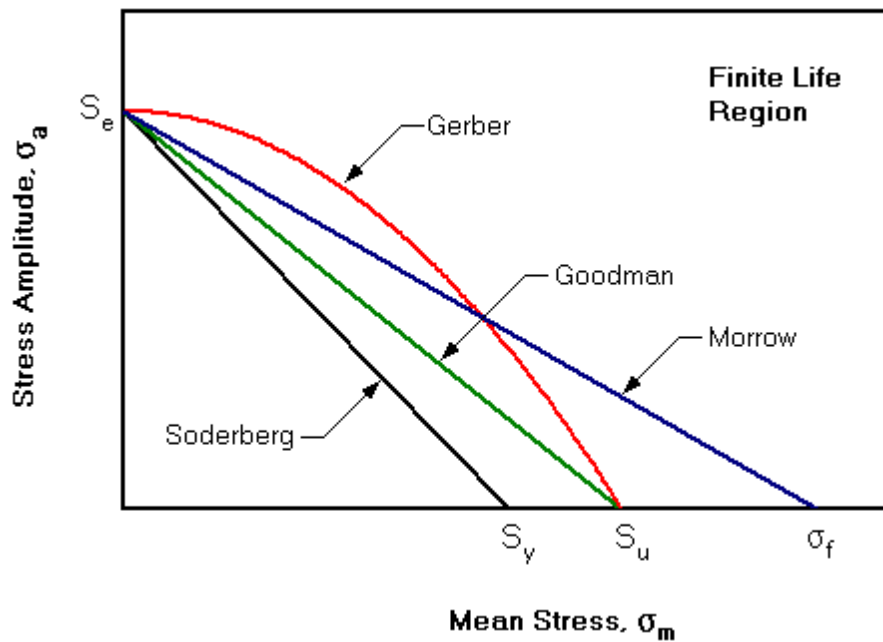


Figure 2 -14: Comparison of mean stress correction equations

2.8 Rain Flow Cycle Counting

It was stated earlier in previous sections of this chapter that it is desirable to have constant amplitude cyclic loading, due to the simplicity in counting the cycles and computing the fatigue life estimate. However, this is not usually the case in most fatigue situations, instead variable amplitude load sequences are prevalent. To carry out fatigue analysis in this scenario of variable amplitude loading the load sequence must be converted into blocks of constant amplitude loading. Once this has been done, the stress amplitude and mean stresses from each of the loading blocks can then be used to compute the number of remaining cycles to failure from stress-life curves. This procedure of converting the variable amplitude load sequences into constant amplitude loading blocks is called ‘*cycle counting*’. There exist several cycle counting methods as recommended by ASTM in their publication in ASTM E1049-85 for ‘*Standard Practices for Cycle Counting in Fatigue Analysis*’ (ASTM, 2017). Among these methods the most reliable are the range pair counting method and the rainflow counting method. In this thesis the rainflow counting method will be used to convert the variable stress history into constant amplitude stress blocks due to its accuracy.

The rainflow cycle counting method was developed in 1968 by Endo and Matsuishi in their work on fatigue of materials (Matsuishi and Endo, 1968). This method involves comparing the stress cycle reversals to the streams of rainwater that flow down the edges of the roof of a Pagoda, this can be seen in Figure 2-15 below.



Figure 2-15 : Rainwater flowing down the roof of a Pagoda (Irvine, 2013)

There are four main steps in Rainflow counting as prescribed in ASTM E1049-85, these are:

1. Hysteresis filtering:

In this step small cycles that do not contribute to fatigue can be filtered out. To do this an amplitude range is set and any cycle that is below this range is filtered out of the loading history (Hiatt, 2016).

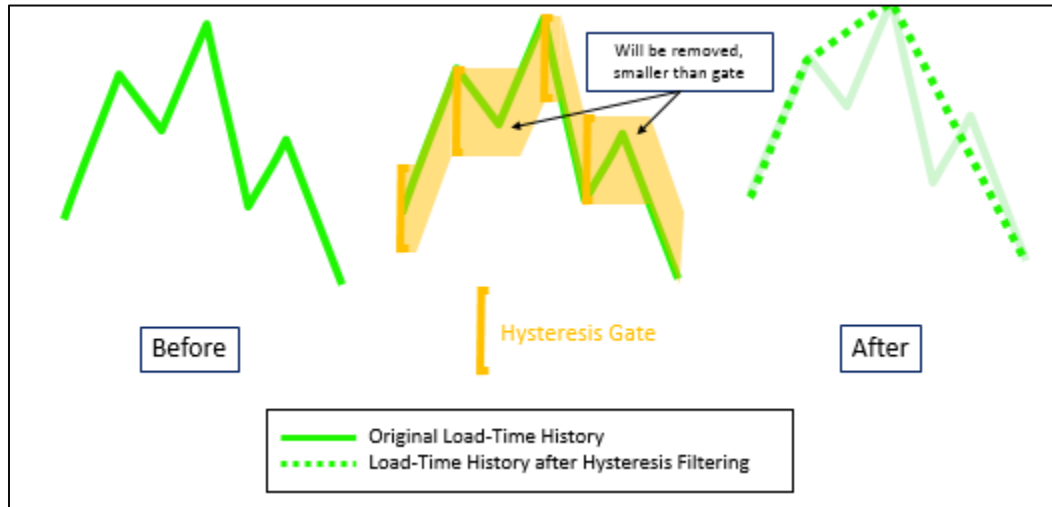


Figure 2-16: Removal of cycles smaller than amplitude range from load history (Hiatt, 2016)

2. Peak-Valley filtering:

In this step only loading data points which have reversals are retained. The reason for this is that it is only the maximum and minimum values in a cycle that are needed for fatigue life calculation. After carrying out this step a turning point sequence will be obtained which will be used for the discretization step of this analysis (Hiatt, 2016).

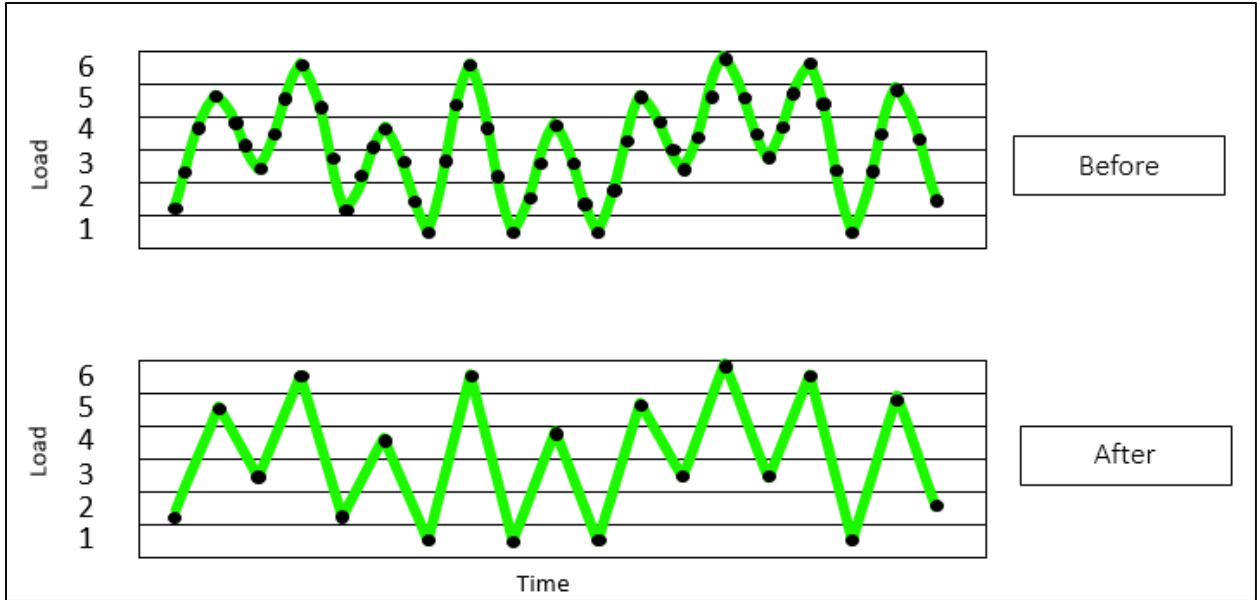


Figure 2-17: Peak-Valley Filtering retaining loading data points (black dots) which represent reversals (Hiatt, 2016)

3. Discretization:

In this step discrete bins are set on the Y-axis to take account of the fixed amplitude ranges that have been set. Here the amplitude of the loading data points is centred according to their bins. it is necessary to pick a bin size that does not significantly adjust the amplitude of the loading data points. According to the ASTM E-1049-85 standard it is recommended to use 64 bins during this discretization step (Hiatt, 2016).

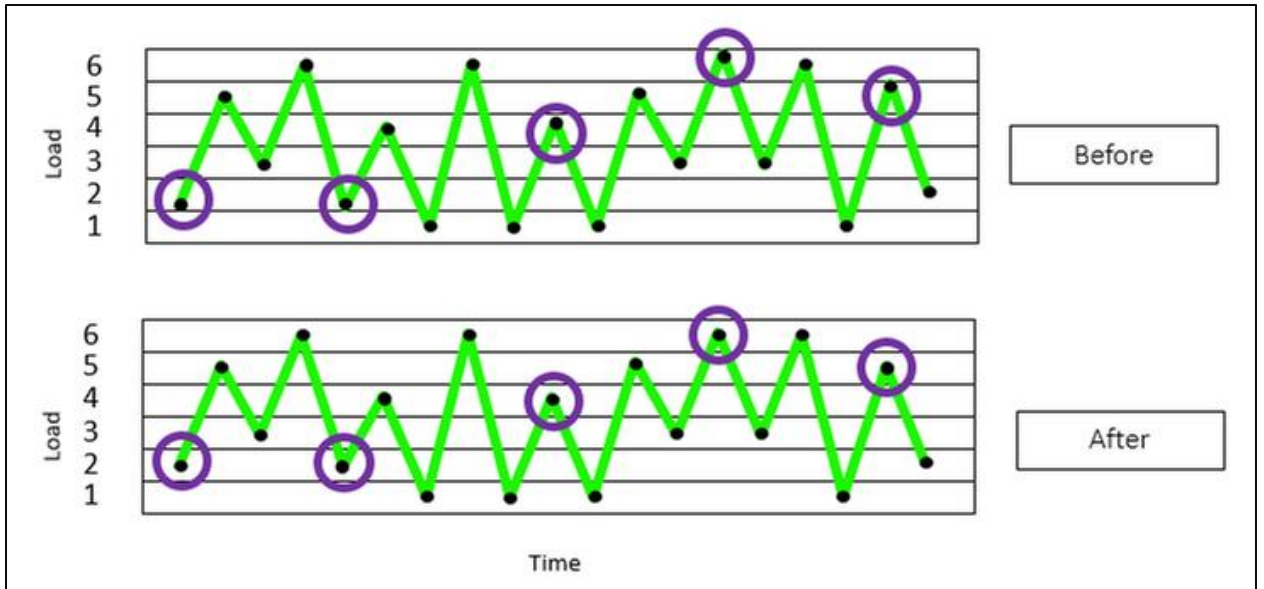


Figure 2-18: Binning of data points. Black dots amplitudes are adjusted to the centre of the bins. Data points whose amplitude is affected by binning are circled in purple.(Hiatt, 2016)

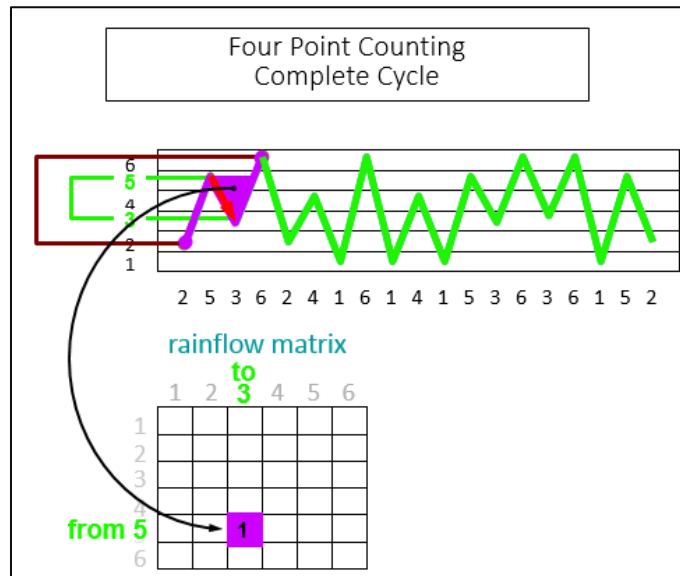
4. Four Point Counting Method:

In this step the cycles that are obtained from the previous three steps can be counted taking account of the mean stress and stress amplitude from each counted cycle. To carry out this four-point counting method the following steps need to be carried out.

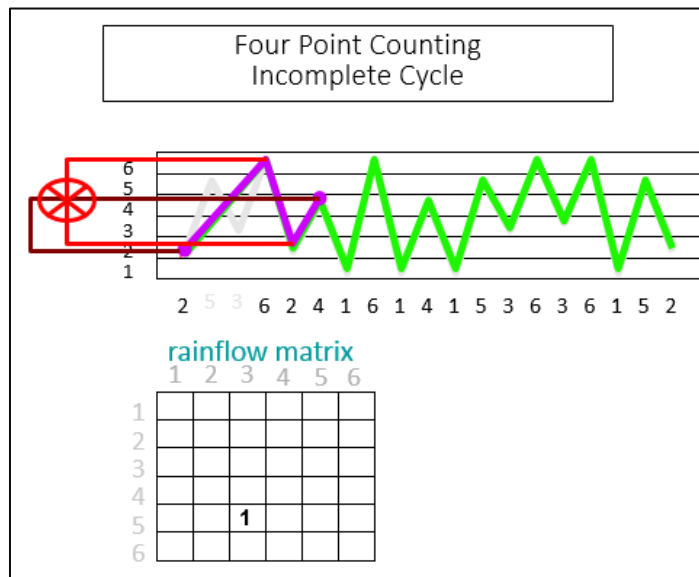
- i. Select four consecutive stress data points (S1, S2, S3, S4)
- ii. Identify the inner stress [S2-S3]
- iii. Identify the outer stress [S1-S4]
- iv. A cycle is counted if the inner stress range is less than or equal to the outer stress range and if the inner stress range is bordered by the outer stress range. If these conditions are not met the cycle is not counted (Hiatt, 2016).

This procedure is continued until all full complete cycles are extracted and counted from the stress loading history. The incomplete cycles are kept as residue in a rainflow matrix and will be used for further analysis of fatigue over a specific time period for example if the extracted complete cycles are for 1 loading block then if the damage for

2000 loading blocks is needed the residue of incomplete cycles will then be multiplied by 2000 and added to the rainflow matrix.



(a)



(b)

Figure 2-19: Illustration showing complete and incomplete cycles using the four point counting method (Hiatt, 2016)

3 Review of Selected Fatigue Damage Models

In this chapter three selected fatigue damage models will be presented; these are the models that have been used for fatigue damage assessment in this research work. The selected models are Palmgren Miner's, Manson's and Subramanyan's fatigue damage models. These models suggest different approaches to fatigue life assessment: Palmgren-Miner's model is a linear based model; Manson's is a double linear model while Subramanyan's is a non-linear model. A brief overview of on key aspects of these models will be presented and advantages and drawbacks of each models will be put forward.

3.1 Palmgren-Miner's Linear Damage Model

Miner's rule was popularised in 1945 by M.A Miner in his work on fatigue involving tension-tension axial fatigue data for aircraft skin material (Miner, 1945) , this was a development of an earlier cumulative damage model proposed by G.A Palmgren in 1924 (Palmgren, 1924). This model is commonly known as Miner's rule or Palmgren-Miner's linear damage hypothesis. Palmgren Miner's model operates on two major assumptions: the load spectra is assumed to be fully reversed sinusoidal cycle and it is assumed that the total work absorbed by the system will result in failure occurring. This model postulates that “where there are k different stress magnitudes in a spectrum, S_i ($1 \leq i \leq k$), each contributing $n_i(S_i)$ cycles, then if $N_i(S_i)$ is the number of cycles to failure of a constant stress reversal S_i (determined by uniaxial fatigue tests), failure occurs when damage(D) i.e. the ratio of the applied cycles to the number of cycles to failure is equal to 1” (Miner, 1945). Usually the value of 1 is used to express when failure of a material due to fracture will occur. However, this value for damage (D) varies in different industries for example in the aerospace industry a value of 0.7 is used for D due to the conservative restrictions that are needed for the design of aerospace parts or equipment. This relationship is expressed in equation 3-1 and 3-2 below and Figure 3-1 shows the sinusoidal loading that is assumed in Miner's rule.

$$D = \sum_{i=1}^k \frac{n_i}{N_i} \quad \text{Eqn. 3- 1}$$

$$n_r = N_m \left(1 - \sum_{i=1}^k \frac{n_i}{N_i} \right) \quad \text{Eqn. 3- 2}$$

Where:

- n_i is the number of cycles accumulated at stress S_i .
- N_i is the number of cycles a material can take until failure at the given stress
- D is the fraction of life consumed by exposure to the cycles at the different stress levels.
- n_r is the remaining life of a material
- N_m is the number of cycles at the given multi stress level

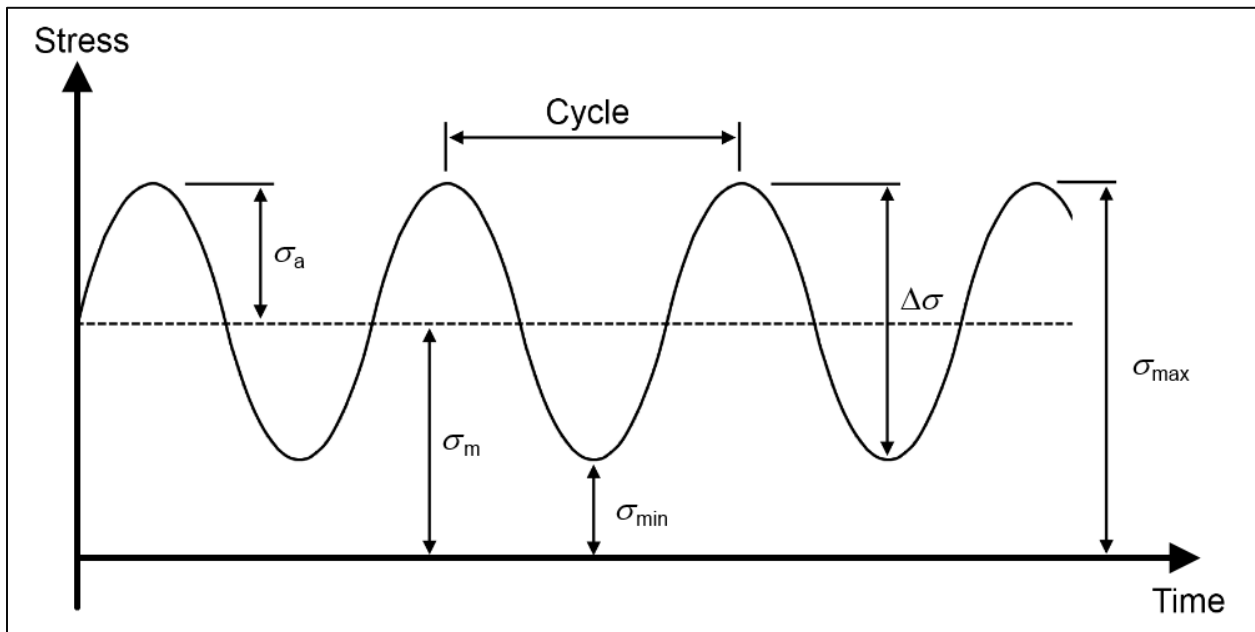


Figure 3-1: Sinusoidal loading spectra that is assumed to apply Miner's rule

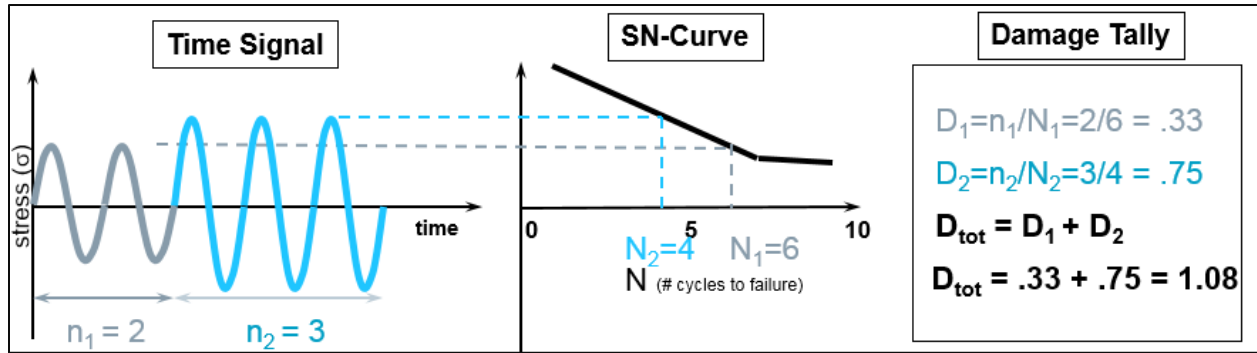


Figure 3-2: Schematic showing the application of Miner's rule in this case D exceeds 1 so failure will occur (Hiatt, 2016)

Palmgren-Miner's linear damage model is the most popular model used in various industries for analysing fatigue life and expressing damage that a material is being subjected to, this is due to the simplicity in utilising this model. Also, most of the stress-life curves available in standards such as DNV-RP-C203 were developed from experimental data based on Miners rule.

Some of the main limitations that exists in the usage of Miner's rule is that it does not take into account the load sequences, effects of load level and the load interactions a material is subjected to, and because of this Miner's rule tends to underestimate fatigue life in a scenario where stress amplitudes increase and it overestimates fatigue life in a scenario where stress amplitudes are decreasing. To overcome these shortcoming various probabilistic methods have been used to counteract the load sequence effects thus resulting in acceptable predictions for fatigue life under random loading (Blason et al., 2016, Fernández-Canteli et al., 2014, Pavlou, 2002, Pavlou, 2018)

3.2 Manson's Double Linear Damage Model

This model was developed by S.S Manson in 1967 where he considered fatigue to be occurring in two major stages namely: crack initiation and crack propagation. The main assumption in this initial postulate by Manson, was that the crack initiation period N_p could be used to express the total life of a material by using Eqn 3-3 – Eqn 3-4. Various revisions have been made to this model until 1981 where Manson abandoned the use of the terminologies of crack initiation and crack propagation, rather he chose to call this Phase I and Phase II, he also presented equations to implement the double linear damage rule. This was done to achieve simplicity in the application of this principle in comparison to the damage curve approach that he had suggested in his previous

publications (Ensign et al., 1966, Manson, 1966). Manson's double linear damage rule can be regarded as Miner's rule applied to two phases of fatigue damage. According to Manson, (Manson and Halford, 1981) when block loading exceeds two levels the following equations can be used to compute damage in the two phases.

Total fatigue life is expressed as:

$$N_f = N_I + N_{II} \quad \text{Eqn. 3-3}$$

The relationship between Phase I damage and total fatigue life is then expressed as

$$N_I = N_f \exp (ZN_f^\Phi) \quad \text{Eqn. 3- 4}$$

Z and Φ are constants and can be determined from the knee points of the curve for Phase I damage. The knee points are the same for all materials and can be determined from the maximum and minimum lives present in the loading cycle.

$$N_{I,N1,f} = N_{1,f} \left(\frac{n_1}{N_{1,f}} \right)_{knee} = 0.35 N_{1,f} \left(\frac{N_{1,f}}{N_{2,f}} \right)^{0.25} \quad \text{Eqn. 3-5}$$

$$N_{I,N2,f} = N_{2,f} \left(1 - \left(\frac{n_{2,f}}{N_{2,f}} \right)_{knee} \right) = N_{2,f} \left(1 - 0.65 \left(\frac{N_{1,f}}{N_{2,f}} \right)^{0.25} \right) \quad \text{Eqn. 3-6}$$

By substituting equations 3-5 and 3-6 into equations 3-3 and 3-4 a solution can be obtained for the constants Z and Φ as shown by the equations below.

$$\Phi = \frac{1}{\ln\left(\frac{N_{1f}}{N_{2f}}\right)} \ln \left[\frac{\ln\left(0.35\left(\frac{N_{1f}}{N_{2f}}\right)^{0.25}\right)}{\ln\left(1-0.65\left(\frac{N_{1f}}{N_{2f}}\right)^{0.25}\right)} \right] \quad \text{Eqn. 3-7}$$

$$Z = \frac{\ln\left(0.35\left(\frac{N_{1f}}{N_{2f}}\right)^{0.25}\right)}{N_{1,f}^{\Phi}} \quad \text{Eqn. 3-8}$$

Therefore, N_{II} can be expressed as:

$$N_{II} = N_f - N_I = N_f \left(1 - \exp(ZN_f^{\Phi}) \right) \quad \text{Eqn. 3-9}$$

Where:

- N_f is the total number of cycles to failure
- N_I is the number of cycles to failure in phase one
- N_{II} is the number of cycles to failure in phase two
- Z and Φ are constants

This can be further explained using Figures 3-3 and 3-4 below to show the damage phases considered in this model.

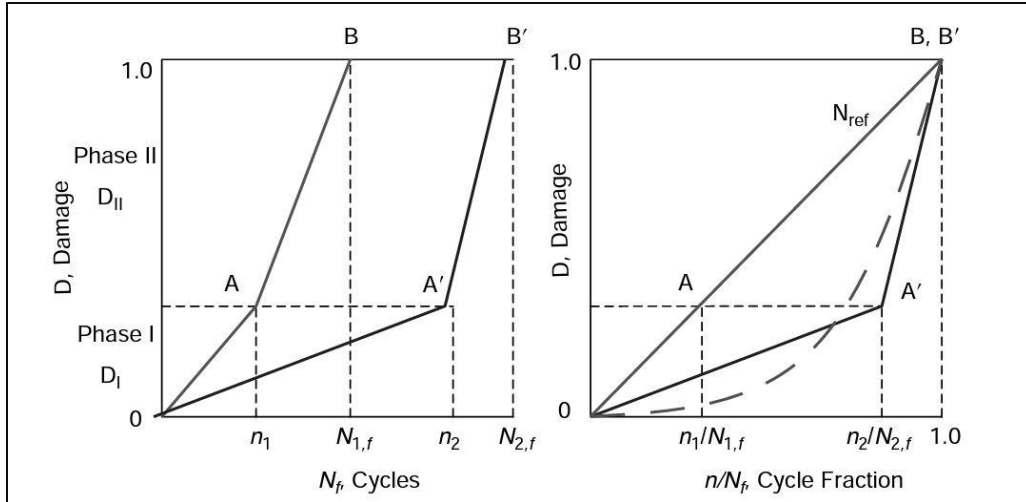


Figure 3-3: Double linear damage accumulation occurring in the two phases for a material (Lee et al., 2004)

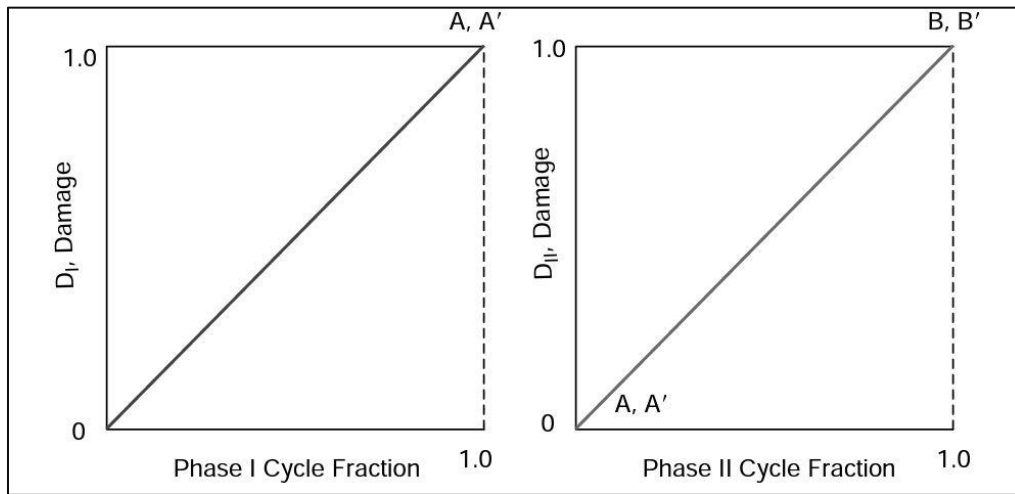


Figure 3-4: Linear damage rules for Phase I and Phase II (Lee et al., 2004)

Manson's double linear damage model has been shown to conform with experimental results as demonstrated by the research work carried out by Manson et al for NASA (Manson and Halford, 1981) and other publications from notable researchers within the fatigue subject area (Fissolo et al., 2015, Lee et al., 2004). By utilising two linear damage phases for fatigue, the ease in the use of Miner's rule can be carried over into this model, like it was stated earlier the double linear damage rule is similar to applying Miner's rule in two phases of damage. It eliminates the

deficiencies that are present in Miner's rule by having the co-ordinates for the knee-point of the S-N-curve and due to its linear nature, application of this model for designing components or analysing fatigue is easily done. The drawbacks when utilising this model is that the knee-point of the S-N curve has to be determined to properly implement this model, also Manson's model does not take into account the retardation mechanisms for crack growth (Pavlou, 2000, Pavlou et al., 2004) and mixed mode cracks (Mikkelsen et al., 2017, Pavlou, 2015, Pavlou et al., 2003).

3.3 Subramanyan's Non-Linear Damage Model

This non-linear model was developed by S. Subramanyan in 1976, in this model the concept of iso-damage lines that converge at the knee-point of an S-N curve is utilised when analysing fatigue damage. This postulate of iso-damage lines is where Subramanyan's model deviates from Miner's rule, because in Miner's rule it is assumed that a constant damage line lies on an S-N curve and this constant damage line is parallel to the S-N curve for all the stress and number of cycles to failure combinations (Subramanyan, 1976). This cumulative damage model operates under the assumption of 100% damage existing on the S-N curve of a material. When stress and equivalent number of cycles to failure below the endurance limit of a material are read off an S-N curve their combinations will result in no damage (0% damage). The interval between the S-N curve (100 % damage) and stress and cycle combinations below the endurance limit (0% damage) will have a set of straight iso-damage lines which will converge at the knee-point of the S-N curve. Revisions were made to this model in 1978 to account for the reduction in the endurance limit of a material at various stress levels (Srivatsavan and Subramanyan, 1978).

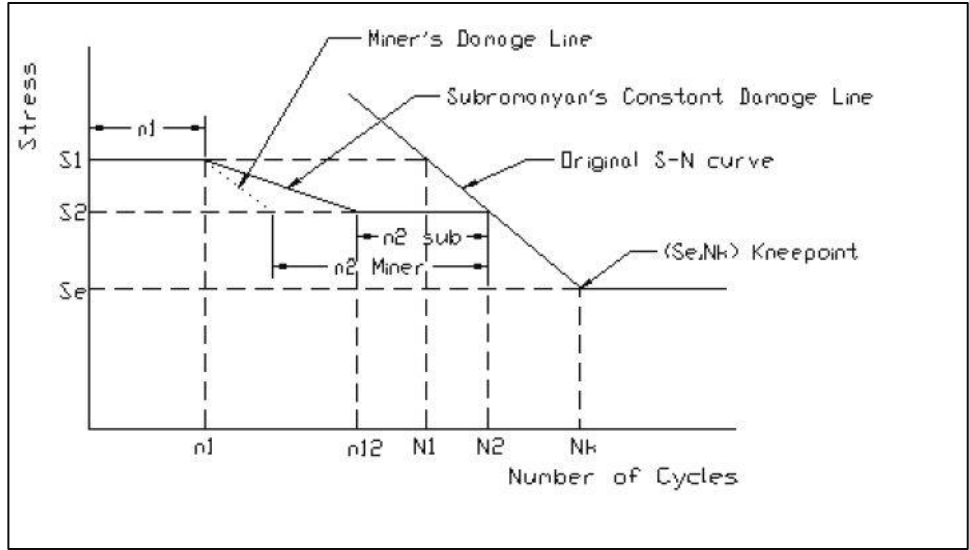


Figure 3-5: Comparison between Subramanyan's model of iso-damage lines to Miner's approach for estimating the number of cycles until failure (Subramanyan, 1976)

Consider Figure 3-5 above for an applied load i with n_i cycles with constant stress amplitudes, the damage accumulated is:

$$D = \frac{\log N_k - \log N_1}{\log N_k - \log n_1} = \frac{\log N_k - \log N_2}{\log N_k - \log n_{12}} \quad \text{Eqn. 3-10}$$

Equation 3-10 can be transformed to obtain the term α

$$\alpha = \frac{\log n_{12} - \log N_2}{\log n_1 - \log N_1} \quad \text{Eqn. 3-11}$$

The cycle ratio of this stress loading combinations is ratio between the loading cycles and the number of cycles to failure which is obtained from the S-N curve.

$$C_n = \frac{n_n}{N_n} \quad \text{Eqn. 3-12}$$

And

$$n_2 = N_2 - n_{12} \quad \text{Eqn. 3-13}$$

By substituting this expression into equation 3-11 we then have:

$$\alpha \log C_1 = \alpha \log(1 - C_2) \quad \text{Eqn. 3-14}$$

Given that ($\log n_{12} \leftrightarrow -S_e$, $\log n_1 \leftrightarrow -S_e$, $\log N_1 \leftrightarrow -S_1$, $\log N_2 \leftrightarrow -S_2$) a new expression for α is then obtained as:

$$\alpha = \frac{S_2 - S_e}{S_1 - S_e} = \frac{\log N_k - \log N_2}{\log N_k - \log N_1} \quad \text{Eqn. 3-15}$$

Where:

- N_k is the number of cycles to failure at the knee/point of the S-N curve
- n_n is the number of counted load cycles at the given stress level n
- n_{12} is the equivalent number of load cycles at the given stress level 2 for a two-step loading
- N_n is the number of cycles to failure at a given stress level n on the S-N curve
- C_n is the cycle ratio at a given stress level n
- S-N is the stress at a given level n
- S_e is the endurance limit of the material

Revisions were made to this model in 1978 by Srivatsavan and Subramanyan to adjust the endurance limit of a material at various stress levels, this was achieved by making use of the expressions below:

For the remaining life of a two-step loading from N_1 - N_2 :

$$N_{21} = \left[1 - \left(\frac{n_1}{N_1} \right) \right]^{\frac{S_2 - S_{e1}}{S_1 - S_{e1}}} \quad \text{Eqn. 3-16}$$

The remaining lives of the load sequence can be plotted on an S-N diagram to obtain a “remaining life line” (Srivatsavan and Subramanyan, 1978)

According to Subramanyan, since the material has been stressed for one cycle (C_1) with a stress level S_1 , its fatigue limit would be reduced. For a two-step loading this reduced fatigue limit can be expressed as S_{e2} and the reduced fatigue limit can be obtained by using the expression below:

$$S_{e2} = \left[S_{e1} \left(\frac{S_1}{S_{e1}} \right) \right]^{-C_1 \beta} \quad \text{Eqn. 3-17}$$

Where:

- S_1 is the stress at level 1
- S_{e1} is the endurance limit of the virgin material
- C_1 is the cycle ratio at a given stress level 1
- β is the yield strength of the material

Subramanyan’s model has shown slightly non-conservativeness when compared to actual experimental results for SAE 4130 (Lee et al., 2004) which makes its usage acceptable. However, application of this model to analyse fatigue must be carried out with caution. According to Fatemi and Yang (Fatemi and Yang, 1998) Subramanyan’s model is not applicable in cases where the stress amplitudes are near the endurance limit of the material, because S-N curves exhibit non-linearity close to their knee-point and because there is singularity at the knee point since all iso-damage lines will converge at this point.

4 Data Quality and Diagnostics

In this chapter the importance of data quality and diagnostics checks will be presented. Recommendations based on DNV-RP-0497 will be reviewed in tandem with the practices for data quality checking adopted in this research work. Justification will be provided on the choice for analysis methods to assess data quality.

This chapter will also cover the statistical parameters used in assessing data quality as well as the tools and techniques that were adopted in this thesis for data diagnosis. The results from the data quality test will be presented in the results section of this thesis and additional tables and graphs can be seen in [Appendix B](#).

4.1 Importance of Data Quality and Diagnostics

The rise of industry 4.0 and its use of tools such as internet of things (IoT), cloud computing with vast amount of data termed ‘big data’ has forced a rethink among asset managers and stakeholders within various engineering sectors to look for ways to leverage this data to create value. A brief definition of key terms will be given to provide more clarity on concepts that will be used in this chapter.

Industry 4.0 can also be referred to as Industrial intelligence, and it has been termed as the ‘Fourth Industrial Revolution,’ which will transform the manufacturing industry by combining internet of things, data integration and cloud computing into the manufacturing systems. The main difference between industry 4.0 and traditional manufacturing is that industry 4.0 is a departure from the centralized offline system without interconnectivity being used in traditional manufacturing. The two main features of industrial intelligence are cloud computing and IoT (internet of things) where cloud computing allows for remote access to data and services, while IoT utilizes the cloud to automate processes in facilities or equipment linked to the internet. In a nutshell industrial intelligence eliminates processes that were managed by people and machines physically and transfers them to the cloud to be managed remotely from any location (Tessitore, 2018). When we refer to ‘big data’ this refers to vast chunks of data that are acquired through sensors and are transmitted to cloud storage facilities for post processing this data covers three aspects volume, variety and velocity. A schematic is provided in Figure 4-2 to show how these tools interact at NOV. Although there is presence of big data from obtained by sensors for the various components

on rigs, this data will not be useful in creating value if it does not meet the quality standards set by the organization or recommended by regulators.

Good quality data is a key driver for decision making in an organization, the more quality a data has will influence how much confidence asset managers have in the outputs from their decisions. This will enable a reduction in inefficiency and help in reducing risk when making critical decisions about an asset. Also, good quality data helps to eliminate lost man-hours that will be spent fixing the data to eliminate errors thus resulting in an increase in productivity.

In contrast to these points bad quality data will lead to reduction in the confidence of asset managers about the outcomes of their decisions. Also bad quality data can lead to a company missing out on valuable insights that could have been gotten from their data, which will result in a loss of competitiveness and revenue to other companies that are utilising better quality data (Moreno, 2019).

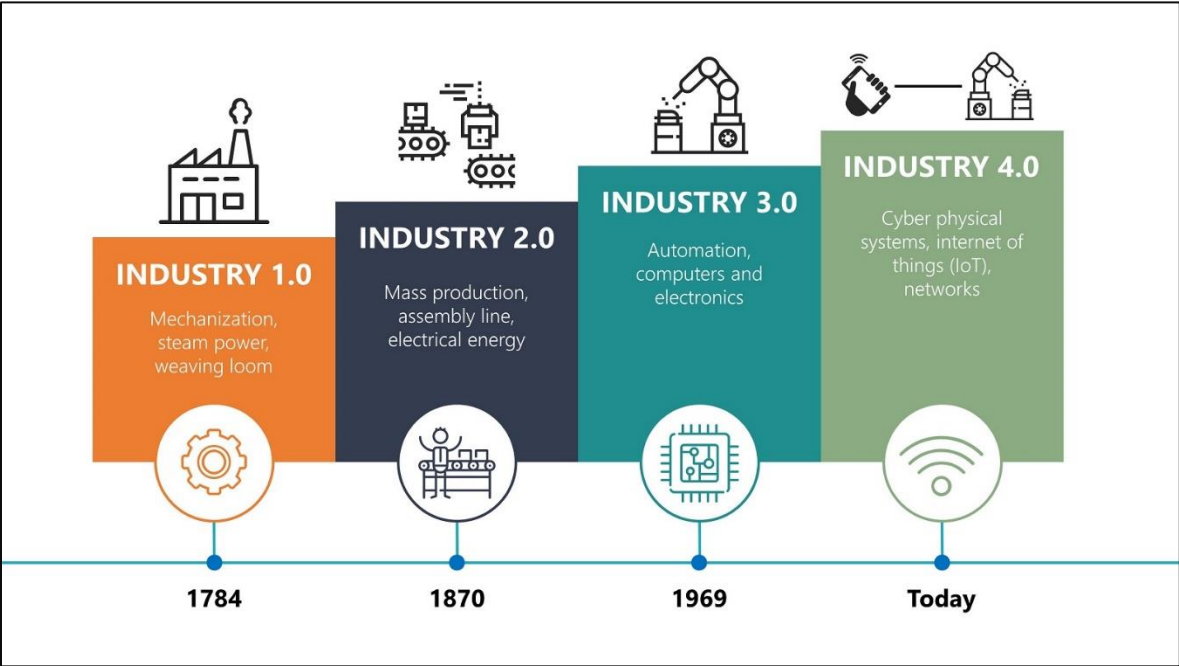


Figure 4-1: The Rise of Big Data and Industry 4.0

4.2 Data Acquisition and Storage In-house

In this thesis, data from three (3) NOV drilling rigs were analysed, these rigs had data from a main well and an auxiliary well. The main well refers to rigs that were used for heavier more complex operations and they had more components that were mounted on the top-drive meanwhile the auxiliary well were used for easier operations and required less components mounted on the top-drive. The hook load and torque signal data analysed in this thesis were from January 2014 until June 2016.

The data from rig equipment, in this case the HPS-03 1000T top drives are collected with the aid of a Data Vault server which is installed on the rig to collect data from the control system. The Data Vault securely and efficiently collects, stores and replicates equipment data to MAX.

MAX is the digital foundation at NOV, it is an advanced data infrastructure and a core team of experts that provide facilities for cloud computing, data storage, data science, and data access.

Data analytics and reports are provided to Rigsentry subscribers through a multipurpose web portal called 'Access-NOV'. The asset frameworks for rig data, analytics and equipment information is structured in Data Vault and MAX per the taxonomies defined in the SLATE system.

An illustration is given below to elaborate on this process of data acquisition, storage and utilisation for analytics.

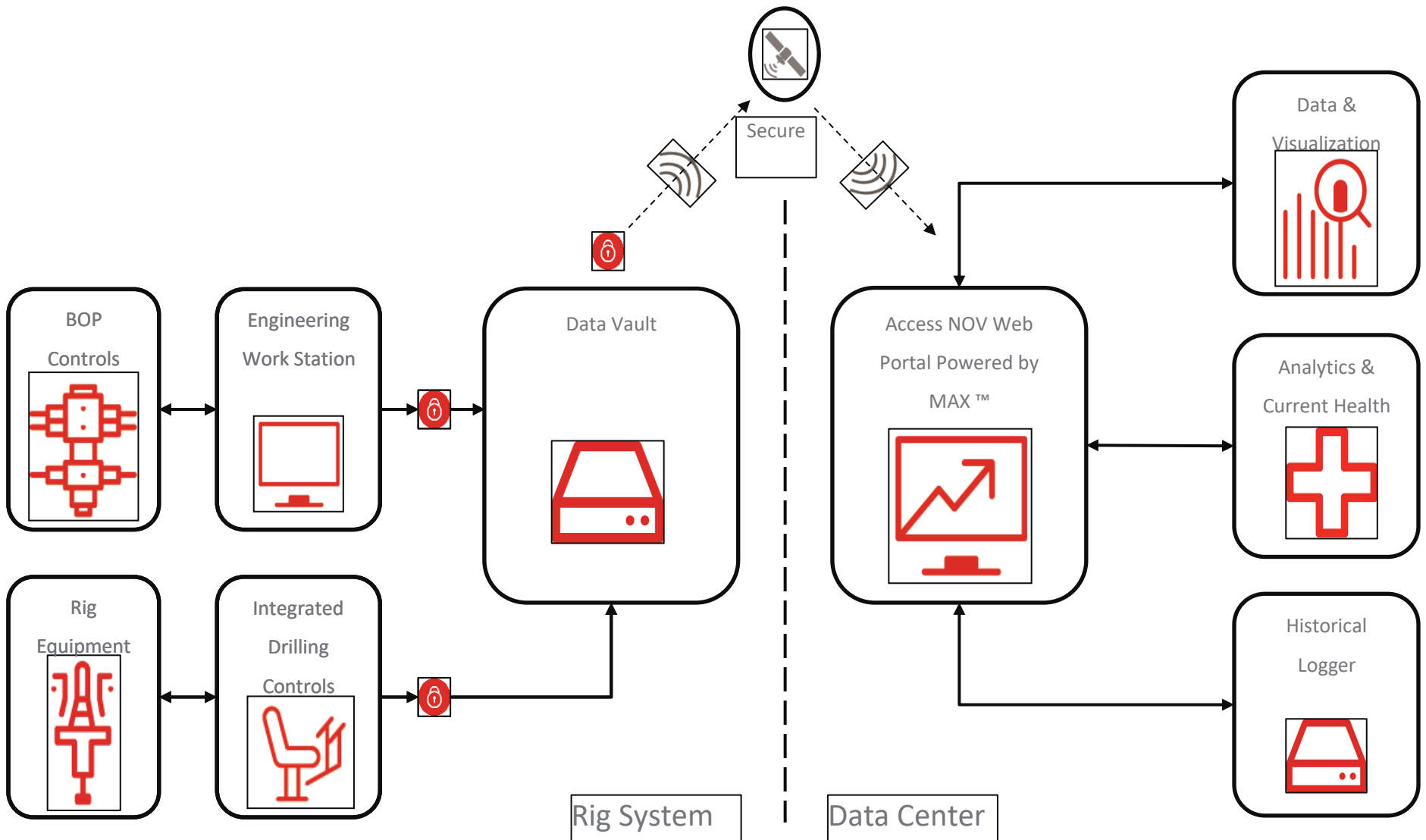


Figure 4-2: Illustration showing the process flow of data from Rigs to the data collection centre at NOV (Zec, 2018)

4.3 Data Quality Assessment

According to ISO 8000-8 (Information and data quality) there are three classes that can be used when assessing the quality of data these are:

- Syntactic quality: This refers to the conformance of data to its particular syntax which is set by the metadata. This is evaluated by a verification process.
- Semantic quality: This refers to the data properly corresponding to what it is trying to represent. That is data should be factual and true if torque signal from data reads 100 Nm at 1200 on a specific day the actual measurement in real time on that specific day at 1200 should be 100 Nm. Similar to the syntactic quality this is also evaluated by a verification process.
- Pragmatic quality: This refers to usefulness to data to fulfill a function and this is evaluated by a validation process.

In practice data obtained directly from sensors and IoT will have a higher quality than data which passes through analytics systems. This is because the data will undergo various transformations when it passes through the analytics process which will affect the quality of data (DNV-GL, 2017). This scenario was seen in this research work and this is the reason why quality checks were put in place to ensure that the data was fulfilling the requirements. The goal of a data quality assessment is to obtain uniformity and correctness in the data and ensure the data meets the expectations for the users of this data or the systems where this data will be applied.

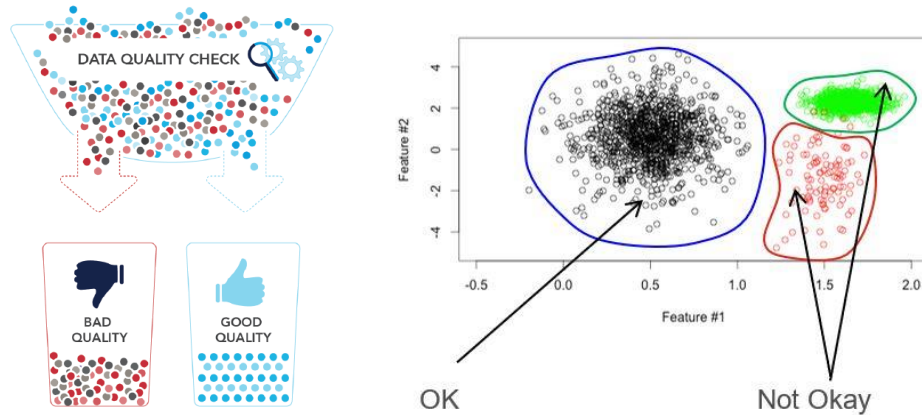


Figure 4-3: (a) The outcome of a data quality check (ISO, 2015) (b) Filtering of bad data from good quality data (Zec, 2018)

According to DNV-GL in their standard on data quality assessment (DNV-GL-RP-0497), when assessing data quality, the following steps should be taken namely:

- Define a scope taking into account the datasets that will be used and if these datasets meet the expectations for its users.
- Acquire the data and carry out transformations on this data to prepare it for exploration.
- Carry out a data quality assessment which entails identifying and setting the requirements for the data. In this step a maturity assessment will be carried out on the organization to determine the capabilities of personnel as well as their practices when handling data.
- A risk assessment should be carried out on the data where the causes of bad quality data will be identified and the consequences for making decisions based on this faulty data will be computed.
- Set up an improvement system to implement the recommendations from the data quality check. this is to ensure data quality is kept at a high level continuously.

In this thesis only the first two steps were carried out because the other steps were outside the scope of this research work.

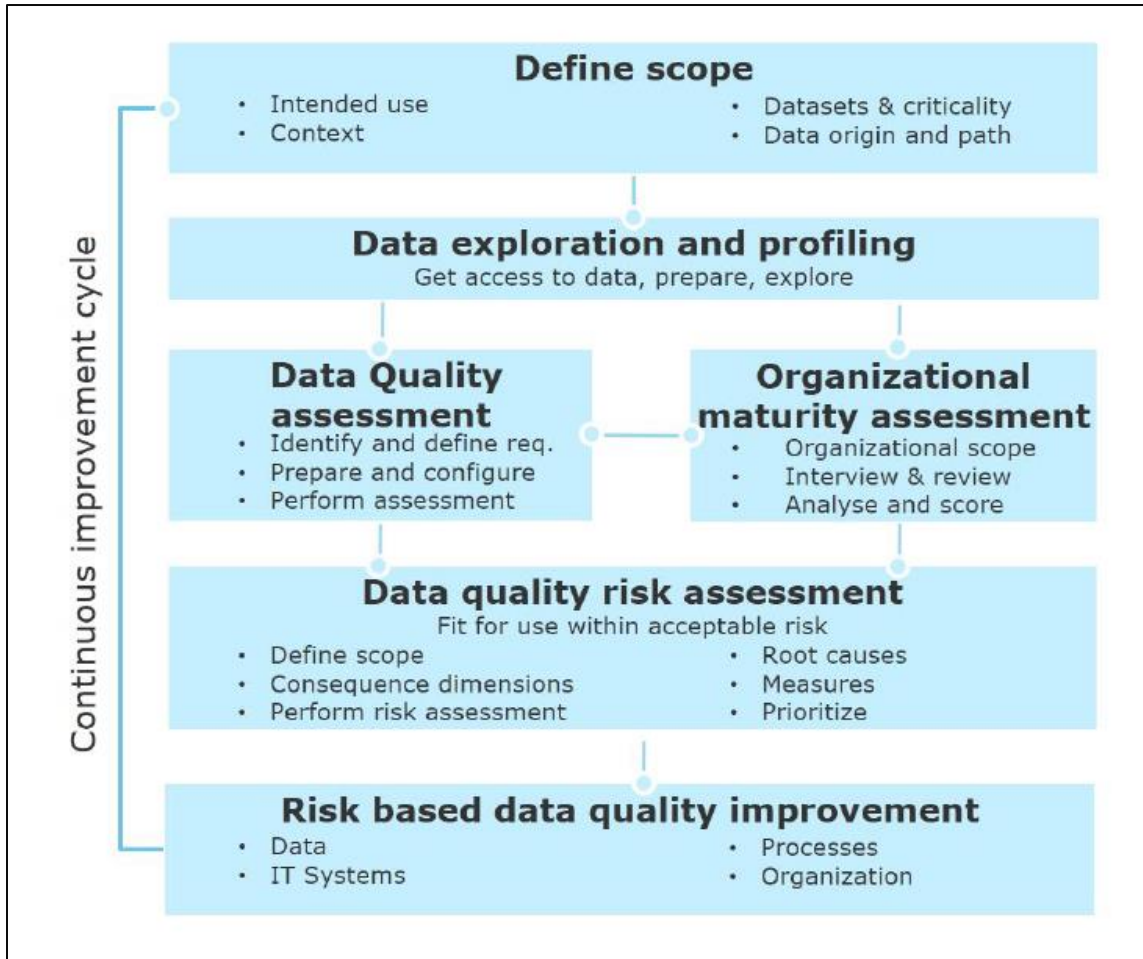


Figure 4-4: The Data quality process (DNV-GL, 2017)

4.4 Data Quality Parameters and Tools

It was stated earlier in the previous section that there are three categories of tests for data quality namely: syntactic, semantic and pragmatic these three data quality test categories were utilised in assessing data quality in this research work.

Addressing syntactic quality involved checking the formatting of the data for example if the date-timestamps were in a uniform format of year, month and day (YYYY-MM-DD) as well as checking that the dates were in the right language format.

To address semantic quality information from the equipment manual was checked to ascertain the standard operating conditions of the equipment and the expected limits for revolutions per minute. This was necessary to filter out noise from the torque signal data in cases where exceptionally high

values above the operating limits of the top drive are obtained. For example, if we have a torque signal reading of at a speed of 500rpm and the specification of the device is 300rpm, this reading will be filtered out since it does not conform to the actual real-world situation.

Pragmatic quality was addressed based on the fitness of purpose of this data, which is for fatigue analysis. This data has been verified by external parties such as DNV-GL when scheduled inspections are carried out on the equipment's.

Given that the datasets that were used in this thesis were very large spanning two years with 30 million entries expected every year. There was a need for robust tools to enable processing of the data to be carried out smoothly. In this research work R was chosen as the reference software to carry out data profiling and exploration, due to the robust research that is behind most of the libraries available in R. Data quality checking tools from R repositories such as 'Dplyr', 'Dlookr', 'Lubridate' and 'Summarytools' were used in this research work to verify that the syntactic quality of the data was met. These tools were also used to check the completeness of the datasets, semantic consistency, presence of duplicates and presence of outliers in the data.

Firstly, 'Dplyr' was used to access the classes of data types (numeric, date) available in the raw datasets, the null count, and to populate empty entries with NA values.

Secondly, 'Lubridate' was used in conjunction with 'Dplyr' to create full time series of 1 second interval for each dataset. This was necessary to ensure uniformity in the length of datasets since some datasets were missing entries when the rigs were idle, and the top-drive was not in operation. 'Lubridate' was also used to ensure all the date-timestamps were in the right format (YYYY-MM-DD) and to replace entries that had Norwegian words for months like ('mai->May', 'oktober->October', 'desember->December')

Lastly, 'Dlookr' and 'Summarytools' were used to get statistical insights into the data such as the mean, inter-quartile range, standard deviation as well as the unique rate, missing values and the presence of outliers. In this thesis the outliers identified with these tools were not filtered from the data because it was stated by the equipment operators that those values termed as outliers would have been generated during the times the equipment was idle. More details about the results from this data quality analysis will be presented in the results section of this thesis with additional results in [Appendix B](#).

5. Analysis Methods and Tools

This chapter will start with a brief description of the HPS-03 1000T top-drive and the tie-rods that were chosen for fatigue analysis, this is necessary to enhance the readers understanding of the machine part that was analysed for fatigue. This description will focus on the drive system of the top-drive and the suspension system that contains the tie-rods and this will also serve as the foundation for the choice of analysis methods and tools in this thesis. The tie rod is calculated according to API 8C "*Specification of Drilling and Production Hoisting Equipment*" and F.E.M.1.001 "*Rules for the Design of Hoisting Appliances*".

The procedures that were adopted when using the selected fatigue damage methods for fatigue calculations will be presented. Justification will also be given on the choice of tools for the various aspects of this research work.

5.1 Description of the HPS-03 1000T Top Drive

The Hydralift Power Swivel (HPS) is a fully integrated swivel concept with an efficient pipe handling system. The compact and rugged design of the machine allows it to fit in the shortest derricks, and still meet the high demands of drilling deep and tough wells in harsh environments all over the world.

Technical data for the tie rod:

- Load rating for pair: 1060 short tons (962 tonnes)
- Required safety factor (API 8C): 2.25

A basic HPS-03 1000T consists of the following assemblies:

1. Drive system:

The main part of the drive system is the Gearbox including Main Shaft, and the drilling motors. The following components are found under the drive system:

- Gearbox with Main shaft assembly:

The Gearbox is designed and manufactured using the latest technology in helical cut gearwheels, air purged Inpro upper seal system, and a dual bottom lip seal system. A housing made of high strength cast steel supports

the thrust bearing as well as all gearwheels with bearings. The bull gear is heat shrunk to the Main shaft thrust shoulder. A set of springs provides preloading of both main thrust bearing and axial upward thrust bearing, preventing shock loading on both, when top hole drilling and jarring.

The Main shaft is radially supported by two separate radial bearings. Power is transmitted from motor to Drill Stem through the Gearbox. The vital part of the Gearbox in this transmission is the Main shaft, made of forged high alloy steel for use in demanding environments. The Main shaft connects to the Drill Stem via a Crossover Sub.



Figure 5-1: Illustration showing the upper part of the HPS-03 1000T top drive with its drive system

- Drilling Motors
 - Motor cooling system
 - Parking brake

- Suspension system

The Suspension system includes suspension (Tie Rods) connecting the Top Drive to the Travelling Block/Hook via an Adaptor Link, and Thread Compensating system. This is the most critical part of the top-drive, hence why it was chosen for this fatigue analysis.

- Thread compensating

The Thread Compensating System, called ‘Smartcomp’, is a state-of-the-art automated thread compensating (weight cancelling) system providing minimum “pin on box” loads during spin-in and break-out sequences of HPS operation. The Thread comp system consists of four hydraulic cylinders, position sensing device and a hydraulic control manifold. Smartcomp utilizes modern control technology and hydraulic actuation mechanics to cancel a prescribed amount of the HPS’ weight from the saver sub pin at all vertical positions of the HPS. Variations in mud specific gravity can also be accommodated by the control system. A self-tuning sequence is employed to calibrate the system for a given HPS configuration (accounting for total installed component weight and mud specific gravity).

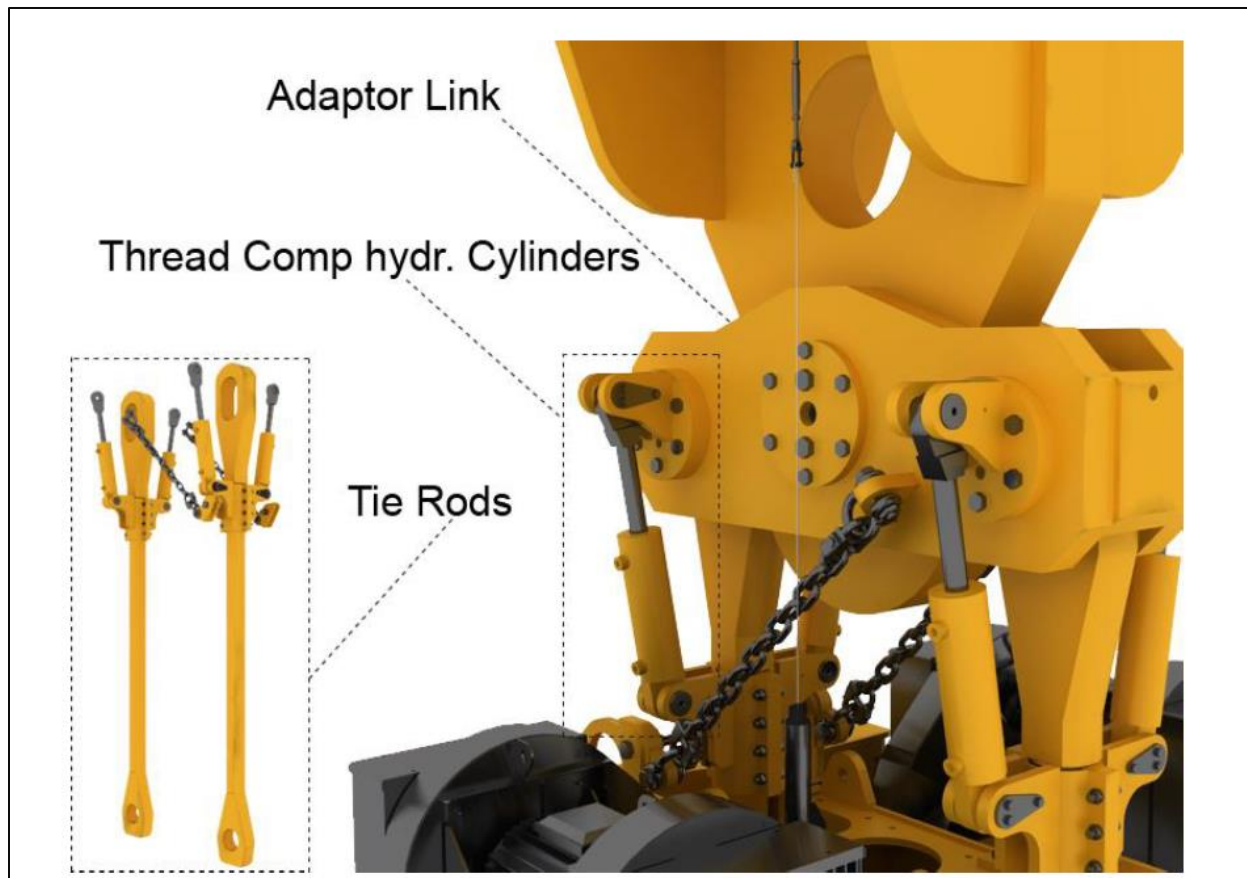


Figure 5-2: Illustration showing the suspension system of the top drive with the tie-rods which are analysed in this thesis

- Water Course
- Drill Stem and IBOP
- Support Frame
- Protection Frame

2. Pipe handler System, including:

- Rotating head
- Torque Arrestor
- Link Tilt system

- Suspension for Torque Wrench
- Torque Wrench
- IBOP Actuator system

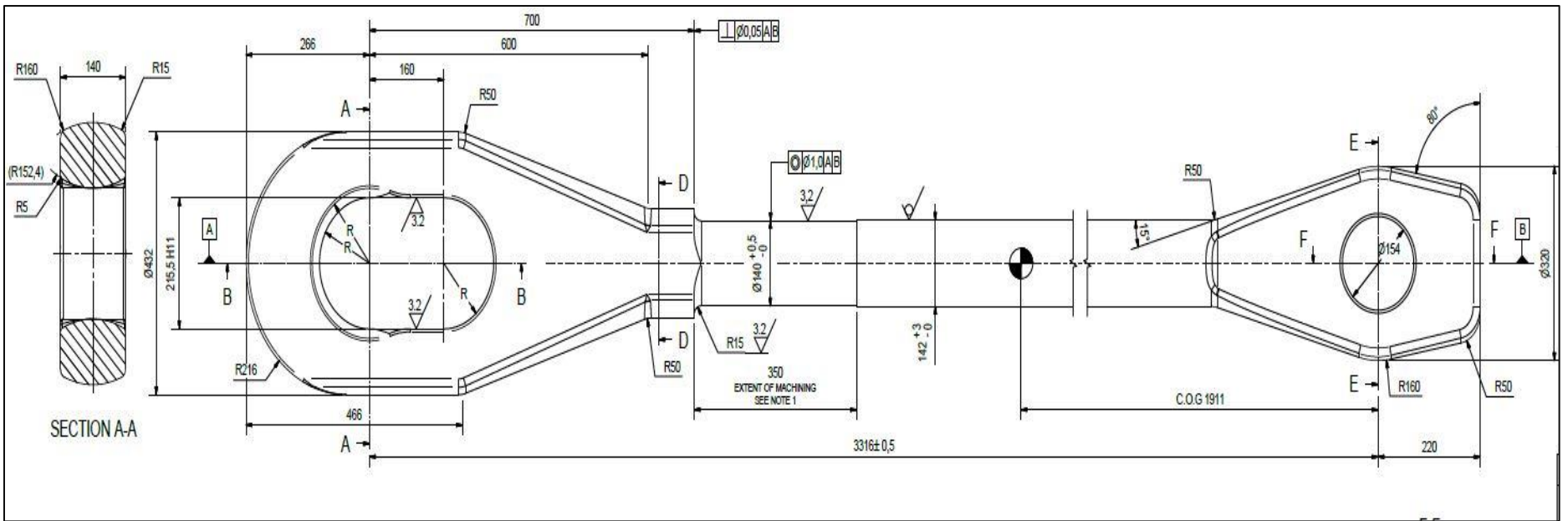


Figure 5-3: Detailed drawing of the cross-section of the Tie-rods

3. Top Drive Guiding/Support system (Dolly)

- Retractable Dolly

4. Control system

- Service loops
- PLC Cabinet
- Operator control panel
- Hydraulic control valve unit
- Derrick junction boxes
- Derrick hydraulic/pneumatic junction manifold

5. Auxiliary equipment:

- Handling equipment
- Special tools

5.2 Fatigue Damage Model Tests

It was mentioned in the previous chapter that upon acquiring torque signal and hook load data from the data vault, quality checking had to be carried out as recommended by DNV-RP-0497. This was done to ensure consistency and accuracy in the results that will be obtained from the fatigue calculations.

After processing the raw data to obtain error free torque signal and hook loads datasets the corresponding shear stress and stress in the x-direction were calculated as follows:

Shear stress (T_{xy}):

Given: radius of lower part of tie-rod = 0.077m as seen from Figure 5-3

$$\text{Polar moment of inertia} = \frac{\pi D^4}{32} = 5.52183E-05$$

The shear stress for each time stamp is then calculated using the relation for shear stress and torque signal where T_{xy} is computed as

$$T_{xy} = \frac{\text{Torque x radius}}{\text{Polar moment of inertia}}$$

Stress in the X-direction(σ_x):

Given: We have two tie-rods for the top drive with the following dimensions and parameters

$g = 9.80665 \text{ m/s}^2$, thickness = 0.11m, width = 0.32m diameter of hole = 0.154m as seen in Figure 5-3

σ_x is computed as follows:
$$\frac{\text{Hookloads X } g}{2 \text{ X thickness} * (\text{width} - \text{diameter of hole})}$$

The Von-Mises equivalent stress approach **Equation 2-3** was utilised to get the equivalent stresses for each of the shear stress and stress in the x-direction combinations. This equivalent stress approach was adopted because the axial and torsional loads obtained from the loading history of the top-drive were considered to be proportional and in the same phases. According to Juvinall, “In situations in which we can reasonably expect an overloaded part in service to fail in the same manner as the standard tensile test bar made of the same material, it is recommended that the maximum-distortion-energy theory be used to predict ductile yielding”. The material of construction of the top-drive is high strength steel which exhibits ductile behaviour, this is additional justification why Von-Mises equivalent stress approach was utilised. It should be noted that Von-Mises equivalent stress approach is an approximation and there are more robust models such as those proposed by Fatemi and Papadopoulos, however these more robust equivalent stress approaches are more complicated for implementation in engineering applications and due to time restrictions were not considered to be feasible for use in this research work. Due to these reasons Von- Mises equivalent stress approach was chosen as a reasonable approximation for the equivalent stresses.

After this was done the equivalent stress datasets were extracted from R and the WAFO rainflow counting toolbox in Python was used to count the complete cycles for the extracted equivalent stress histories.

WAFO (Wave Analysis for Fatigue and Oceanography) is a package in Python which can be used for rainflow cycle counting as well as other statistical analysis of waves or random load cycles. WAFO's rainflow counting toolbox was chosen as the tool for counting cycles because of the extensive research that has been put into this tool. This has made WAFO a good choice as a rainflow cycle counting tool. The processed rainflow cycle counts gotten using WAFO's rainflow counting toolbox had mean stresses, alternating stresses and the number of complete cycles for each equivalent stress in the load history.

It was seen from the post processed rainflow counts that there was a non-zero mean stress and to apply the selected fatigue damage models completely reversed cycles will be needed. Goodman's mean stress correction formula **Equation 2-18** was applied for each stress load level containing mean stresses and alternating stresses to obtain Goodman adjusted stresses. These Goodman adjusted stresses are equivalent fully reversed stresses that will give the same amount of damage as the inputted stress loads. The Goodman adjusted stresses were then read off the bi-linear S-N curve given in the F.E.M 1.001 standard in section 4.1.3.5, this S-N curve is shown below in Figure 5-4. This was done to obtain the number of cycles remaining until failure for each of the applied stresses. The S-N curve has a knee-point at 2,000,000 cycles with an endurance limit at 157 MPa, since it is a bi-linear S-N curve there are two slopes for this curve between the cycle ranges (8,000-2,000,000) and for cycles greater than 2,000,000 cycles. The cycle count range between 8,000 - 2,000,000 cycles is termed the region of limited endurance for stresses above or equal to the endurance limit. For cycle counts greater than 2,000,000 cycles this region is termed the region of the endurance limit. More details of this S-N curve are presented in [Appendix A](#).

The steps taken to prepare the load histories for analysis using the selected fatigue damage models have been shown so far. In the sections that follow it will be shown how the selected fatigue damage models were applied, evaluation will also be given on the selected models taken into account their ease of use.

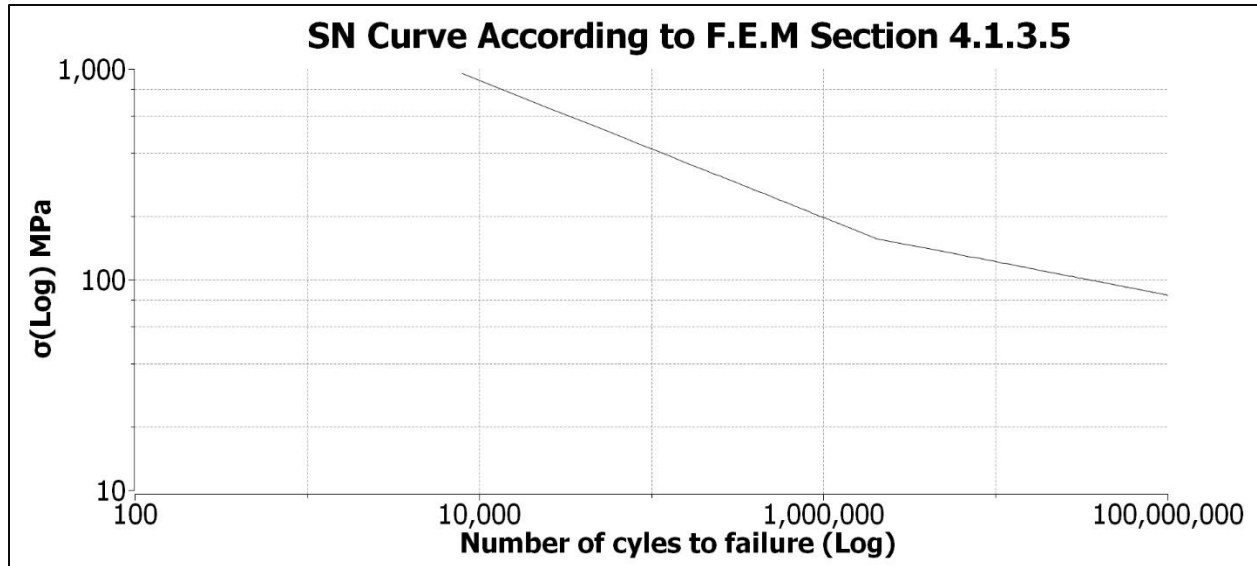


Figure 5-4: S-N curve according to F.E.M section 4.1.3.5 used in this thesis (F.E.M, 1998)

5.2 Palmgren Miner's Linear Damage Model

5.2.1 Parameter Calculation and Model Evaluation

Palmgren-Miner's linear damage model was applied by using the formula's shown below to compute damage and the number of cycles remaining until failure.

$$D = \sum_{i=1}^k \frac{n_i}{N_i}$$

$$n_r = N_m \left(1 - \sum_{i=1}^k \frac{n_i}{N_i} \right)$$

n_i was obtained from the processed rainflow cycle counts gotten from the WAFO toolbox, the Goodman adjusted stresses were used with the slopes of the Wohler curves to obtain N_i (the number of cycles until failure) these two parameters were then used to compute damage.

Palmgren-Miner's damage model is an easy model to use due to its assumption of linear damage, the drawbacks of this model is that it neglects the load sequences. With the aid of probabilistic methods such as Weibull this load sequence effects can be mitigated resulting in acceptable fatigue life predictions.

5.3 Manson's Double Linear Damage Model

5.3.1 Parameter Calculation and Model Evaluation

Manson's double linear damage rule was applied by using the formula's below to obtain Φ and Z . These two parameters were then used with Equation 3-3 and 3-4 to obtain the number of cycles until failure in the two fatigue phases. Damage was then calculated for each phase using the ratio of the number of rainflow counted cycles to the number of cycles until failure for phase I and II.

$$\Phi = \frac{1}{\ln\left(\frac{N_{1f}}{N_{2f}}\right)} \ln \left[\frac{\ln\left(0.35\left(\frac{N_{1f}}{N_{2f}}\right)^{0.25}\right)}{\ln\left(1-0.65\left(\frac{N_{1f}}{N_{2f}}\right)^{0.25}\right)} \right]$$

$$Z = \frac{\ln\left(0.35\left(\frac{N_{1f}}{N_{2f}}\right)^{0.25}\right)}{N_{1,f}^{\Phi}}$$

Manson's double linear damage model is also quite easy to use since it is similar to applying Miner's rule in two fatigue phases. This model is more accurate in taking into account load sequences since it takes the co-ordinates from the knee-point of the S-N curve when determining the number of cycles until failure.

5.4 Subramanyan's Non-linear Damage Model

5.4.1 Parameter Calculation and Model Evaluation

Subramanyan's non-linear damage model was applied by using the formula's shown below to obtain the equivalent number of cycles until failure for each stress load level. These formulas are based on the revised work by Srivatsavan and Subramanyan to take into account the reduction in the fatigue limit of a material.

$$N_{21} = \left[1 - \left(\frac{n_1}{N_1} \right) \right]^{\frac{S_2 - S_{e1}}{S_1 - S_{e1}}}$$

$$S_{e2} = \left[S_{e1} \left(\frac{S_1}{S_{e1}} \right) \right]^{-C_1\beta}$$

Among the selected models that were reviewed Subramanyan's model required a fair bit of effort to apply. This model is slightly non-conservative, but its usage is acceptable although some caution must be taken when applying it in cases where the stress loads are close to the endurance limit of the material.

5.5 Modelling Probability of Failure of HPS-03 1000T Tie Rods

This probabilistic model is based on the existing fatigue calculation of the tie rod according to F.E.M rules. Some modifications are done according to the actual behaviour of the material (expected yielding on first occurrence of high load above yield point).

There are several methods to compute numerical prediction result in a probabilistic approach, here a simple distribution model computation is used, if material properties are lognormal-distributed, and their natural logarithms are normal-distributed. This prevents negative strength occurrence and is the most recognized strength distribution model, besides Weibull-distribution.

All variables are assumed to be independent in the way they are used (the explicit dependency between ultimate tensile strength and fatigue limit cancels out in the model).

Lognormal-distributions give exact results in expressions where the various variables are multiplied, divided and raised to powers where the exponent is deterministic, just as normal-distributions give exact results in expressions where the various variables are added, subtracted and multiplied by a deterministic parameter. Where exponents themselves are stochastic, approximative expressions are used to find the resulting distribution parameters. This is acceptable when the coefficients of variation are small.

5.5.1 Fatigue resistance modelling

The model is based on the linear section of the S-N curve. This is expressed as:

$$S^m \cdot N = C \qquad \text{Eqn. 5-1}$$

Taking the logarithm on both sides:

$$m \cdot \log(S) + \log(N) = \log(C) \quad \text{Eqn. 5-2}$$

The first known point is the nominal ultimate tensile strength f_u at a given number of cycles N_1 :

$$m \cdot \log(f_u) + \log(N_1) = \log(C) \quad \text{Eqn. 5-3}$$

The second known point is the fatigue limit σ_D (including all strength reduction factors) at a given number of cycles N_2 :

$$m \cdot \log(\sigma_D) + \log(N_2) = \log(C) \quad \text{Eqn. 5-4}$$

Equating the two expressions:

$$m \cdot \log(f_u) + \log(N_1) = m \cdot \log(\sigma_D) + \log(N_2)$$

$$m = \frac{\log(N_2) - \log(N_1)}{\log(f_u) - \log(\sigma_D)} \quad \text{Eqn. 5-5}$$

The fatigue limit can be expressed as a fraction η of the ultimate tensile strength:

$$\sigma_D = \eta \cdot f_u \rightarrow \log(\sigma_D) = \log(\eta) + \log(f_u) = 0.4343 \cdot \ln(\eta) + \log(f_u) \quad \text{Eqn. 5-6}$$

$$m = \frac{\log(N_2) - \log(N_1)}{\log(f_u) - 0.4343 \cdot \ln(\eta) - \log(f_u)} = \frac{\log(N_1) - \log(N_2)}{0.4343 \cdot \ln(\eta)} \quad \text{Eqn. 5-7}$$

$$\frac{1}{m} = c \cdot \ln(\eta) ; c = \frac{0.4343}{\log(N_2) - \log(N_1)} = -0.181 \quad \text{Eqn. 5-8}$$

For completeness, the S-N curve constant is found as:

$$C = N_1 \cdot f_u^m \quad \text{Eqn. 5-9}$$

5.5.2 Load modelling

The equivalent stress of the load spectrum is:

$$S = \sqrt[m]{k} \cdot S_{\max} = x \cdot S_{\max} \rightarrow Sm = x^m \cdot S_{\max}^m = k \cdot S_{\max}^m \quad \text{Eqn. 5-10}$$

The equivalent stress is the stress level that will give the same fatigue damage as the entire load spectrum, if all n applied stress cycles of the spectrum is equal:

$$\sum_{i=1}^n S_i^m = n \cdot S^m = n \cdot k \cdot S_{\max}^m \quad \text{Eqn. 5-11}$$

The number of stress cycles until fatigue failure at the equivalent stress level is:

$$N = \frac{C}{S^m} = \frac{N_1 \cdot f_u^m}{S^m} = \frac{N_1 \cdot f_u^m}{k \cdot S_{\max}^m} = \frac{N_1 \cdot f_u^m}{k} \cdot \left(\frac{f_u}{S_{\max}} \right)^m \quad \text{Eqn. 5-12}$$

The cumulative fatigue damage is:

$$D = \sum_{i=1}^n \frac{1}{N_i} = \frac{n}{N} = \frac{n \cdot k}{N_1} \cdot \left(\frac{S_{\max}}{f_u} \right)^m = \frac{n \cdot k}{N_1} \cdot Y^m = \frac{n \cdot k}{N_1} \cdot g \quad \text{Eqn. 5-13}$$

$$Y = \frac{S_{\max}}{f_u} \quad g = Y^m \quad \ln(g) = m \cdot \ln(Y)$$

With an allowable limit of the fatigue damage given as Δ , the fatigue safety factor is:

$$Z = \frac{\Delta}{D}$$

The criterion for predicted fatigue fracture is:

$$Z \leq 1$$

5.5.3 Variables and parameters data:

Nominal ultimate tensile strength f_u is adjusted according to actual material certificate values R_m :

$$f_u = 950 \text{ MPa} \quad f_u = R_m \quad \mu f_u = \frac{1}{0.91} \cdot f_u = 1044 \text{ MPa} \quad V f_u = 0.063 \quad \sigma f_u = V f_u \cdot \mu f_u = 66 \text{ MPa}$$

$$f_u \sim \text{LN}(\nu f_u, \zeta f_u) \quad \nu f_u = \ln\left(\frac{\mu f_u}{\sqrt{1 + V f_u^2}}\right) = 6.947 \quad \zeta f_u = \sqrt{\ln(1 + V f_u^2)} = 0.063$$

First point of S-N curve according to FEM (considered deterministic):

$$N_1 = 8\ 000 \text{ cycles}$$

Second point of S-N curve according to FEM (considered deterministic):

$$N_2 = 2\ 000\ 000 \text{ cycles}$$

Fatigue limit ratio:

$$\eta = \frac{\sigma_D}{f_u} = 0.165 \quad \mu \eta = 0.165 \quad V \eta = 0.063 \quad \sigma \eta = V \eta \cdot \mu \eta = 0.010$$

$$\boldsymbol{\eta} \sim \text{LN}(\nu_{\eta}, \zeta_{\eta}) \quad \nu_{\eta} = \ln\left(\frac{\mu_{\eta}}{\sqrt{1+V_{\eta}^2}}\right) = -1.806 \quad \zeta_{\eta} = \sqrt{\ln(1+V_{\eta}^2)} = 0.063$$

$$\ln(\boldsymbol{\eta}) \sim \text{N}(\nu_{\eta}, \zeta_{\eta})$$

Slope of S-N curve:

$$\frac{1}{m} = c \cdot \ln(\boldsymbol{\eta}) \quad \frac{1}{m} \sim \text{N}(c \cdot \nu_{\eta}, |c| \cdot \zeta_{\eta}) \quad |c| \cdot \zeta_{\eta} = 0.327 \quad c \cdot \zeta_{\eta} = 0.011 \quad V_{1/m} = 0.035$$

$$\boldsymbol{m} \sim \text{N}(\mu_m, \sigma_m) \quad \mu_m \approx \frac{1}{c \cdot \nu_{\eta}} = 3.06 \quad \sigma_m \approx \frac{|c| \cdot \zeta_{\eta}}{c^2 \cdot \nu_{\eta}^2} = 0.107 \text{ for } V_m = V_{1/m} = 0.035 \ll 1$$

Stress at maximum load rating (it is for simplicity assumed that the very local peak stress at load rating is limited to the yield stress and creates a compressive residual stress after first occurrence:

$$f_y = 735 \text{ MPa} \quad S_{\max} = f_y = R_{p0.2}$$

$$\mu_{S_{\max}} = \frac{1}{0.78} \cdot f_y = 936 \text{ MPa} \quad V_{S_{\max}} = 0.09 \quad \sigma_{S_{\max}} = V_{S_{\max}} \cdot \mu_{S_{\max}} = 84 \text{ MPa}$$

$$S_{\max} \sim \text{LN}(\nu_{S_{\max}}, \zeta_{S_{\max}}) \quad \nu_{S_{\max}} = \ln\left(\frac{\mu_{S_{\max}}}{\sqrt{1+V_{S_{\max}}^2}}\right) = 6.834$$

$$\zeta_{S_{\max}} = \ln\left(\sqrt{1+V_{S_{\max}}^2}\right) = 0.090$$

Load factor:

$$Y = \frac{S_{\max}}{f_u} \quad \boldsymbol{Y} \sim \text{LN}(\nu_Y, \zeta_Y) \quad \nu_Y = \nu_{S_{\max}} - \nu_{f_u} = -0.113$$

$$\zeta Y = \zeta_{\text{smax}}^2 + f_u^2 = 0.110$$

$$Y \sim \text{LN}(v_Y, \zeta Y) \rightarrow \ln(Y) \sim N(v_Y, \zeta Y)$$

$$\ln(g) = m \cdot \ln(Y)$$

$$\mu \ln(g) = \mu_m \cdot \mu \ln(Y) = \mu_m \cdot v_Y = -0.345$$

$$\sigma \ln(g) \approx \sqrt{\mu_m^2 \cdot \sigma_{\ln Y}^2 + \mu_{\ln Y}^2 \cdot \sigma_m^2 + \sigma_m^2 \cdot \sigma_{\ln Y}^2} = \sqrt{\mu_m^2 \cdot \zeta_Y^2 + v_Y^2 \cdot \sigma_m^2 + \sigma_m^2 \cdot \zeta_Y^2} = 0.336$$

Eqn. 5- 14

$$g \sim \text{LN}(v_g, \zeta_g) \quad v_g = \mu \ln(g) \quad \zeta_g = \sigma \ln(g)$$

Load spectrum factor computed from $m=3.07$ applied to the load spectrum is deterministic:

$$k=0.0125$$

Total number of load cycles in the spectrum is deterministic:

$$n_{\text{tot}}=545\ 000$$

Let i be the number of equal parts that the load spectrum is divided into, where there is no inspection during each part. Then the relevant number of load cycles are:

$$n = \frac{n_{\text{tot}}}{i} = \frac{545\ 000}{i}$$

Cumulative fatigue damage index:

$$D = \frac{n \cdot k}{N_1} \cdot g$$

$$D \sim \text{LN}(\nu_D, \zeta_D) \quad \nu_D = \ln(n) - \ln(i) + \ln(k) + \nu_g - \ln(N_1) = -0.506 - \ln(i) \quad \zeta_D = \zeta_g = 0.336$$

Partial fatigue damage limit (NB: from tests there is a widespread in this variable):

$$\Delta = 1 \quad \mu_\Delta = \Delta = 1 \quad \sigma_\Delta = 0.325$$

$$\Delta \sim \text{LN}(\nu_\Delta, \zeta_\Delta) \quad N\delta = \ln\left(\frac{\mu_\Delta}{\sqrt{1 + \left(\frac{\sigma_\Delta}{\mu_\Delta}\right)^2}}\right) = -0.100 \quad \zeta_\Delta = \sqrt{\ln\left(1 + \left(\frac{\sigma_\Delta}{\mu_\Delta}\right)^2\right)} = 0.317$$

Safety factor against fatigue fracture:

$$Z = \frac{\Delta}{D}$$

$$Z \sim \text{LN}(\nu_Z, \zeta_Z) \quad \nu_Z = \nu_D - \nu_\Delta = -0.406 - \ln(i)$$

$$\zeta_Z = \sqrt{\zeta_D^2 + \zeta_\Delta^2} = 0.462$$

The probability of fatigue failure within the inspection period, given equal usage in each period, is:

$$p_f = P(Z \leq 1) = \Phi\left(\frac{\ln(1) - N\nu_Z}{\zeta_Z}\right) = \Phi\left(-\frac{N\nu_Z}{\zeta_Z}\right)$$

On the assumption that the design load spectrum covers exactly 20 years of service, the probabilities of developing fatigue fracture for various inspection intervals are

Inspection interval:	Predicted probability of fatigue failure:
1 years	$9 \cdot 10^{-14} \cong 0$
2 years	$2 \cdot 10^{-9}$
4 years	$6 \cdot 10^{-6}$
5 years	$5 \cdot 10^{-5}$
10 years	$9 \cdot 10^{-3}$
20 years	0.19

Table 5-1: Probability of fatigue failure for the inspection intervals

6 Results and Discussion

This chapter will focus on the results obtained from the FEM analysis, data diagnosis and the fatigue damage model results. Discussions of this results will also be made in tandem with the presentation of the results to give better clarity on the results.

6.1 Finite Element Method Results

6.1.1 General

This section describes the ANSYS Workbench analysis of the structure of the tie rod for the HPS-03-1000T top-drive. The geometry of the structure is shown in **Figure 5-3** in Chapter 5

6.1.2 Model

6.1.2.1 Geometry

The geometry is taken from the **Figure 5-3**. Only a quarter of the tie rod geometry is used in the model due to symmetry. The bounding box for the model measures 216 mm by 3802 mm by 70 mm along the global x, y and z axes. The model weighs a total of 163 kg.

6.1.2.2 Axis co-ordinate system

The axis co-ordinate system has x in horizontal direction parallel to the pin hole axis, y upwards and z horizontally perpendicular to x-direction.

6.1.2.3 Material

The tie rod material is defined as structural steel with the following properties:

- Modulus of elasticity 2.0E5 N/mm²
- Poisson's ratio 0.3
- Mass density 7.85E-6 kg/mm³

6.1.2.4 Bodies

The model contains one body, which is volume meshed.

6.1.2.5 Contact

No contact is defined in the model.

6.1.2.6 Mesh

The mesh is given an overall element sizing of 30 mm. The model has a total of 11,118 nodes and 5,996 elements.

6.1.2.7 Boundary conditions

The following boundary conditions are defined:

- The cut face at the plane of mirror symmetry is held by frictionless support.
- One vertex at the top of the upper hole is fixed for translation in y-direction (given displacement).

6.1.2.8 Loads

The following loads are defined:

- The upper hole is loaded with 1179 kN in positive y-direction (bearing load).
- The lower hole is loaded with 1179 kN in negative y-direction (bearing load).

6.1.3 Structural Results

6.1.3.1 Reaction forces

The analysis gives the following reaction forces:

- 0 kN in x, 1.5 kN in y and 0 kN in z

The reaction force in y-direction is a result of an unbalance between the bearing loads.

6.1.3.2 Deformations

The analysis shows a maximum total deformation of 5.53 mm.

6.1.3.3 Stresses

The analysis shows a maximum Von-Mises equivalent stress of 900 MPa, maximum utilisation factor from detail calculation of 0.94 and maximum utilisation for fatigue of 0.40.

The tie rod has yield strength of 735 MPa. The applicable safety factor is 2.25 according to API 8C. Allowable stress for the tie rod is then 327 MPa. The areas with stresses above allowable are limited to local stress concentrations. The maximum stress is below ultimate strength, and the areas with stress above yield strength are extremely local. Hence the stress level is acceptable.

6.1.4 ANSYS FEM Plots

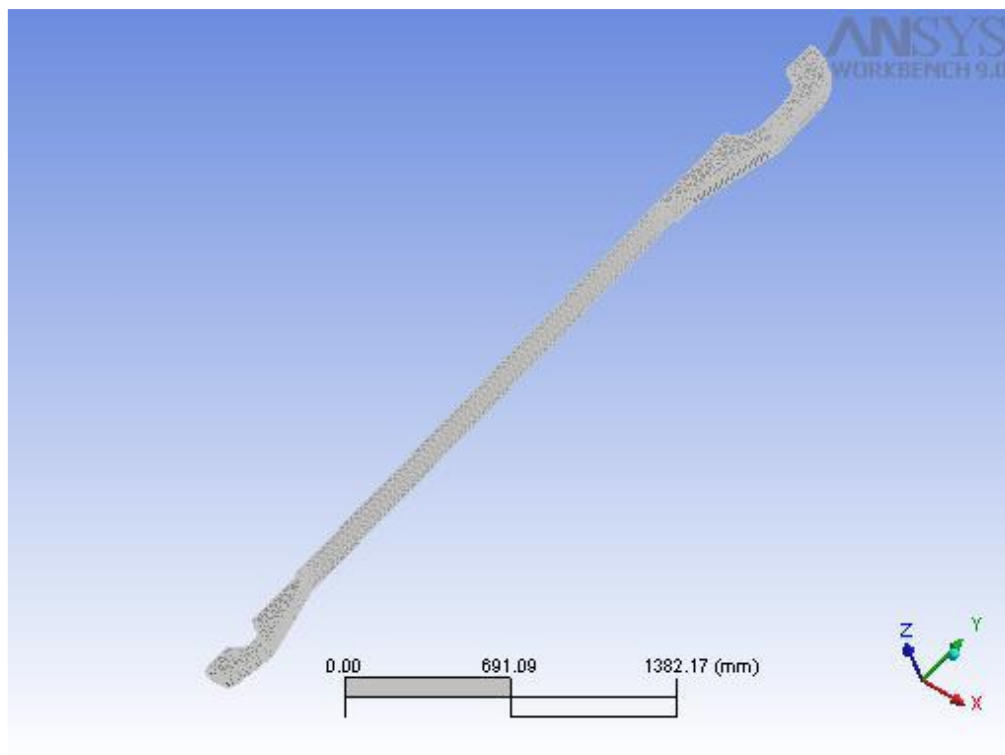


Figure 6-1: Mesh Geometry

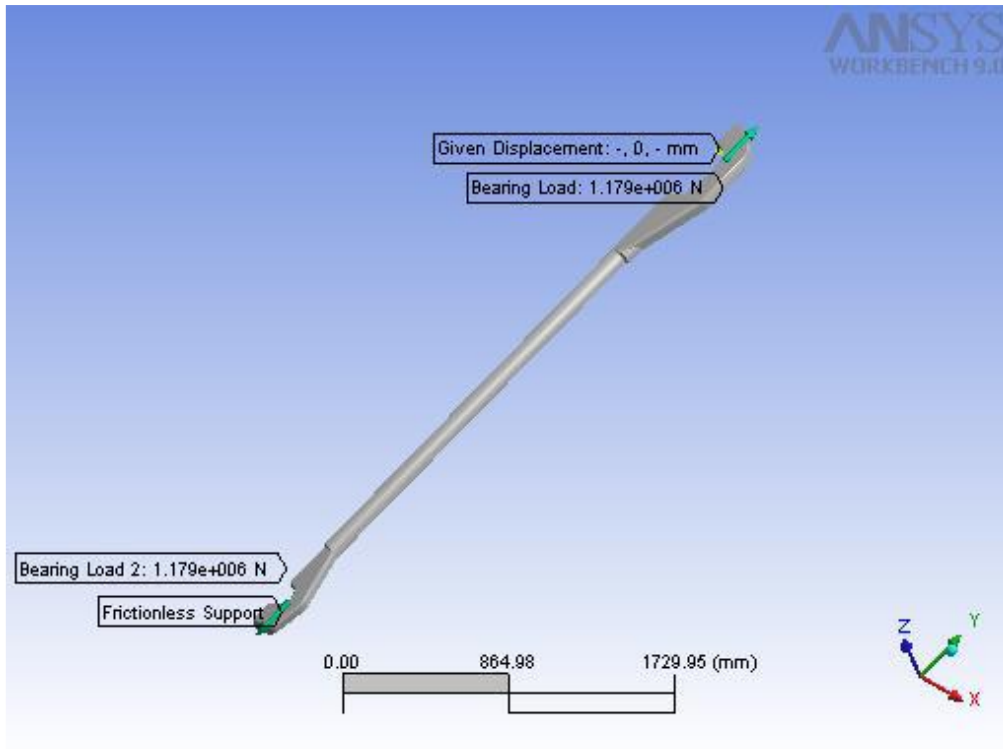


Figure 6-2: Environment Geometry

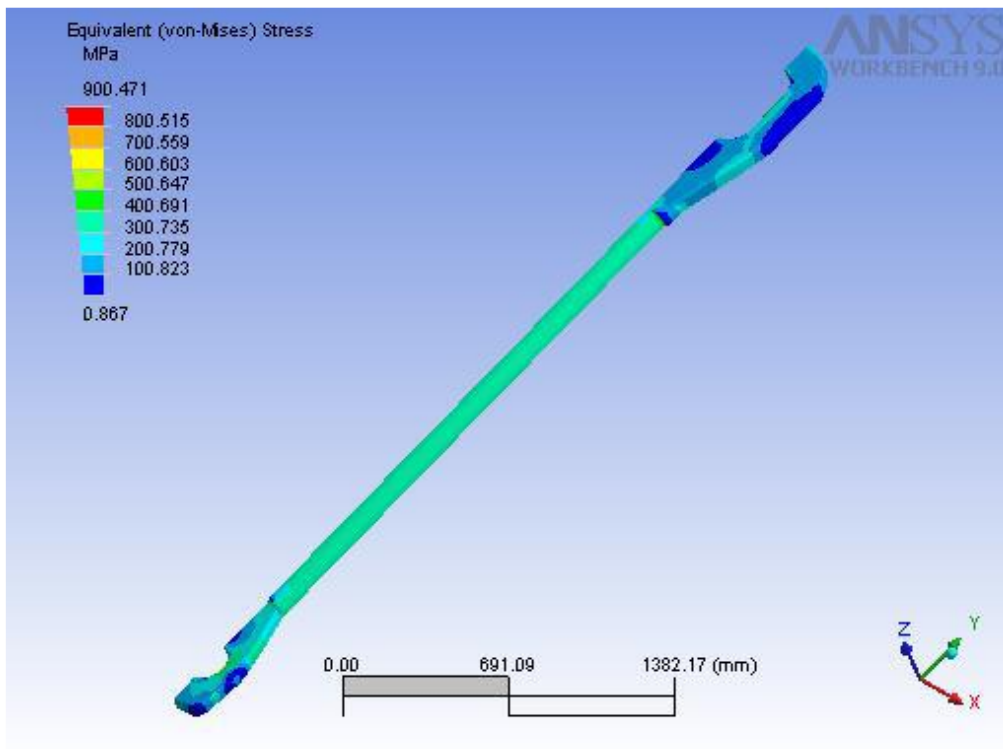


Figure 6-3: Equivalent Stress Contours(a)

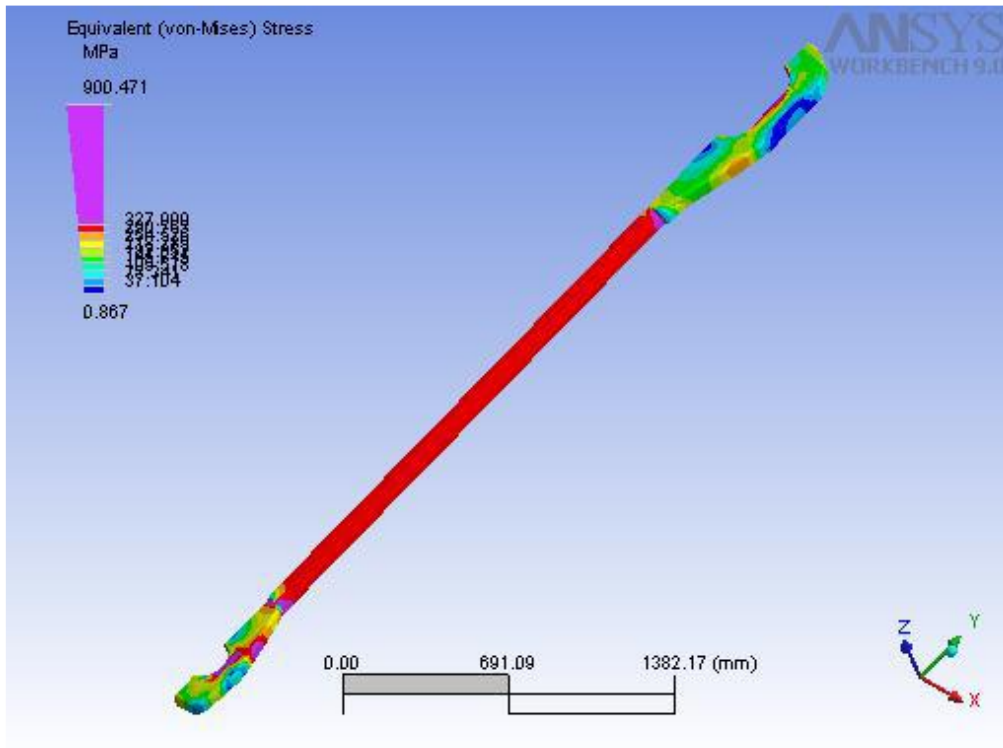


Figure 6-4: Equivalent Stress Contours(b)

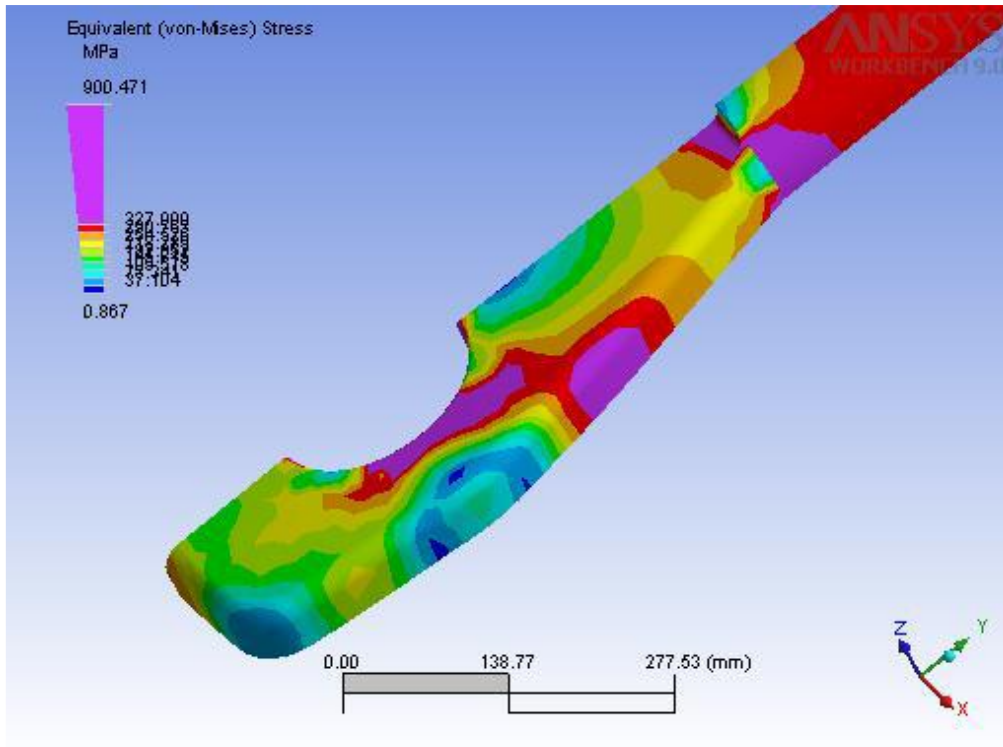


Figure 6-5: Equivalent Stress Contours (c)

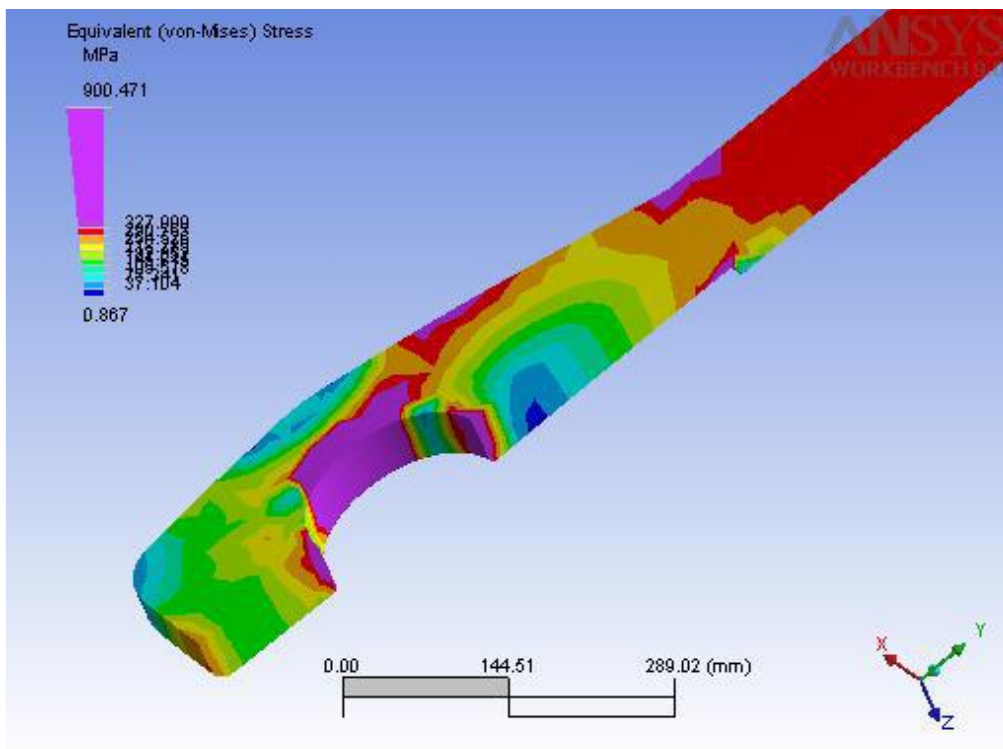


Figure 6-6: Equivalent Stress Contours (d)

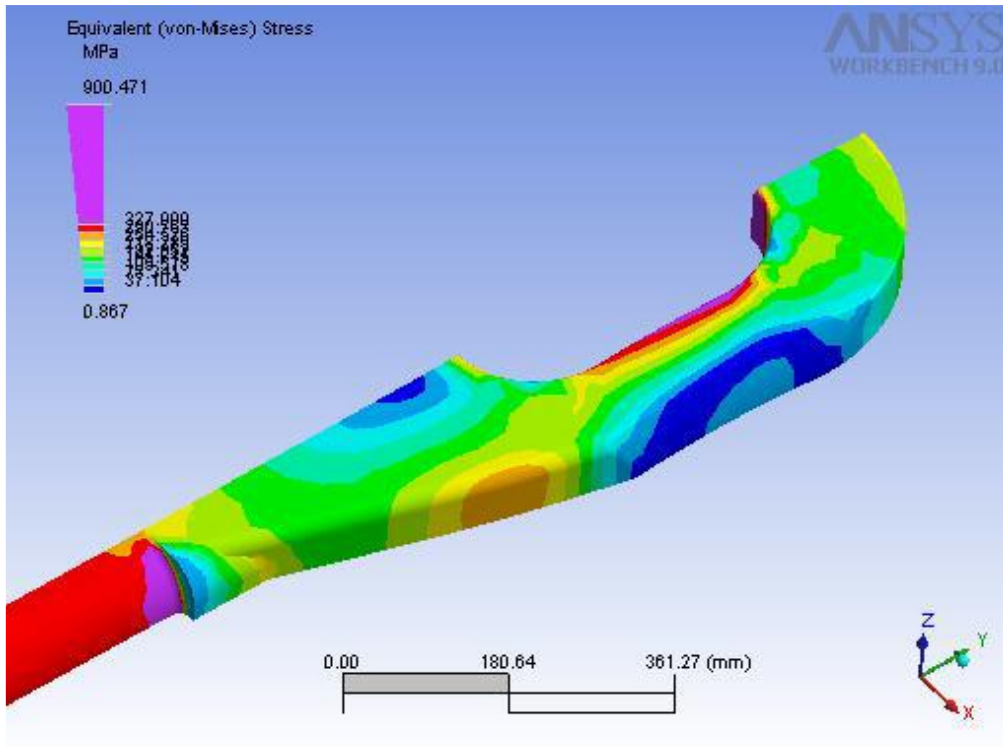


Figure 6-7: Equivalent Stress Contours (d)

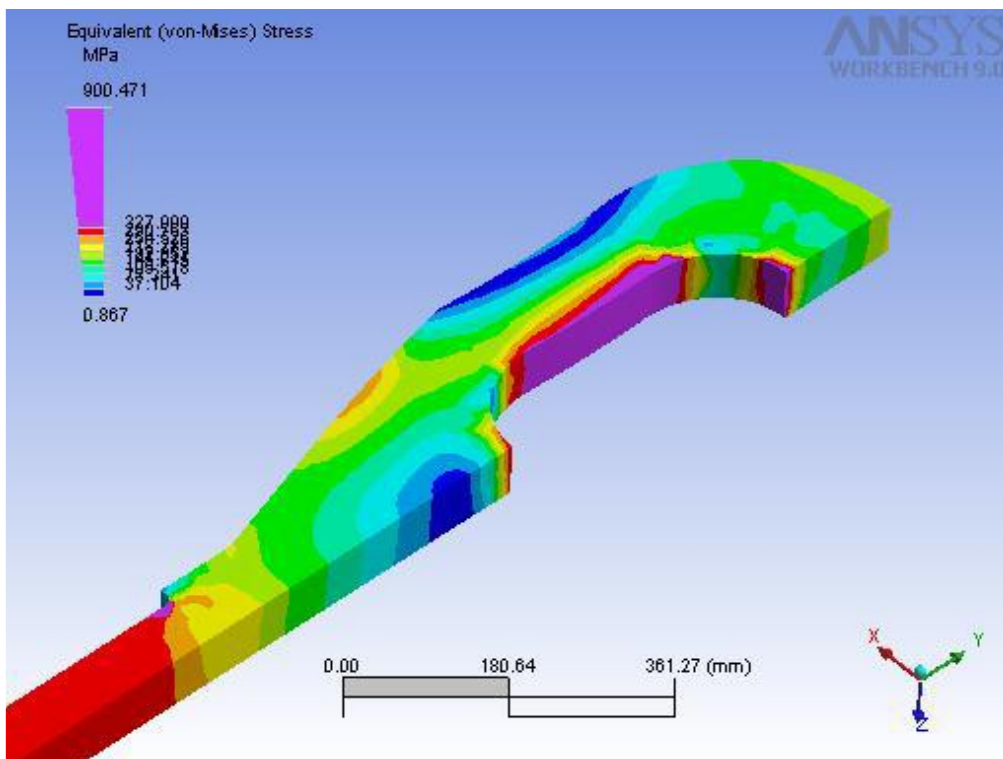


Figure 6-8: Equivalent Stress Contours (e)

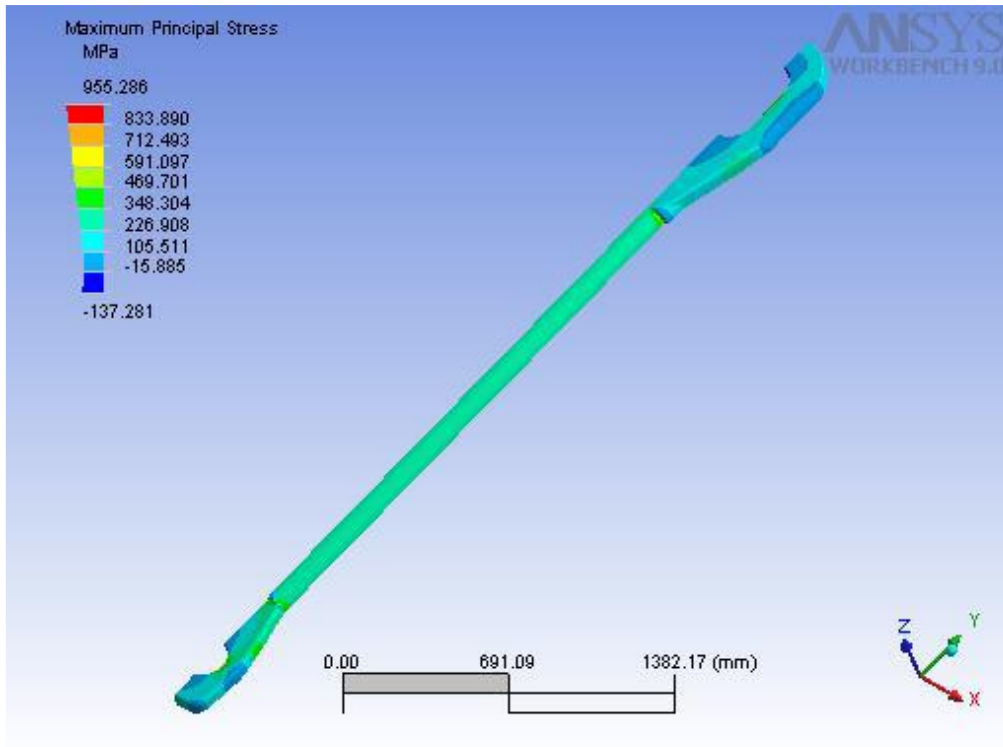


Figure 6-9: Maximum Principal Stress Contours

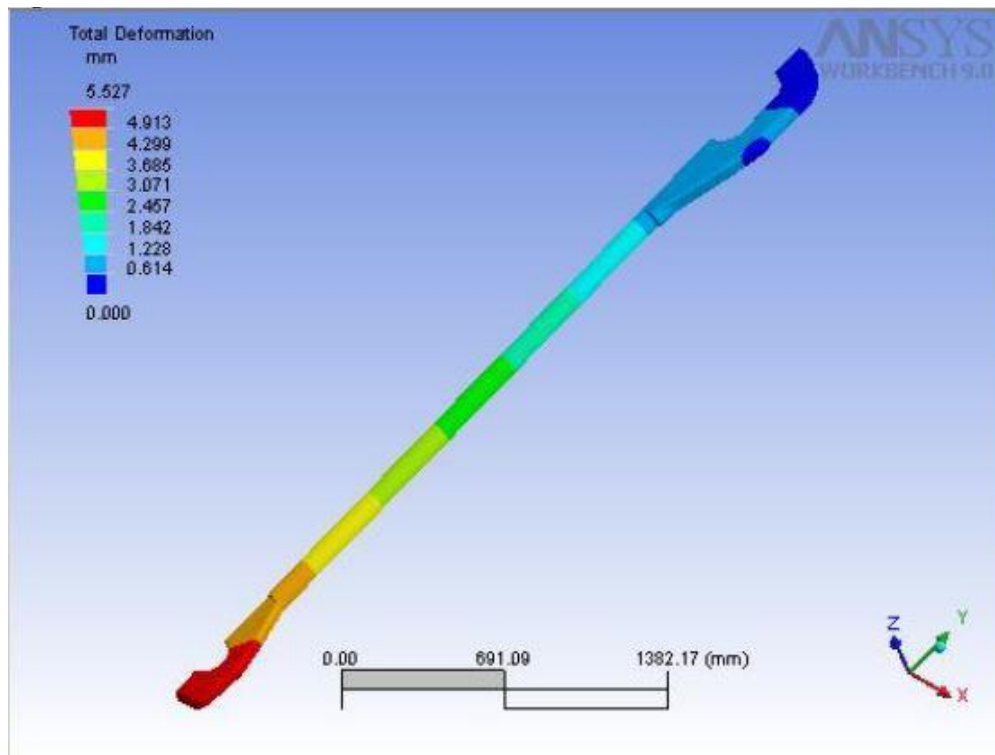


Figure 6-10 : Total Deformation Contours

6.2 Data Diagnosis Results

Rig 1: Main Well

Variable	Sigma_eq (January-July 2014)	Sigma_eq (July-December 2014)
n	9510667	13657275
na	0	0
mean	25.93	65.12826
sd	22.7	49.37109
se_mean	0.01	0.01336
IQR	1	87
skewness	4.21	0.632875
kurtosis	18.36	-0.85427
p10	19	20
p90	32	140
p95	52	151
p99	149	181
p100	287	287

Table 6-1: Data Description for Rig 1 Main Well Datasets between January-December 2014

Table 6-1 above contains the results of a data quality check that was carried out on signals from Rig 1 Main Well between January 2014 – December 2014. The two datasets above have different number of entries, so the skewness, standard error in the mean and kurtosis properties will be good metrics in comparing these datasets. The procedure adopted here was implemented for quality checking all the datasets obtained from the three (3) rigs which were analysed in this research work. After carrying out data transformations on the datasets to ensure syntactic quality was met, the null entries were eliminated, hence why the NA count is zero in both datasets in Table 6-1.

For the dataset for Rig 1 Main Well between January-July 2014, the mean of the dataset (25.93 MPa) is not so far from the standard deviation (22.7 MPa) and median of the data set (20 MPa). The histogram plot in Figure 6-11 shows that this dataset is skewed to the right since the mass of

the values of this dataset are congregated on the left side of the histogram and the tail of the histogram is on the right side. Since this distribution is skewed and not normally distributed, the median (20 MPa) is a better measure of the centrality of the data. With a kurtosis of 18.36 this implies that the data is heavy tailed and possesses a lot of outliers which was confirmed by the boxplots in the outlier diagnosis shown in Figure 6-11. Meanwhile, the dataset for Rig 1 Main Well between July-December 2014 has a mean of (65.13 MPa) which deviates significantly from the standard deviation of (49.37 MPa) and the median of (50 MPa). The histogram plot in Figure 6-12 shows that this dataset is also skewed to the right, although it has a lower skewness than the dataset for the first half of 2014. The kurtosis for the dataset from July-December 2014 is also considerably lower than the kurtosis obtained in the dataset for the first half of 2014. This signifies that there are fewer outliers in the dataset for July-December 2014, which is confirmed by the results obtained from the outlier test in Figure 6-12 where the outliers in the dataset from July-December 2014 (419 outliers) is significantly lower than those in the dataset for the first half of 2014 (2,378, 441 outliers)

The standard error of the mean obtained in the dataset for the first half of 2014 is (0.01 MPa) and this is quite close to the standard error in the mean obtained in the dataset for the second half of 2014 (0.01336 MPa). This implies that there is a 95 percent chance that the error obtained in estimates of the mean (25.93 MPa) for the dataset from January -July 2014 will be within two times the standard error (0.02 MPa) and there is certainty it will be within three times the standard error (0.03 MPa). Additionally, the interquartile range in this dataset (January -July 2014) is (1 MPa) therefore most data in this dataset lie at 1 MPa which a low stress level.

Furthermore, the p estimates shown in Table 6-1 refer to the percentiles of the data and by what extent data can exceed the given percentile, where p10 of (19 MPa) refers to 10 percent of the data exceeding 19 (MPa).

Lastly, the outlier diagnosis results shown in figure 6-11 details the extent to which outliers are present in this dataset. As mentioned in the chapter on data quality checking of this thesis, outliers were only eliminated from the dataset in scenarios where the values did not meet requirements for semantic quality. This can be explained with two scenarios, one where torque speeds exceed the top-drive specifications and another where there is a sudden instantaneous torque speed increase which violates standard operating conditions during drilling. In the first scenario if the torque

signal reading was above the specification for the top-drive this signal will be filtered out as noise from the dataset. Also, in the second scenario if the torque speed suddenly spiked from let's say 20 to 200 this reading will also be filtered out because it will violate physical operating condition when drilling. This sudden torque speed increase will result in there been a huge vibration that will cause significant movement of the platform. The Drilling engineers involved with these rigs were consulted prior to filtering out those signals that do not meet semantic quality to ensure the right assumptions were being made.

Additional results from the data quality checks and outlier diagnosis can be seen in [Appendix C](#) of this thesis.

Rig 1: Main Well

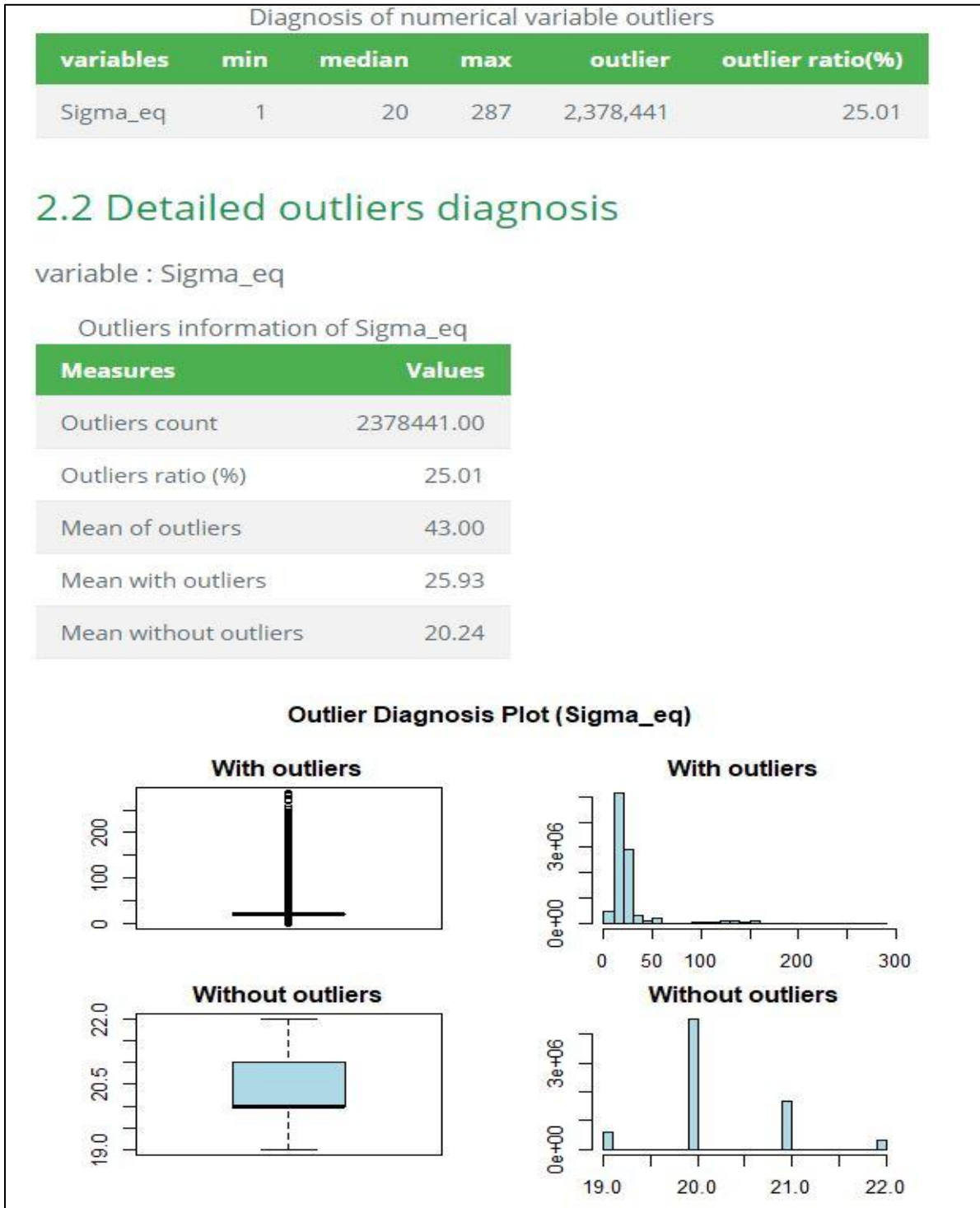


Figure 6-11: Outlier Diagnosis Results for Rig 1 Main Well Datasets from January -July 2014

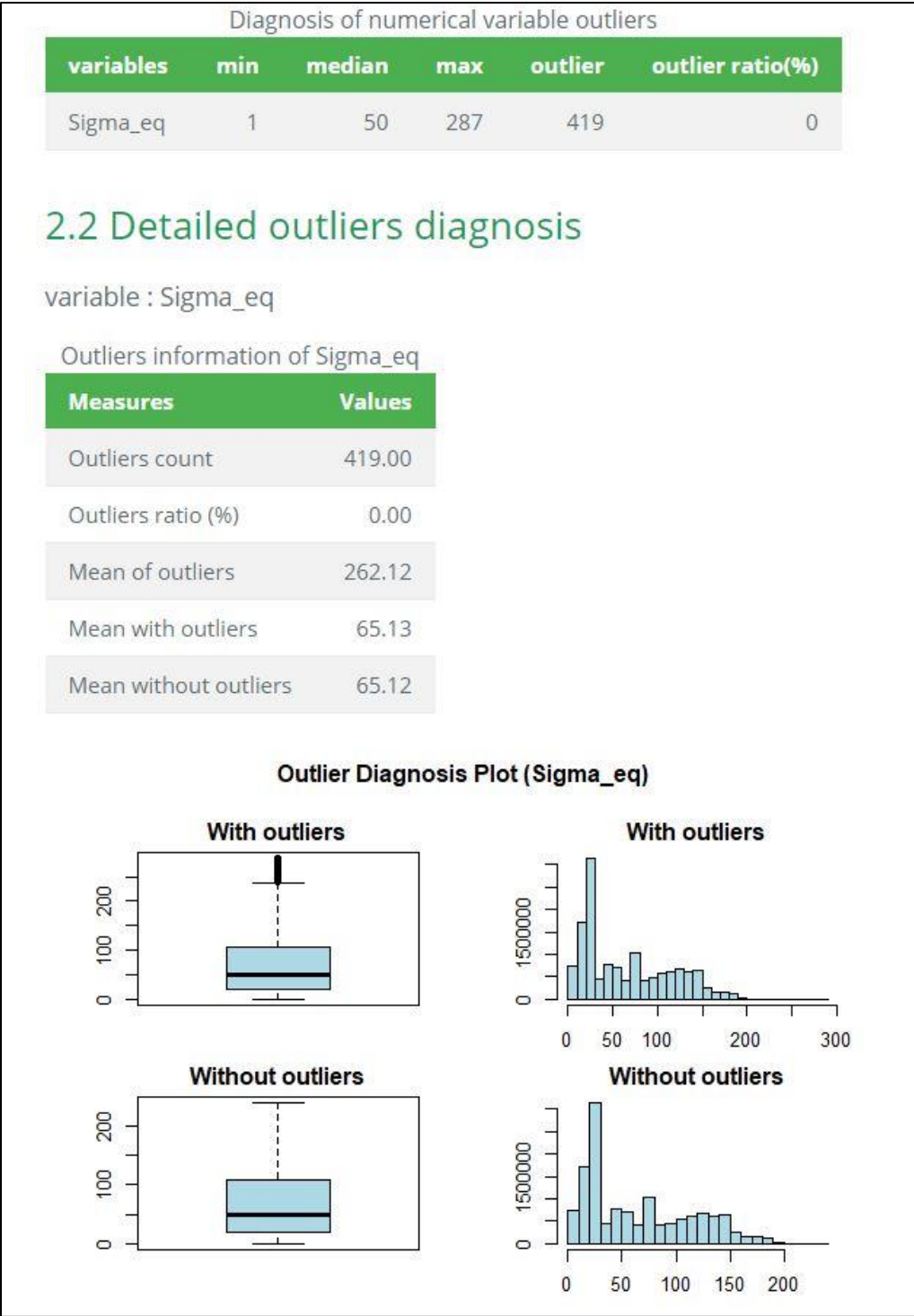


Figure 6-12: Outlier Diagnosis Results for Rig 1 Main Well Datasets from July - December 2014

6.3 Comparison Results for Miner's linear damage rule, Manson's double linear damage rule and Subramanyan's non-linear damage rule models

This section of the thesis contains the results obtained from using Miner's linear damage rule, Manson's double linear damage rule and Subramanyan's non-linear damage rule. The comparison of results obtained from the various fatigue damage models will focus on two (2) key areas, damage results, and number of loading blocks until failure results. Here, emphasis will be placed on how the fatigue damage models compare to each other on the Main well and Auxiliary well. This discussion will cover both conservative and non-conservative fatigue damage and number of loading blocks until failure estimates. Where conservative estimates take account of undamaging stresses (below the endurance limit and not having a high enough cycle count to cause damage) and non-conservative estimates filters out stresses that are undamaging. The reason for this is that conservative estimates are used in-house at NOV when carrying out fatigue analysis, this discussion will show the variations in damage results and number of loading blocks until failure from these approaches.

It was mentioned earlier that the top-drive on the Main well was used for more challenging operations that required additional components to be mounted on the top-drive compared to the top-drive on the auxiliary well which required less components and was used for simpler operations. Another key difference is the top-drive for the Main well was used for more operations than the top-drive on the Auxiliary well. Summary results will be presented from the three (3) Rigs that were analyzed for the year 2014 for both the top-drives used on the Main Well and the Auxiliary well. More comprehensive results for 2015 and 2016 for the top-drives used on the Main Well and Auxiliary Well for the three rigs can be seen in [Appendix-F](#) of this thesis.

6.3.1 Comparison of Fatigue Damage Results

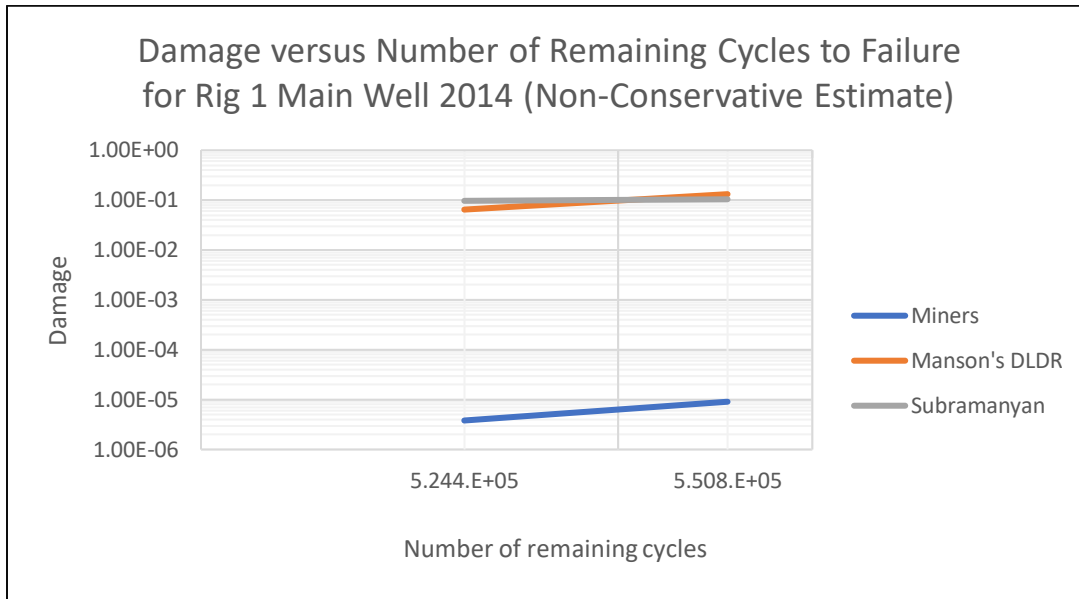


Figure 6-13: Non-conservative estimates of damage versus the number of remaining cycles until failure from the selected fatigue damage models for Rig 1 Main Well in 2014

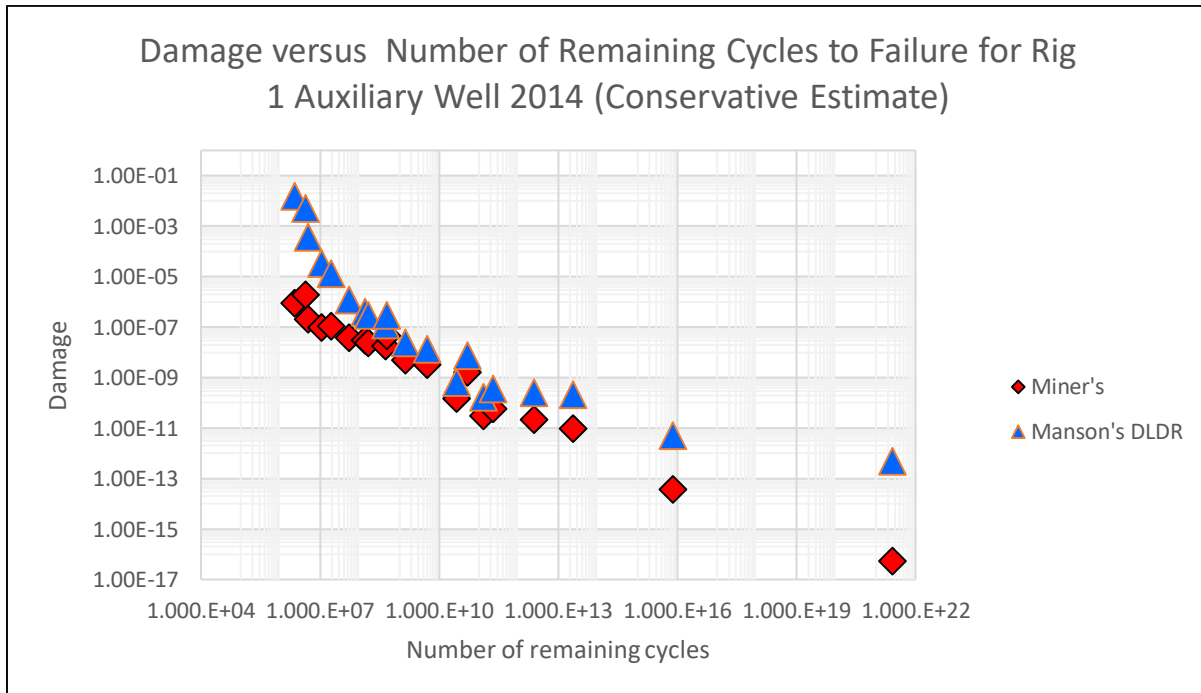


Figure 6-14: Conservative estimates of damage versus the number of remaining cycles until failure from the selected fatigue damage models for Rig 1 Auxiliary Well in 2014

In a non-conservative fatigue damage estimate the results from top-drive on the Main well of Rig 1 shows slight increases in damage from Manson's double linear damage rule and Subramanyan's non-linear damage rule. Damage increases by 50 percent from 0.065 to 0.13 in Manson's DLDR model, while in Subramanyan's model there is an 8 percent increase in damage from 0.096 to 0.104. In Miner's linear damage rule there is a 60 percent increase in damage from 3.81E-6 to 9.08E-6.

From these damage results it can be observed that Subramanyan's non-linear model and Manson's DLDR are quite close in their estimates for accumulated damage. Subramanyan's model gives the most damage accumulation of 0.2 which is slightly higher than damage accumulation in Manson's DLDR model (0.195). Meanwhile, the accumulated damage from Miner's rule (1.289E-5) is quite low in comparison to Manson and Subramanyan's models. This has significant implications on the operational life of this top-drive, because according to the damage accumulation obtained from Miner's rule this equipment can go on in operation without experiencing fatigue failure for a much longer time in comparison to the damage accumulation results from Manson's double linear damage rule and Subramanyan's non-linear damage which predict a shorter operational life for the top-drive. These deviations in the damage accumulation results from Subramanyan's model, Manson's and Miner's model are in agreement with variable amplitude tests that have been carried out by (Blason et al., 2016, Fernández-Canteli et al., 2014, Pavlou, 2002, Pavlou, 2018) that show Miner's rule overestimates fatigue life when there is a decrease in applied stresses in a high-low loading sequence.

The conservative results from the Auxiliary well for Rig 1 are presented to show the deviations between Miner's and Manson's models and to follow the conservative methodology that is utilised in-house at NOV for fatigue analysis. With a non-conservative estimate it would have been shown clearly that no damage occurred on this top-drive due to the applied stresses being below the endurance limit and also since the number of applied cycles were below number of remaining cycles (2,000,000) for the endurance limit region on the S-N curve. This S-N curve was presented in the previous chapter and more details on this S-N curve can be seen in [Appendix A](#). There are no conservative results obtained using Subramanyan's model because a key assumption in this model is that stresses below the endurance limit which is at the knee-point of the S-N curve do not contribute to damage. The conservative estimate result in Figure 6-14 shows significant deviations

in damage estimates between Miner's rule and Manson's double linear damage rule. According to Miner's rule there is a damage accumulation of $3.39E-6$ while Manson's DLDR gives a damage accumulation of 0.02. These results show an overestimation of the fatigue life of the top drive for the Auxiliary well by Miner's rule this follows the same trend as in the non-conservative damage estimates for the top-drive on Rig 1 Main well and this can be attributed to the fact that there is a reduction in the applied stresses for each loading step in this loading history.

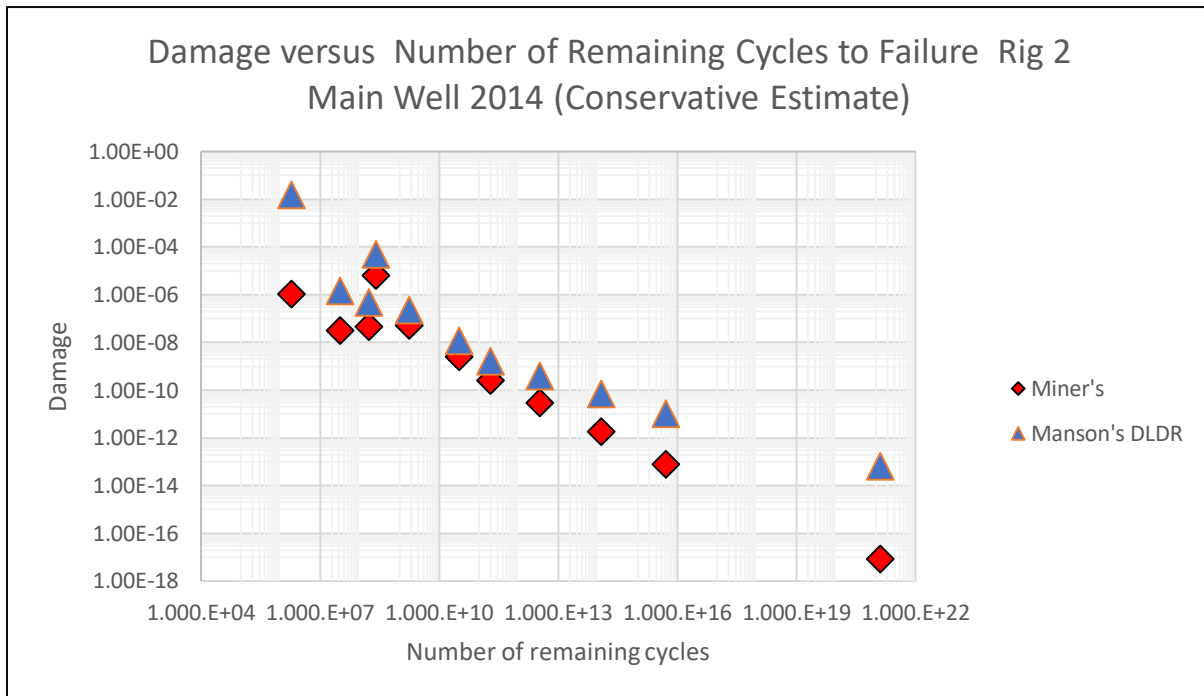


Figure 6-15: Conservative estimates of damage versus the number of remaining cycles until failure from the selected fatigue damage models for Rig 2 Main Well in 2014

For the top-drive on the Main well on Rig 2 the conservative damage estimates also show an overestimation of fatigue life from Miner's rule in comparison to Manson's DLDR. Here, the accumulated damage gotten from Miner's rule is $7.56E-06$ in comparison to Manson's DLDR which gives an accumulated damage of 0.0154. This underestimation of damage from Miner's rule will result in a higher operational life predicted for this top-drive in comparison to Manson's DLDR which will have a more conservative prediction for the fatigue life of this equipment.

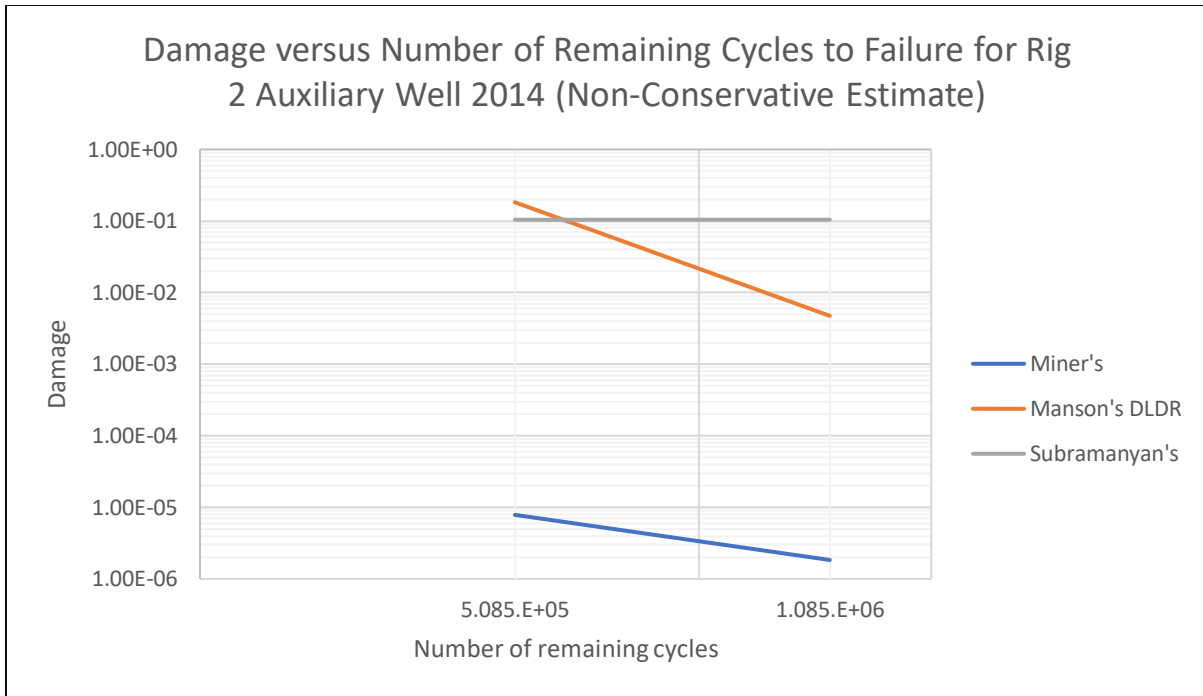


Figure 6-16: Non-conservative estimates of damage versus the number of remaining cycles until failure from the selected fatigue damage models for Rig 2 Auxiliary Well in 2014

In this non-conservative damage estimate for the top-drive on the Auxiliary well on Rig 2 it can be observed that the accumulated damage results from Manson’s DLDR and Subramanyan’s model are more conservative than the accumulated damage predicted by Miner’s rule. Here, the accumulated damage from Subramanyan’s model is 0.208 while that from Manson’s DLDR is 0.1876, this still shows some close correlation between the damage results obtained from these models. Meanwhile, the accumulated damage results obtained from using Miner’s rule is 9.71E-6 which is significantly lower than the accumulated damage results obtained from Manson’s DLDR or Subramanyan’s model, this continues in the trend of overestimation of the fatigue life by Miner’s rule that has been seen in the previous results.

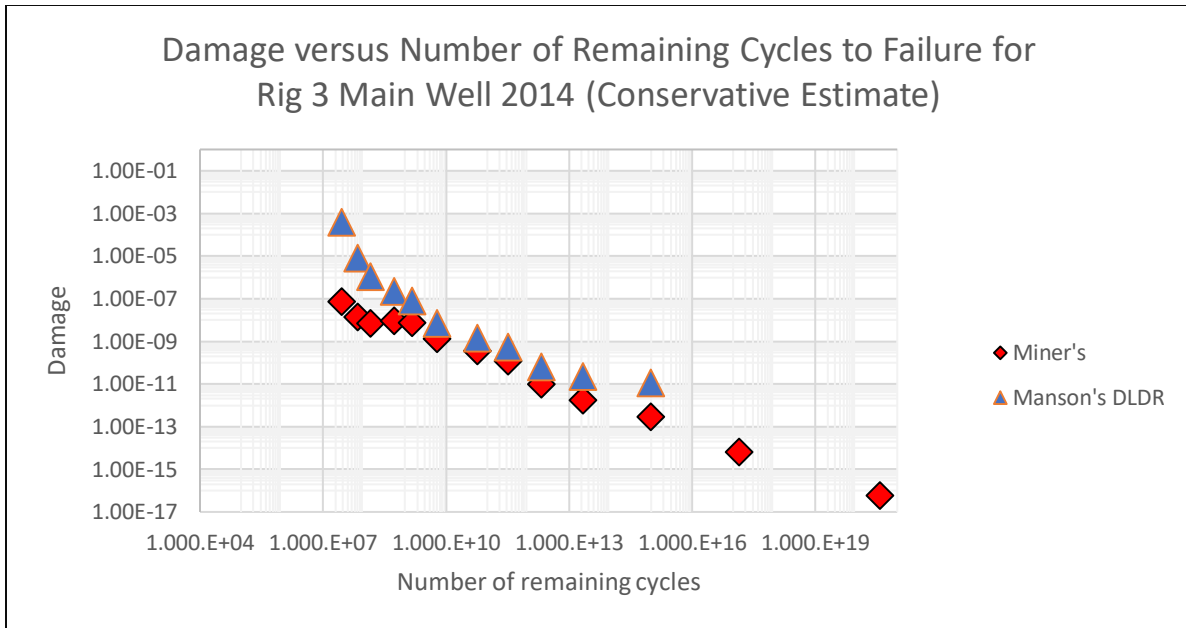


Figure 6-17: Conservative estimates of damage versus the number of remaining cycles until failure from the selected fatigue damage models for Rig 3 Main Well in 2014

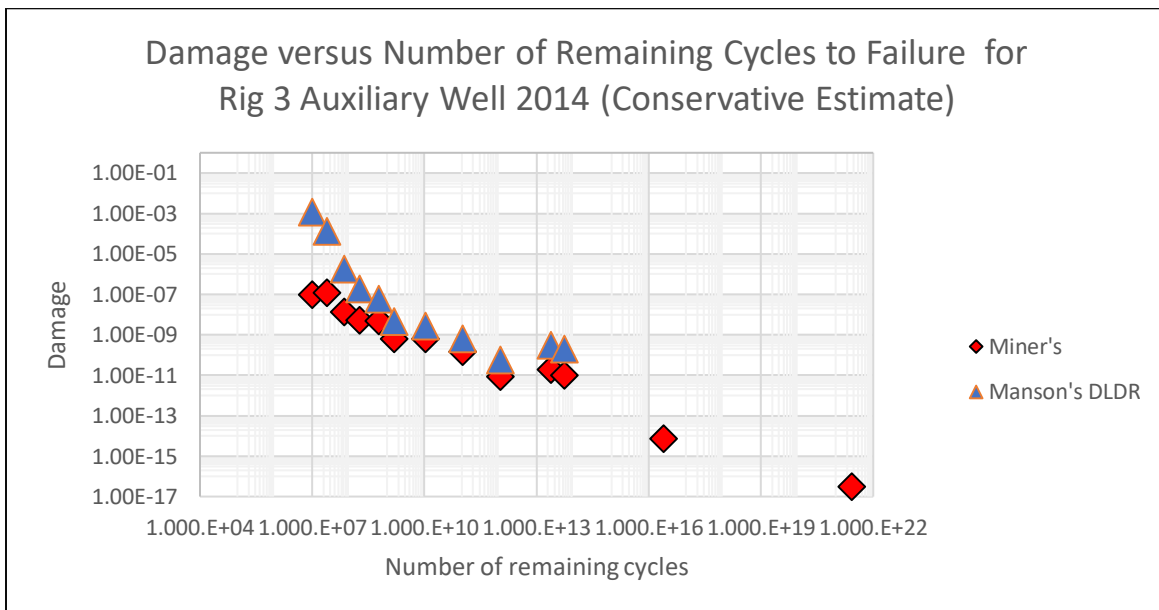


Figure 6-18: Conservative estimates of damage versus the number of remaining cycles until failure from the selected fatigue damage models for Rig 3 Auxiliary Well in 2014

In the conservative damage estimate results shown above in Figures 6-17 and 6-18 for the main and auxiliary well on Rig 3, it can be observed that the trend of Miner's rule overestimating the fatigue life of the top-drive continues. Here, the damage accumulated for the Main well when using Miner's rule is $1.11E-7$ in comparison to a damage accumulation of $3.998E-4$ from Manson's DLDR. This same scenario is present for the top-drive on the auxiliary well where Miner's rule predicts an accumulated damage of $2.43E-7$ while Manson's DLDR predicted an accumulated damage of $1.2568E-3$. In both results from Rig 3 Miner's rule overestimates the fatigue life of the analysed component on the top-drive.

In summary, the damage results obtained from the three rigs for the year 2014 shows close correlations between the damage results obtained using Manson's double linear damage rule and Subramanyan's non-linear damage rule with Subramanyan's model being slightly less conservative than Manson's model. In the results obtained, Miner's rule consistently overestimated the fatigue life for the analysed top-drive members in comparison to the fatigue life estimates gotten from Manson's and Subramanyan's models.

Given that these three models and take into account different mechanisms and assumptions when measuring damage this brings into question how much information can be derived from their damage estimates. It is because of this that the number of loading blocks until failure was computed using each model. It is believed that this will be more informative when comparing the results from these three fatigue damage models. This comparison using the number of loading blocks until failure will be shown the next section of this discussion.

6.3.3 Comparison of the number of loading blocks until failure results for Miners linear damage rule and Manson's double linear damage rule models

In this comparison the analysed top-drive members are subjected to a stress loading history which results in damage when these applied stresses are above the endurance limit of the top-drive. This loading history is assumed to represent one (1) loading block of applied stresses on the top-drive, from this analogy the number of loading blocks until failure is computed as the number of applied stress loading blocks that will result in a damage value of unity (1).

For Miner's rule and Manson's DLDR, the number of loading blocks until failure was computed as the inverse of the total damage accumulation, where in Manson's model this was computed for

the two damage phases considered in this model. While in Subramanyan's model the stress block iterations were done until damage was equal to unity (1), the stress block where damage was equal to (1) was taken as the predicted number of loading blocks until failure.

Non-conservative estimates and conservative estimates were also taken when considering the number of loading blocks until failure, justification for this has been provided in the previous sections of this discussion. The conservative estimates only show results from Miner's rule and Manson's double linear damage rule because Subramanyan's model cannot be used to take into account stresses below the endurance limit of the analysed top-drive member.

Non-Conservative Estimates

Rig 1

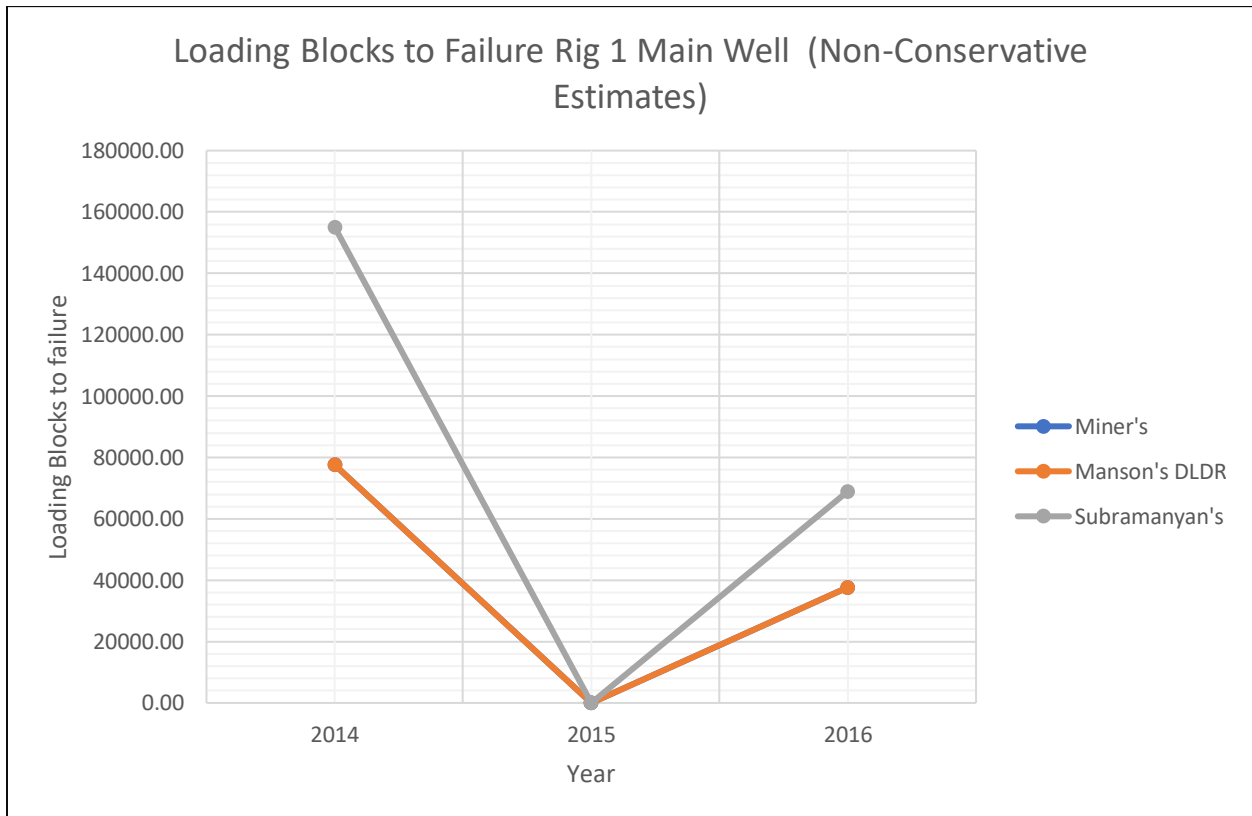


Figure 6-19: Non-conservative estimates of the number of loading blocks until failure from the selected fatigue damage models for Rig 1 Main Well

The non-conservative estimate result shown above in Figure 6-19 covers the predicted number of loading blocks until failure for the Main Well on Rig 1. It can be observed that Miner's rule and Manson's DLDR show close similar predictions for the number of loading blocks until failure. This can also be seen in Table 6-1, there is very little between Miner's rule and Manson's DLDR. Meanwhile, Subramanyan's model shows big deviations in its predictions of number of loading blocks until failure in comparison to Miner's rule and Manson's DLDR. In 2014 the deviations between the predictions from Subramanyan's non-linear damage rule from Miner's rule and Manson's DLDR was 49 percent, with zero damage from all the models in 2015, this deviation decreased slightly in 2016 to 45 percent. These results show a trend of Miner's rule and Manson's double linear damage rule having more conservative estimates for the number of loading blocks of the applied stresses that the top-drive can take before it experiences fatigue failure, Subramanyan's non-linear damage rule shows less conservative estimates. The implication of this is that the top-drive will to be recertified or replaced much earlier if the estimates from Miner's rule and Manson's DLDR are used in comparison to Subramanyan's model.

The non-conservative estimates for the Auxiliary well on Rig 1 can be seen in Figure 6-20 and Table 6-2 below. It can be observed that there is no damage in 2014 and 2015 from all the models considered. The predictions for the number of loading blocks until failure estimates from Miner's rule and Manson's double linear damage rule and Subramanyan's non-linear damage rule are equivalent for the year 2016. This can be due to the very low stress loading for the top-drive on the Auxiliary well and its infrequency of use, from the rainflow count there was just one counted cycle (1) of a damaging stress that was applied to this top-drive.

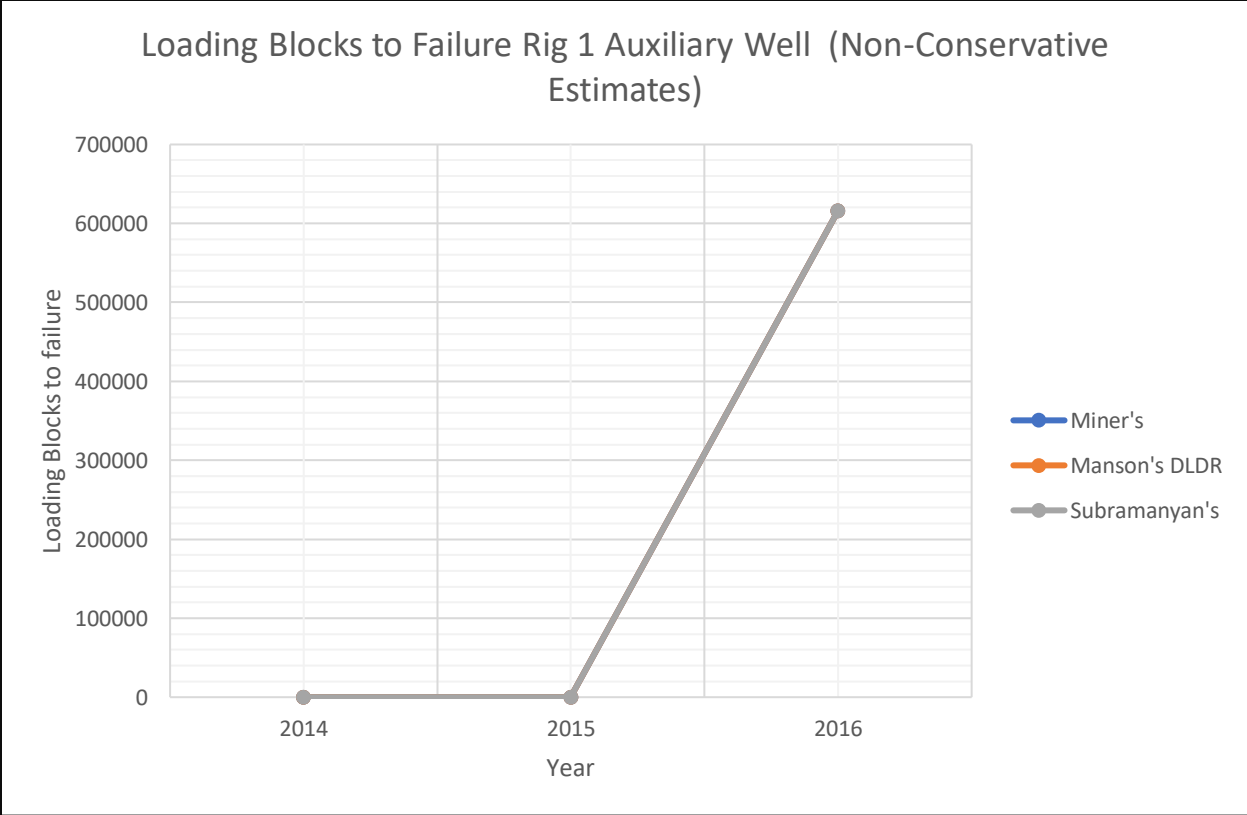


Figure 6-20: Non-conservative estimates of the number of loading blocks until failure from the selected fatigue damage models for Rig 1 Auxiliary Well

Main Well							
Year	Loading Blocks to Failure			Subramanyan's Damage Rule	Miner's vs DLDR Percentage Difference	Miner's vs Subramanyan's Percentage Difference	
	Miner's Linear Damage Rule	Double Linear Damage Rule					
2014		77563.87	77563.84533	155080	0.000000331112	0.499846073	
2015	No Damage	No Damage	No Damage	No Damage	0.000000000000	0	
2016		37562.51	37558.85643	68848.00	0.000097151784	0.454413989	

Table 6-2: Non-conservative estimates of the number of loading blocks until failure from the selected fatigue damage models for Rig 1 Main Well

Auxiliary Well							
Year	Loading Blocks to Failure			Subramanyan's Damage Rule	Miner's vs DLDR Percentage Difference	Miner's vs Subramanyan's Percentage Difference	
	Miner's Linear Damage Rule	Double Linear Damage Rule					
2014	No Damage	No Damage	No Damage	No Damage	0	0	
2015	No Damage	No Damage	No Damage	No Damage	0	0	
2016		615923.75	615923.7589	615922	0	2.82264E-06	

Table 6-3: Non-conservative estimates of the number of loading blocks until failure from the selected fatigue damage models for Rig 1 Auxiliary Well

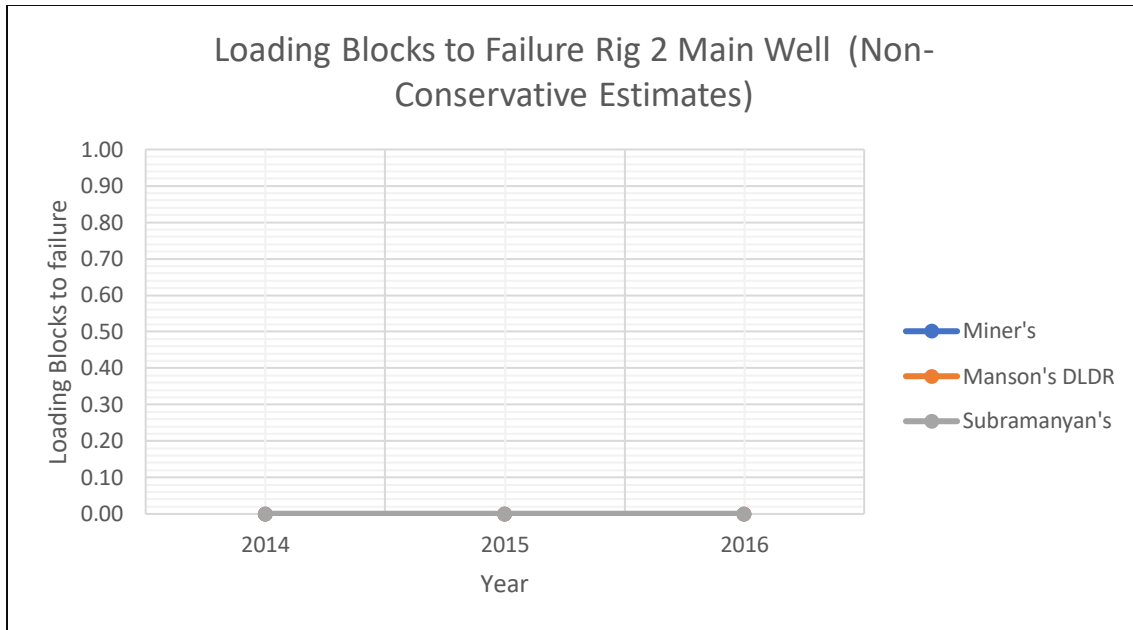


Figure 6-21: Non-conservative estimates of the number of loading blocks until failure from the selected fatigue damage models for Rig 2 Main Well

The non-conservative results for the Main well on Rig 2 shown in Figure 6-21 above reveals that there was no damage from any of the selected models. This is because the applied stresses on the top-drive of this Rig were below the endurance limit so therefore they do not contribute to fatigue damage.

For the Auxiliary on Rig 2, the non-conservative estimates continue in the trend of Miner's and Manson's model being virtually equivalent in their estimates for the number of loading blocks until failure of this top-drive member. Subramanyan's model is less conservative in its estimate of the number of loading blocks until failure in comparison to the other selected models with deviations ranging from 40- 49 percent.

The non-conservative results from Rig 3 for the Main well and Auxiliary well show no damage from any of the selected models for all the years that have been considered.

In summary, the results from the non-conservative estimates for the three (3) Rigs show that Subramanyan's non-linear damage rule is less conservative in its assessment of the number of loading blocks until failure in comparison to Miner's rule and Manson's double linear damage rule

which are more conservative in their estimates. This observation is in agreement with experimental results from tests carried out Lee et al on SAE 4130 (Lee et al., 2004) where it was shown that Subramanyan's model was less conservative in its predictions of number of loading blocks until failure.

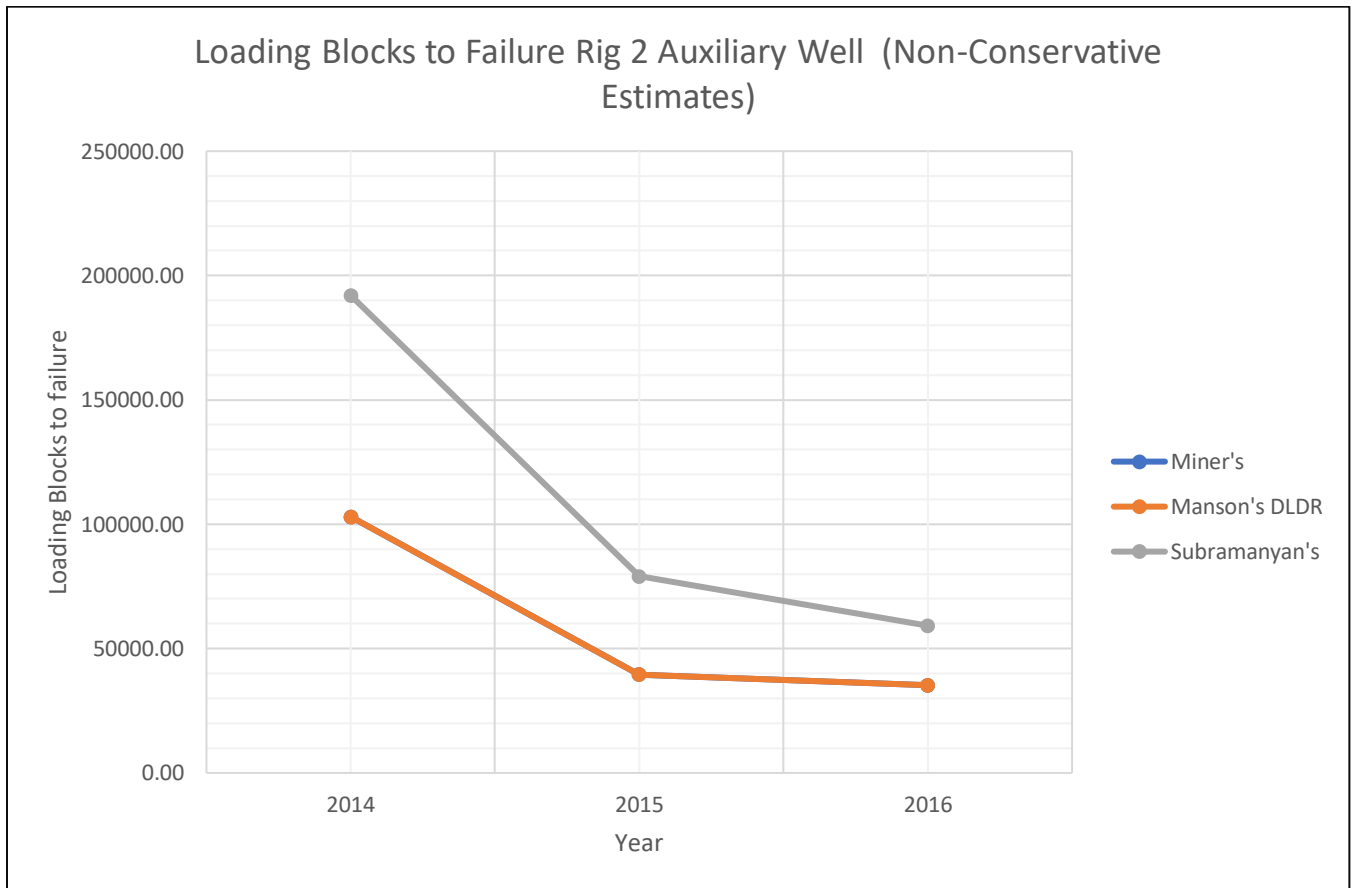


Figure 6-22: Non-conservative estimates of the number of loading blocks until failure from the selected fatigue damage models for Rig 2 Auxiliary Well

Main Well					
Year	Loading Blocks to Failure			Miner's vs DLDR	Miner's vs Subramanyan's
	Miner's Linear Damage Rule	Double Linear Damage Rule	Subramanyan's Damage Rule	Percentage Difference	Percentage Difference
2014	No Damage	No Damage	No Damage	0.000000000000	0
2015	No Damage	No Damage	No Damage	0.000000000000	0
2016	No Damage	No Damage	No Damage	0.000000000000	0

Table 6-4: Non-conservative estimates of the number of loading blocks until failure from the selected fatigue damage models for Rig 2 Main Well

Auxiliary Well					
Year	Loading Blocks to Failure			Miner's vs DLDR	Miner's vs Subramanyan's
	Miner's Linear Damage Rule	Double Linear Damage Rule	Subramanyan's Damage Rule	Percentage Difference	Percentage Difference
2014	102999.65	102993.79	191989.00	0.000056958120	0.463512733
2015	39509.12	39509.11	79013.00	0.000000042193	0.49996689
2016	35290.94	35287.01	59224.00	0.000111138	0.404110886

Table 6-5: Non-conservative estimates of the number of loading blocks until failure from the selected fatigue damage models for Rig 2 Auxiliary Well

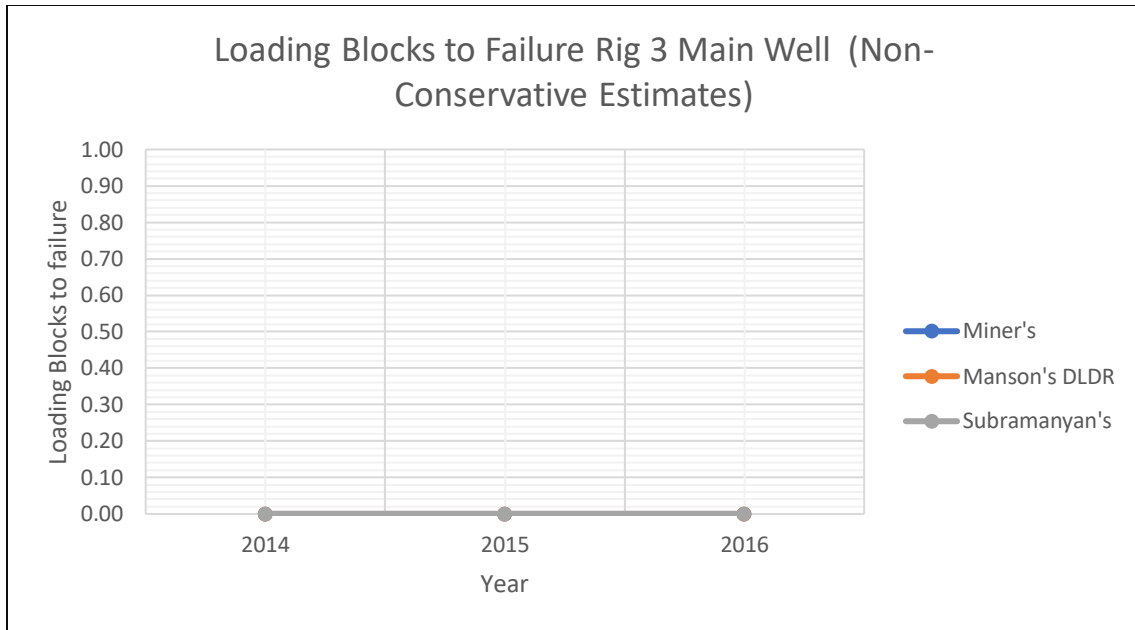


Figure 6-23: Non-conservative estimates of the number of loading blocks until failure from the selected fatigue damage models for Rig 3 Main Well

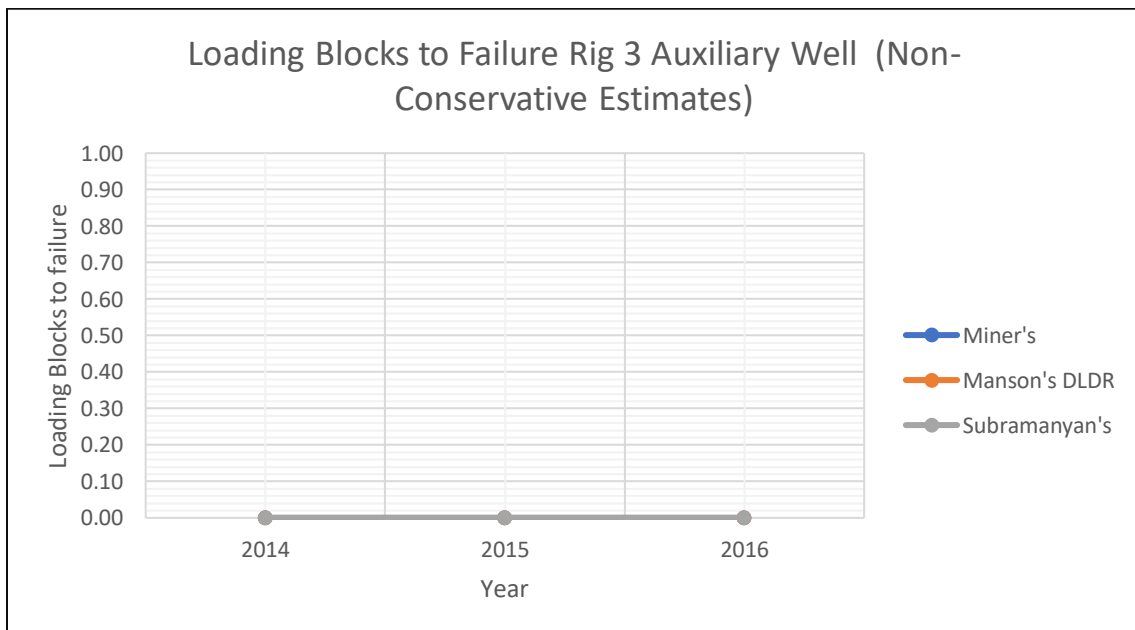


Figure 6-24: Non-conservative estimates of the number of loading blocks until failure from the selected fatigue damage models for Rig 3 Auxiliary Well

Main Well					
Year	Loading Blocks to Failure		Miner's vs DLDR	Miner's vs Subramanyan's	
	Miner's Linear Damage Rule	Double Linear Damage Rule	Subramanyan's Damage Rule	Percentage Difference	Percentage Difference
2014	No Damage	No Damage	No Damage	0	0
2015	No Damage	No Damage	No Damage	0	0
2016	No Damage	No Damage	No Damage	0	0

Table 6-6: Non-conservative estimates of the number of loading blocks until failure from the selected fatigue damage models for Rig 3 Main Well

Auxiliary Well					
Year	Loading Blocks to Failure		Miner's vs DLDR	Miner's vs Subramanyan's	
	Miner's Linear Damage Rule	Double Linear Damage Rule	Subramanyan's Damage Rule	Percentage Difference	Percentage Difference
2014	No Damage	No Damage	No Damage	0	0
2015	No Damage	No Damage	No Damage	0	0
2016	No Damage	No Damage	No Damage	0	0

Table 6-7: Non-conservative estimates of the number of loading blocks until failure from the selected fatigue damage models for Rig 3 Auxiliary Well

Conservative Estimates

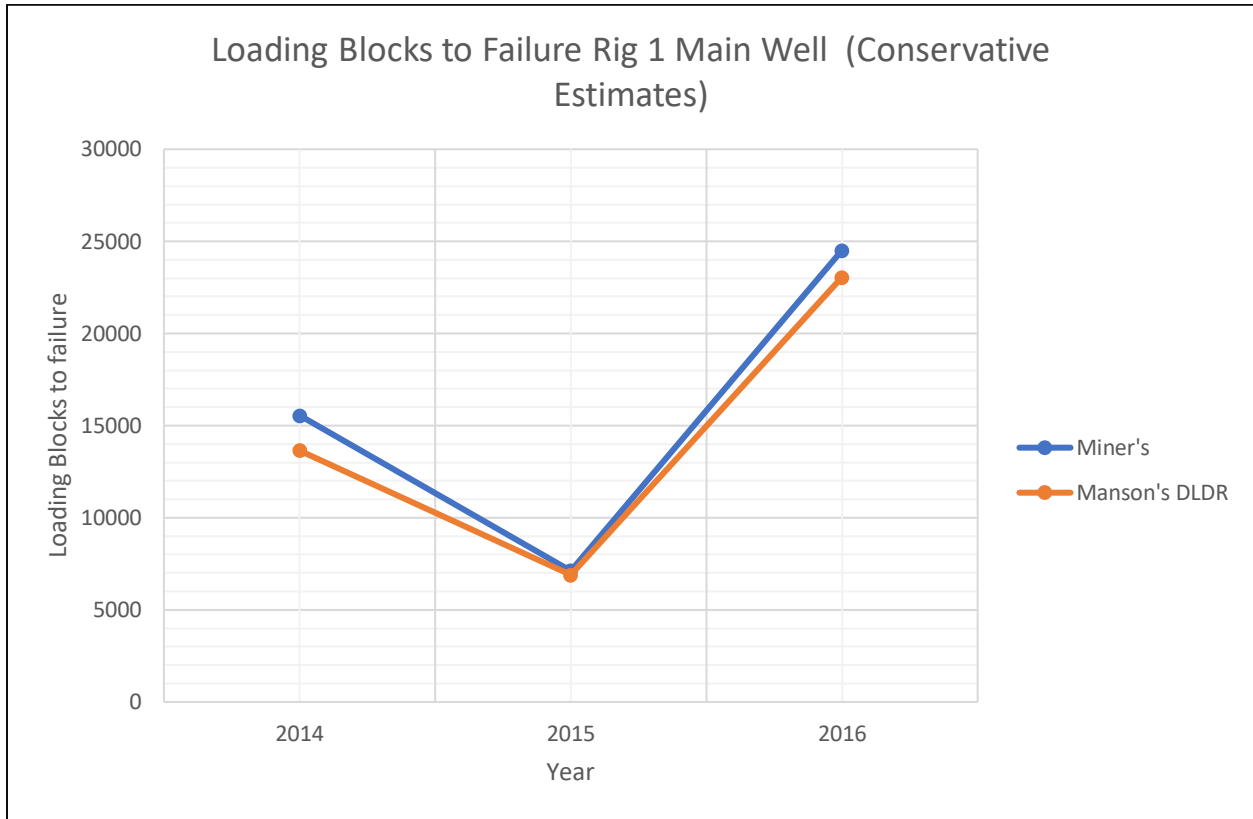


Figure 6-25: Conservative estimates of the number of loading blocks until failure from the selected fatigue damage models for Rig 1 Main Well

Main Well			
Year	Loading Blocks to Failure		Percentage Difference
	Miner's Linear Damage Rule	Double Linear Damage Rule	
2014	15545.28304	13655.00152	12.15983981
2015	7116.608943	6898.219818	3.068724528
2016	24515.87887	23057.10754	5.950312196

Table 6-8: Conservative estimates of the number of loading blocks until failure from the selected fatigue damage models for Rig 1 Main Well

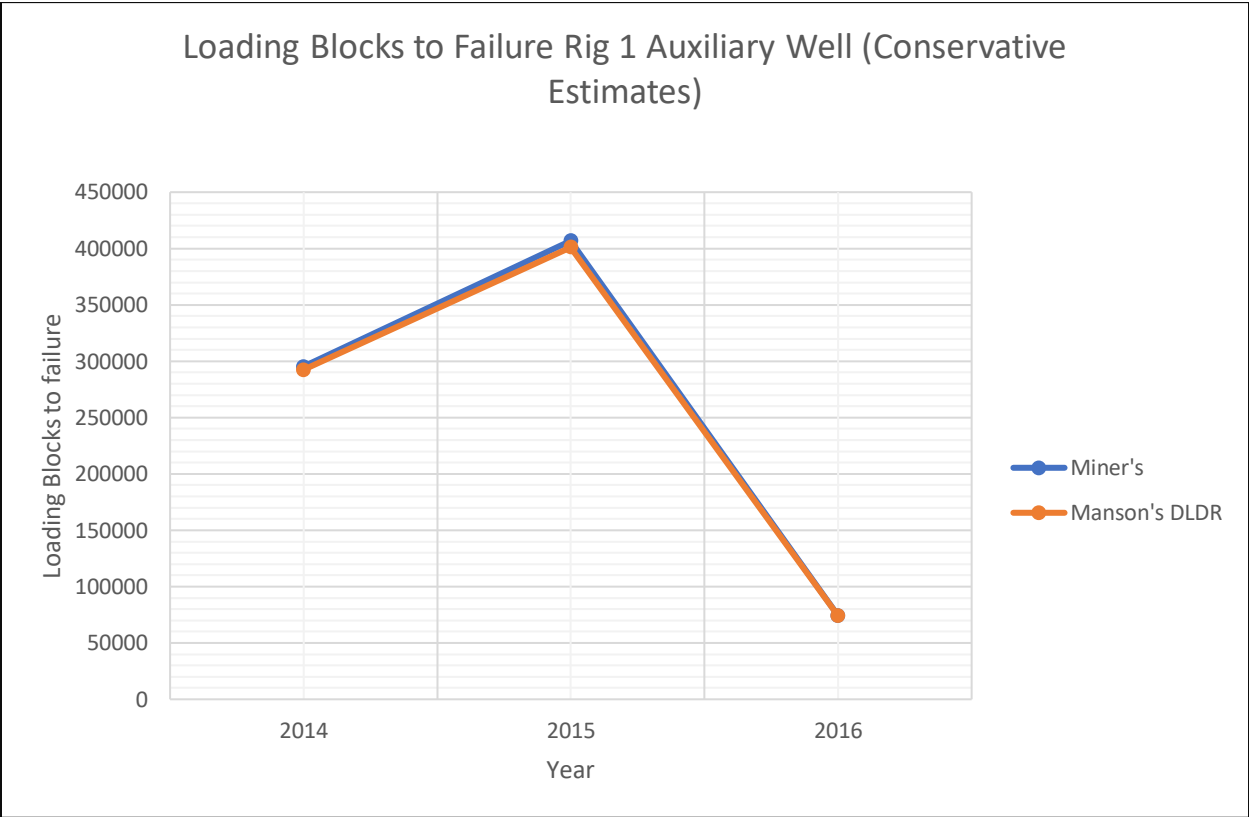


Figure 6-26: Conservative estimates of the number of loading blocks until failure from the selected fatigue damage models for Rig 1 Auxiliary Well

Auxiliary Well			
Year	Loading Blocks to Failure		Percentage Difference
	Miner's Linear Damage Rule	Double Linear Damage Rule	
2014	295260.7235	292487.0861	0.939385847
2015	406772.7963	400986.9686	1.42237331
2016	74366.41212	74149.95719	0.29106544

Table 6-9: Conservative estimates of the number of loading blocks until failure from the selected fatigue damage models for Rig 1 Auxiliary Well

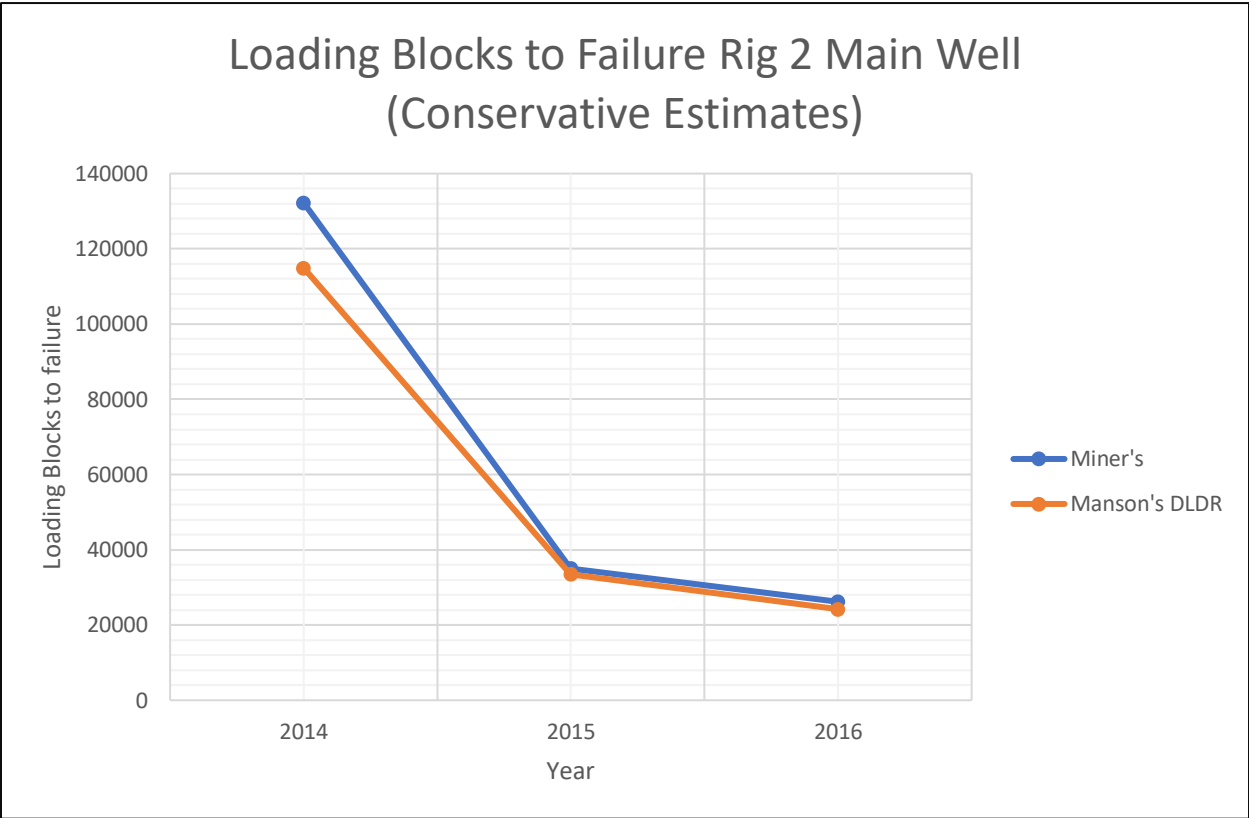


Figure 6-27: Conservative estimates of the number of loading blocks until failure from the selected fatigue damage models for Rig 2 Main Well

Main Well			
Year	Loading Blocks to Failure		Percentage Difference
	Miner's Linear Damage Rule	Double Linear Damage Rule	
2014	132237.5778	114920.4265	13.09548436
2015	35046.61408	33481.42569	4.466018855
2016	26179.18984	24211.43501	7.516484842

Table 6-10: Conservative estimates of the number of loading blocks until failure from the selected fatigue damage models for Rig 2 Main Well

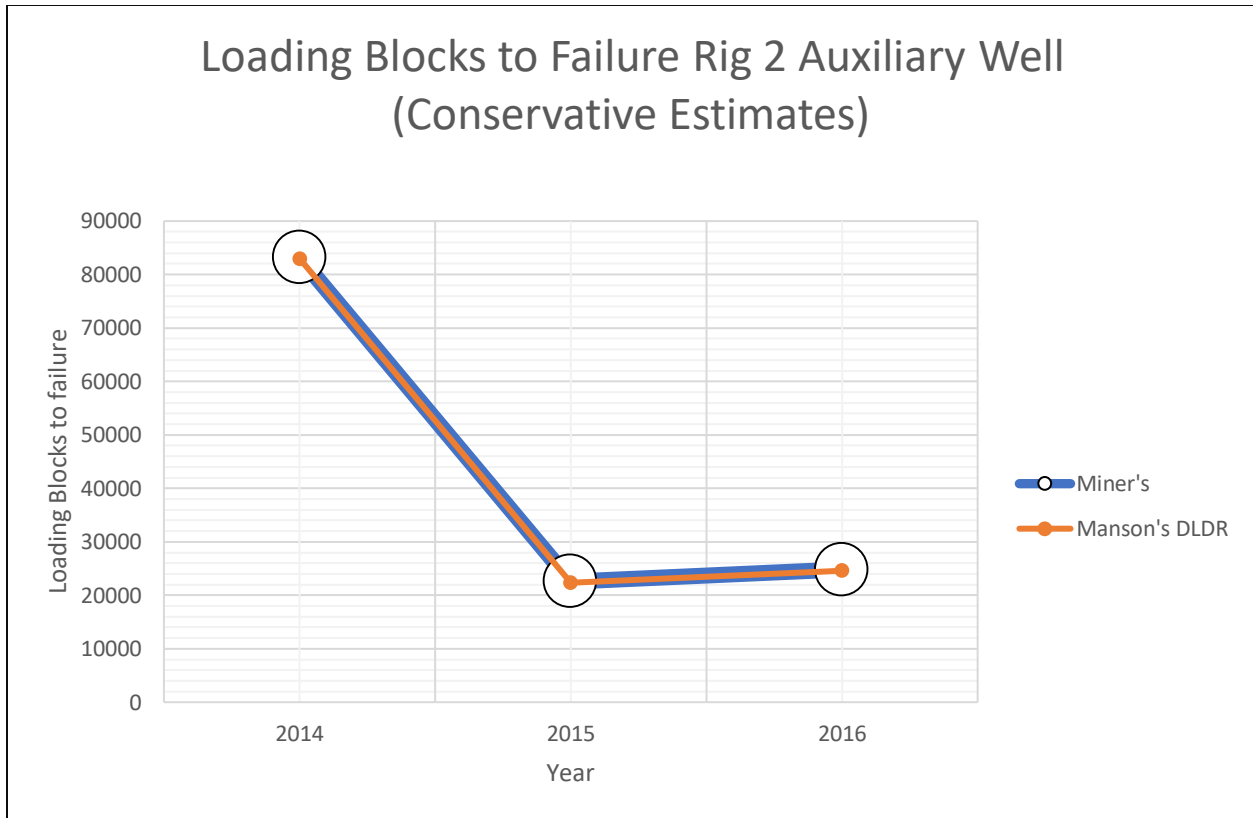


Figure 6-28: Conservative estimates of the number of loading blocks until failure from the selected fatigue damage models for Rig 2 Auxiliary Well

Auxiliary Well			
Year	Loading Blocks to Failure		Percentage Difference
	Miner's Linear Damage Rule	Double Linear Damage Rule	
2014	83229.09254	83002.99927	0.271651721
2015	22559.85834	22340.51577	0.972269282
2016	24795.46176	24592.32712	0.819241193

Table 6-11: Conservative estimates of the number of loading blocks until failure from the selected fatigue damage models for Rig 2 Auxiliary Well

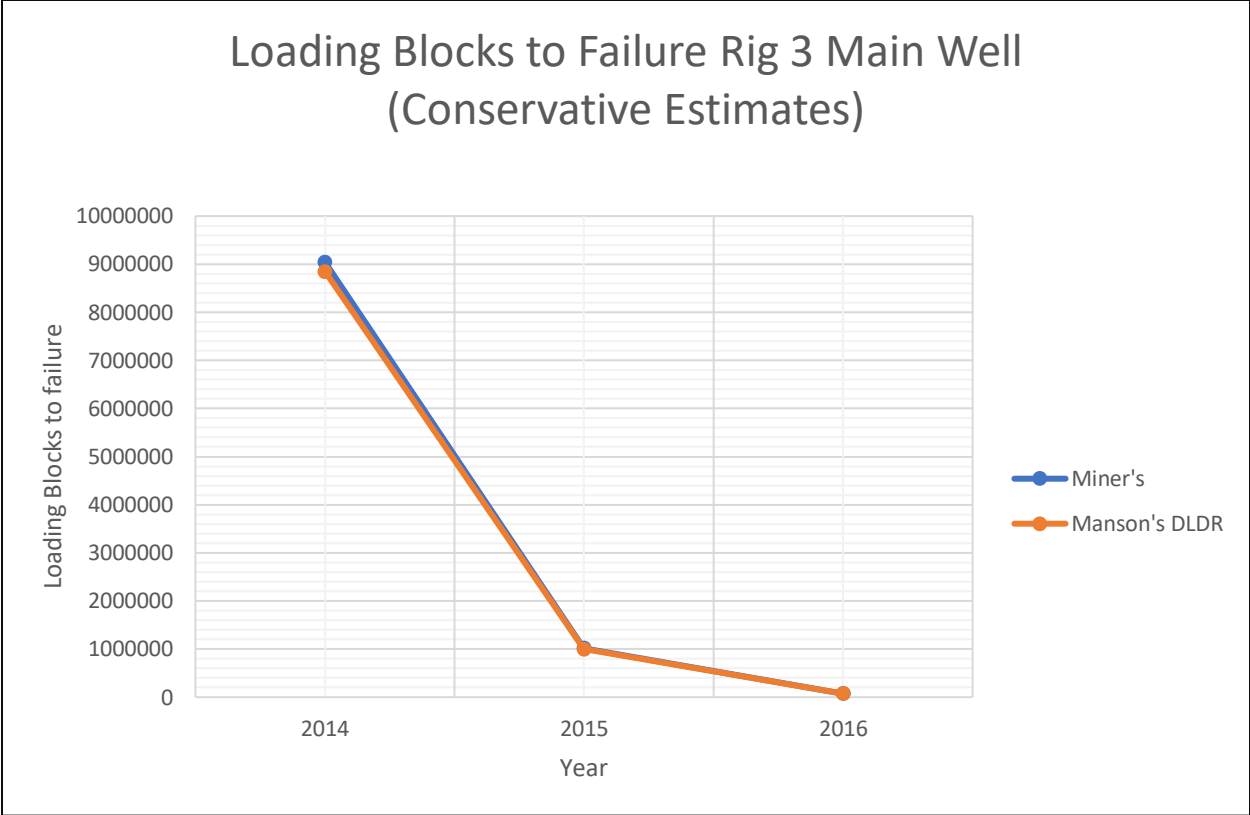


Figure 6-29: Conservative estimates of the number of loading blocks until failure from the selected fatigue damage models for Rig 3 Main Well

Main Well			
Year	Loading Blocks to Failure		Percentage Difference
	Miner's Linear Damage Rule	Double Linear Damage Rule	
2014	9044105.074	8851108.502	2.133948805
2015	1020552.67	998045.1065	2.205428922
2016	73073.04148	72294.91124	1.06486636

Table 6-2: Conservative estimates of the number of loading blocks until failure from the selected fatigue damage models for Rig 3 Main Well

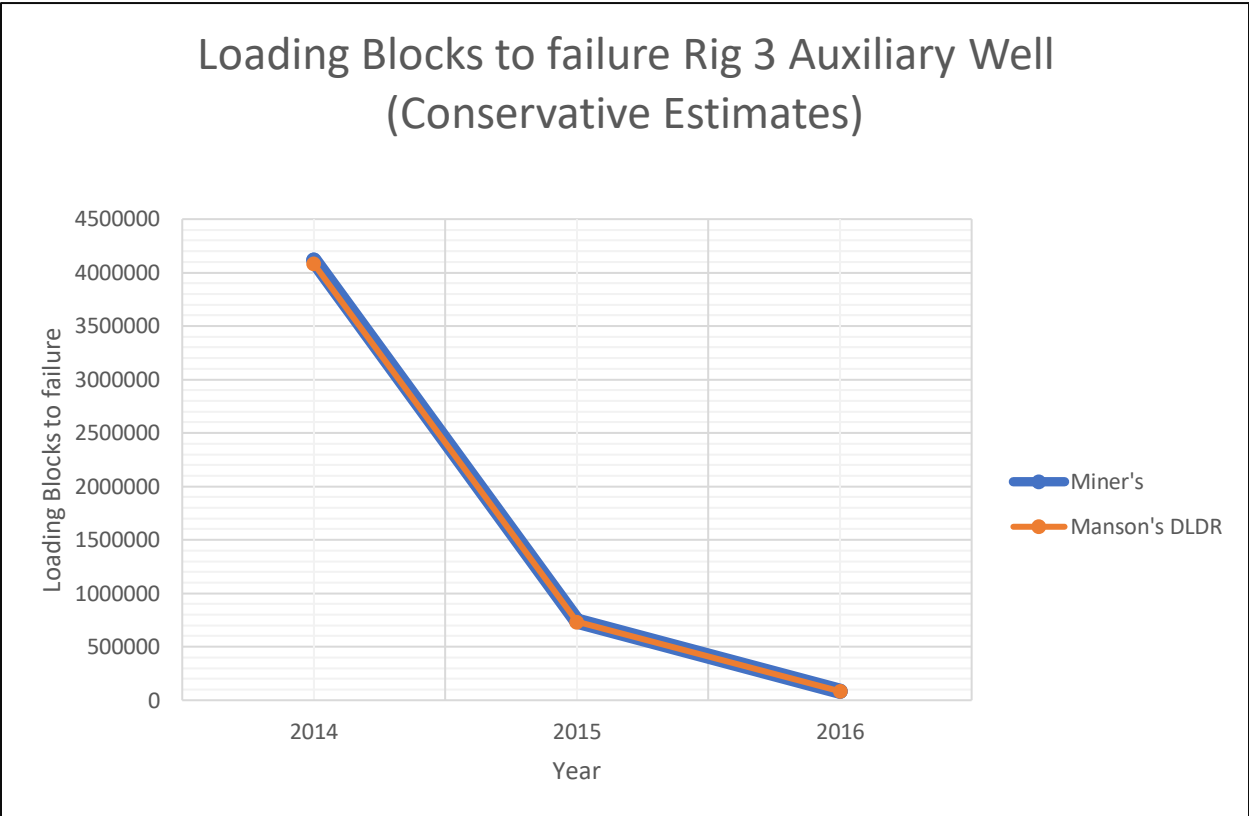


Figure 6-30: Conservative estimates of the number of loading blocks until failure from the selected fatigue damage models for Rig 3 Auxiliary Well

Auxiliary Well			
Year	Loading Blocks to Failure		Percentage Difference
	Miner's Linear Damage Rule	Double Linear Damage Rule	
2014	4117119.601	4082199.887	0.848158853
2015	739490.8565	733934.3048	0.751402353
2016	84165.50807	83565.26153	0.713174026

Table 6-13: Conservative estimates of the number of loading blocks until failure from the selected fatigue damage models for Rig 3 Auxiliary Well

The results from the conservative estimates of the number of loading blocks until failure (where stresses below the endurance limit) were considered when calculating damage are shown from Figure 6-25 through to Figure 6-30. These results are shown for consistency with the methodology adopted in-house.

The results from the top-drive on the Main well of Rig 1 shows that Manson's double linear damage rule is more conservative in its estimates of the number of loading blocks until failure in comparison to Miner's rule with deviations ranging between (3-12 percent). For the top-drive on the Auxiliary well of Rig 1 there is very little difference between the predicted number of loading blocks until failure from both models, this is because the top-drive on the Auxiliary well had a low frequency of use and was subjected to small applied stresses which is confirmed by most of the results that have been obtained for the top-drives on the Auxiliary well in the three (3) rigs.

Also, the results from the top-drive on the Main well of Rig 2 continue in the trend of Miner's rule being less conservative than Manson's double linear damage rule in estimating the number of loading blocks until failure. Here, the deviations between Manson's double linear damage rule and Miner's rule range from (4-13 percent). There was also very little difference between both models for the top-drive on the Auxiliary well on Rig 2 due to its low frequency of use and low applied stresses.

Lastly, the results from the top-drives on the Main well and Auxiliary well on Rig 3 show very little difference. This rig was idle for some time due to low activity on the Norwegian Continental Shelf in 2015 and 2016 and because of this there was low cycles counts for applied stresses on the top-drives on this rig.

In summary, the conservative estimation methodology adopted in-house will lead to overestimation of damage which will result in shorter operational life predictions for the top-drives on the drilling rigs. From a business standpoint the current conservative methodology is accepted because there is not so much difference in the inspection interval when computing the mean time between failures (MTBF) for the top-drive. The current regulations suggested by DNV-GL is that the top-drive on the Rigs should be revalidated every 5 years with more intrusive inspections done every 10 years. Investigation into this is outside the scope of this thesis since a deterministic approach for fatigue assessment has been adopted so far in this research work.

7 Conclusion and Recommendations

7.1 Conclusion

The central focus of this project was on the area of multiaxial fatigue on offshore equipment. This project was aimed at the implementation of linear, double linear and non-linear damage accumulation rules for prediction of fatigue life of the tie-rods on an offshore drilling top-drive. The selected damage accumulation models were built and coded in Python to enable an implementation of hybrid models which are based on linear algebra and vector calculus. This was done to accelerate calculations, reduce internal IT dependency when changes need to be made and allow for implementation of machine learning techniques to obtain optimized results.

The goals of this project were accomplished to a fairly high degree and it is believed that the results will serve as decision support for Asset Managers of offshore equipment.

The literature survey of this research work uncovered key concepts about fatigue, its mechanisms, contributing factors and ways in which fatigue can be classified. Also, it was established that the stress-life (S-N) approach is the most commonly used method for analysing high cycle fatigue because of the vast amount of data available from experiments and material testing. The stress life (S-N) approach is also the chosen method for utilisation in multiaxial fatigue cases that involve long-life with applied strains that are mainly elastic. Equivalent stress approaches were investigated and it was shown that Von-Mises equivalent stress approach was the most accepted approach for approximating equivalent stresses for multiaxial fatigue problems where the axial and torsional forces are in-phase and proportional as recommended by standards such as DNV-GL- RP-C-203 and F.E.M 1.001. Mean stress correction methods such as Goodman, Gerber, Soderberg, Morrow and Smith-Watson-Topper were also analysed, and it was established that the modified Goodman method was the most accepted mean stress correction method. The modified Goodman mean stress correction method is widely accepted due to its simplicity and its reasonable amount of conservativeness. Also, most data from experimental tests fall between the curves for Goodman and Gerber. Cycle counting techniques were evaluated and it was seen that the range pair and rainflow counting techniques were two of the more reliable cycle counting techniques. However, the rainflow cycle counting technique was shown to be more accurate in converting variable stress histories into constant amplitude stress blocks.

Fatigue assessment was carried out using Palmgren-Miner's, Manson's and Subramanyan's models to represent linear, double-linear and non-linear damage accumulation rules respectively. The results obtained from using these damage accumulation rules were quite reasonable and follow established trends from past research carried out by (Blason et al., 2016, Fernández-Canteli et al., 2014, Pavlou, 2002, Pavlou, 2018) whereby variable amplitude test experiments were performed to establish the fatigue life predictions from these models. The key variables that were observed while comparing the fatigue life predictions of the selected models were: damage accumulation and the number of loading blocks until failure.

The damage accumulation results obtained from the selected models show that Miner's rule was consistently less conservative in its prediction for the accumulated damage in comparison to Manson's double linear damage rule and Subramanyan's non-linear damage rule. The selected double-linear and non-linear damage accumulation rules showed close correlations in their predictions of the amount of damage that had been accumulated by the tie-rods on the drilling top-drives which was in most cases more than the damage accumulation that was predicted by Palmgren Miner's rule. It can be concluded from these results that Palmgren Miner's rule underestimates the amount of accumulated damage which will result in an overestimation of the number of cycles remaining before the component experiences a failure. This finding is consistent with the research carried out by (Fatemi and Yang, 1998, Fissolo et al., 2015, Mesmacque et al., 2005, Schoenborn et al., 2015, Theil, 2016) where it was proven that Palmgren Miner's rule predicts longer life for components when the stress amplitude is decreasing. Manson's and Subramanyan's damage accumulation rules should be utilised to provide more reliable damage accumulation estimates.

The number of loading blocks until failure results showed close correlations between Miner's and Manson's models when non-conservative fatigue damage estimates were made without filtering out stresses below the endurance limit. These models were found to be more conservative in their predictions for the number of loading blocks until failure. Subramanyan's non-linear damage rule had less- conservative predictions on the number loading blocks until failure. This finding is consistent with experimental results from tests carried out Lee et al on SAE 4130 (Lee et al., 2004) where it was shown that Subramanyan's model was slightly less conservative in its predictions of number of loading blocks until failure. However, the number of loading blocks until failure results

in the scenario where conservative fatigue damage estimates were made where stresses below the endurance limit were not filtered out, showed that Miner's rule was more conservative in comparison to Manson's double linear damage rule in predictions. In view of this more analysis should be performed using Manson's double linear damage rule and Subramanyan's non-linear damage rule. Here, more robust equivalent stress determination methods such as those proposed by Fatemi and Papadopoulos should be utilised.

It can be concluded that the results from this project will serve as an enabler for the utilization of more comprehensive fatigue life estimation techniques such as Manson's double linear damage rule and simplified non-linear damage rules which capture the true nature of the fatigue that equipment's are subjected to, and thus to improve the reliability of the fatigue life predictions.

7.2 Recommendations

The following recommendations are suggested for future research work on multiaxial fatigue on the tie-rods of offshore drilling top-drives

- A more robust and accurate equivalent stress approximation method should be utilized. Due to the time constraints of this project, the Von-Mises equivalent stress approximation method was used to determine the equivalent stresses that were applied to the tie-rods. This approach is a rough but reasonable estimation of the equivalent stress.
- Additional research should be carried out using other mean stress correction methods such as Smith-Watson-Topper, Gerber or Morrow to compare the results from these methods with the modified Goodman approach.
- A probabilistic based fatigue analysis should be done in tandem with Manson's double linear damage rule and simplified non-linear damage rules to enable the estimation of key reliability metrics such as the mean time between failures (MTBF), mean time to failure (MTTF) and the mean time to repair (MTTR). This is essential to provide additional justification to decision makers on the need to adopt a different approach other than Palmgren-Miner's rule for multiaxial fatigue assessments.
- Given the results obtained from Subramanyan's model other simplified non-linear damage models such as Rege's "one-parameter nonlinear fatigue damage accumulation" and Pavlou's "S-N fatigue damage envelope" should be tested to compare predictions.

- Further research should be geared towards integrating the double linear and non-linear damage models into a blockchain database for easy validation of structural integrity of various equipment by validators such as DNV-GL and suppliers or users of these equipment's.

8 References

1. ALMAR-NÆSS, A. 1985. Fatigue Handbook - Offshore Steel Structures.
2. ANAEE, R. & HAMEED, M. 2016. Tribocorrosion.
3. ARCHIVES, B. O. A. A. 1954. CRASH OF A DE HAVILLAND DH.106 COMET 1 OFF ELBE ISLAND: 35 KILLED.
4. ASTM 2017. Standard Practices for Cycle Counting in Fatigue Analysis.
5. BLASON, S., CORREIA, J. A. F. O., JESUS, A. M. P. D., CALCADA, R. A. B. & FERNANDEZ-CANTELI, A. 2016. 60.
6. COFFIN, L. F. 1954. A study of the effects of cyclic thermal stresses on a ductile metal. Transactions of the ASME. 76: 931–950.
7. COURTNEY, T. H. 1990. *Graph showing fatigue failure as a function of strain amplitude.*
8. DNV-GL 2017. Data quality assessment framework. *RP-0497.*
9. DOWLING, N. E. A. 1993. *Mechanical behavior of materials : engineering methods for deformation, fracture, and fatigue*, Boston :.
10. DOWLING, N. E. A. 2004. Mean Stress Effects in Stress-Life and Strain-Life Fatigue.
11. ENSIGN, C. R., FRECHE, J. C. & MANSON, S. S. 1966. Application of a double linear damage rule to cumulative fatigue - NASA-TM-X-52226. Sponsoring Organization: NASA Lewis Research Center.
12. EUROCODE 1993. Eurocode 3: "Design of Steel Structures": ENV1993-1-1: Part 1.1, General rules and rules for buildings, CEN, 1993.
13. F.E.M 1998. RULES FOR THE DESIGN OF HOISTING APPLIANCES. *CHECKING FOR FATIGUE AND CHOICE OF MECHANISM COMPONENTS*
14. FEDERATION EUROPEENNE DE LA MANUTENTION.
15. FATEMI, A. 2018. Multiaxial Stresses.
16. FATEMI, A. & YANG, L. 1998. Cumulative fatigue damage and life prediction theories: a survey of the state of the art for homogeneous materials. *International Journal of Fatigue*, 20, 9-34.
17. FERNÁNDEZ-CANTELI, A., BLASÓN, S., CORREIA, J. A. F. O. & JESUS, A. M. P. D. 2014. A probabilistic interpretation of the Miner number for fatigue life prediction. *Frattura ed Integrità Strutturale*, 8, 327-339.
18. FINDLEY W. N. 1959. A theory for the effect of mean stress on fatigue of metals under combined torsion and axial load or bending. *Journal of Engineering for Industry*. Vol. 81, 1959, pp. 301-306.
19. FISSOLO, A., GOURDIN, C., CHEN, Y., PEREZ, G. & STELMASZYK, J. M. 2015. Investigations into the cumulative fatigue life of an AISI 304L austenitic stainless steel used for pressure water reactors: Application of a double linear damage rule. *International Journal of Fatigue*, 77, 199-215.
20. GUSTAFSSON, J. & SAARINEN, J. 2007. "Multi-axial fatigue in welded details.", *Master's Thesis in the Master Degree Programme Civil Engineering, Chalmers University Of Technology.*
21. HIATT, J. 2016. *Rainflow Counting* [Online]. [Accessed].
22. IRVINE, T. 2013. Rainflow Cycle Counting for Random Vibration Fatigue Analysis
23. ISO 2015. Data quality -- Part 8: Information and data quality: Concepts and measuring. *8000-8.*
24. JUVINALL, R. C. & MARSHEK, K. M. 2006. *Fundamentals of machine component design*, New York, Wiley.
25. KUSSMAUL K. F., M. D. L., SOCIE D. F. 1991. Fatigue under biaxial and multiaxial loading. Mechanical Engineers Publications Limited, Publication 10, London, United Kingdom, 1991, 480 pp.
26. LABORATORY, TESTING & INC. 2019. *Specimen Testing* [Online]. [Accessed].

27. LEE, Y.-L., BARKEY, M., HATHAWAY, R. & PAN, J. 2004. *Fatigue Testing and Analysis : Theory and Practice*, Oxford, UNITED STATES, Elsevier Science & Technology.
28. LEESE G. E. & SOCIE D. 1989. Multiaxial fatigue: Analysis and Experiments. Society of Automotive Engineers. Warrendale, USA, 1989, 162 pp.
29. MADDOX, S. J. & RAZMJOO, G. R. 2001. Interim fatigue design recommendations for fillet welded joints under complex loading. *Fatigue & Fracture of Engineering Materials & Structures*, 24, 329-337.
30. MANSON, S. 1966. Interfaces between fatigue, creep, and fracture. *International Journal of Fracture Mechanics*, 2, 327-363.
31. MANSON, S. & HALFORD, G. 1981. Practical implementation of the double linear damage rule and damage curve approach for treating cumulative fatigue damage. *International Journal of Fracture*, 17, 169-192.
32. MANSON, S. S. 1953. Behavior of materials under conditions of thermal stress" (PDF). National Advisory Committee for Aeronautics. NACA TN-2933.
33. MATSUSHI, M. & ENDO, T. 1968. Fatigue of metals subjected to varying stress, Japan Soc. Mech. Engineering.
34. MESMACQUE, G., GARCIA, S., AMROUCHE, A. & RUBIO-GONZALEZ, C. 2005. Sequential law in multiaxial fatigue, a new damage indicator. *International Journal of Fatigue*, 27, 461-467.
35. MIKKELSEN, O., REGE, K., HEMMINGSEN, T. & PAVION, D. G. Numerical estimation of the stop holes-induced fatigue crack growth retardation in offshore structures taking into account the corrosion effect. The 27th International Ocean and Polar Engineering Conference, 2017. International Society of Offshore and Polar Engineers.
36. MINER, M. A. 1945. Cumulative damage in fatigue". *Journal of Applied Mechanics*. 12: 149–164. *Journal of Applied Mechanics*. 12: 149–164.
37. .
38. MORENO, H. 2019. *The Importance Of Data Quality -- Good, Bad Or Ugly* [Online]. Available: <https://www.forbes.com/sites/forbesinsights/2017/06/05/the-importance-of-data-quality-good-bad-or-ugly/#13058fe110c4> [Accessed].
39. NOV. 2019. *National Oilwell Varco Reports Fourth Quarter and Full Year 2018 Results* [Online]. Available: [https://nov.com/News/National Oilwell Varco Reports Fourth Quarter and Full Year 2018 Results.aspx](https://nov.com/News/National_Oilwell_Varco_Reports_Fourth_Quarter_and_Full_Year_2018_Results.aspx) [Accessed].
40. OOTW. 2013. *ALEXANDER L. KIELLAND PLATFORM CAPSIZE ACCIDENT – INVESTIGATION REPORT* [Online]. [Accessed].
41. PALMGREN, A. G. 1924 "Die Lebensdauer von Kugellagern" [Life Length of Roller Bearings]. *Zeitschrift des Vereines Deutscher Ingenieure* (in German). 68 (14): 339–341.
42. PAPADOPOULOS I. V. 2001. Long life fatigue under multiaxial loading". *International Journal of Fatigue*, Vol. 23, 2001, page. 839-849.
43. PAPADOPOULOS I. V., DAVOLI P., GORLA C., FILIPPINI M. & BERNASCONI A. 1997. "A comparative study of multiaxial high-cycle fatigue criteria for metals". *International Journal of Fatigue*. Vol.19, 1997, page. 219-235.
44. PARK, J. & NELSON, D. 2000. Evaluation of an energy-based approach and a critical plane approach for predicting constant amplitude multiaxial fatigue life (vol 22, pg 23, 2000). *Int. J. Fatigue*, 22, 349-349.
45. PAVLOU, D. 2000. Prediction of fatigue crack growth under real stress histories. *Engineering Structures*, 22, 1707-1713.

46. PAVLOU, D. 2015. Fatigue crack deflection-induced retardation based on the principle of the minimum potential energy. *International Review of Mechanical Engineering*, 9, 324-330.
47. PAVLOU, D., LABEAS, G., VLACHAKIS, N. & PAVLOU, F. 2003. Fatigue crack propagation trajectories under mixed-mode cyclic loading. *Engineering structures*, 25, 869-875.
48. PAVLOU, D., VLACHAKIS, N., PAVLOU, M. & VLACHAKIS, V. 2004. Estimation of fatigue crack growth retardation due to crack branching. *Computational materials science*, 29, 446-452.
49. PAVLOU, D. G. 2002. A phenomenological fatigue damage accumulation rule based on hardness increasing, for the 2024-T42 aluminum. *Engineering Structures*, 24, 1363-1368.
50. PAVLOU, D. G. 2018. The theory of the S-N fatigue damage envelope: Generalization of linear, double-linear, and non-linear fatigue damage models. *International Journal of Fatigue*, 110, 204-214.
51. QUOC-VIET L.T. 2016. *Application of Multiaxial Fatigue Analysis Methodologies for the Improvement of the Life Prediction of Landing Gear Fuse Pins*.
52. RAABE, D. 1980. *Dramatic failure of materials in drilling platforms at sea* [Online]. [Accessed].
53. SCHIJVE J. 2009. *Fatigue of structures and materials, 2nd ed., Springer, 2009*.
54. SCHOENBORN, S., KAUFMANN, H., SONSINO, C. M. & HEIM, R. 2015. Cumulative Damage of High-strength Cast Iron Alloys for Automotive Applications. *Procedia Engineering*, 101, 440-449.
55. SIMSCALE. 2019. *What is von Mises Stress?* [Online]. Available: <https://www.simscale.com/docs/content/simwiki/fea/what-is-von-mises-stress.html> [Accessed].
56. SMITH, J. O. 1942. "The Effect of Range of Stress on the Fatigue Strength of Metals," Bulletin No. 334, University of Illinois, Engineering Experiment Station, Urbana, IL, Feb. 1942. See also Bulletin No. 316, Sept. 1939. .
57. SMITH, K. N., P. WATSON & AND T. H. TOPPER 1970. "A Stress Strain Function for the Fatigue of Metals," *Journal of Materials*, ASTM, Vol. 5, No. 4, Dec. 1970, pp. 767- 778. .
58. SOLIDWORKS 2009. Preventing Mechanical Fatigue, Technical paper. SolidWorks Corp., 300 Baker avenue, Concord MA 01742 USA.
59. SRIVATSAVAN, R. & SUBRAMANYAN, S. 1978. A Cumulative Damage Rule Based on Successive Reduction in Fatigue Limit. *Journal of Engineering Materials and Technology*, 100, 212-214.
60. SUBRAMANYAN, S. 1976. A Cumulative Damage Rule Based on the Knee Point of the S-N Curve. *Journal of Engineering Materials and Technology*, 98, 316-321.
61. SURESH, S. 1992. *Fatigue of materials*, Cambridge, Cambridge University Press.
62. TESSITORE, D. 2018. *What is industry 4.0?* [Online]. Available: <https://www.industrialintelligence.net/industry-4-0/> [Accessed].
63. THEIL, N. 2016. Fatigue life prediction method for the practical engineering use taking in account the effect of the overload blocks. *International Journal of Fatigue*, 90, 23-35.
64. UIS. 2016. *Mean Stress Effects* [Online]. [Accessed].
65. WANG Y.Y. & W.X., Y. 2003. Evaluation and comparison of several multiaxial fatigue criteria", *International Journal of Fatigue*, Vol. 26, 2004, page.17-25.
66. WANHILL, R. J. H. 2002. Milestone Case Histories in Aircraft Structural Design. National Aerospace Laboratory. NLR-TP-2002-521.
67. WIKIPEDIA. 2019. *Versailles train disaster* [Online]. [Accessed].
68. YONGMING L. 2006. *Stochastic modelling of multiaxial fatigue and fracture. Ph.D. Thesis. Graduate School of Vanderbilt University, Nashville, Tennessee, 2006, 187 pp.*
69. YOU B.R. & LEE S.B. 1995. A critical review on multiaxial fatigue assessments of metals", *International Journal of Fatigue*. Vol. 18, No. 4, 1996, page. 235-244.
70. ZEC, J. 2018. Asset Management, services and innovation in digital era.

9 Appendices

Appendix A: Wohler Curve

According to the F.E.M 1.001 standard (F.E.M, 1998) "WOHLER curve" in this context means an endurance curve representing the number n of stress cycles which can be withstood before fatigue failure, as a function of the maximum stress σ (T), when all stress cycles present the same amplitude and the same ratio κ between extreme values.

Regarding this WOHLER curve, the following hypotheses are made respectively:

- **For $n = 8 * 10^3$:**

$$\sigma = \sigma_R$$

or

$$\tau = \sigma_R / 3^{0.5}$$

Where: σ_R is the ultimate strength of the material

σ_d is the endurance limit of the material

τ_d is the endurance limit of the material

- **For $8 * 10^3 \leq n \leq 2 * 10^6$:**

The area of limited endurance, the function is represented by a straight-line TD in a reference system comprising two logarithmic scale axes (Figure 9-1)

The slope of the WOHLER curve, in the interval considered, is characterised by the factor:

$$c = \tan(\phi) = [\log(2 * 10^6) - \log(8 * 10^3)] / (\log \sigma_R - \log \sigma_d)$$

or

$$c = \tan(\phi) = [\log(2 * 10^6) - \log(8 * 10^3)] / [(\log (\sigma_R / 3^{0.5}) - \log \tau_d)]$$

- For $n = 2 * 10^6$:

$$\sigma = \sigma_d$$

or

$$\tau = \tau_d$$

- For $n > 2 * 10^6$:

The so-called region of endurance limit, the function is represented, in the same reference system as above, by the straight fine DN, bisector of the angle formed by the extension of TD and a fine parallel to the axis of the n values, passing through D. The slope of the WOHLER curve for $n > 2 * 10^6$ is characterised by the factor:

$$c' = \tan(\phi') = c + (c^2 + 1)^{0.5}$$

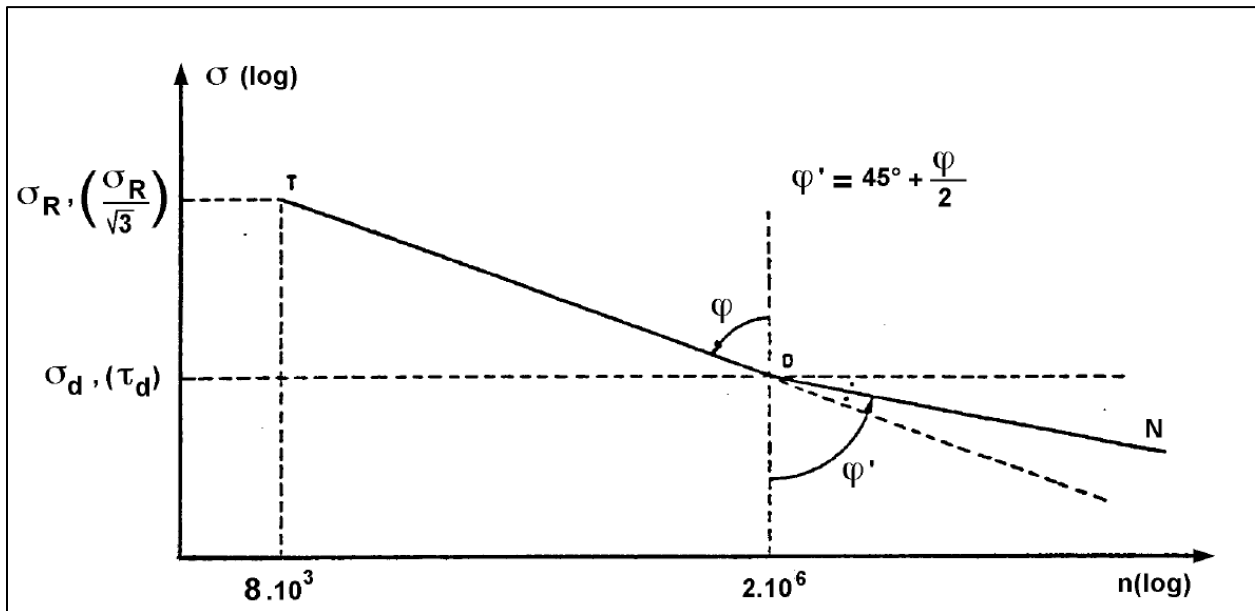


Figure 9-1: S-N curve according to F.E.M section 4.1.3.5 (F.E.M, 1998)

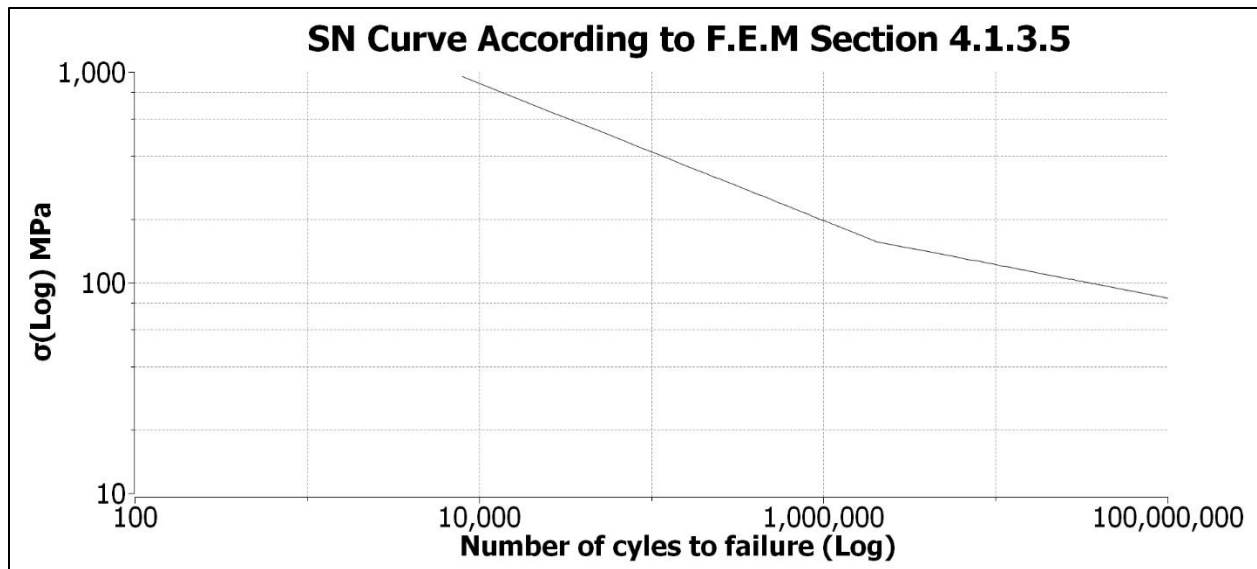


Figure 9-2: S-N curve according to F.E.M section 4.1.3.5 reproduced and used in this thesis (F.E.M, 1998)

Appendix B: Data Quality Checks

Data Description Tables

Rig 1: Main Well

Variable	Sigma_eq (January-July 2014)	Sigma_eq (July-December 2014)
n	9510667	13657275
na	0	0
mean	25.93	65.12826
sd	22.7	49.37109
se_mean	0.01	0.01336
IQR	1	87
skewness	4.21	0.632875
kurtosis	18.36	-0.85427
p10	19	20
p90	32	140
p95	52	151

p99	149	181
p100	287	287

Table 9-1: Data Description for Rig 1 Main Well Datasets between January-December 2014

Variable	Sigma_eq (January-July 2015)	Sigma_eq (July-December 2015)
n	4649854.00	6783167.00
na	0.00	0.00
mean	40.90	55.40
sd	42.74	49.77
se_mean	0.02	0.02
IQR	30.00	73.00
skewness	1.61	1.08
kurtosis	1.84	0.65
p10	4.00	5.00
p90	112.00	127.00
p95	139.00	148.00
p99	190.00	203.00
p100	260.00	298.00

Table 9-2: Data Description for Rig 1 Main Well Datasets between January-December 2015

Variable	Sigma_eq (January-July 2016)
n	7412916.00
na	0.00
mean	56.65
sd	47.59
se_mean	0.02
IQR	66.00
skewness	1.08
kurtosis	0.39
p10	8.00
p90	123.00
p95	160.00
p99	187.00
p100	290.00

Table 9-3: Data Description for Rig 1 Main Well Dataset between January-July 2016

Rig 1: Auxiliary Well

Variable	Sigma_eq (January-July 2014)	Sigma_eq (July-December 2014)
n	9391382.00	12828685.00
na	0.00	0.00
mean	19.80	20.68
sd	4.37	3.31
se_mean	0.00	0.00
IQR	1.00	0.00
skewness	-1.17	-2.63
kurtosis	90.03	128.18
p10	20.00	21.00
p90	21.00	22.00
p95	22.00	22.00

p99	22.00	24.00
p100	248.00	291.00

Table 9-4: Data Description for Rig 1 Auxiliary Well Datasets between January-December 2014

Variable	Sigma_eq (January-July 2015)	Sigma_eq (July-December 2015)
n	2833304	3656517.00
na	0	0.00
mean	20.79694	18.43
sd	4.037312	7.32
se_mean	0.002399	0.00
IQR	2	1.00
skewness	4.254745	-1.26
kurtosis	270.4498	11.93
p10	19	2.00
p90	22	22.00
p95	25	22.00
p99	28	23.00
p100	262	280.00

Table 9-5: Data Description for Rig 1 Auxiliary Well Datasets between January-December 2015

Variable	Sigma_eq (January-July 2016)
n	4173468.00
na	0.00
mean	21.76
sd	3.17

se_mean	0.00
IQR	1.00
skewness	44.11
kurtosis	2592.98
p10	21.00
p90	22.00
p95	22.00
p99	23.00
p100	278.00

Table 9-6: Data Description for Rig 1 Auxiliary Well Dataset between January-July 2016

Rig 2: Main Well

Variable	Sigma_eq (July-December 2014)
n	1843707.00
na	0.00
mean	22.75
sd	8.68
se_mean	0.01
IQR	0.00
skewness	11.26
kurtosis	142.73
p10	21.00
p90	22.00
p95	25.00
p99	37.00
p100	248.00

Table 9-7: Data Description for Rig 2 Main Well Dataset between July-December 2014

Variable	Sigma_eq (January-July 2015)	Sigma_eq (July-December 2015)
n	10996350.00	4438484.00
na	0.00	0.00
mean	22.71	16.10
sd	17.18	15.63
se_mean	0.01	0.01
IQR	1.00	21.00
skewness	5.75	1.96
kurtosis	42.06	10.61
p10	6.00	1.00
p90	32.00	37.00
p95	35.00	47.00
p99	118.00	56.00
p100	293.00	272.00

Table 9-8: Data Description for Rig 2 Main Well Datasets between January-December 2015

Variable	Sigma_eq (January-July 2016)
n	7389491.00
na	0.00
mean	34.57
sd	27.80
se_mean	0.01
IQR	30.00
skewness	1.28
kurtosis	2.05
p10	2.00
p90	77.00
p95	90.00
p99	123.00

p100	289.00
------	--------

Table 9-9: Data Description for Rig 2 Main Well Dataset between January-July 2016

Rig 2: Auxiliary Well

Variable	Sigma_eq (July-December 2014)
n	4648476.00
na	0.00
mean	18.13
sd	6.85
se_mean	0.00
IQR	1.00
skewness	0.08
kurtosis	64.11
p10	2.00
p90	21.00
p95	21.00
p99	22.00
p100	305.00

Table 9-10: Data Description for Rig 2 Auxiliary Well Dataset between July-December 2014

Variable	Sigma_eq (January-July 2015)	Sigma_eq (July- December 2015)
n	12983849.00	111498.00
na	0.00	0.00
mean	21.25	3.39
sd	8.13	15.90
se_mean	0.00	0.05

IQR	1.00	0.00
skewness	12.07	9.50
kurtosis	170.51	100.66
p10	20.00	1.00
p90	21.00	2.00
p95	22.00	7.00
p99	26.00	94.00
p100	293.00	284.00

Table 9-2 : Data Description for Rig 2 Auxiliary Well Datasets between January-December 2015

Variable	Sigma_eq (January-July 2016)
n	4460861.00
na	0.00
mean	21.92
sd	9.90
se_mean	0.00
IQR	0.00
skewness	6.04
kurtosis	76.84
p10	20.00
p90	23.00
p95	24.00
p99	74.00
p100	293.00

Table 9-3 : Data Description for Rig 2 Auxiliary Well Dataset between January-July 2016

Rig 3: Main Well

Variable	Sigma_eq (July-December 2014)
n	1843707.00
na	0.00
mean	22.75
sd	8.68
se_mean	0.01
IQR	0.00
skewness	11.26
kurtosis	142.73
p10	21.00
p90	22.00
p95	25.00
p99	37.00
p100	248.00

Table 9-4 : Data Description for Rig 3 Main Well Dataset between July-December 2014

Variable	Sigma_eq (January -July 2015)	Sigma_eq (July-December 2015)
n	10996350.00	4438484.00
na	0.00	0.00
mean	22.71	16.10
sd	17.18	15.63
se_mean	0.01	0.01
IQR	1.00	21.00
skewness	5.75	1.96
kurtosis	42.06	10.61
p10	6.00	1.00
p90	32.00	37.00

p95	35.00	47.00
p99	118.00	56.00
p100	293.00	272.00

Table 9-5 : Data Description for Rig 3 Main Well Datasets between January-December 2015

Variable	Sigma_eq (January-July 2016)
n	7389491.00
na	0.00
mean	34.57
sd	27.80
se_mean	0.01
IQR	30.00
skewness	1.28
kurtosis	2.05
p10	2.00
p90	77.00
p95	90.00
p99	123.00
p100	289.00

Table 9-6 : Data Description for Rig 3 Main Well Dataset between July-December 2016

Rig 3: Auxiliary Well

Variable	Sigma_eq (January-July 2014)	Sigma_eq (July-December 2014)
n	9391382.00	12828685.00
na	0.00	0.00
mean	19.80	20.68

sd	4.37	3.31
se_mean	0.00	0.00
IQR	1.00	0.00
skewness	-1.17	-2.63
kurtosis	90.03	128.18
p10	20.00	21.00
p90	21.00	22.00
p95	22.00	22.00
p99	22.00	24.00
p100	248.00	291.00

Table 9-7: Data Description for Rig 3 Auxiliary Well Datasets between January-December 2014

Variable	Sigma_eq (January-July 2015)	Sigma_eq ((July-December 2015)
n	2833304.00	3656517.00
na	0.00	0.00
mean	20.80	18.43
sd	4.04	7.32
se_mean	0.00	0.00
IQR	2.00	1.00
skewness	4.25	-1.26
kurtosis	270.45	11.93
p10	19.00	2.00
p90	22.00	22.00
p95	25.00	22.00
p99	28.00	23.00
p100	262.00	280.00

Table 9-8 : Data Description for Rig 3 Auxiliary Well Datasets between January-December 2015

Variable	Sigma_eq (January-July 2016)
n	4173468.00
na	0.00
mean	21.76
sd	3.17
se_mean	0.00
IQR	1.00
skewness	44.11
kurtosis	2592.98
p10	21.00
p90	22.00
p95	22.00
p99	23.00
p100	278.00

Table 9-9 : Data Description for Rig 3 Auxiliary Well Datasets between January-July 2016

Appendix C: Outlier Diagnosis

Rig 1: Main Well

Diagnosis of numerical variable outliers

variables	min	median	max	outlier	outlier ratio(%)
Sigma_eq	1	20	287	2,378,441	25.01

2.2 Detailed outliers diagnosis

variable : Sigma_eq

Outliers information of Sigma_eq

Measures	Values
Outliers count	2378441.00
Outliers ratio (%)	25.01
Mean of outliers	43.00
Mean with outliers	25.93
Mean without outliers	20.24

Diagnosis of numerical variable outliers

variables	min	median	max	outlier	outlier ratio(%)
Sigma_eq	1	50	287	419	0

2.2 Detailed outliers diagnosis

variable : Sigma_eq

Outliers information of Sigma_eq

Measures	Values
Outliers count	419.00
Outliers ratio (%)	0.00
Mean of outliers	262.12
Mean with outliers	65.13
Mean without outliers	65.12

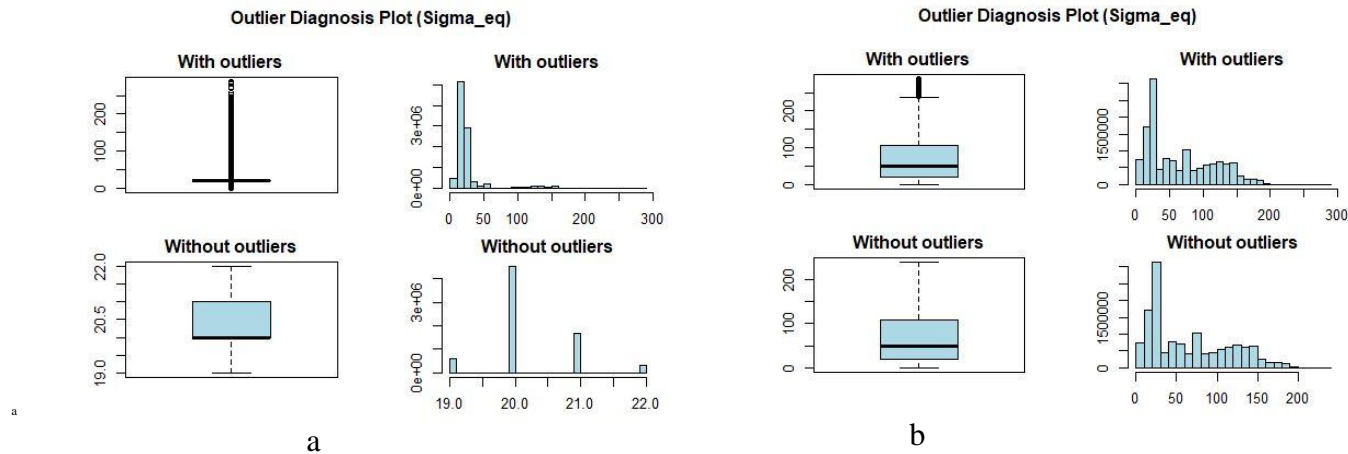


Figure 9-3 : Outlier Diagnosis Results for Rig 1 Main Well Datasets from January 2014 (a)-December 2014 (b)

Diagnosis of numerical variable outliers

variables	min	median	max	outlier	outlier ratio(%)
Sigma_eq	1	21	260	774,205	16.65

2.2 Detailed outliers diagnosis

variable : Sigma_eq

Outliers information of Sigma_eq

Measures	Values
Outliers count	774205.00
Outliers ratio (%)	16.65
Mean of outliers	125.56
Mean with outliers	40.90
Mean without outliers	23.99

Diagnosis of numerical variable outliers

variables	min	median	max	outlier	outlier ratio(%)
Sigma_eq	1	31	298	67,726	1

2.2 Detailed outliers diagnosis

variable : Sigma_eq

Outliers information of Sigma_eq

Measures	Values
Outliers count	67726.00
Outliers ratio (%)	1.00
Mean of outliers	235.25
Mean with outliers	55.40
Mean without outliers	53.58

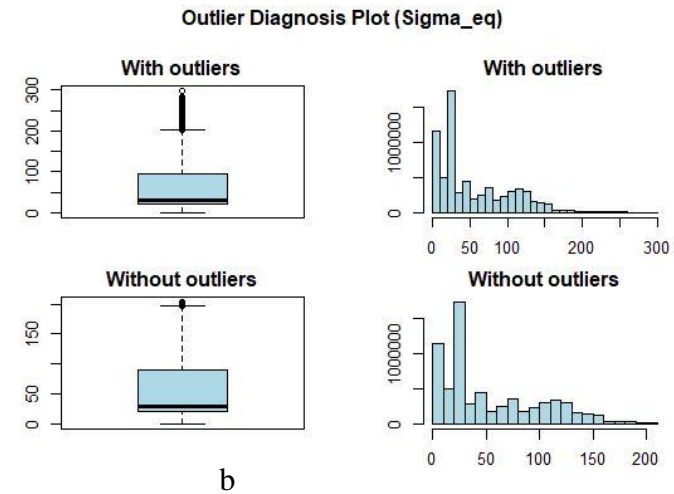
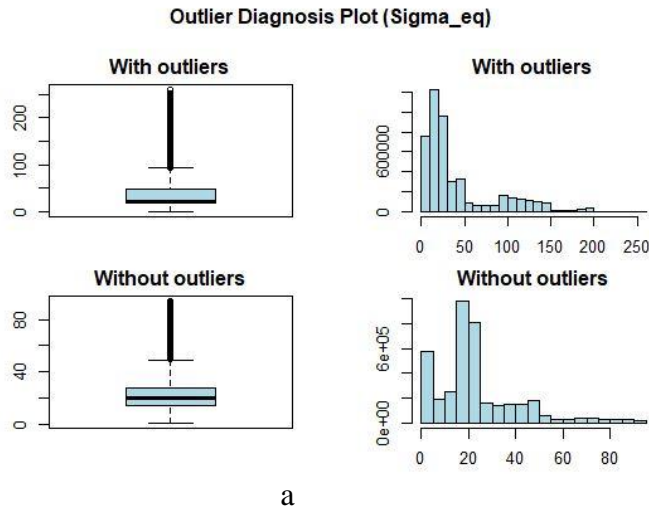


Figure 9-4 : Outlier Diagnosis Results for Rig 1 Main Well Datasets from January 2015 (a)-December 2015 (b)

Diagnosis of numerical variable outliers

variables	min	median	max	outlier	outlier ratio(%)
Sigma_eq	1	36	290	57,768	0.78

2.2 Detailed outliers diagnosis

variable : Sigma_eq

Outliers information of Sigma_eq

Measures	Values
Outliers count	57768.00
Outliers ratio (%)	0.78
Mean of outliers	195.35
Mean with outliers	56.65
Mean without outliers	55.56

Outlier Diagnosis Plot (Sigma_eq)

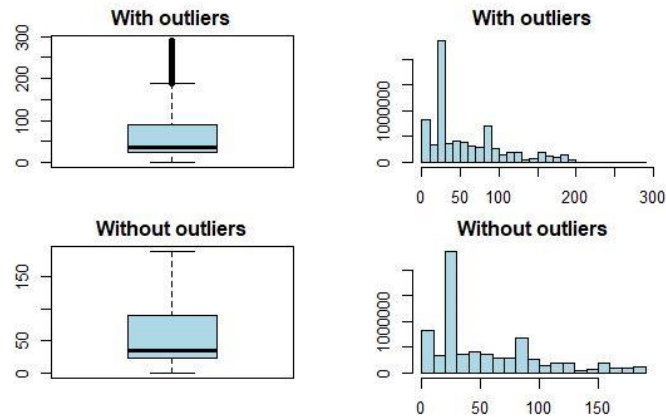


Figure 9-5 : Outlier Diagnosis Results for Rig 1 Main Well Datasets from January-July 2016

Rig 1: Auxiliary Well

Diagnosis of numerical variable outliers

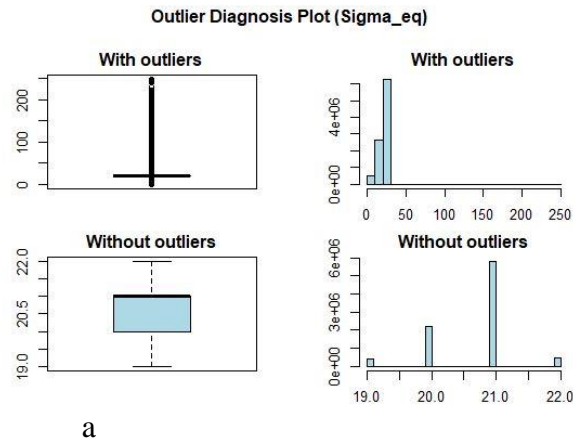
variables	min	median	max	outlier	outlier ratio(%)
Sigma_eq	1	21	248	526,322	5.6

2.2 Detailed outliers diagnosis

variable : Sigma_eq

Outliers information of Sigma_eq

Measures	Values
Outliers count	526322.00
Outliers ratio (%)	5.60
Mean of outliers	4.38
Mean with outliers	19.80
Mean without outliers	20.71



Diagnosis of numerical variable outliers

variables	min	median	max	outlier	outlier ratio(%)
Sigma_eq	1	21	291	3,834,356	29.89

2.2 Detailed outliers diagnosis

variable : Sigma_eq

Outliers information of Sigma_eq

Measures	Values
Outliers count	3834356.00
Outliers ratio (%)	29.89
Mean of outliers	19.94
Mean with outliers	20.68
Mean without outliers	21.00

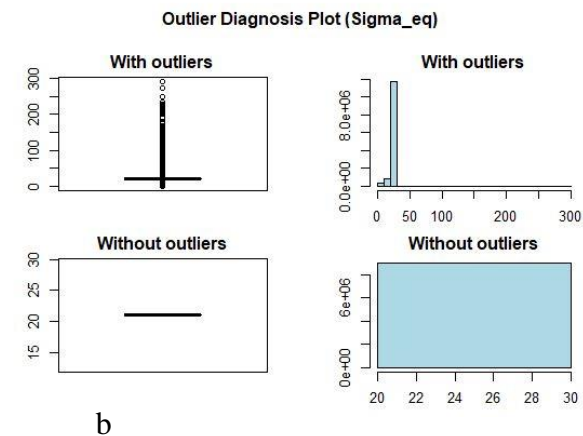


Figure 9-6 : Outlier Diagnosis Results for Rig 1 Auxiliary Well Datasets from January 2014 (a)-December 2014 (b)

Diagnosis of numerical variable outliers

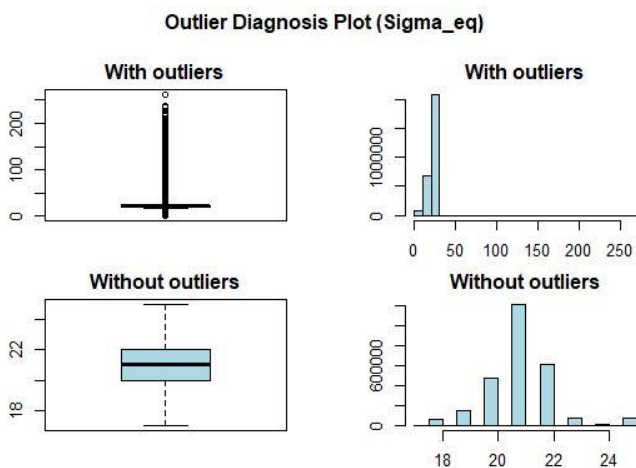
variables	min	median	max	outlier	outlier ratio(%)
Sigma_eq	1	21	262	186,521	6.58

2.2 Detailed outliers diagnosis

variable : Sigma_eq

Outliers information of Sigma_eq

Measures	Values
Outliers count	186521.00
Outliers ratio (%)	6.58
Mean of outliers	17.40
Mean with outliers	20.80
Mean without outliers	21.04



a

Diagnosis of numerical variable outliers

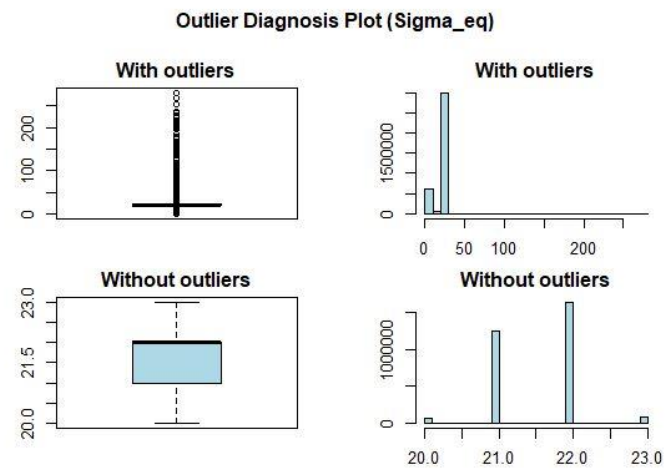
variables	min	median	max	outlier	outlier ratio(%)
Sigma_eq	1	21	280	626,647	17.14

2.2 Detailed outliers diagnosis

variable : Sigma_eq

Outliers information of Sigma_eq

Measures	Values
Outliers count	626647.00
Outliers ratio (%)	17.14
Mean of outliers	3.22
Mean with outliers	18.43
Mean without outliers	21.58



b

Figure 9-7 : Outlier Diagnosis Results for Rig 1 Auxiliary Well Datasets from January 2015 (a)-December 2015 (b)

Diagnosis of numerical variable outliers

variables	min	median	max	outlier	outlier ratio(%)
Sigma_eq	1	22	278	31,050	0.74

2.2 Detailed outliers diagnosis

variable : Sigma_eq

Outliers information of Sigma_eq

Measures	Values
Outliers count	31050.00
Outliers ratio (%)	0.74
Mean of outliers	21.97
Mean with outliers	21.76
Mean without outliers	21.75

Outlier Diagnosis Plot (Sigma_eq)

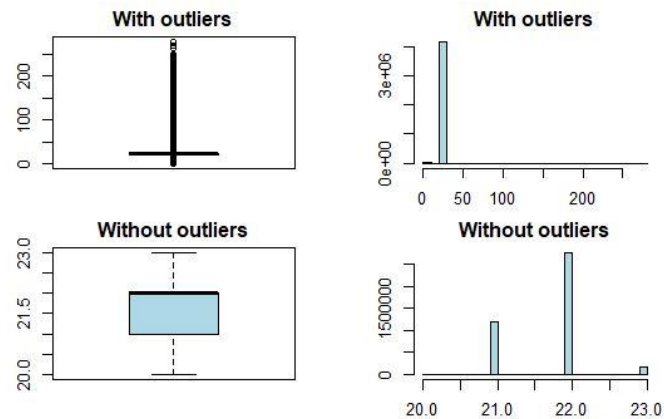


Figure 9-8 : Outlier Diagnosis Results for Rig 1 Auxiliary Well Dataset from January-July 2016

Rig 2: Main Well

Diagnosis of numerical variable outliers

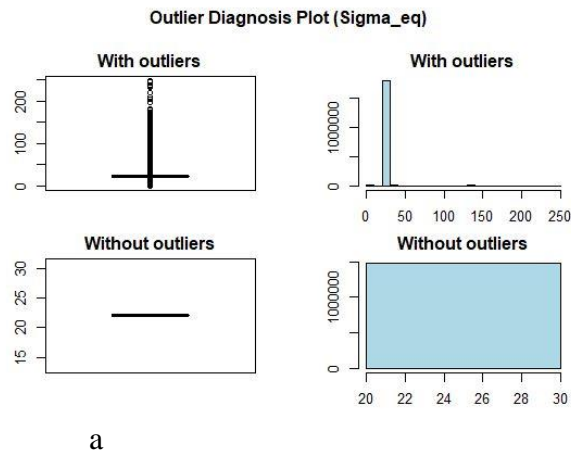
variables	min	median	max	outlier	outlier ratio(%)
Sigma_eq	1	22	248	367,430	19.93

2.2 Detailed outliers diagnosis

variable : Sigma_eq

Outliers information of Sigma_eq

Measures	Values
Outliers count	367430.00
Outliers ratio (%)	19.93
Mean of outliers	25.77
Mean with outliers	22.75
Mean without outliers	22.00



Diagnosis of numerical variable outliers

variables	min	median	max	outlier	outlier ratio(%)
Sigma_eq	1	22	293	3,284,948	29.87

2.2 Detailed outliers diagnosis

variable : Sigma_eq

Outliers information of Sigma_eq

Measures	Values
Outliers count	3284948.00
Outliers ratio (%)	29.87
Mean of outliers	24.51
Mean with outliers	22.71
Mean without outliers	21.95

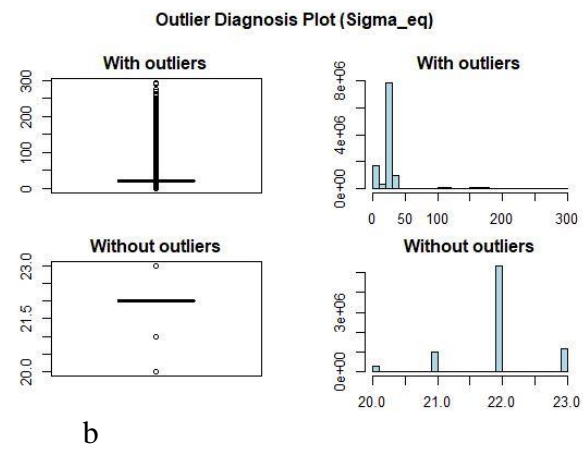


Figure 9-9 : Outlier Diagnosis Results for Rig 2 Main Well Datasets from July 2014 (a)-July 2015 (b)

Diagnosis of numerical variable outliers

variables	min	median	max	outlier	outlier ratio(%)
Sigma_eq	1	13	272	50,878	1.15

2.2 Detailed outliers diagnosis

variable : Sigma_eq

Outliers information of Sigma_eq

Measures	Values
Outliers count	50878.00
Outliers ratio (%)	1.15
Mean of outliers	76.16
Mean with outliers	16.10
Mean without outliers	15.40

Diagnosis of numerical variable outliers

variables	min	median	max	outlier	outlier ratio(%)
Sigma_eq	1	24	289	257,961	3.49

2.2 Detailed outliers diagnosis

variable : Sigma_eq

Outliers information of Sigma_eq

Measures	Values
Outliers count	257961.00
Outliers ratio (%)	3.49
Mean of outliers	114.95
Mean with outliers	34.57
Mean without outliers	31.66

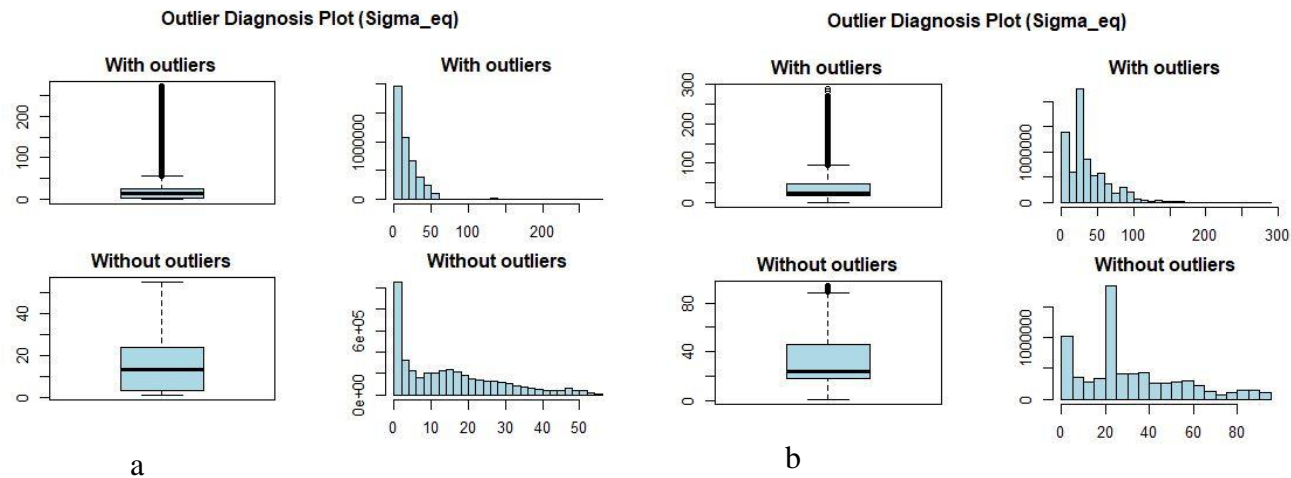


Figure 9-10 : Outlier Diagnosis Results for Rig 2 Main Well Datasets from July 2015 (a)-July 2016 (b)

Rig 2: Auxiliary Well

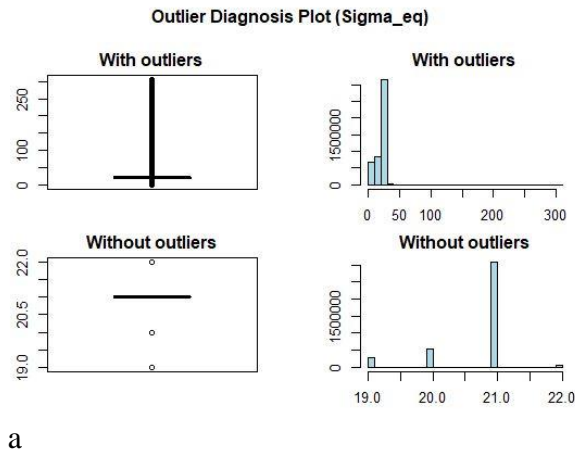
Diagnosis of numerical variable outliers					
variables	min	median	max	outlier	outlier ratio(%)
Sigma_eq	1	21	305	692,340	14.89

2.2 Detailed outliers diagnosis

variable : Sigma_eq

Outliers information of Sigma_eq

Measures	Values
Outliers count	692340.00
Outliers ratio (%)	14.89
Mean of outliers	3.22
Mean with outliers	18.13
Mean without outliers	20.74



Diagnosis of numerical variable outliers					
variables	min	median	max	outlier	outlier ratio(%)
Sigma_eq	1	21	293	447,641	3.45

2.2 Detailed outliers diagnosis

variable : Sigma_eq

Outliers information of Sigma_eq

Measures	Values
Outliers count	447641.00
Outliers ratio (%)	3.45
Mean of outliers	35.31
Mean with outliers	21.25
Mean without outliers	20.74

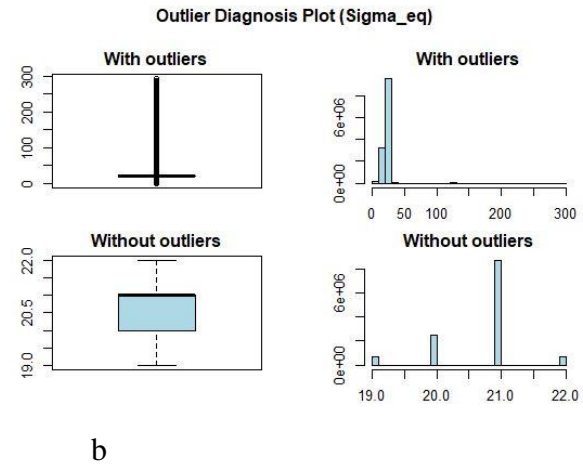


Figure 9-11: Outlier Diagnosis Results for Rig 2 Auxiliary Well Datasets from July 2014 (a) -July 2015 (b)

Diagnosis of numerical variable outliers

variables	min	median	max	outlier	outlier ratio(%)
Sigma_eq	1	1	284	12,367	11.09

Diagnosis of numerical variable outliers

variables	min	median	max	outlier	outlier ratio(%)
Sigma_eq	1	21	293	1,916,111	42.95

2.2 Detailed outliers diagnosis

variable : Sigma_eq

Outliers information of Sigma_eq

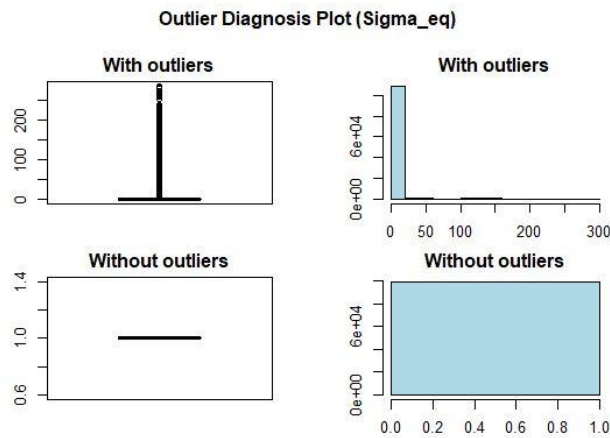
Measures	Values
Outliers count	12367.00
Outliers ratio (%)	11.09
Mean of outliers	22.53
Mean with outliers	3.39
Mean without outliers	1.00

2.2 Detailed outliers diagnosis

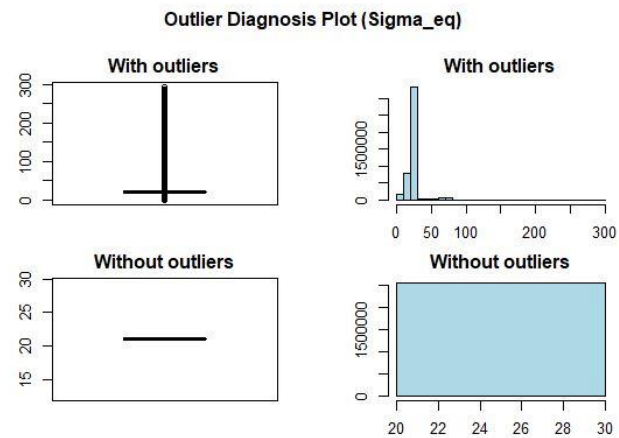
variable : Sigma_eq

Outliers information of Sigma_eq

Measures	Values
Outliers count	1916111.00
Outliers ratio (%)	42.95
Mean of outliers	23.14
Mean with outliers	21.92
Mean without outliers	21.00



a



b

Figure 9-12: Outlier Diagnosis Results for Rig 2 Auxiliary Well Datasets from July 2015 (a) -July 2016 (b)

Rig 3 : Main Well

Outlier Diagnosis Results for Rig 3 Main Well Datasets from July 2014 (a) - July 2015 (b)

Diagnosis of numerical variable outliers

variables	min	median	max	outlier	outlier ratio(%)
Sigma_eq	1	56	227	7	0

2.1.1 Diagnosis of numerical variable outliers

No numeric variables including outliers

2.2 Detailed outliers diagnosis

variable : Sigma_eq

Outliers information of Sigma_eq

Measures	Values
Outliers count	7.00
Outliers ratio (%)	0.00
Mean of outliers	219.14
Mean with outliers	48.49
Mean without outliers	48.48

2.2 Detailed outliers diagnosis

variable : Sigma_eq

Outliers information of Sigma_eq

Measures	Values
Outliers count	0.00
Outliers ratio (%)	0.00
Mean of outliers	NaN
Mean with outliers	20.72
Mean without outliers	20.72

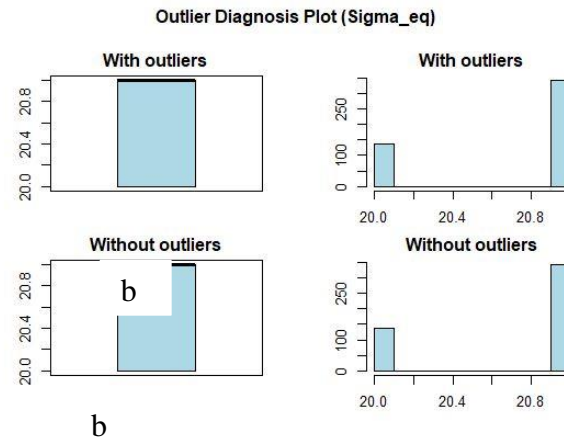
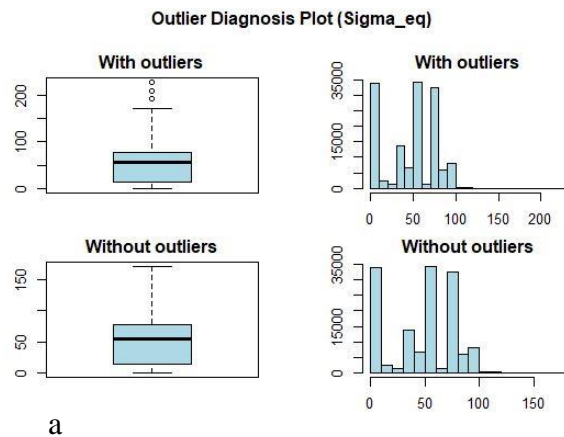


Figure 9-13 : Outlier Diagnosis Results for Rig 3 Main Well Datasets from July 2014 (a) - July 2015 (b)

Diagnosis of numerical variable outliers

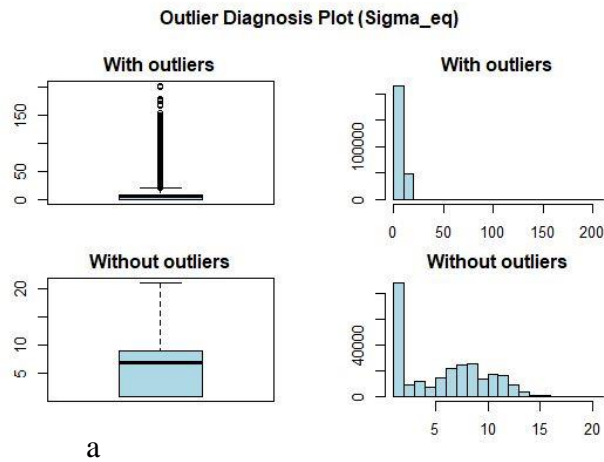
variables	min	median	max	outlier	outlier ratio(%)
Sigma_eq	1	7	203	1,461	0.56

2.2 Detailed outliers diagnosis

variable : Sigma_eq

Outliers information of Sigma_eq

Measures	Values
Outliers count	1461.00
Outliers ratio (%)	0.56
Mean of outliers	94.46
Mean with outliers	6.49
Mean without outliers	6.00



Diagnosis of numerical variable outliers

variables	min	median	max	outlier	outlier ratio(%)
Sigma_eq	1	20	272	86,298	2.64

2.2 Detailed outliers diagnosis

variable : Sigma_eq

Outliers information of Sigma_eq

Measures	Values
Outliers count	86298.00
Outliers ratio (%)	2.64
Mean of outliers	89.52
Mean with outliers	16.21
Mean without outliers	14.22

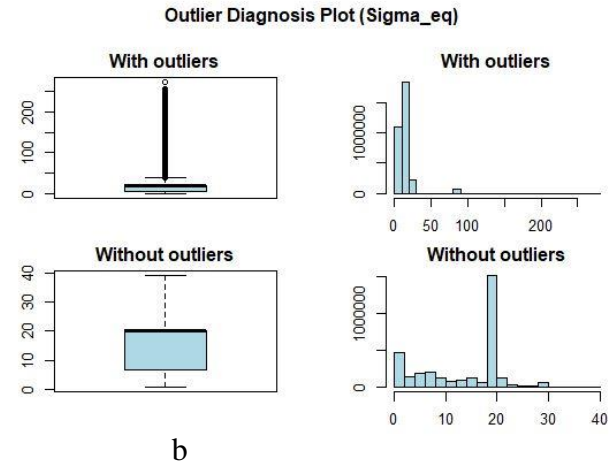


Figure 9-14 : Outlier Diagnosis Results for Rig 3 Main Well Datasets from July 2015 (a) - July 2016 (b)

Rig 3: Auxiliary Well

Diagnosis of numerical variable outliers

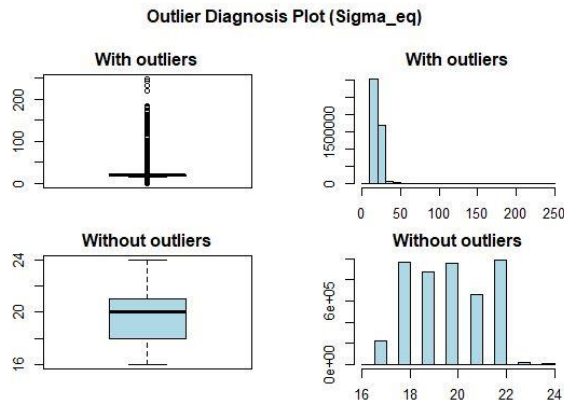
variables	min	median	max	outlier	outlier ratio(%)
Sigma_eq	1	20	248	73,944	1.55

2.2 Detailed outliers diagnosis

variable : Sigma_eq

Outliers information of Sigma_eq

Measures	Values
Outliers count	73944.00
Outliers ratio (%)	1.55
Mean of outliers	33.97
Mean with outliers	20.06
Mean without outliers	19.84



a

Diagnosis of numerical variable outliers

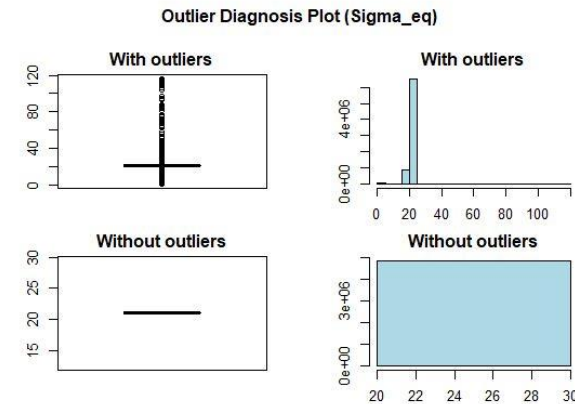
variables	min	median	max	outlier	outlier ratio(%)
Sigma_eq	1	21	116	2,570,114	34.65

2.2 Detailed outliers diagnosis

variable : Sigma_eq

Outliers information of Sigma_eq

Measures	Values
Outliers count	2570114.00
Outliers ratio (%)	34.65
Mean of outliers	20.92
Mean with outliers	20.97
Mean without outliers	21.00



b

Figure 9-15: Outlier Diagnosis Results for Rig 3 Auxiliary Well Datasets from July 2014 (a) - July 2015 (b)

Diagnosis of numerical variable outliers

variables	min	median	max	outlier	outlier ratio(%)
Sigma_eq	1	5	237	39,371	23.14

Diagnosis of numerical variable outliers

variables	min	median	max	outlier	outlier ratio(%)
Sigma_eq	1	22	272	217,363	22.38

2.2 Detailed outliers diagnosis

variable : Sigma_eq

Outliers information of Sigma_eq

Measures	Values
Outliers count	39371.00
Outliers ratio (%)	23.14
Mean of outliers	1.82
Mean with outliers	4.09
Mean without outliers	4.78

2.2 Detailed outliers diagnosis

variable : Sigma_eq

Outliers information of Sigma_eq

Measures	Values
Outliers count	217363.00
Outliers ratio (%)	22.38
Mean of outliers	38.08
Mean with outliers	25.35
Mean without outliers	21.67

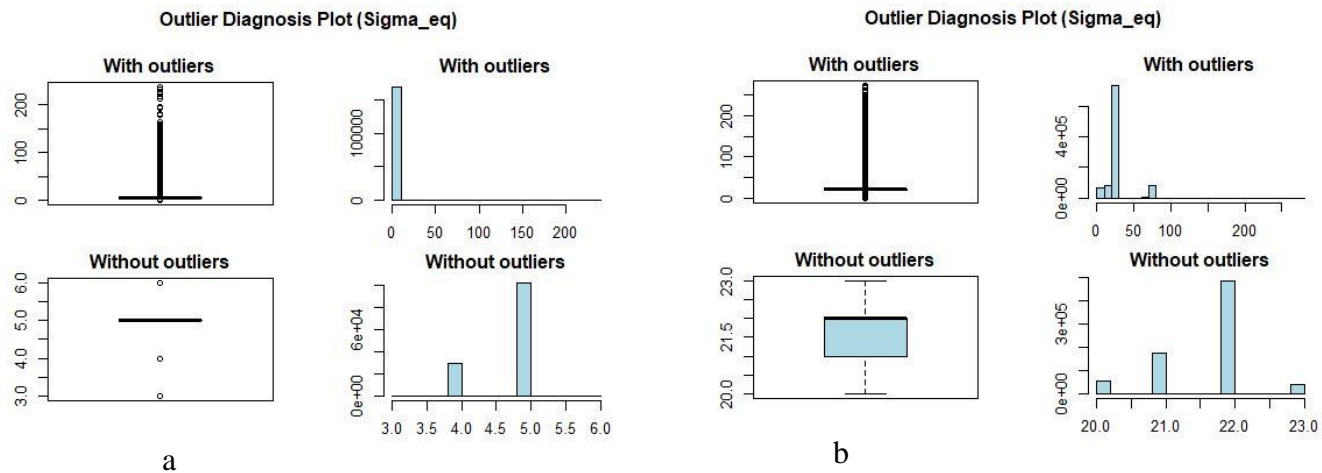


Figure 9-16 : Outlier Diagnosis Results for Rig 3 Auxiliary Well Datasets from July 2015 (a) - July 2016 (b)

Appendix D: Stress Time-Series Graphs

Rig 1: Main Well

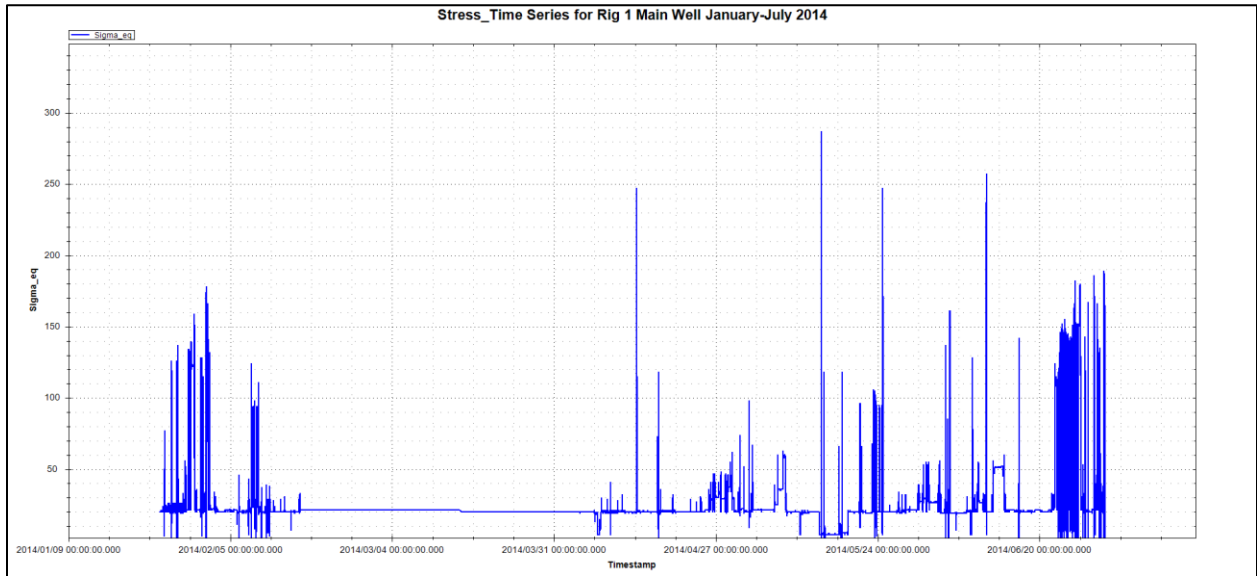


Figure 9-17: Equivalent Stress Time Series Rig 1 Main Well January – July 2014

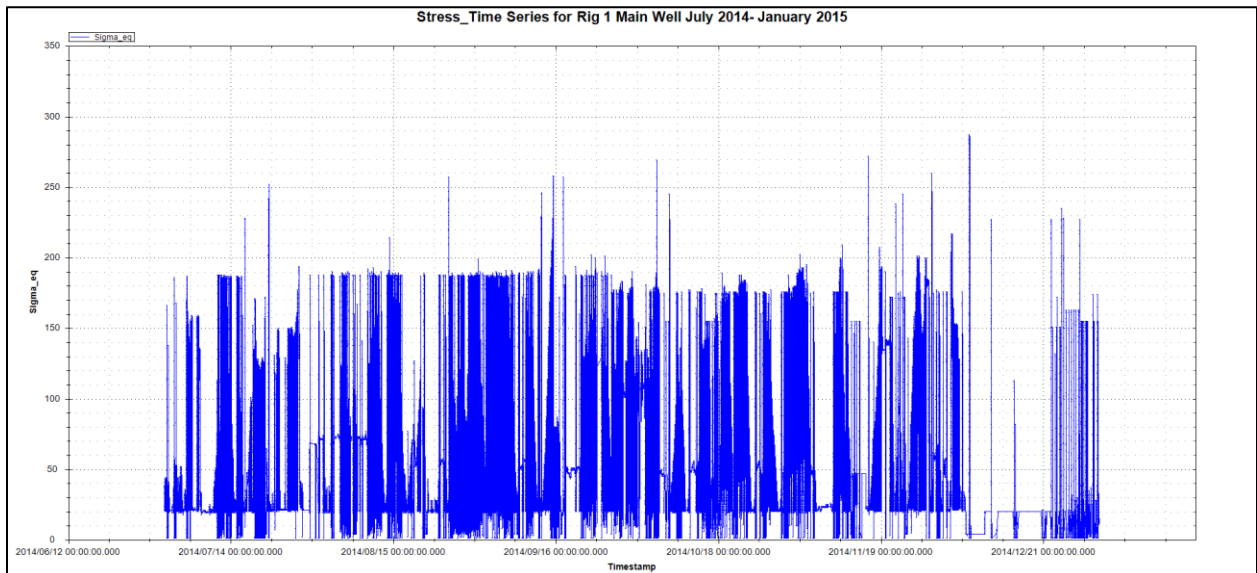


Figure 9-18 : Equivalent Stress Time Series Rig 1 Main Well July 2014- January 2015

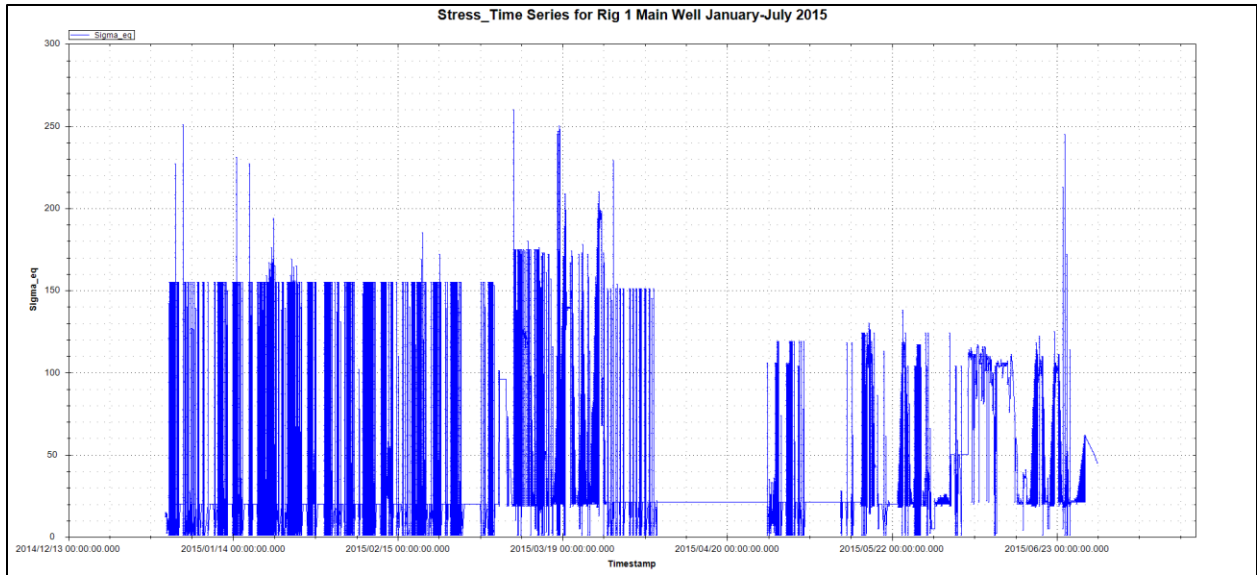


Figure 9-19 : Equivalent Stress Time Series Rig 1 Main Well January - July 2015

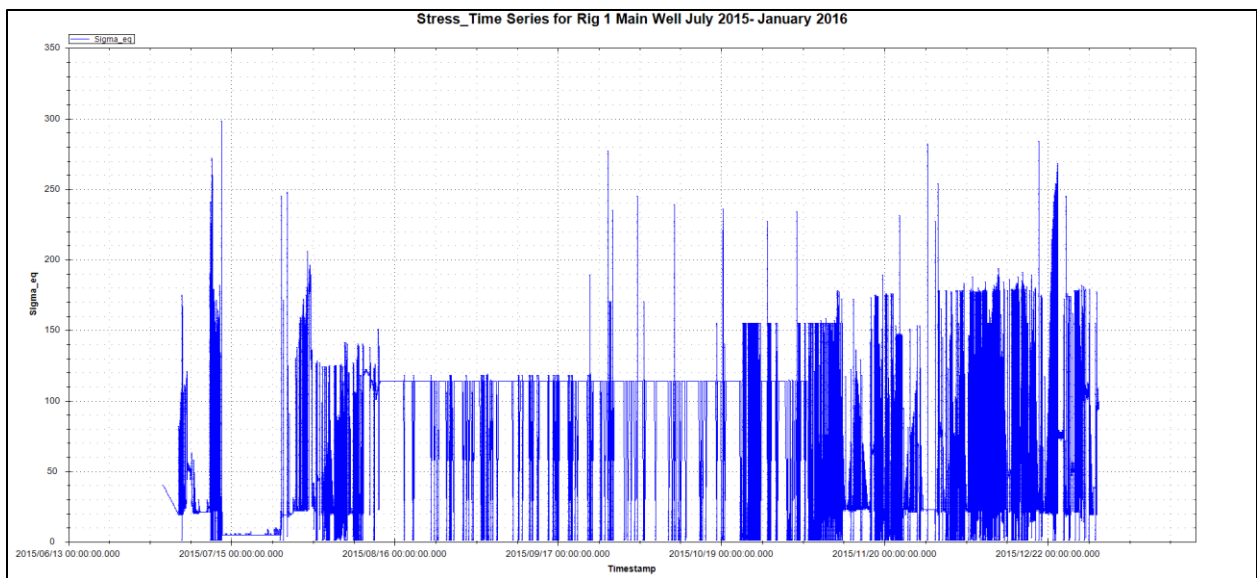


Figure 9-20 : Equivalent Stress Time Series Rig 1 Main Well July 2015- January 2016

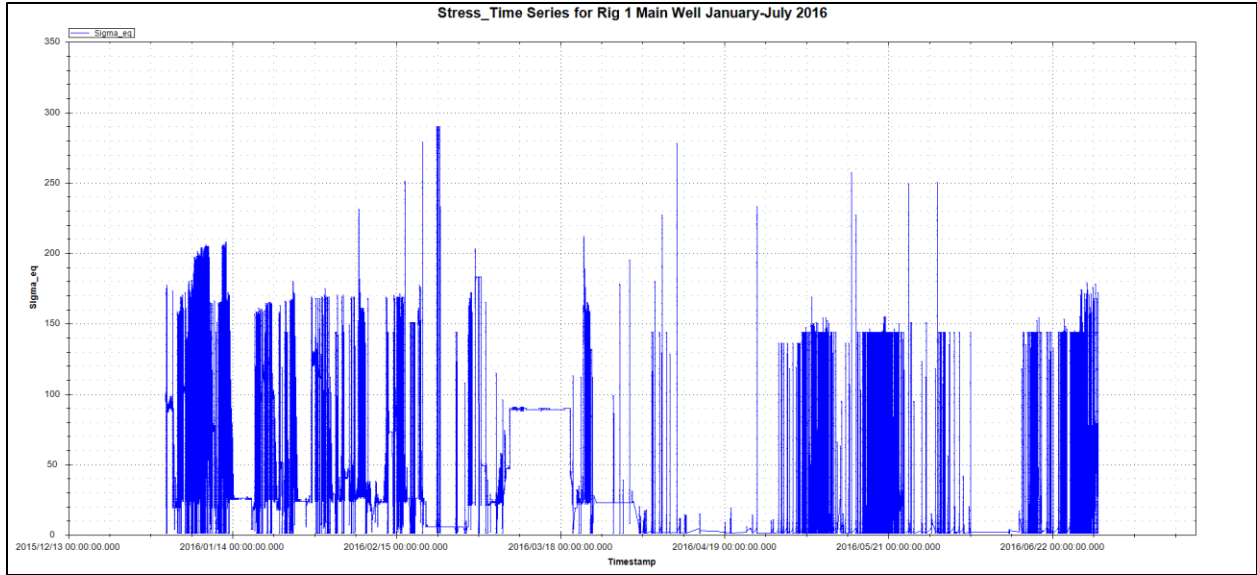


Figure 9-21 : Equivalent Stress Time Series Rig 1 Main Well January - July 2016

Rig 1: Auxiliary Well

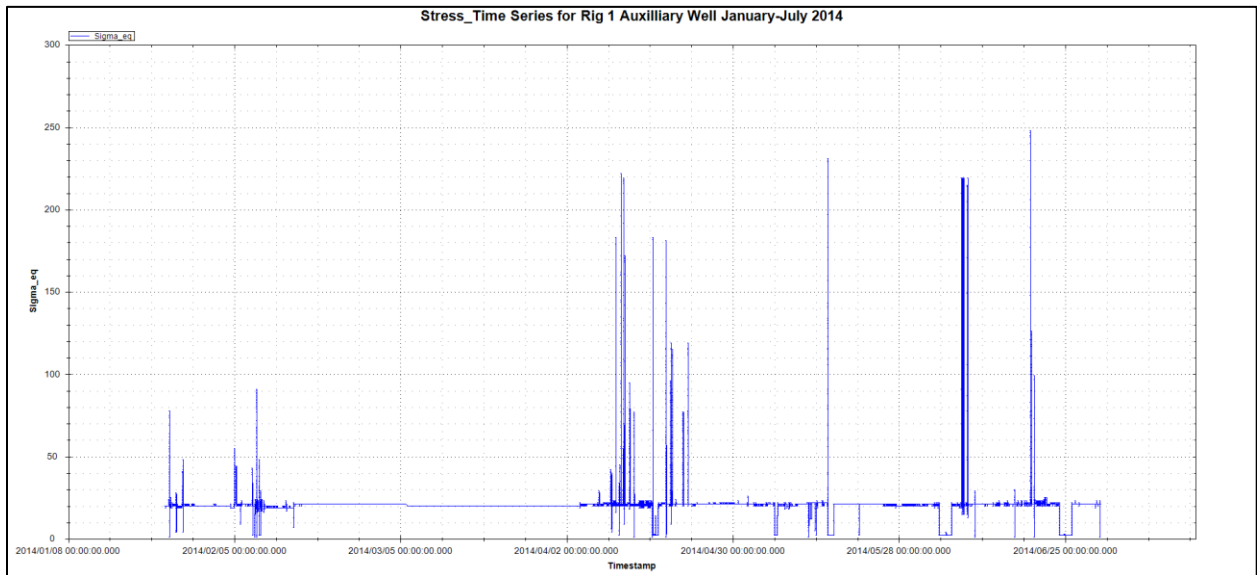


Figure 9-22 : Equivalent Stress Time Series Rig 1 Auxilliary Well January - July 2014

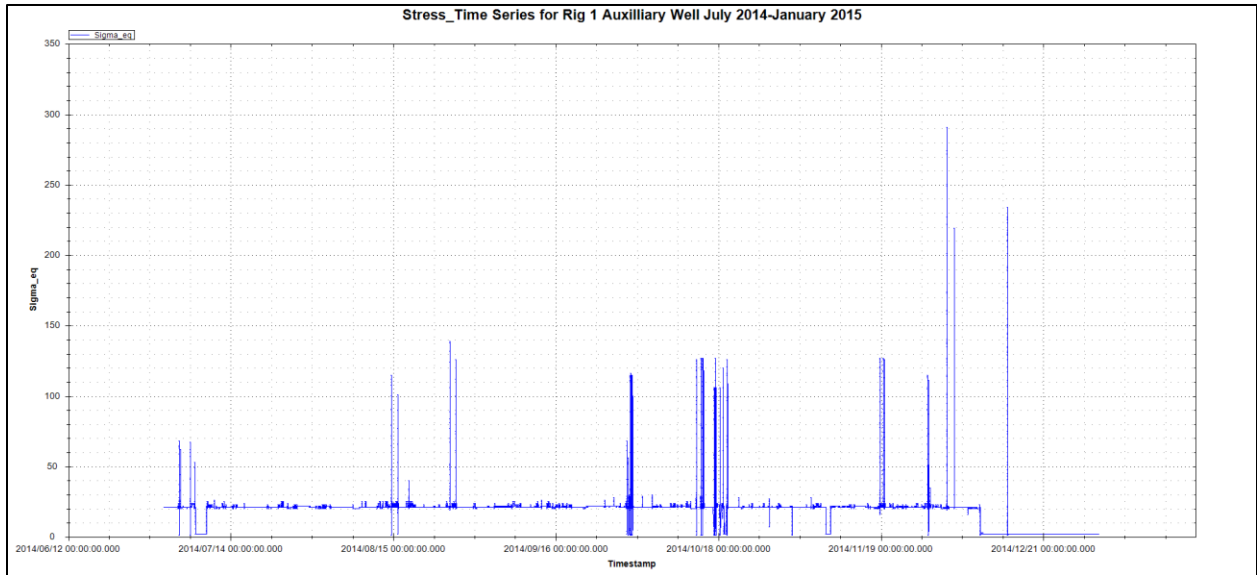


Figure 9-23 : Equivalent Stress Time Series Rig 1 Auxiliary Well July 2014 - January 2015

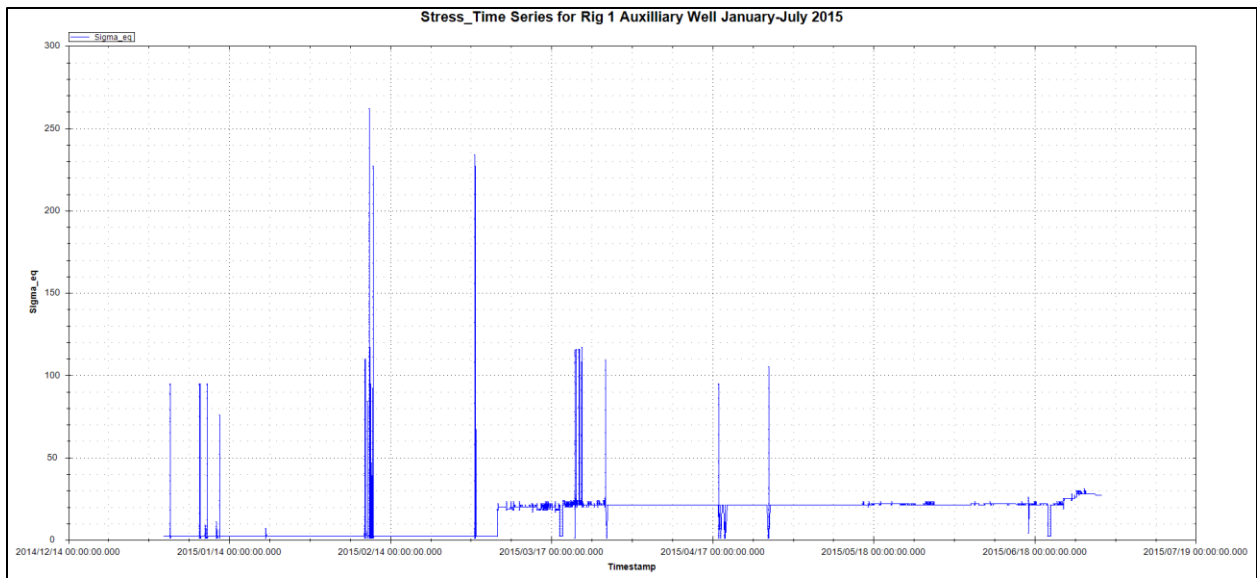


Figure 9-24 : Equivalent Stress Time Series Rig 1 Auxiliary Well January - July 2015

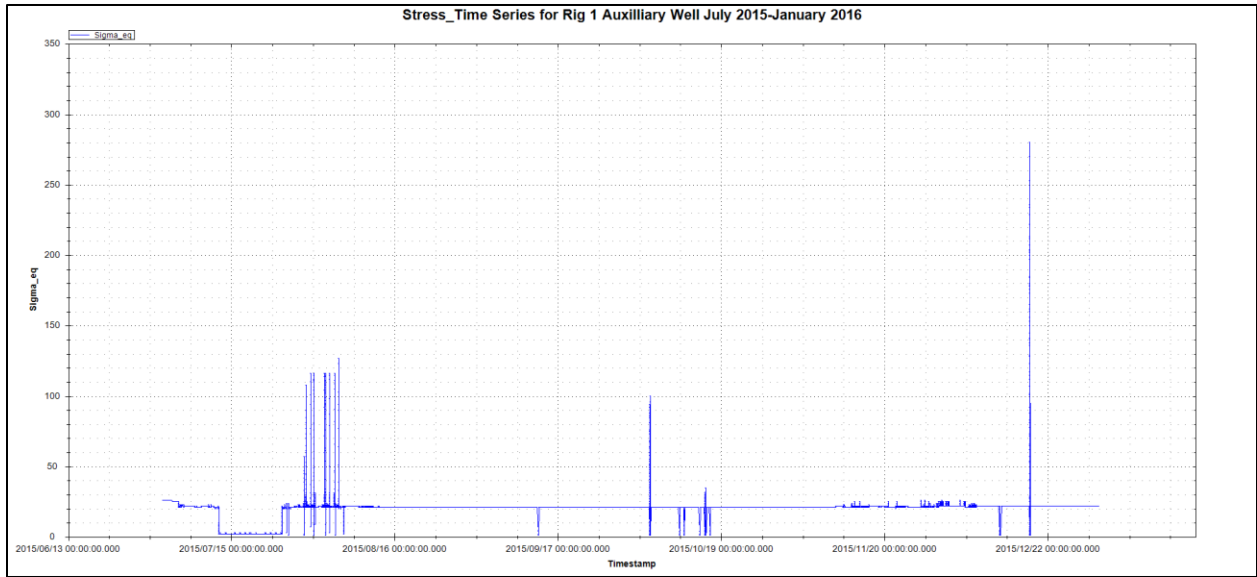


Figure 9-25 : Equivalent Stress Time Series Rig 1 Auxilliary Well July 2015 - January 2016

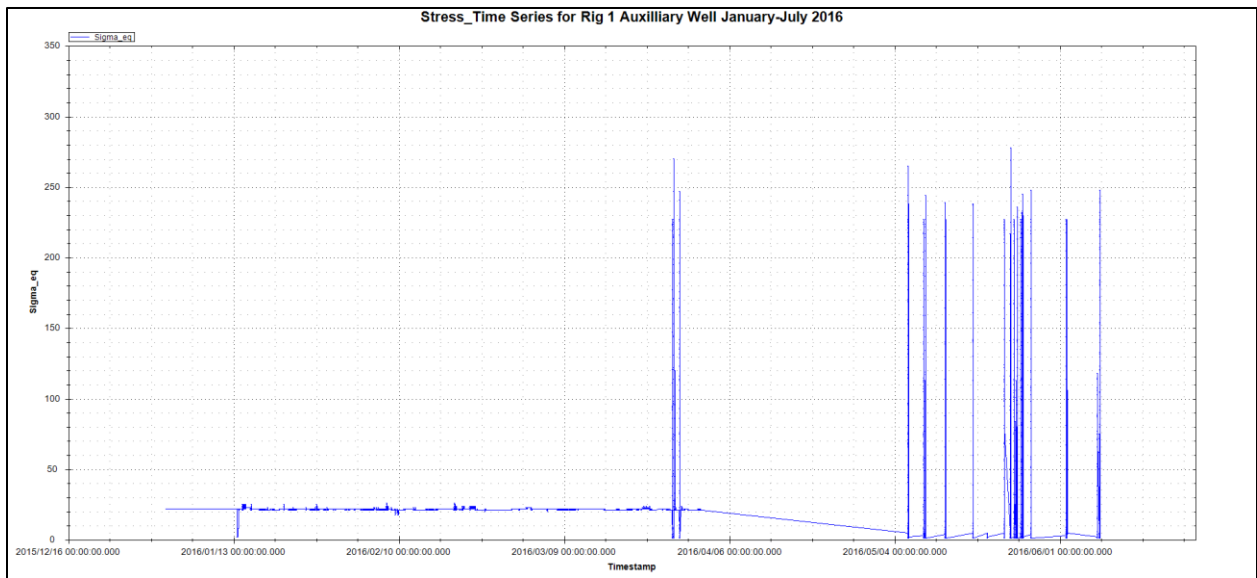


Figure 9-26 : Equivalent Stress Time Series Rig 1 Auxilliary Well January - July 2016

Rig 2: Main Well

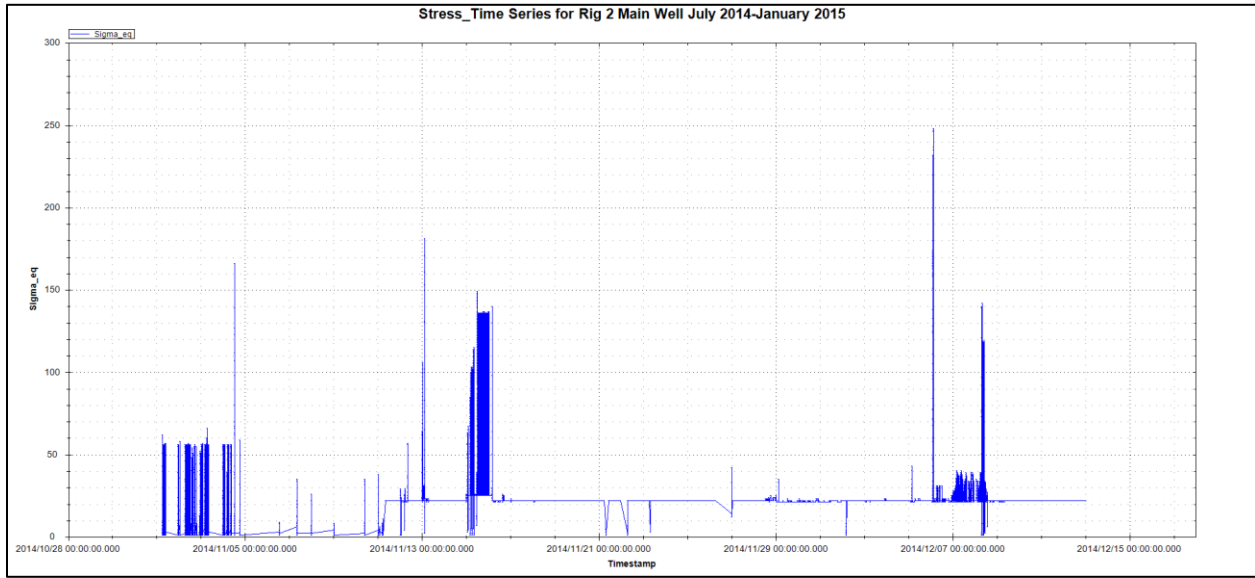


Figure 9-27 : Equivalent Stress Time Series Rig 2 Main Well July 2014 – January 2015

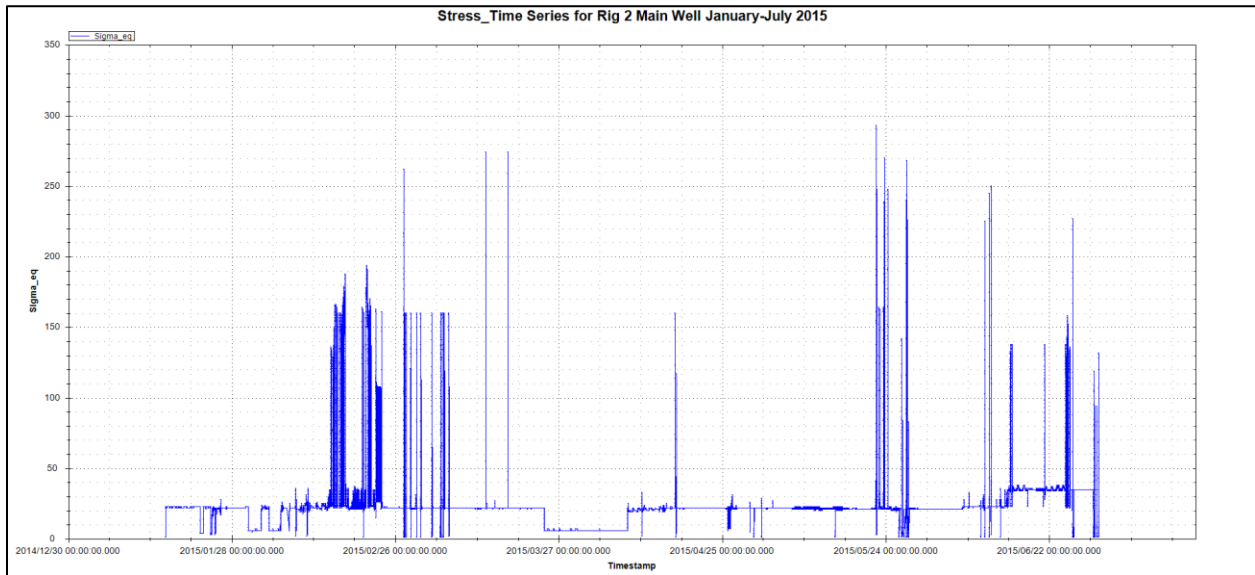


Figure 9-28 : Equivalent Stress Time Series Rig 2 Main Well January- July 2015

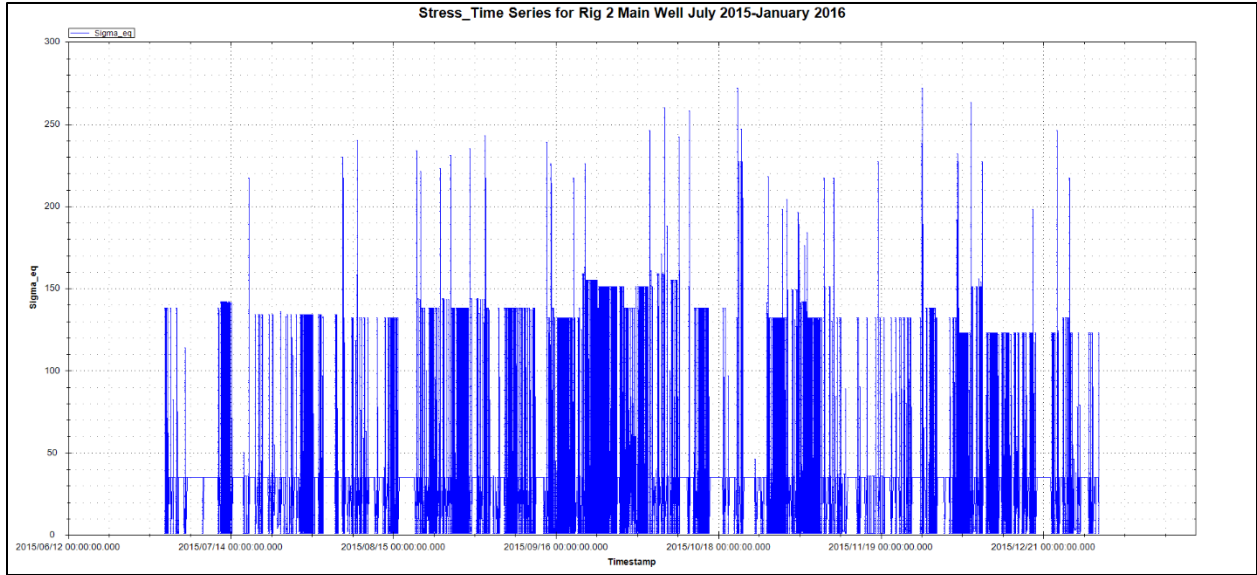


Figure 9-29 : Equivalent Stress Time Series Rig 2 Main Well July 2015 – January 2016

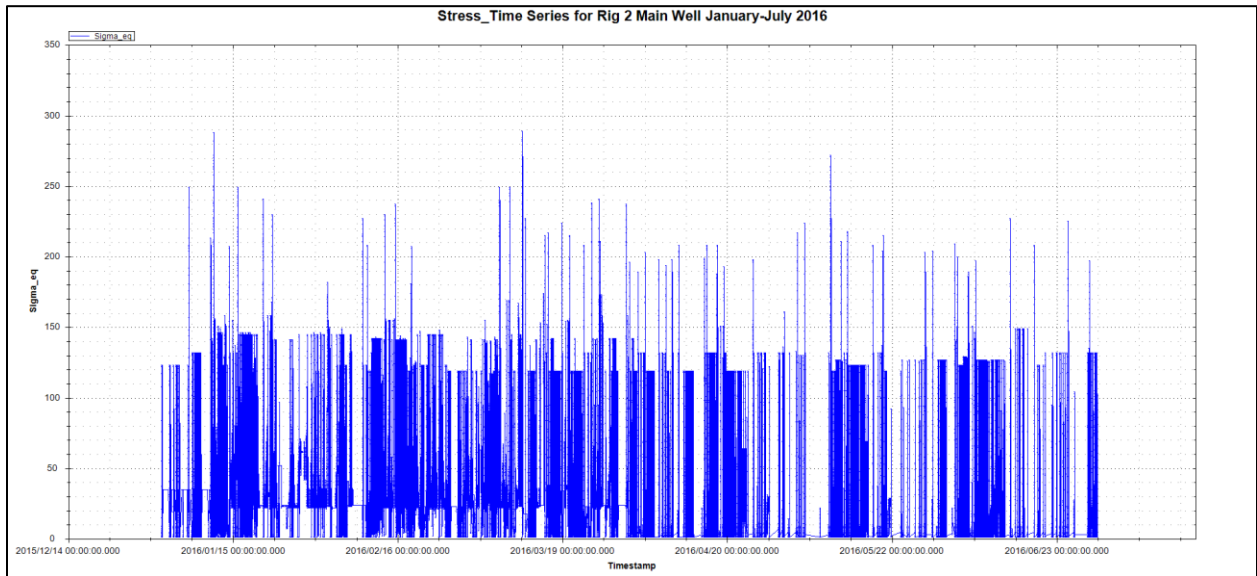


Figure 9-30 : Equivalent Stress Time Series Rig 2 Main Well January - July 2016

Rig 2: Auxiliary Well

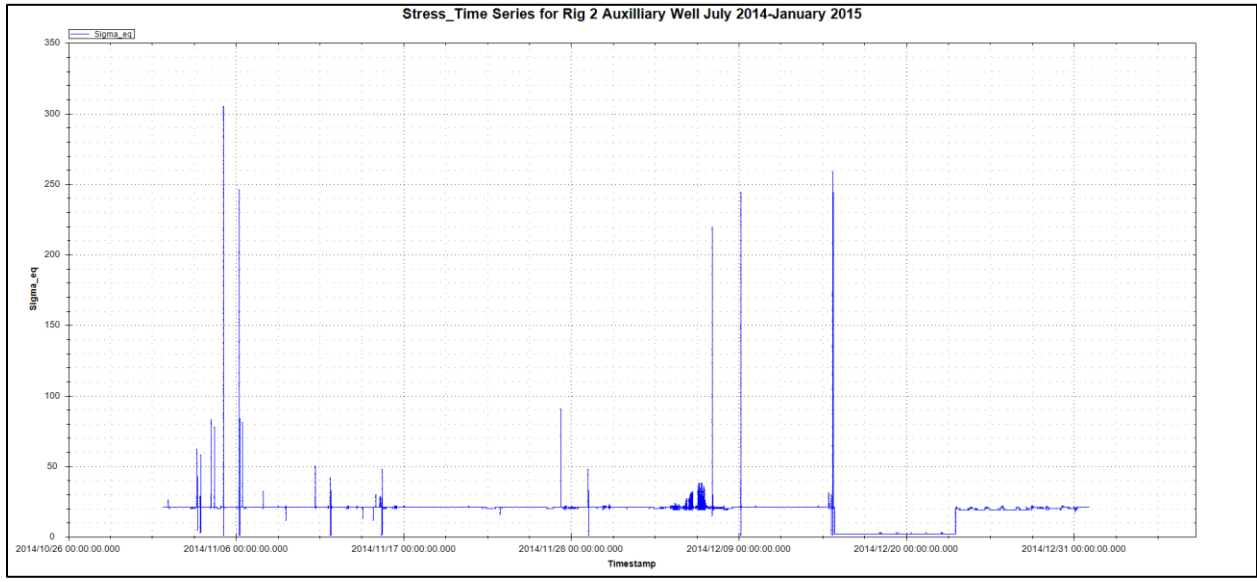


Figure 9-31 : Equivalent Stress Time Series Rig 2 Auxiliary Well July 2014 – January 2015

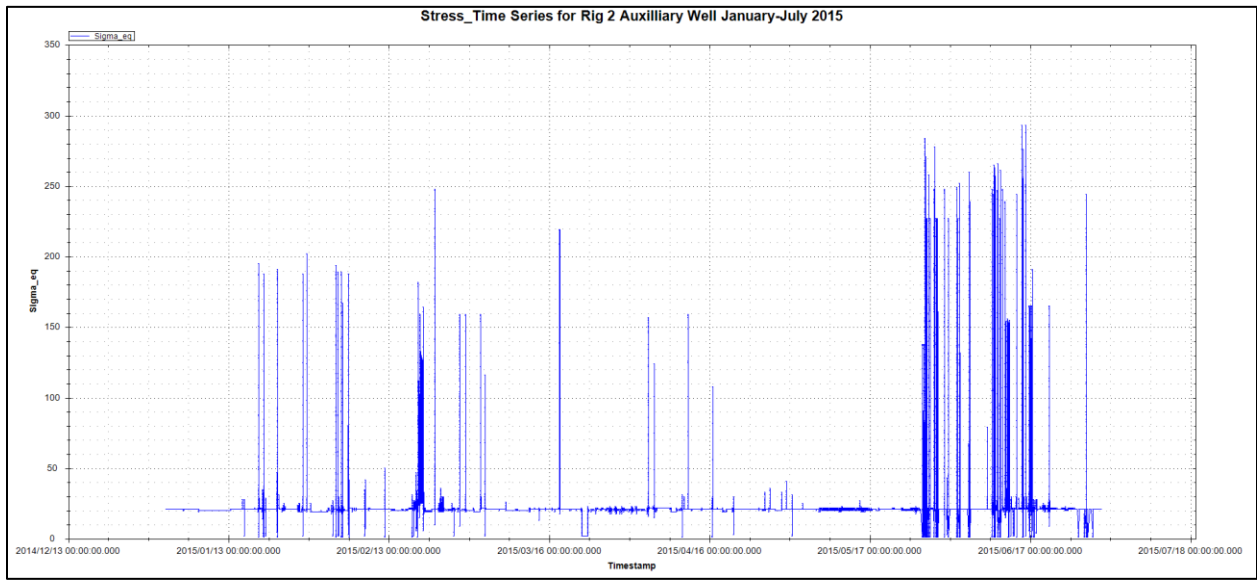


Figure 9-32 : Equivalent Stress Time Series Rig 2 Auxiliary Well January-July 2015

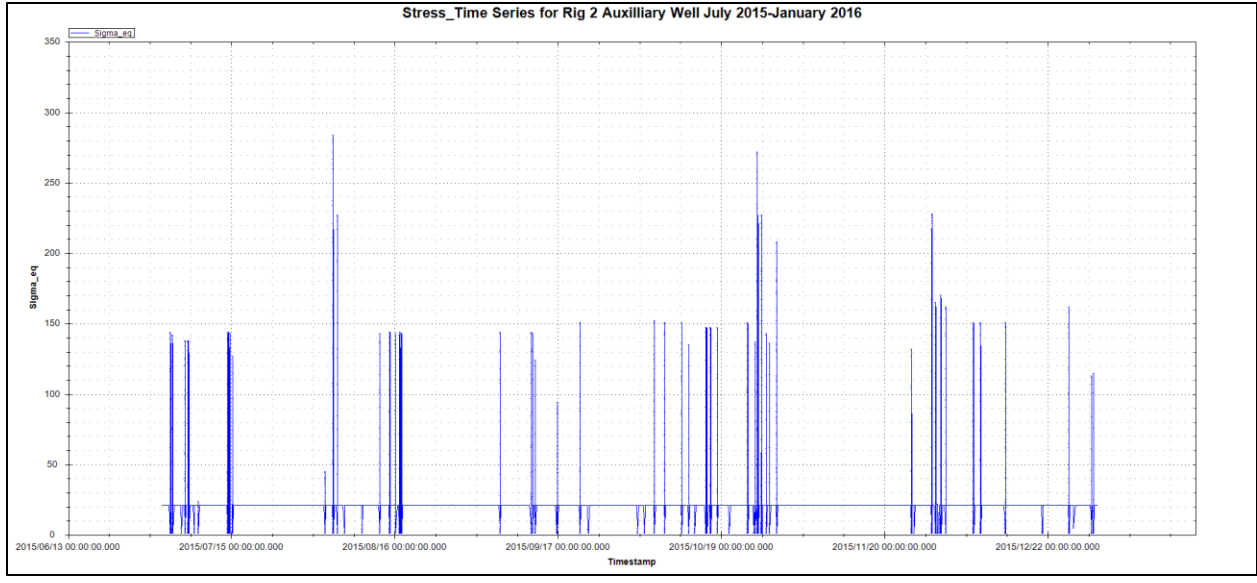


Figure 9-33 : Equivalent Stress Time Series Rig 2 Auxiliary Well July 2015 – January 2016

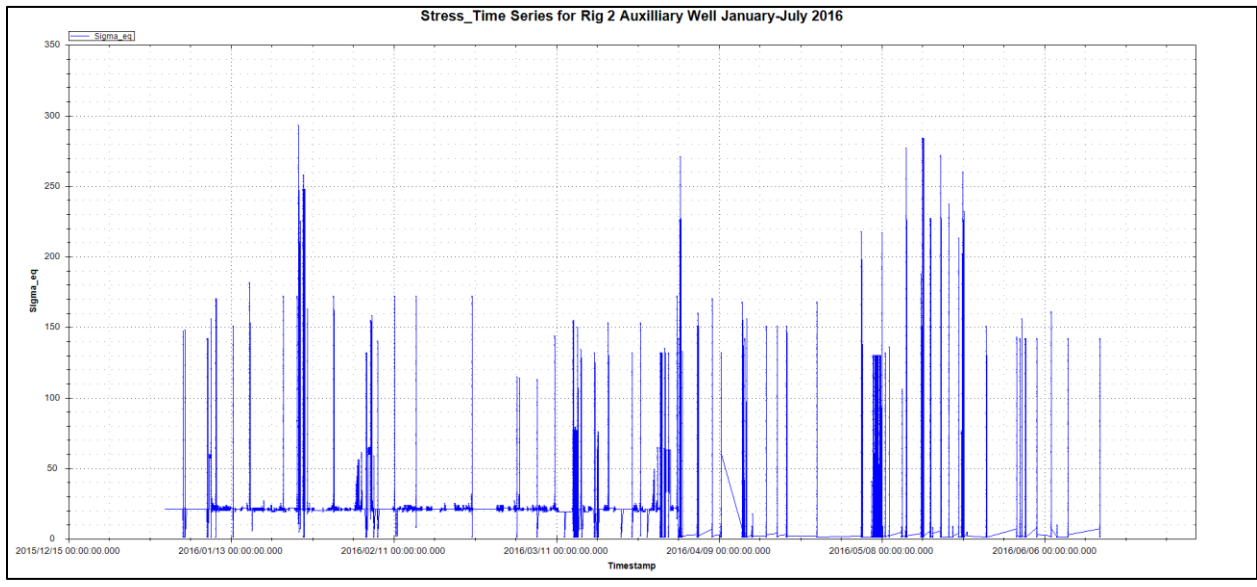


Figure 9-34 : Equivalent Stress Time Series Rig 2 Auxiliary Well January-July 2016

Rig 3: Main Well

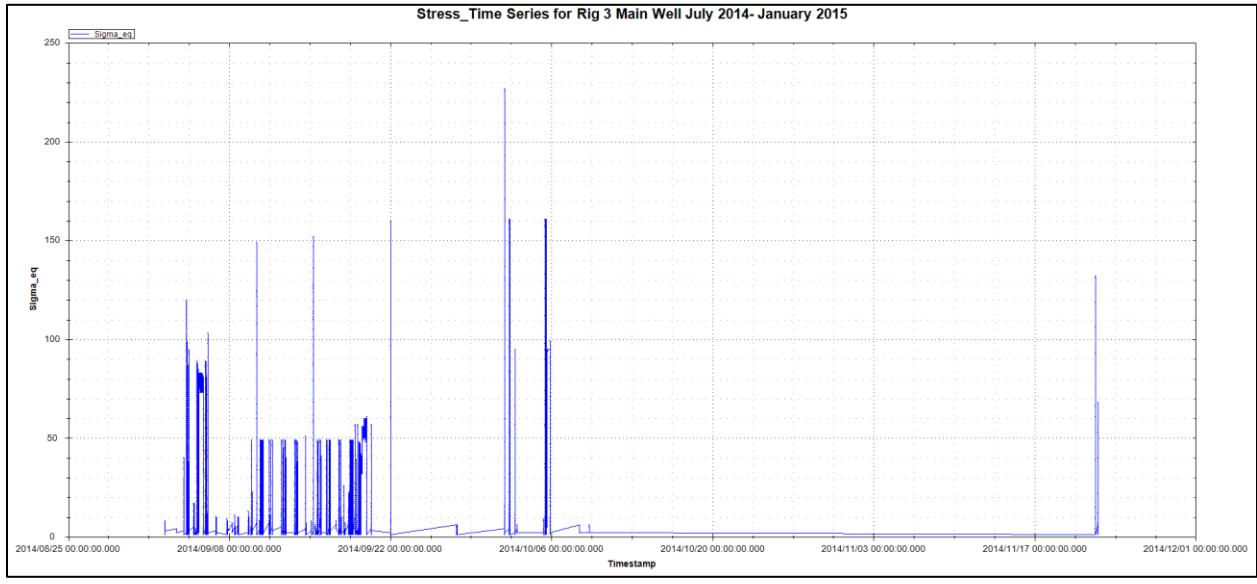


Figure 9-35 : Equivalent Stress Time Series Rig 3 Main Well July 2014 – January 2015

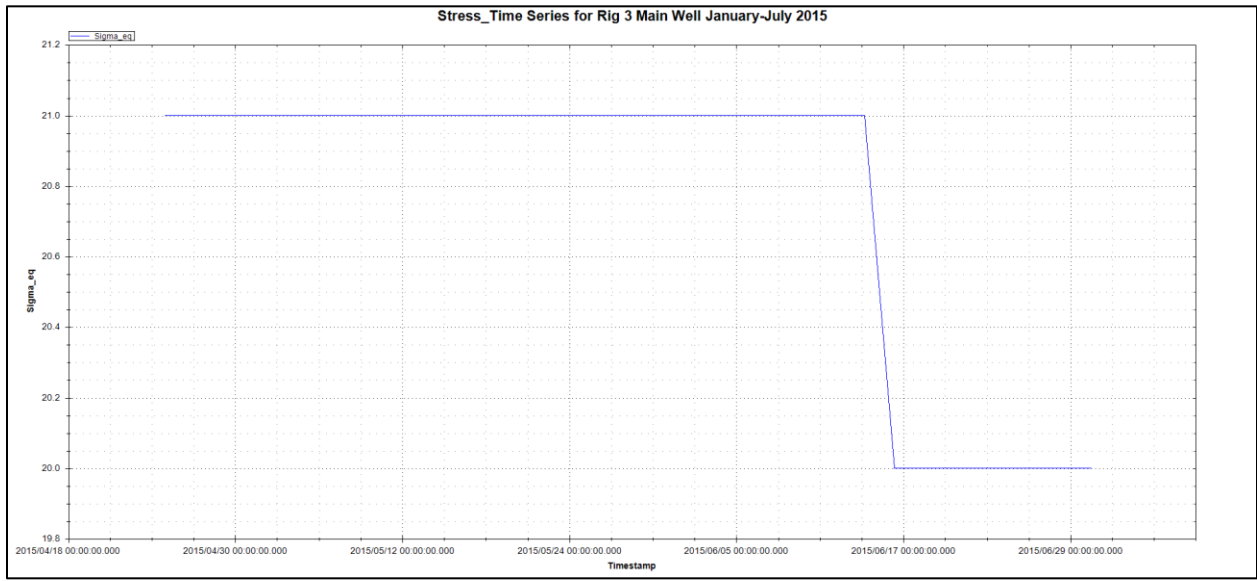


Figure 9-36 : Equivalent Stress Time Series Rig 3 Main Well January - July 2015

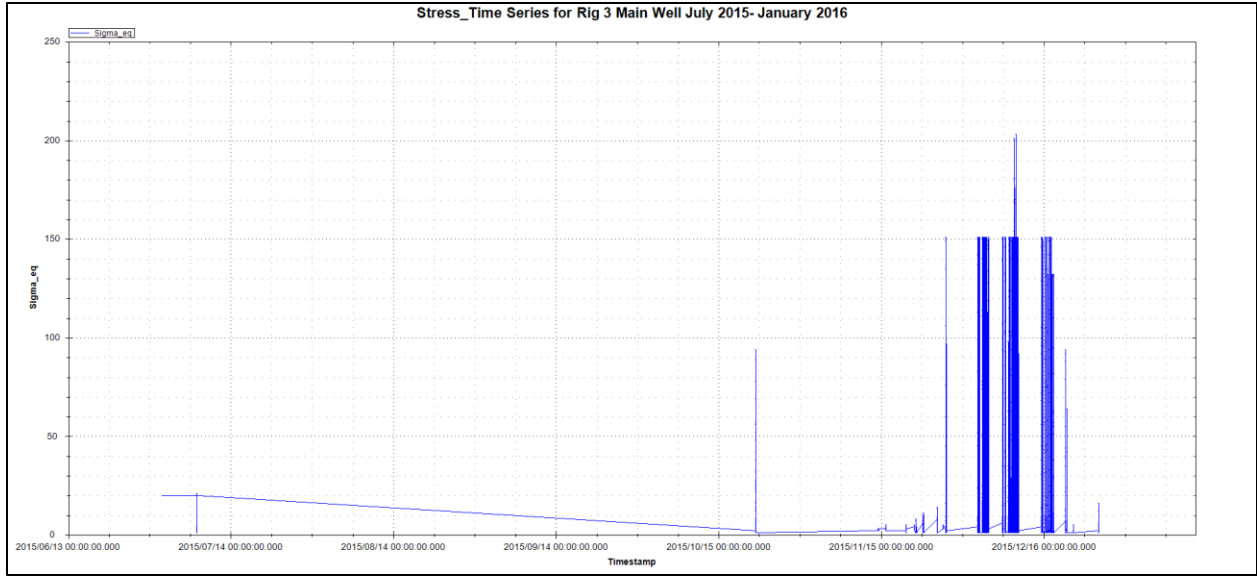


Figure 9-37 : Equivalent Stress Time Series Rig 3 Main Well July 2015 – January 2016

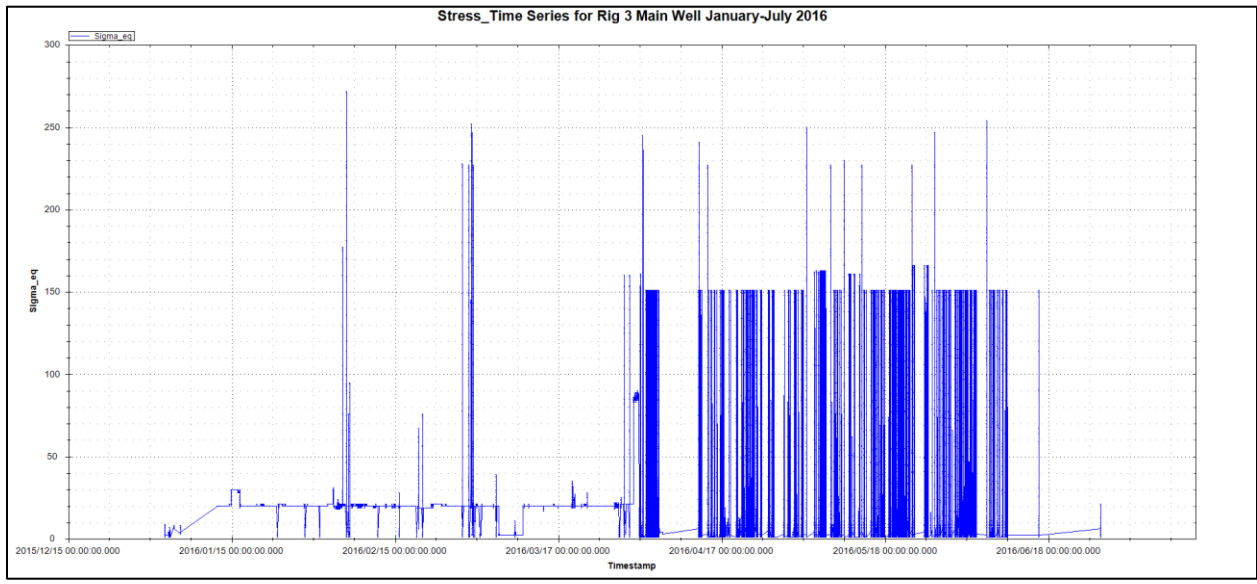


Figure 9-38 : Equivalent Stress Time Series Rig 3 Main Well January -July 2016

Rig 3: Auxiliary Well

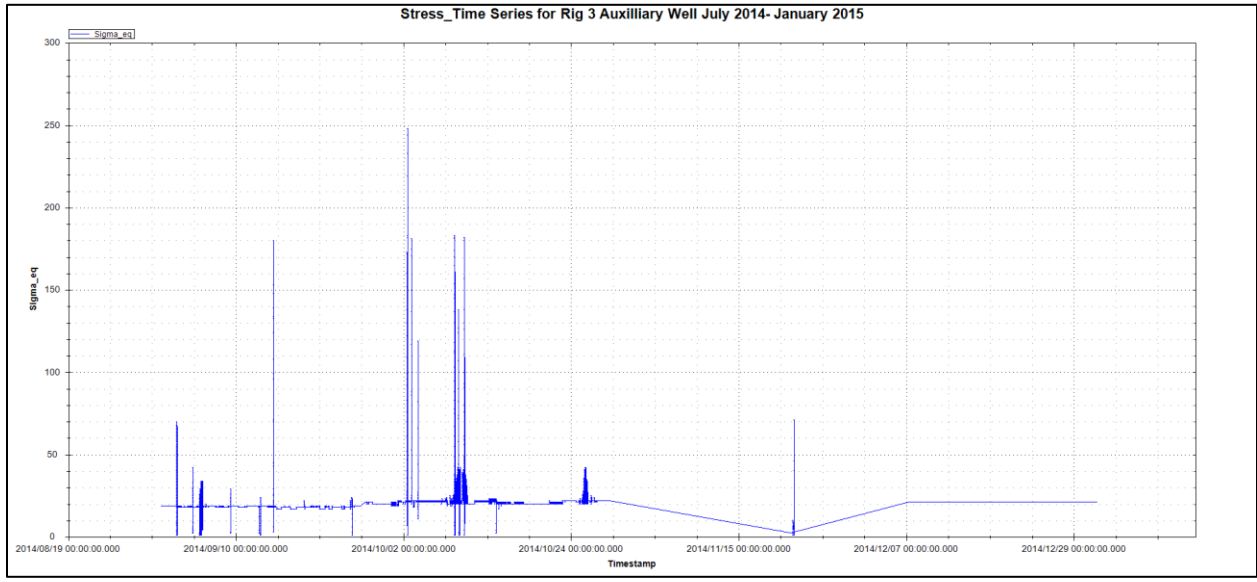


Figure 9-39 : Equivalent Stress Time Series Rig 3 Auxilliary Well July 2014 – January 2015

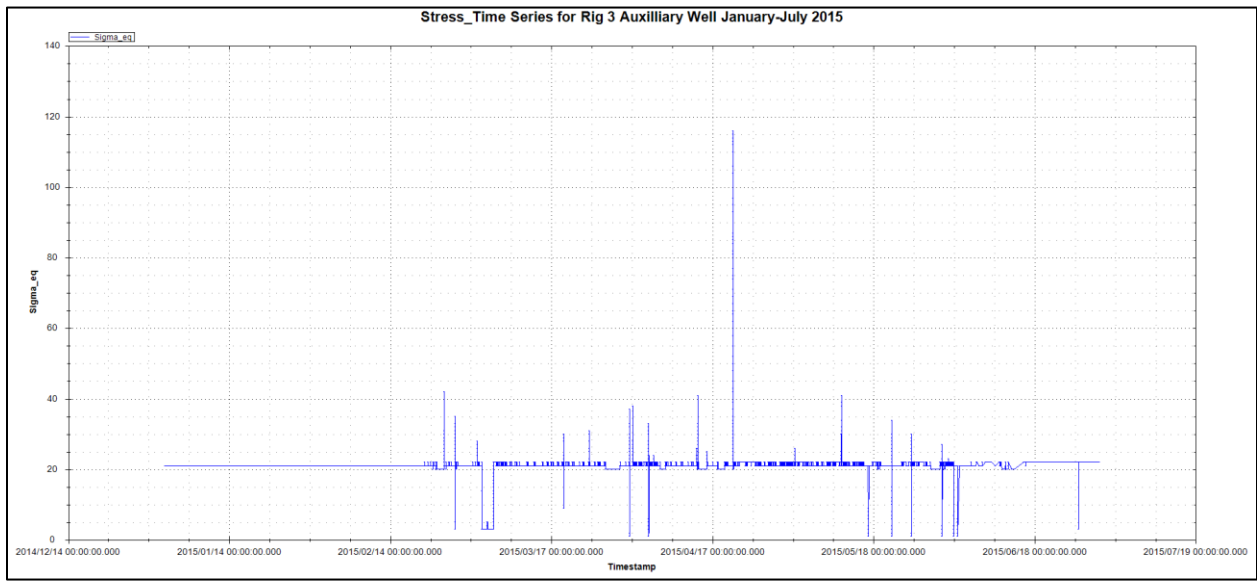


Figure 9-40 : Equivalent Stress Time Series Rig 3 Auxilliary Well January - July 2015

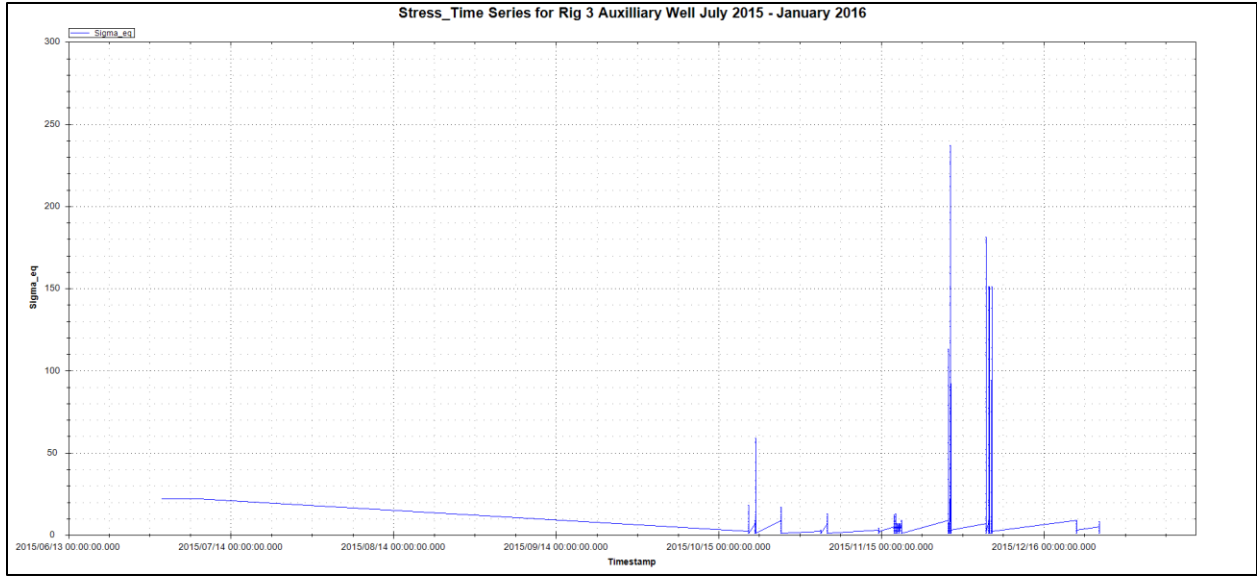


Figure 9-41 : Equivalent Stress Time Series Rig 3 Auxilliary Well July 2015 – January 2016

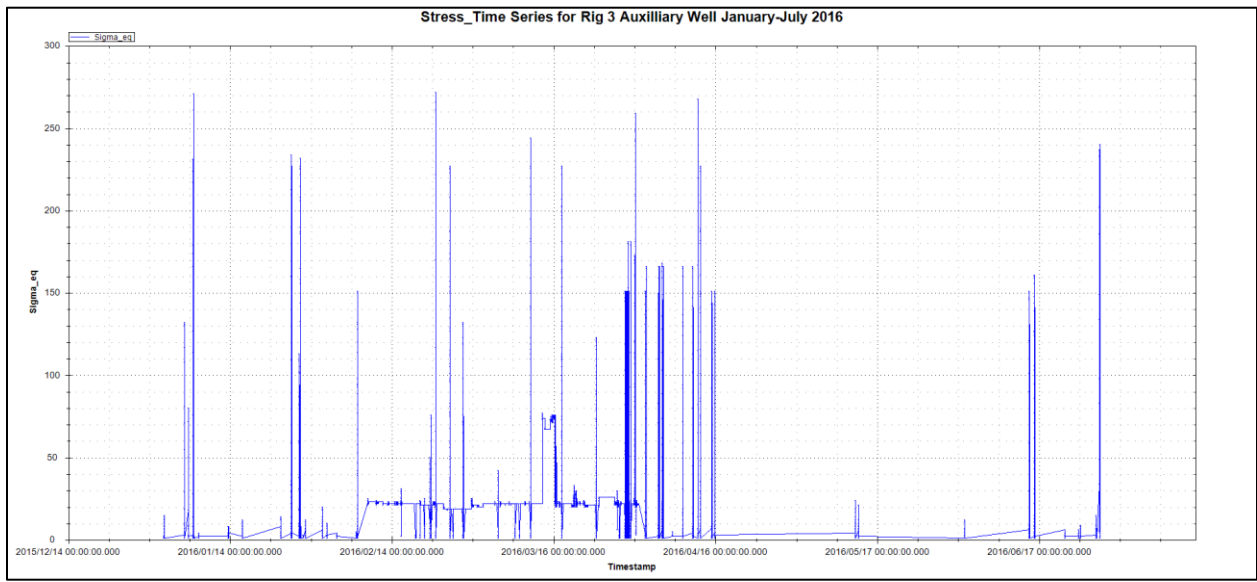


Figure 9-42 : Equivalent Stress Time Series Rig 3 Auxilliary Well January - July 2016

Appendix E: Rainflow Matrixes

Rig 1: Main Well

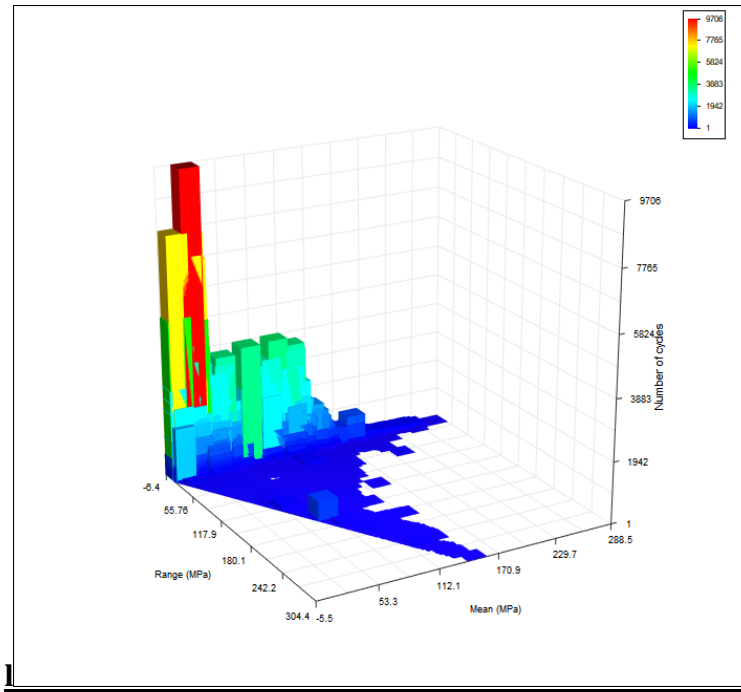


Figure 9-43 : Rainflow Matrix Histogram Rig 1 Main Well 2014

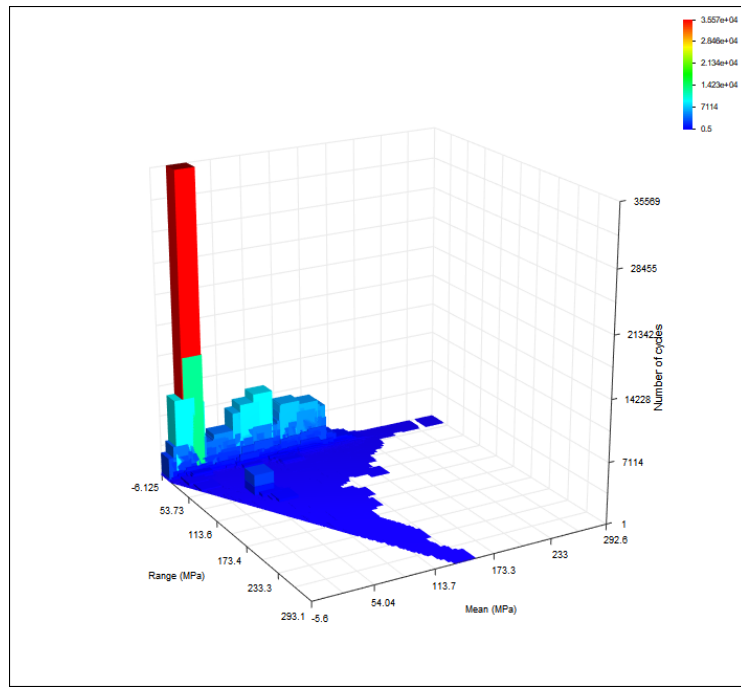


Figure 9-44 : Rainflow Matrix Histogram Rig 1 Main Well 2015

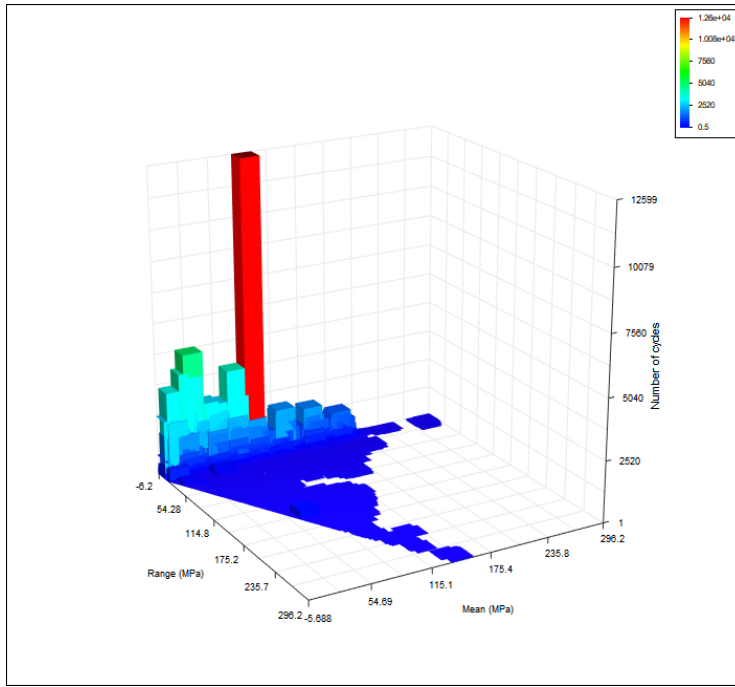


Figure 9-45 : Rainflow Matrix Histogram Rig 1 Main Well 2016

Rig 1: Auxiliary Well

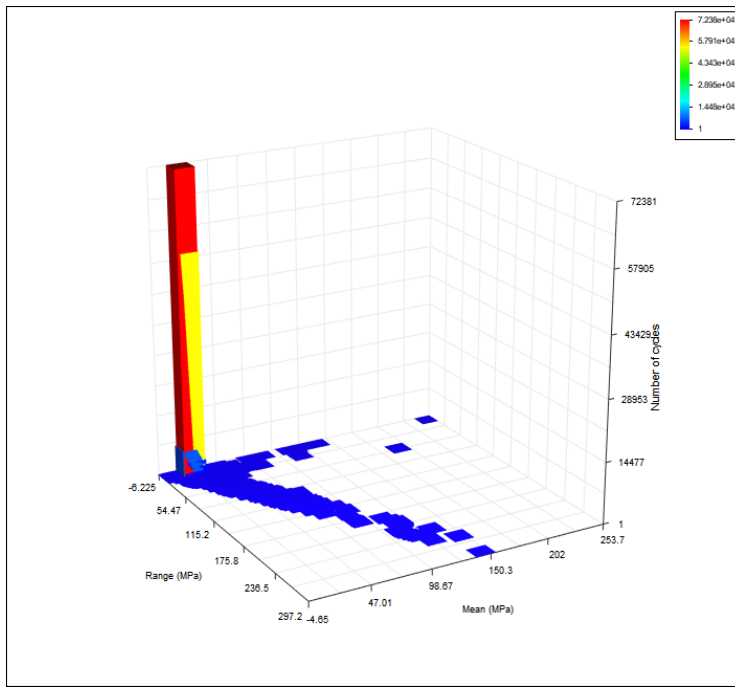


Figure 9-46 : Rainflow Matrix Histogram Rig 1 Auxiliary Well 2014

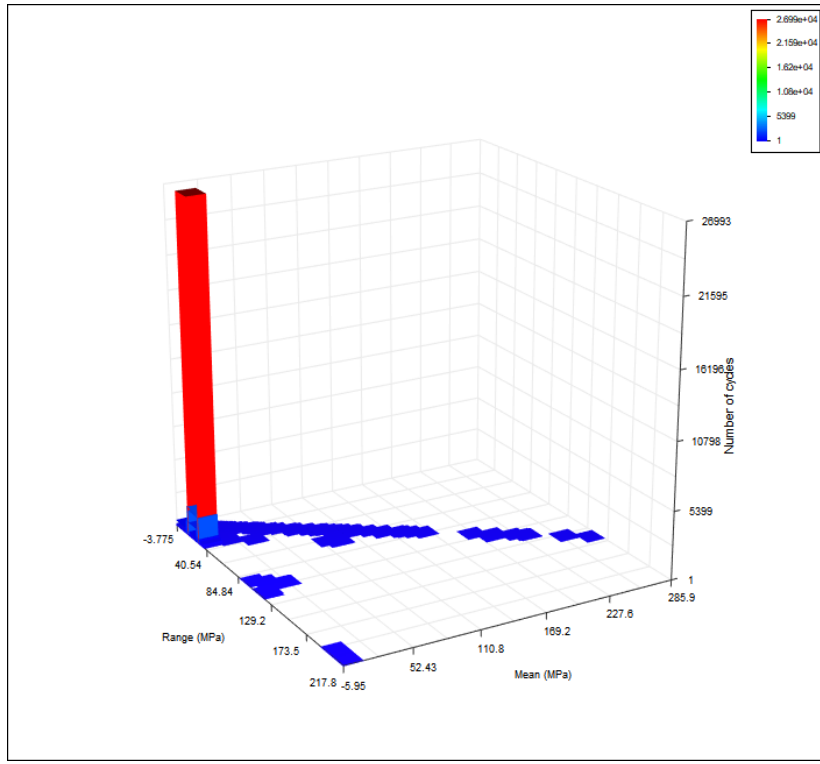


Figure 9-47 : Rainflow Matrix Histogram Rig 1 Auxiliary Well 2015

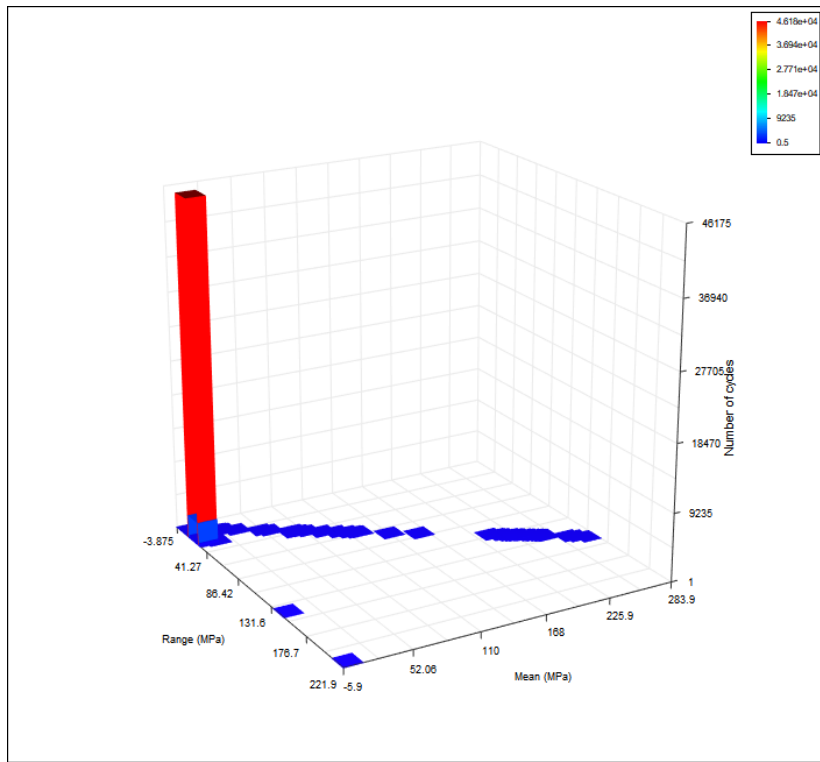


Figure 9-48 : Rainflow Matrix Histogram Rig 1 Auxiliary Well 2016

Rig 2: Main Well

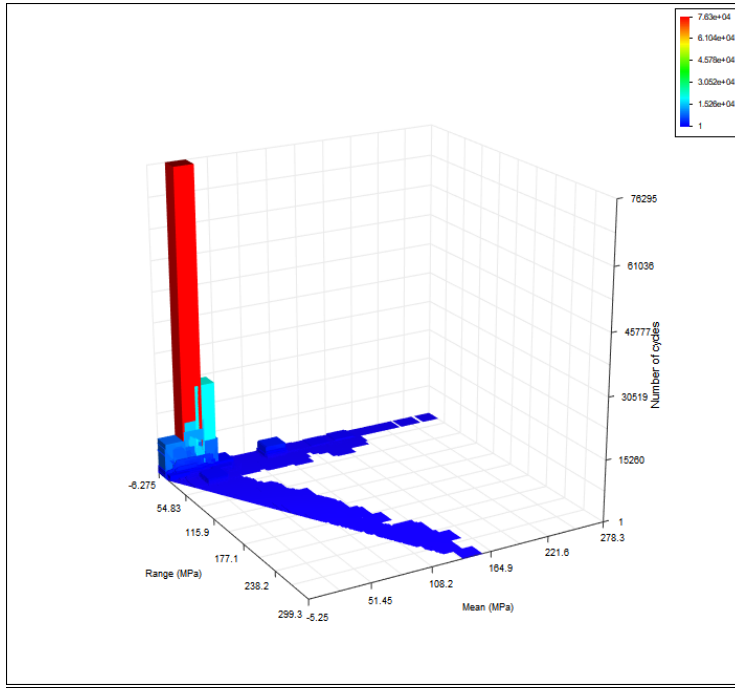


Figure 9-49 : Rainflow Matrix Histogram Rig 2 Main Well 2014

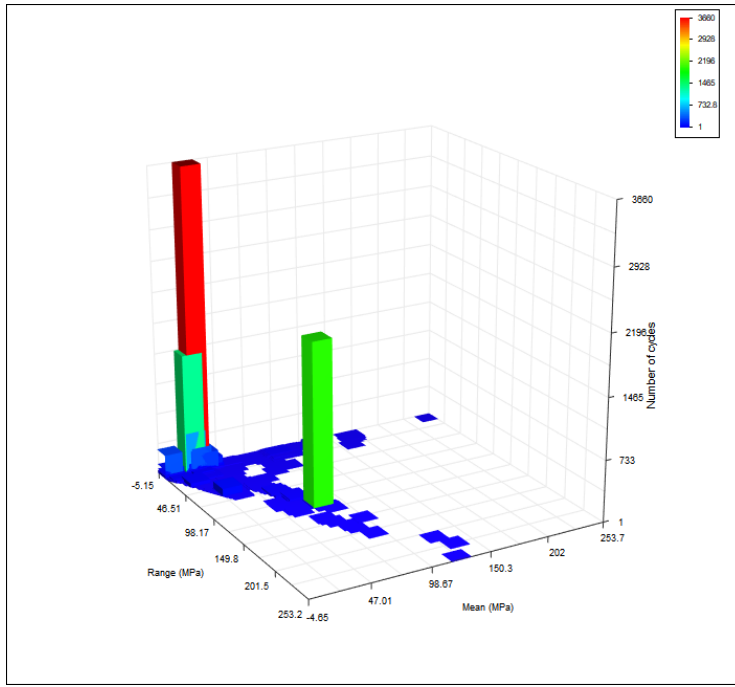


Figure 9-50 : Rainflow Matrix Histogram Rig 2 Main Well 2015

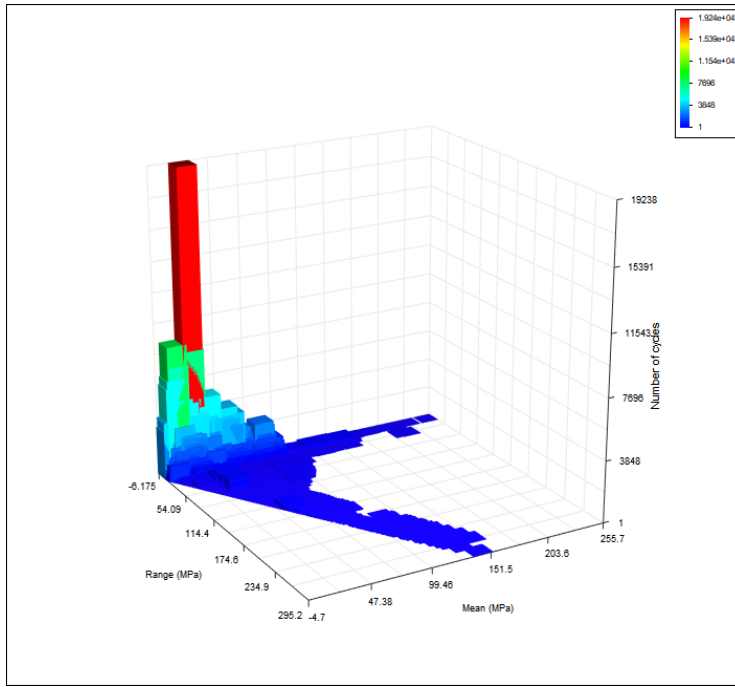


Figure 9-51 : Rainflow Matrix Histogram Rig 2 Main Well 2016

Rig 2: Auxiliary Well

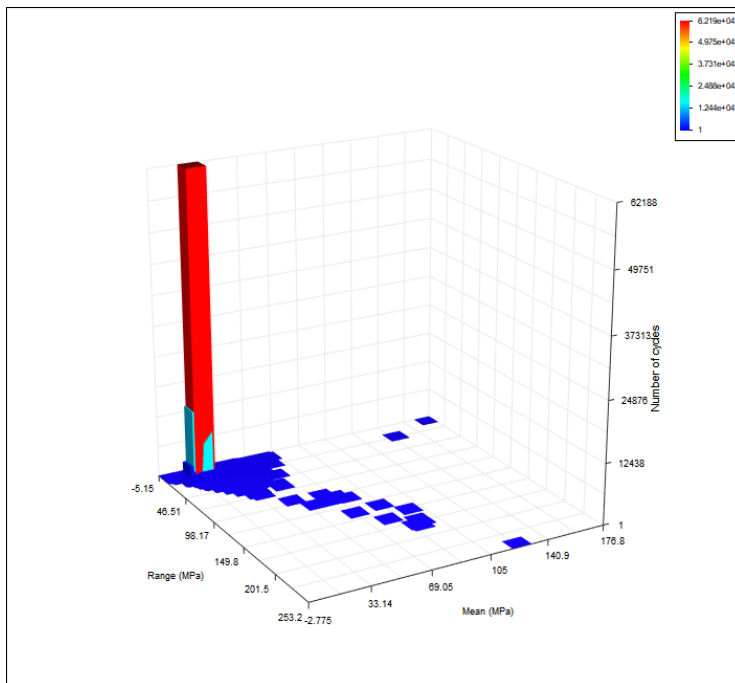


Figure 9-52 : Rainflow Matrix Histogram Rig 2 Auxiliary Well 2014

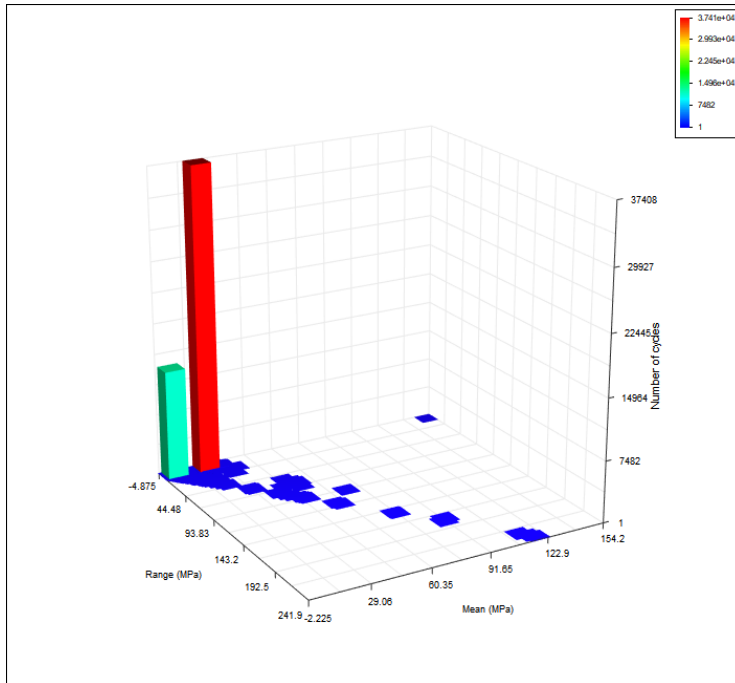


Figure 9-53 : Rainflow Matrix Histogram Rig 3 Auxiliary Well 2015

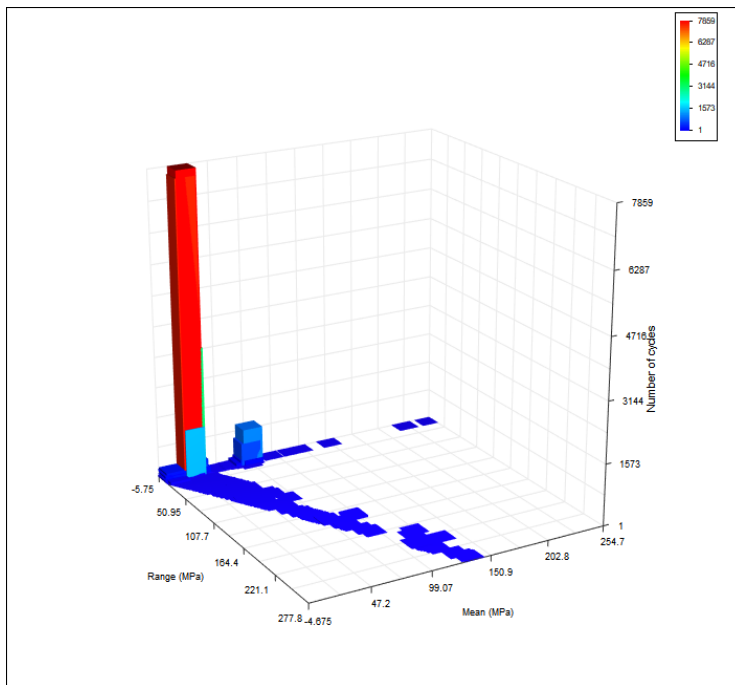


Figure 9-54 : Rainflow Matrix Histogram Rig 3 Auxiliary Well 2016

Rig 3: Main Well

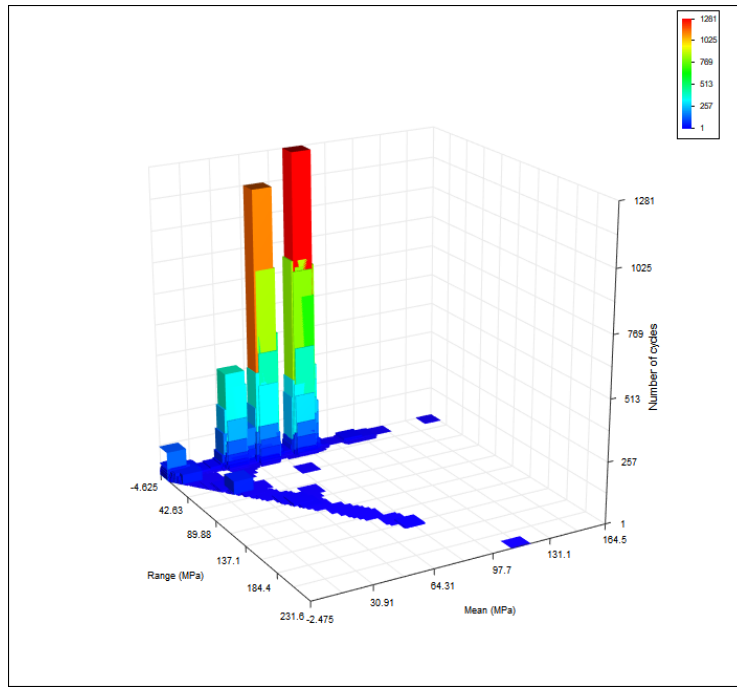


Figure 9-55 : Rainflow Matrix Histogram Rig 3 Main Well 2014

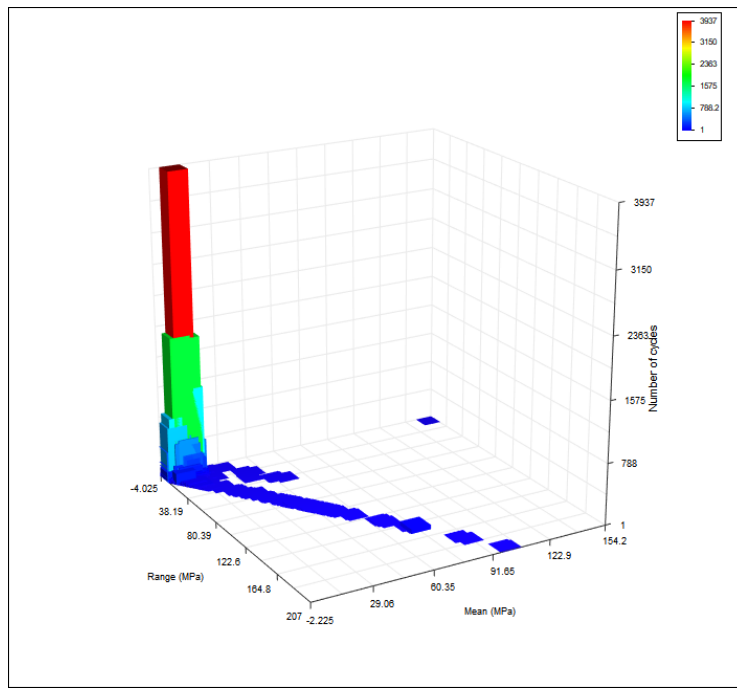


Figure 9-56 : Rainflow Matrix Histogram Rig 3 Main Well 2015

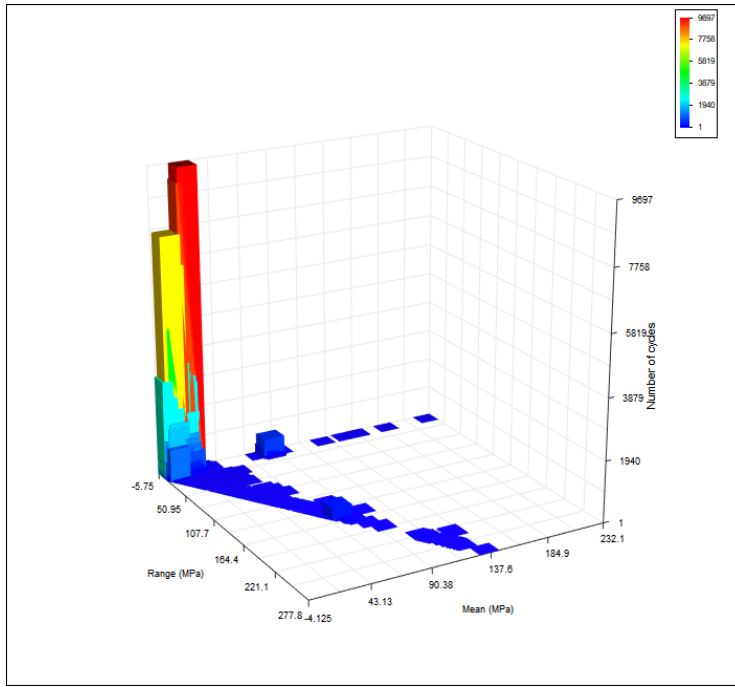


Figure 9-57 : Rainflow Matrix Histogram Rig 3 Main Well 2016

Rig 3: Auxiliary Well

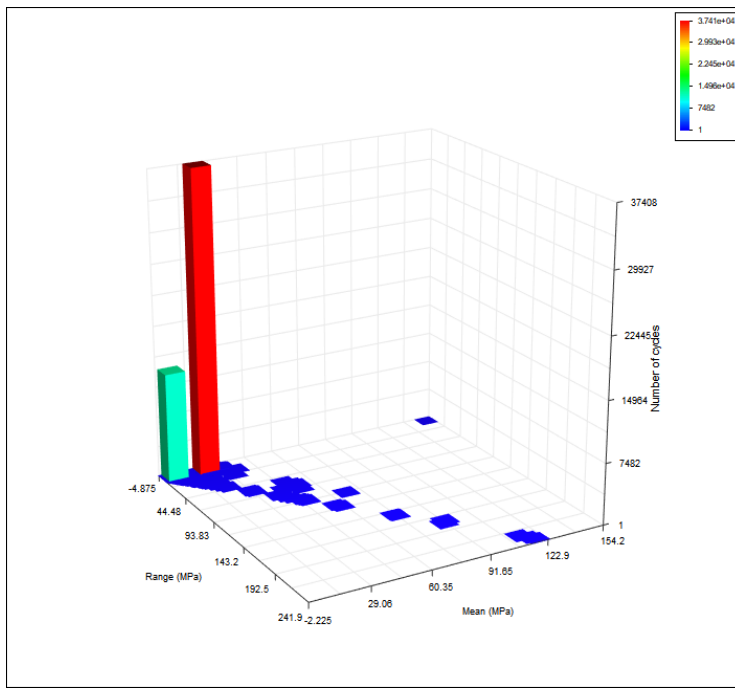


Figure 9-58 : Rainflow Matrix Histogram Rig 3 Auxiliary Well 2014

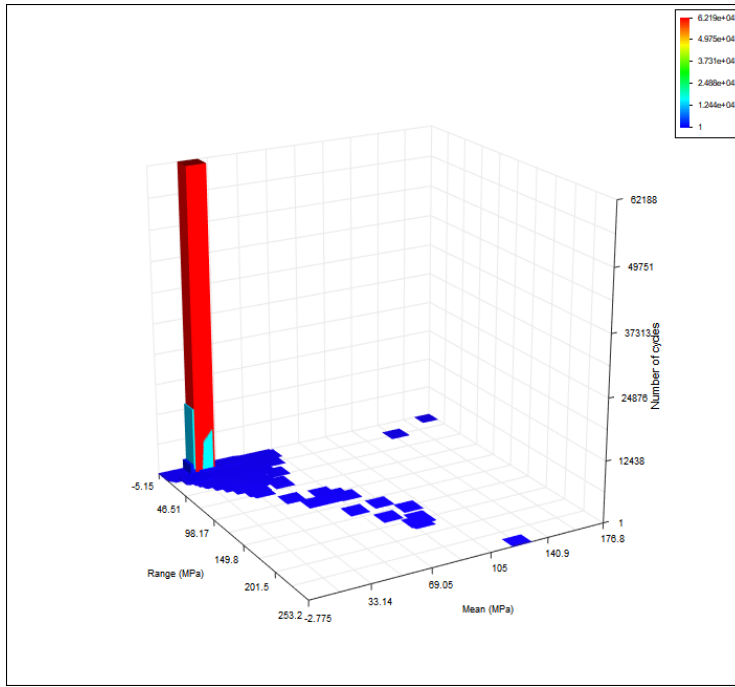


Figure 9-59 : Rainflow Matrix Histogram Rig 3 Auxiliary Well 2015

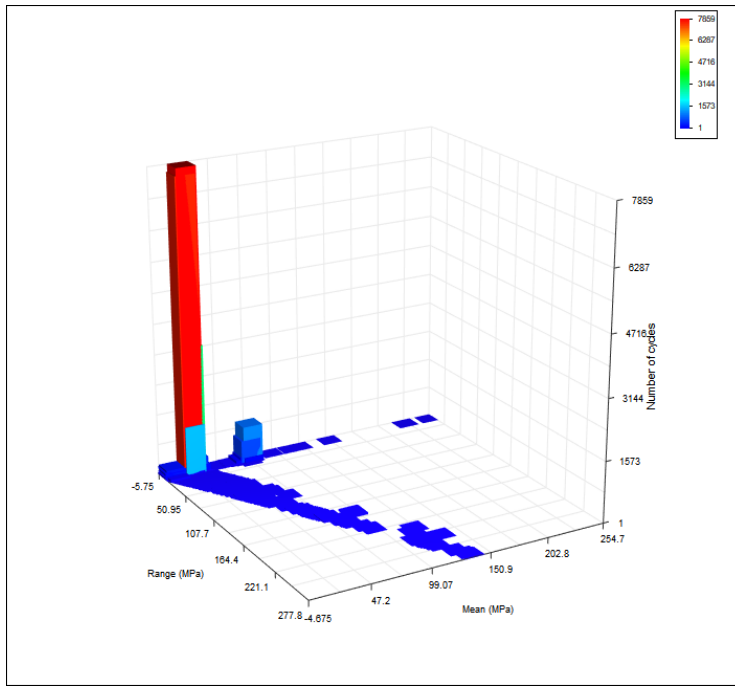


Figure 9-60 : Rainflow Matrix Histogram Rig 3 Auxiliary Well 2016

Appendix F: Comparison of Fatigue Damage Results for Miner's linear damage rule, Manson's double linear damage rule and Subramanyan's non-linear damage rule models
Non-Conservative Estimates

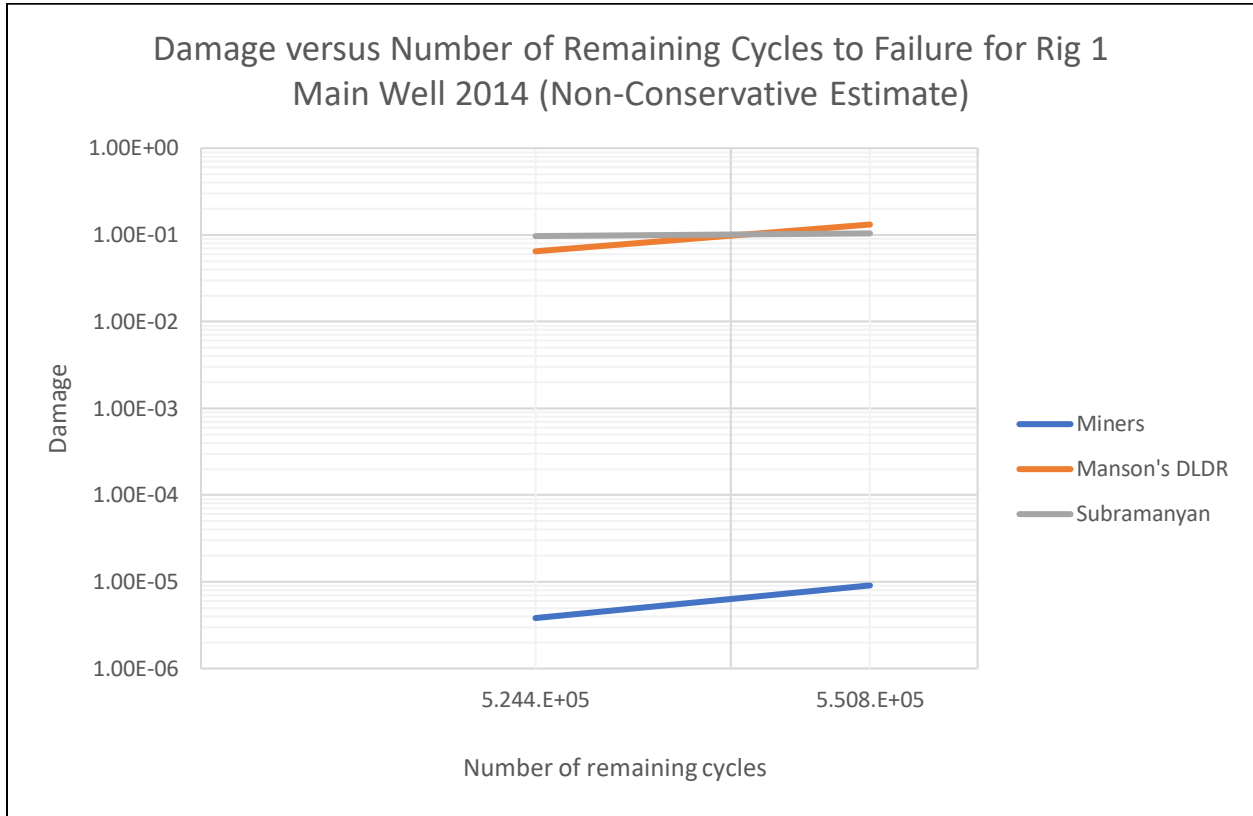


Figure 9-61: Non-conservative estimates of damage versus the number of remaining cycles until failure from the selected fatigue damage models for Rig 1 Main Well in 2014

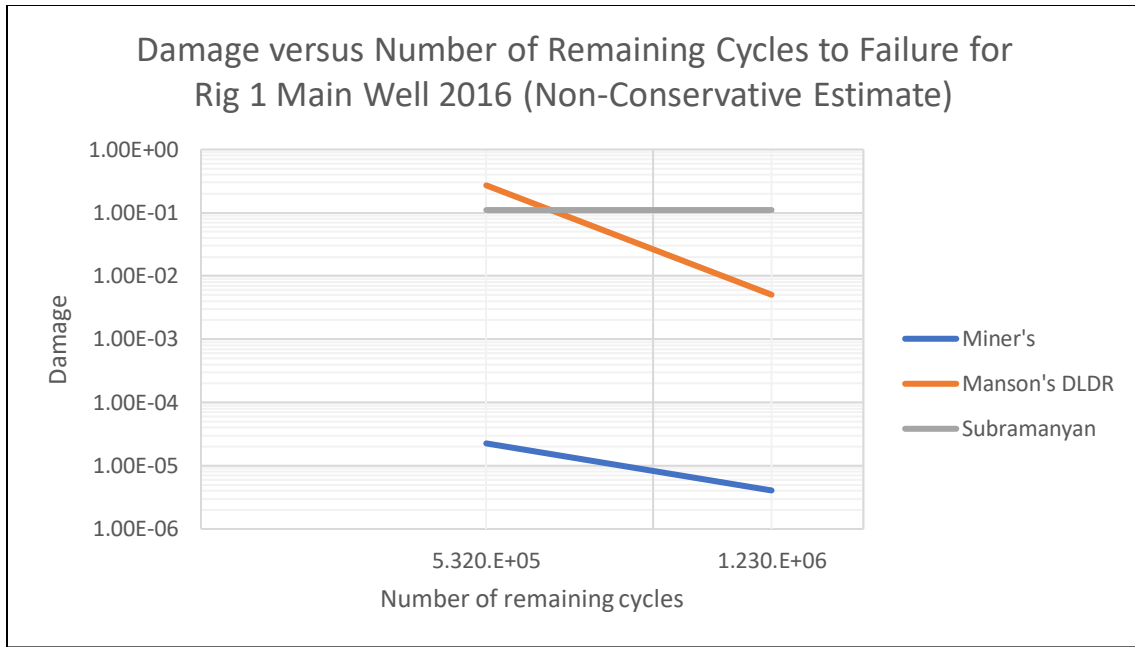


Figure 9-62: Non-conservative estimates of damage versus the number of remaining cycles until failure from the selected fatigue damage models for Rig 1 Main Well in 2016

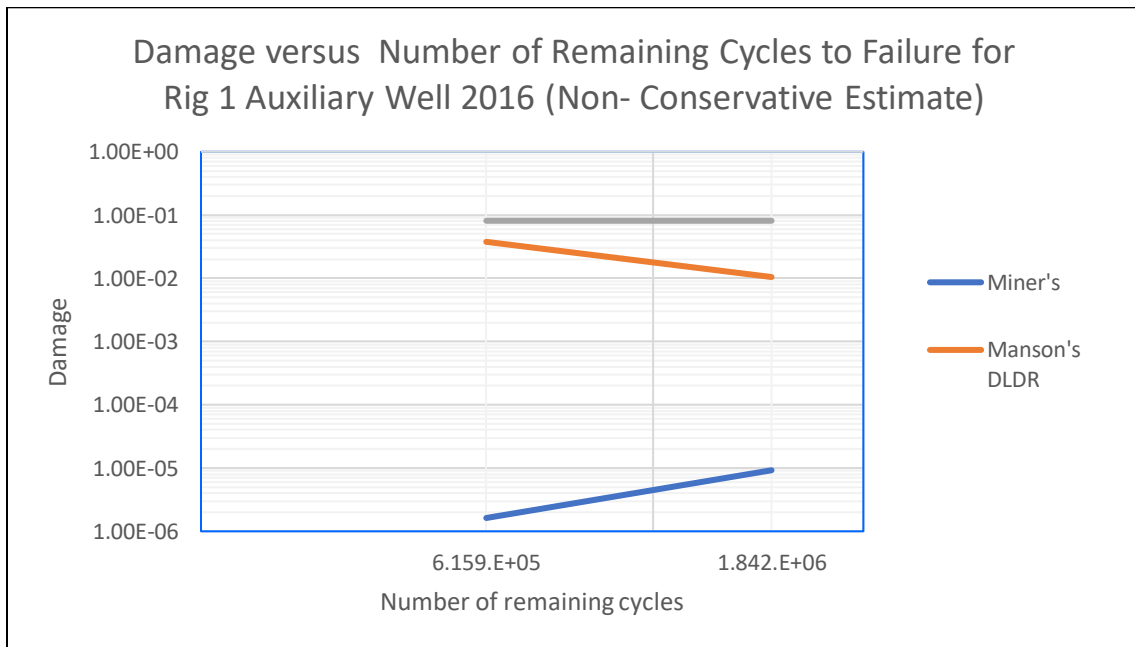


Figure 9-63: Non-conservative estimates of damage versus the number of remaining cycles until failure from the selected fatigue damage models for Rig 1 Auxiliary Well in 2016

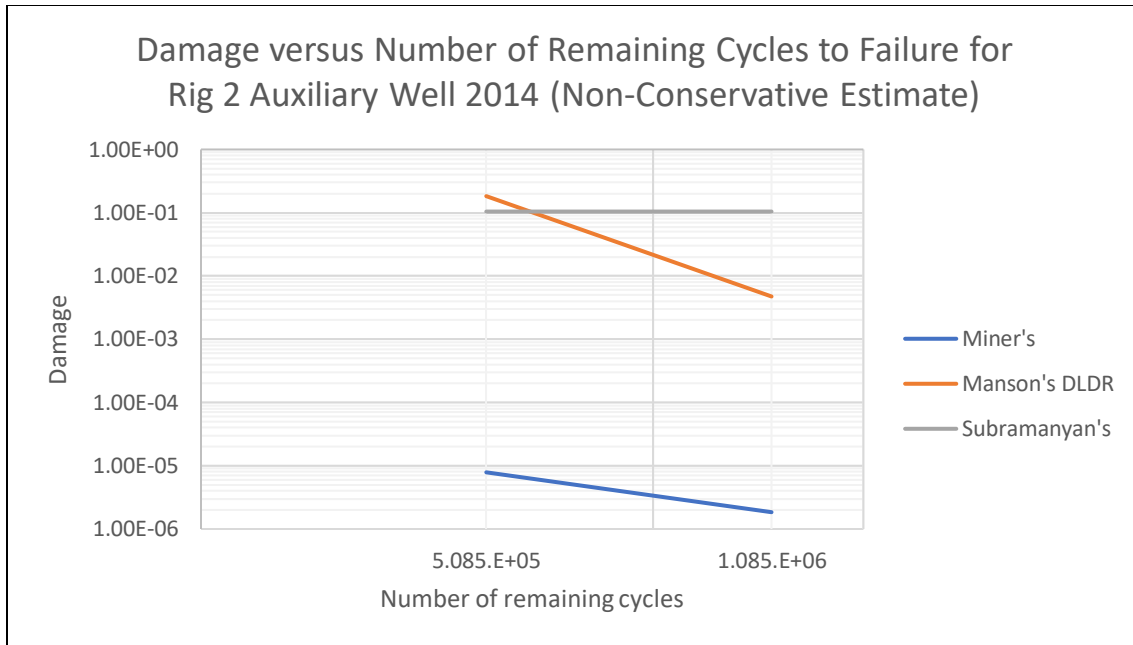


Figure 9-64: Non-conservative estimates of damage versus the number of remaining cycles until failure from the selected fatigue damage models for Rig 2 Auxiliary Well in 2014

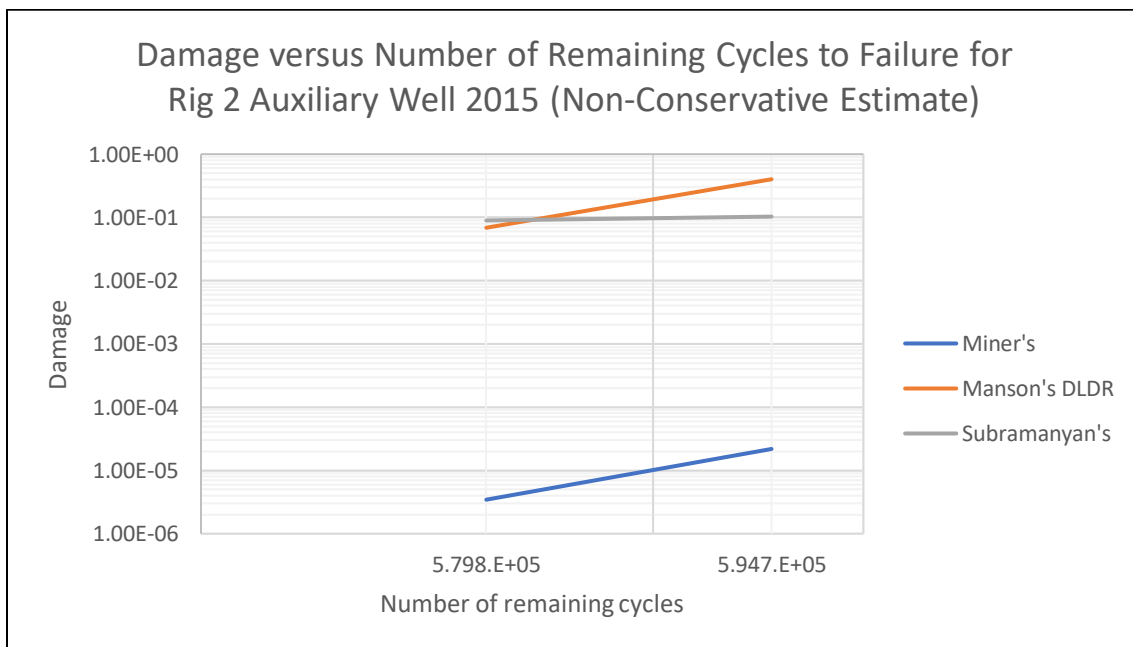


Figure 9-65: Non-conservative estimates of damage versus the number of remaining cycles until failure from the selected fatigue damage models for Rig 2 Auxiliary Well in 2015

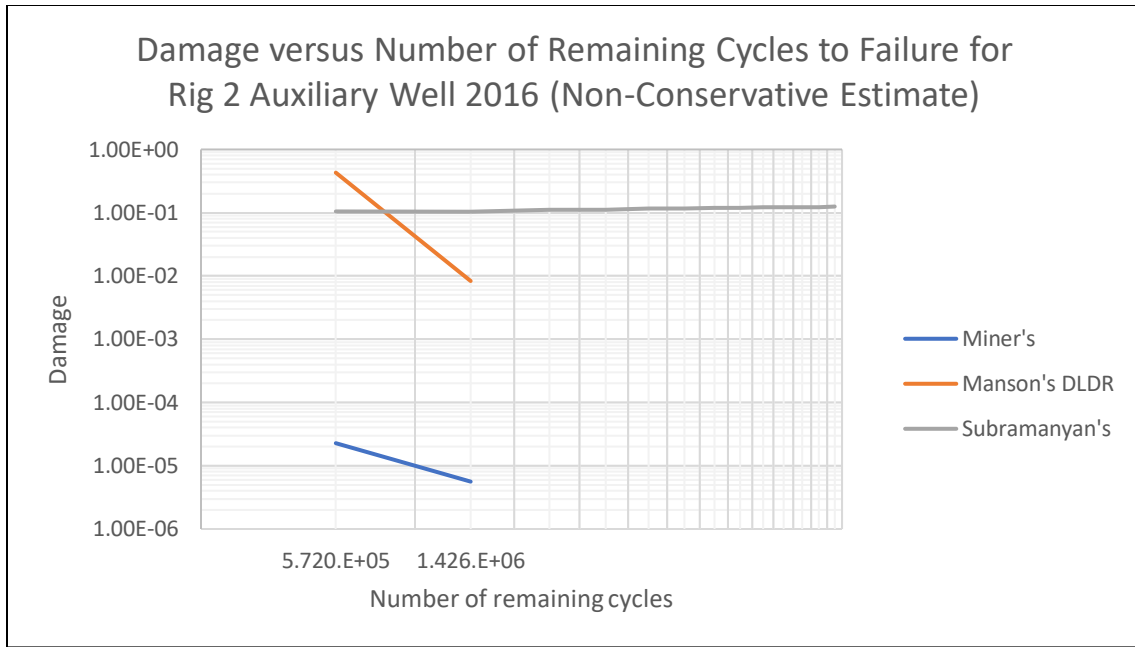


Figure 9-66: Non-conservative estimates of damage versus the number of remaining cycles until failure from the selected fatigue damage models for Rig 2 Auxiliary Well in 2016

Conservative Estimates

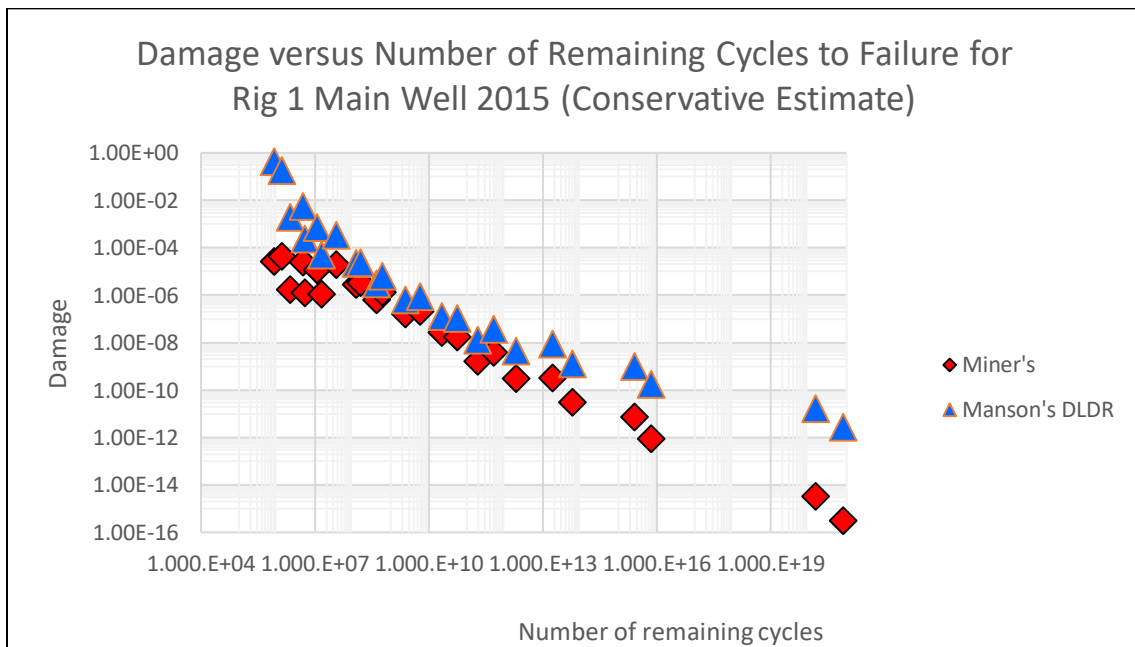


Figure 9-67: Conservative estimates of damage versus the number of remaining cycles until failure from the selected fatigue damage models for Rig 1 Main Well in 2015

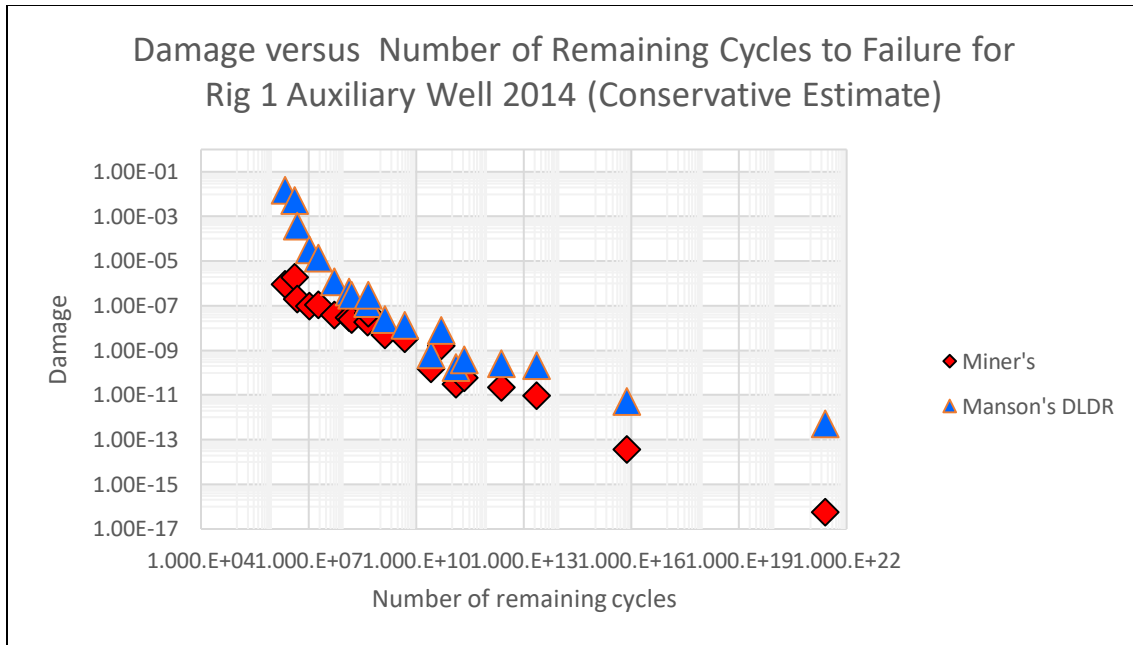


Figure 9-68: Conservative estimates of damage versus the number of remaining cycles until failure from the selected fatigue damage models for Rig 1 Auxiliary Well in 2014

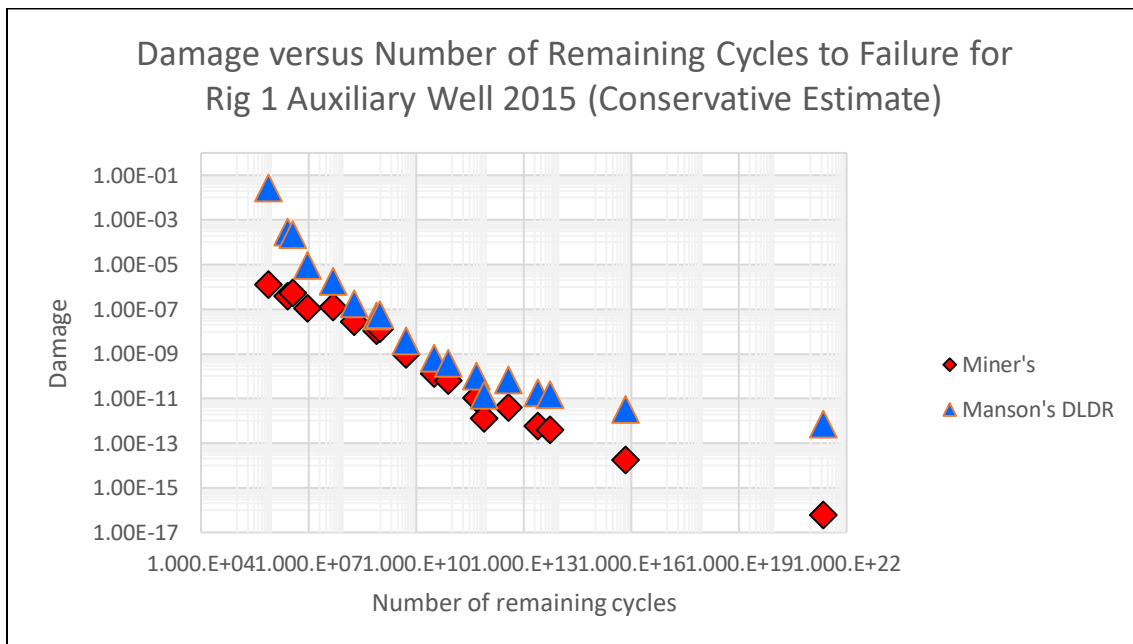


Figure 9-69: Conservative estimates of damage versus the number of remaining cycles until failure from the selected fatigue damage models for Rig 1 Auxiliary Well in 2015

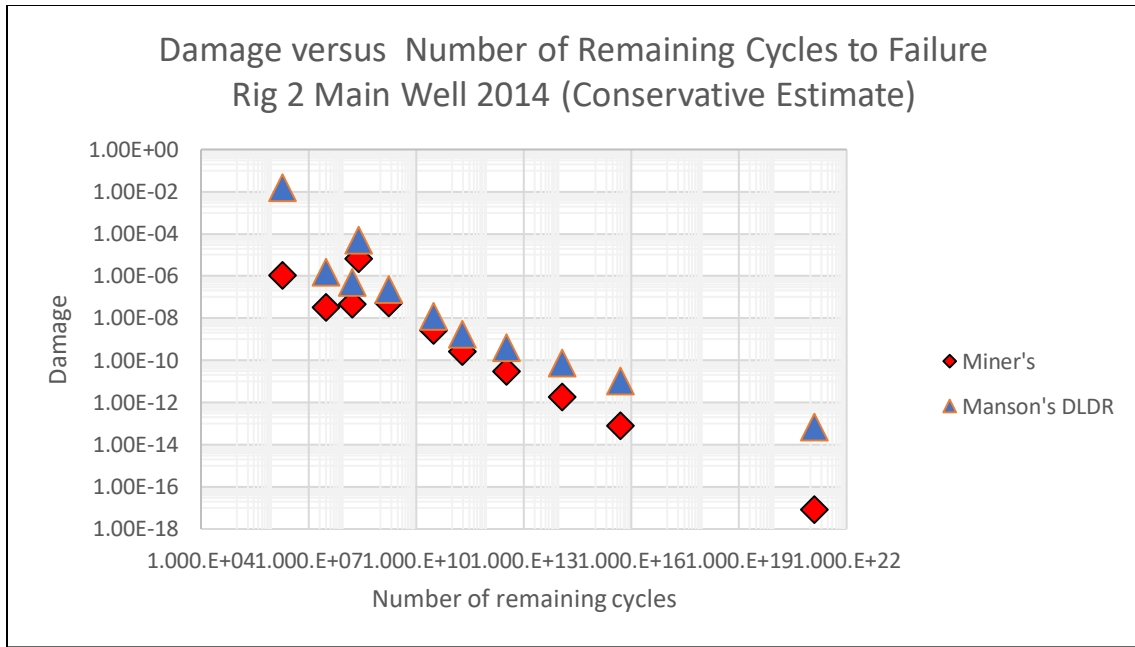


Figure 9-70: Conservative estimates of damage versus the number of remaining cycles until failure from the selected fatigue damage models for Rig 2 Main Well in 2014

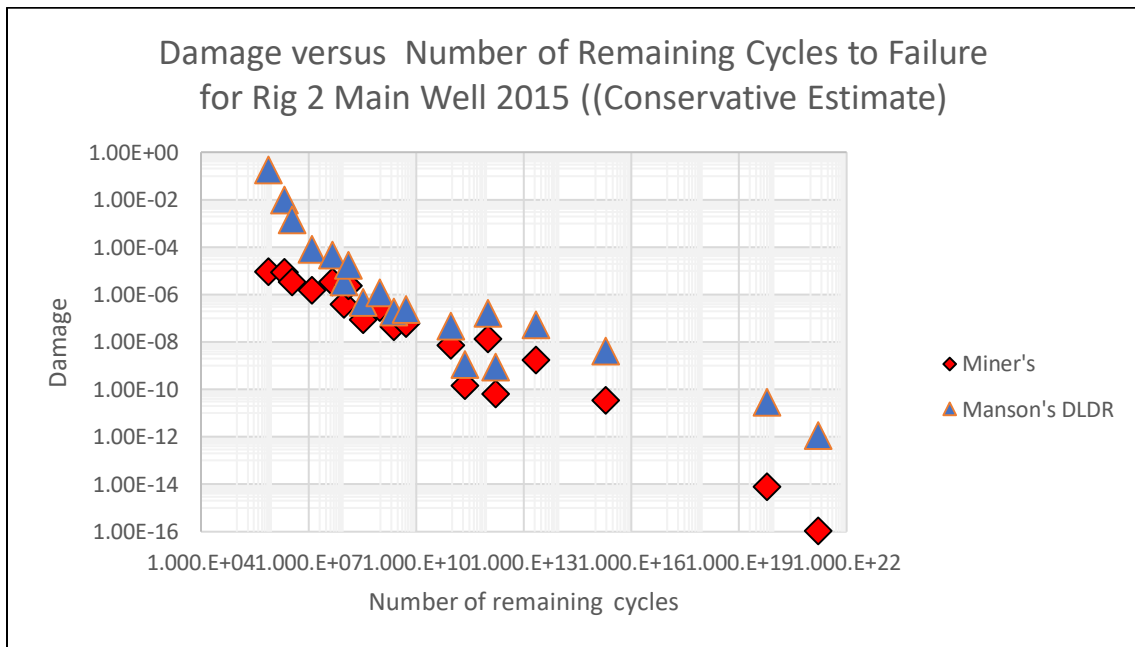


Figure 9-71: Conservative estimates of damage versus the number of remaining cycles until failure from the selected fatigue damage models for Rig 2 Main Well in 2015

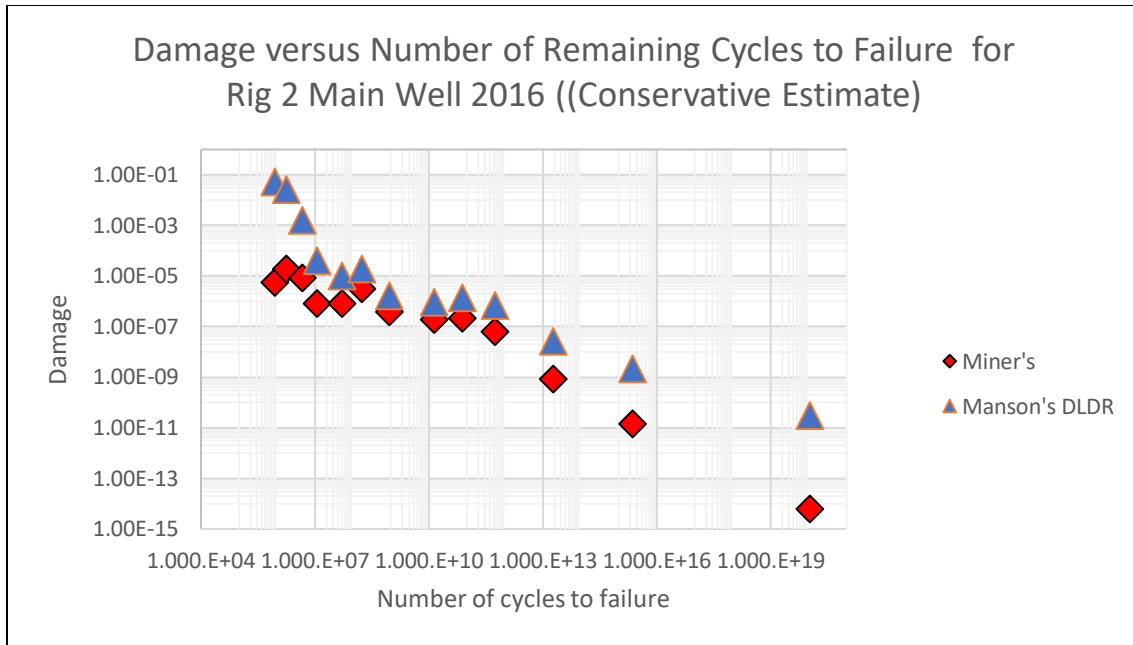


Figure 9-72: Conservative estimates of damage versus the number of remaining cycles until failure from the selected fatigue damage models for Rig 2 Main Well in 2016

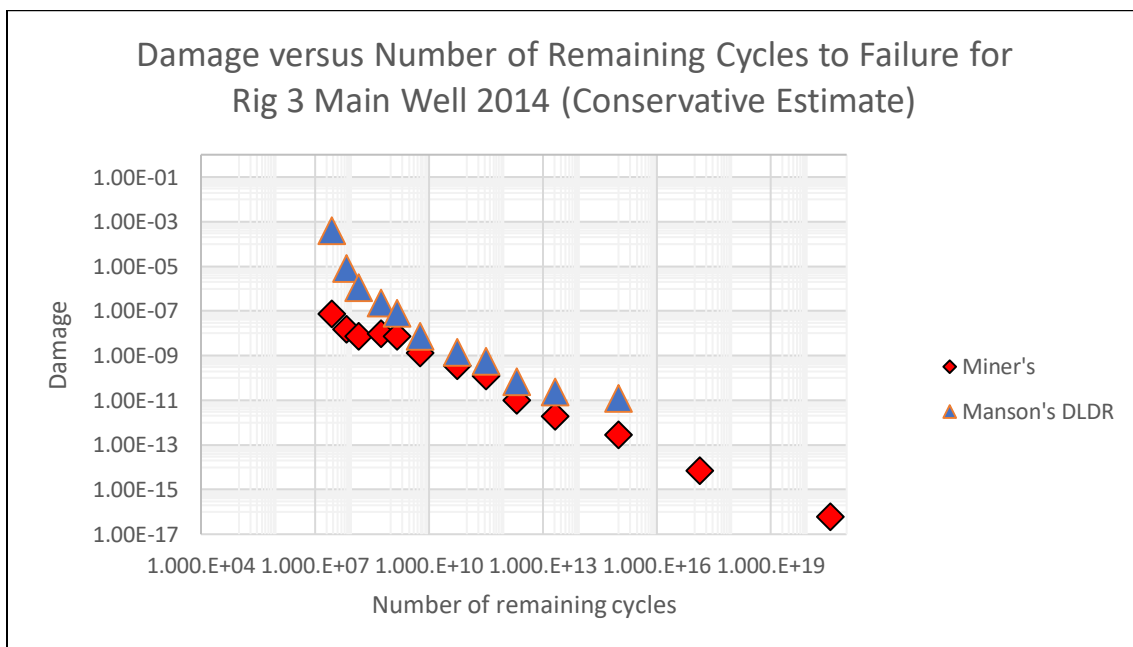


Figure 9-73: Conservative estimates of damage versus the number of remaining cycles until failure from the selected fatigue damage models for Rig 3 Main Well in 2014

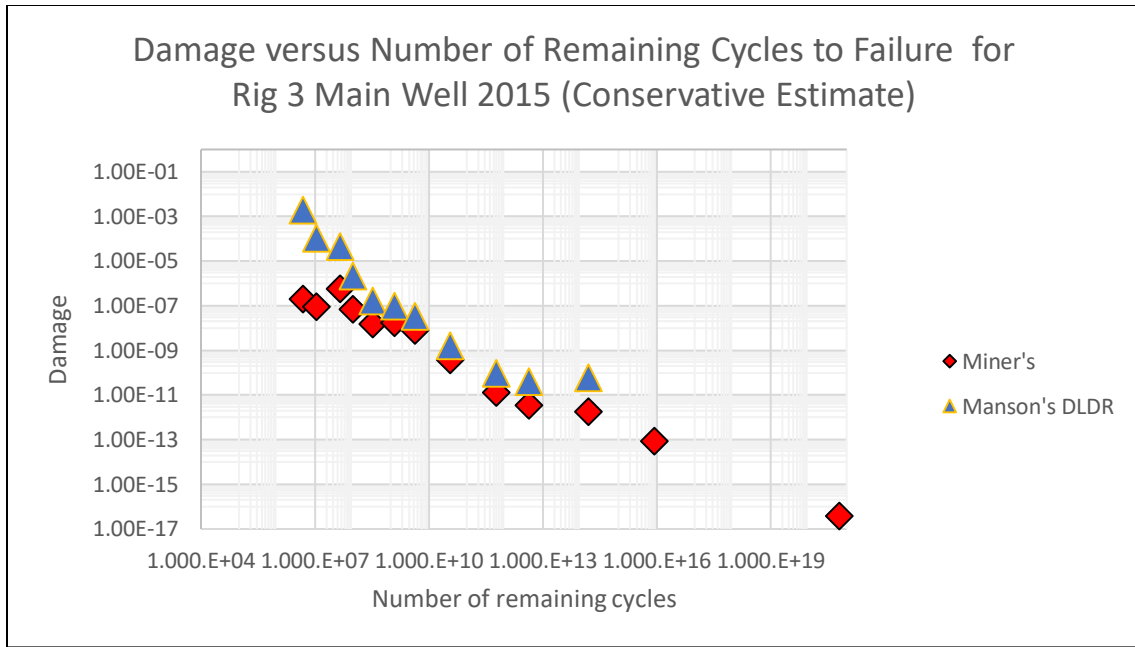


Figure 9-74: Conservative estimates of damage versus the number of remaining cycles until failure from the selected fatigue damage models for Rig 3 Main Well in 2015

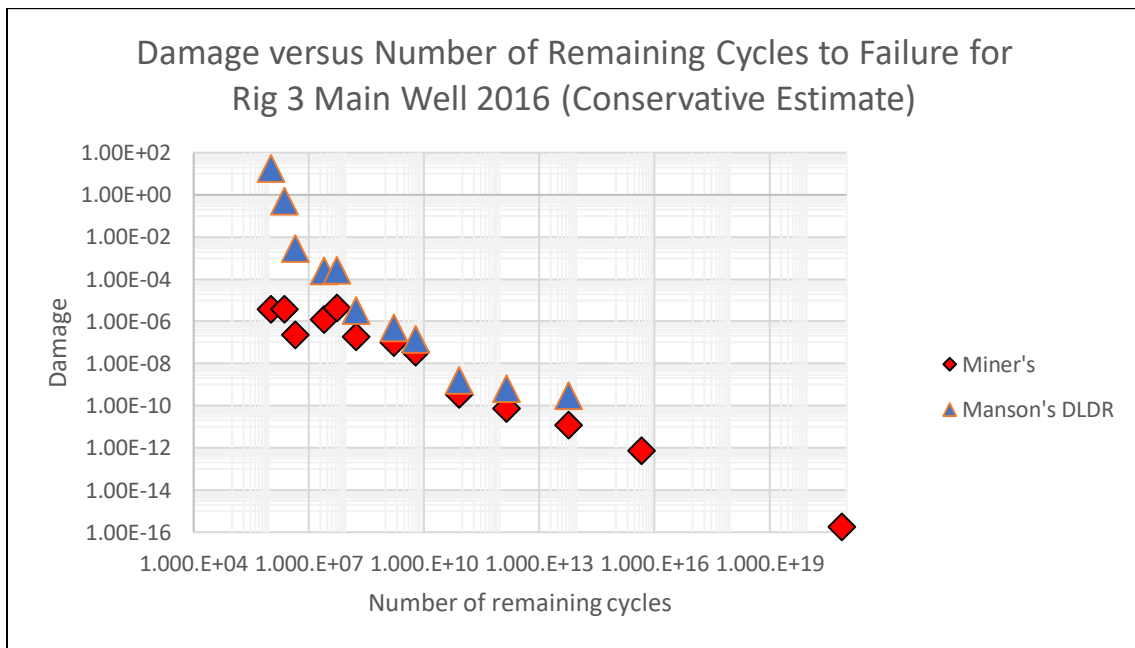


Figure 9-75: Conservative estimates of damage versus the number of remaining cycles until failure from the selected fatigue damage models for Rig 3 Main Well in 2016

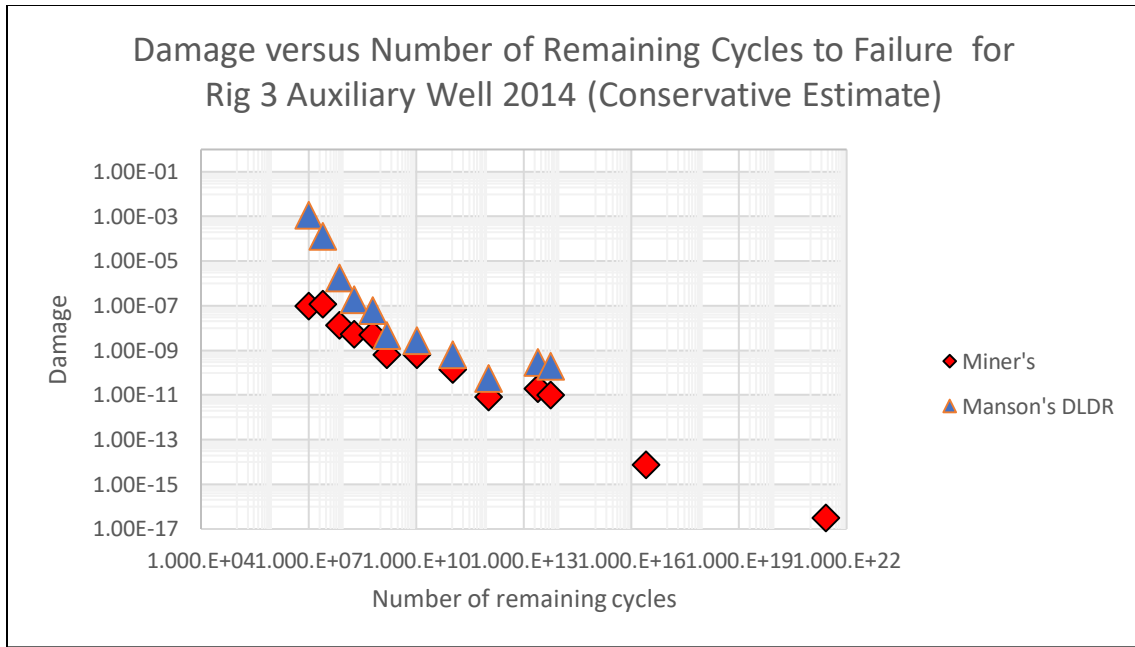


Figure 9-76: Conservative estimates of damage versus the number of remaining cycles until failure from the selected fatigue damage models for Rig 3 Auxiliary Well in 2014

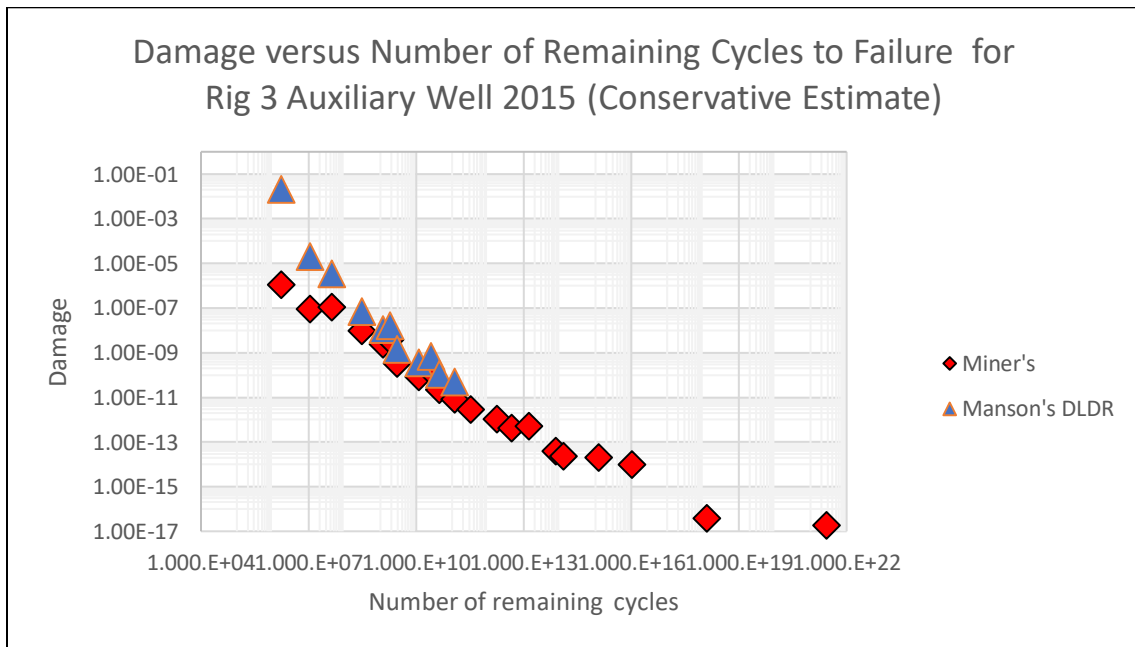


Figure 9-77: Conservative estimates of damage versus the number of remaining cycles until failure from the selected fatigue damage models for Rig 3 Auxiliary Well in 2015

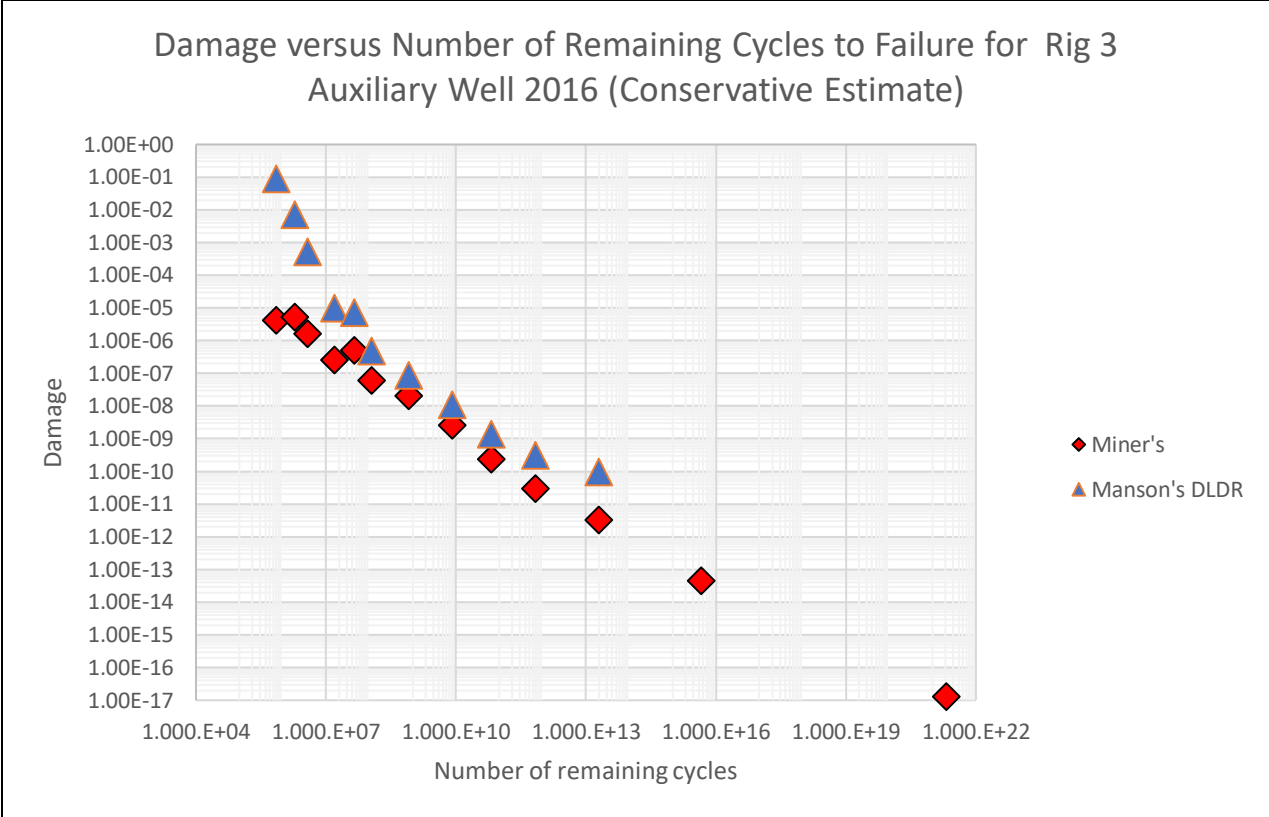


Figure 9-78: Conservative estimates of damage versus the number of remaining cycles until failure from the selected fatigue damage models for Rig 3 Auxiliary Well in 2016

Appendix G: Comparison of the number of loading blocks until failure results for Miners linear damage rule, Manson's double linear damage rule and Subramanyan's non-linear damage models

Non-Conservative Estimates

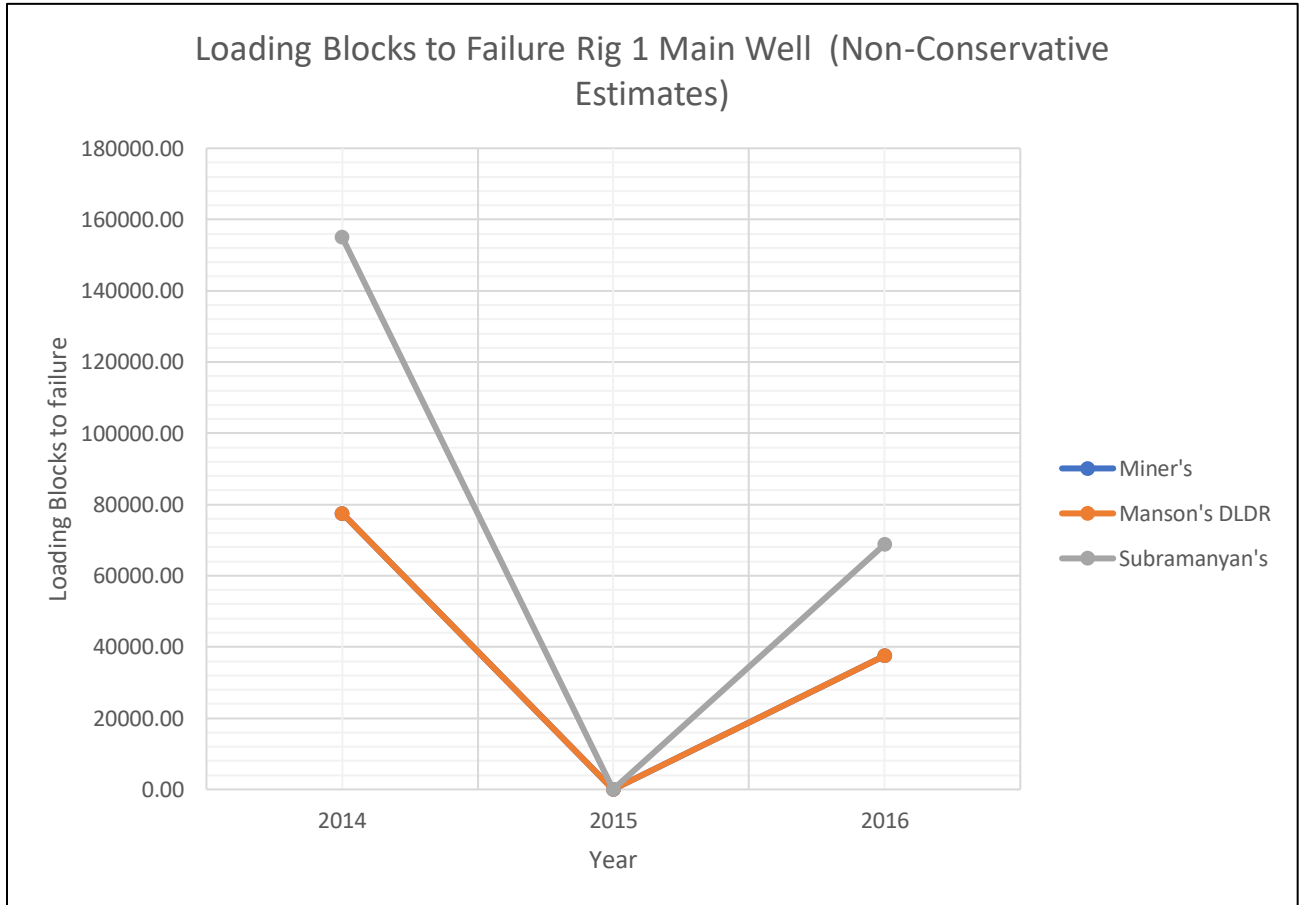


Figure 9-79: Non-conservative estimates of the number of loading blocks until failure from the selected fatigue damage models for Rig 1 Main Well

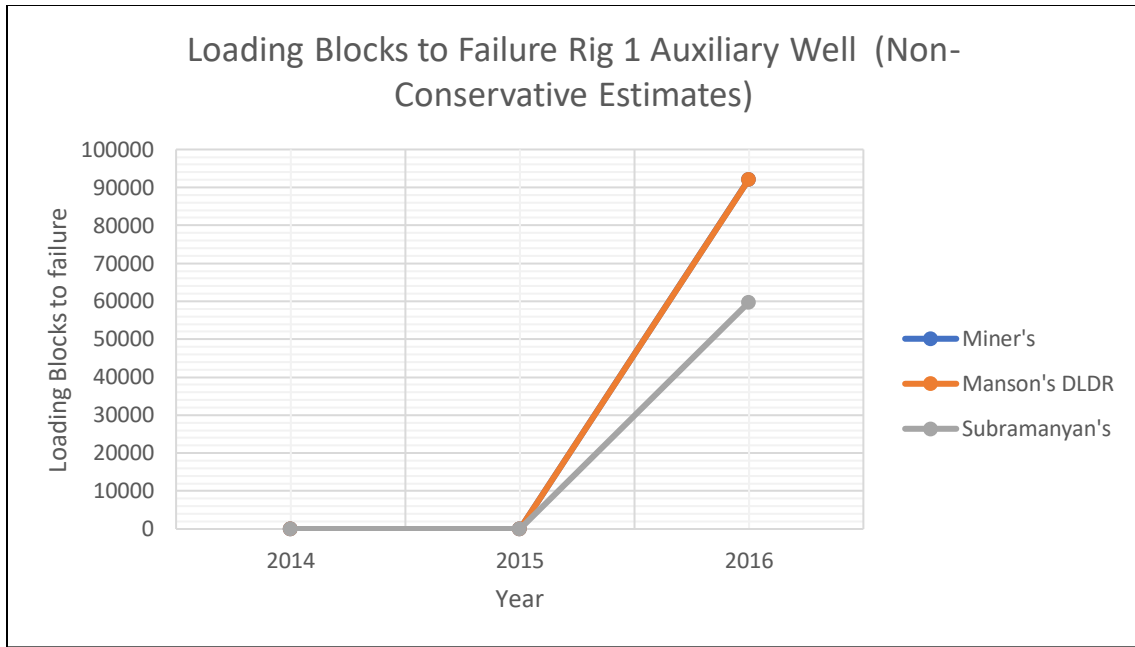


Figure 9-80: Non-conservative estimates of the number of loading blocks until failure from the selected fatigue damage models for Rig 1 Auxiliary Well

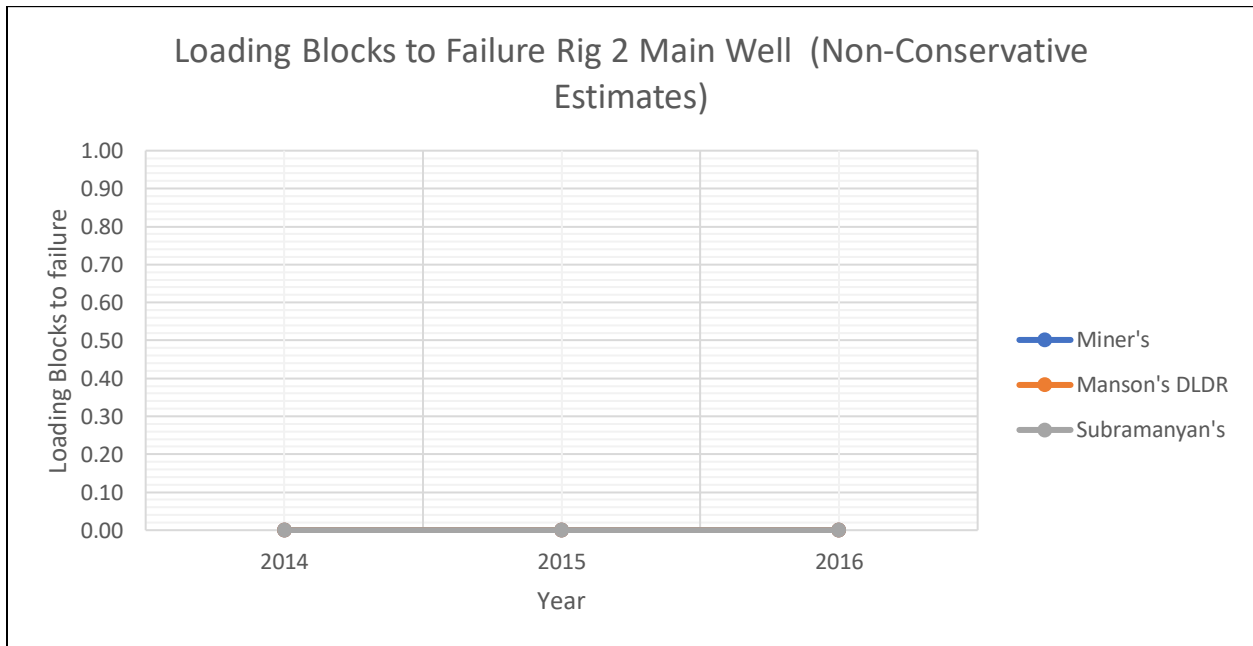


Figure 9-81: Non-conservative estimates of the number of loading blocks until failure from the selected fatigue damage models for Rig 2 Main Well

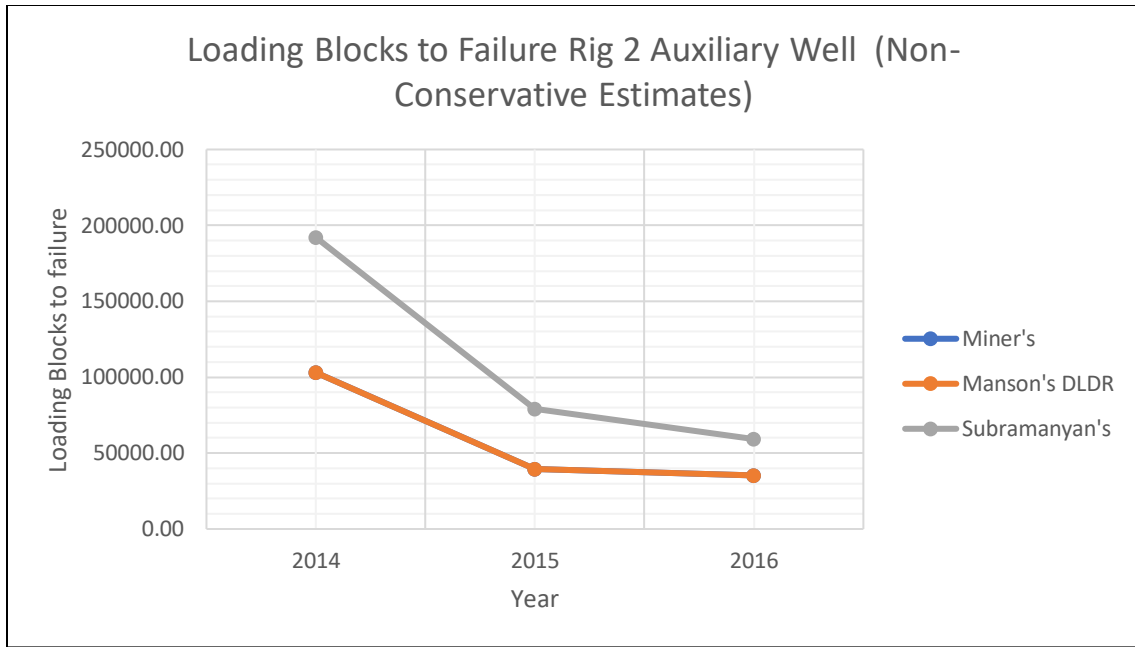


Figure 9-82: Non-conservative estimates of the number of loading blocks until failure from the selected fatigue damage models for Rig 2 Auxiliary Well

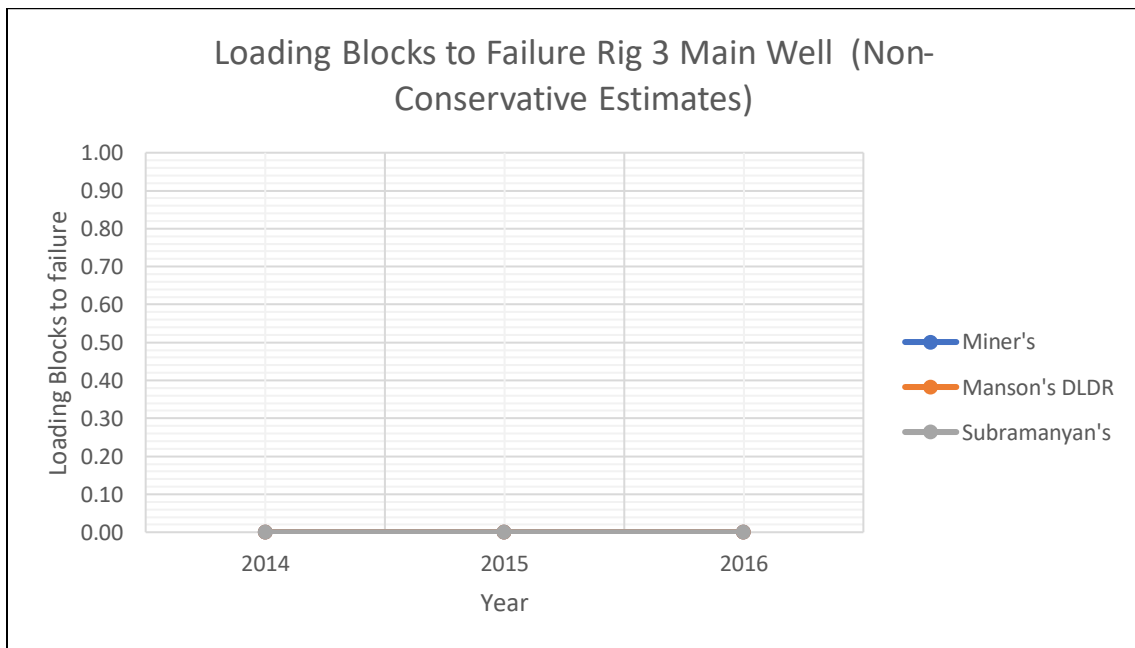


Figure 9-83: Non-conservative estimates of the number of loading blocks until failure from the selected fatigue damage models for Rig 3 Main Well

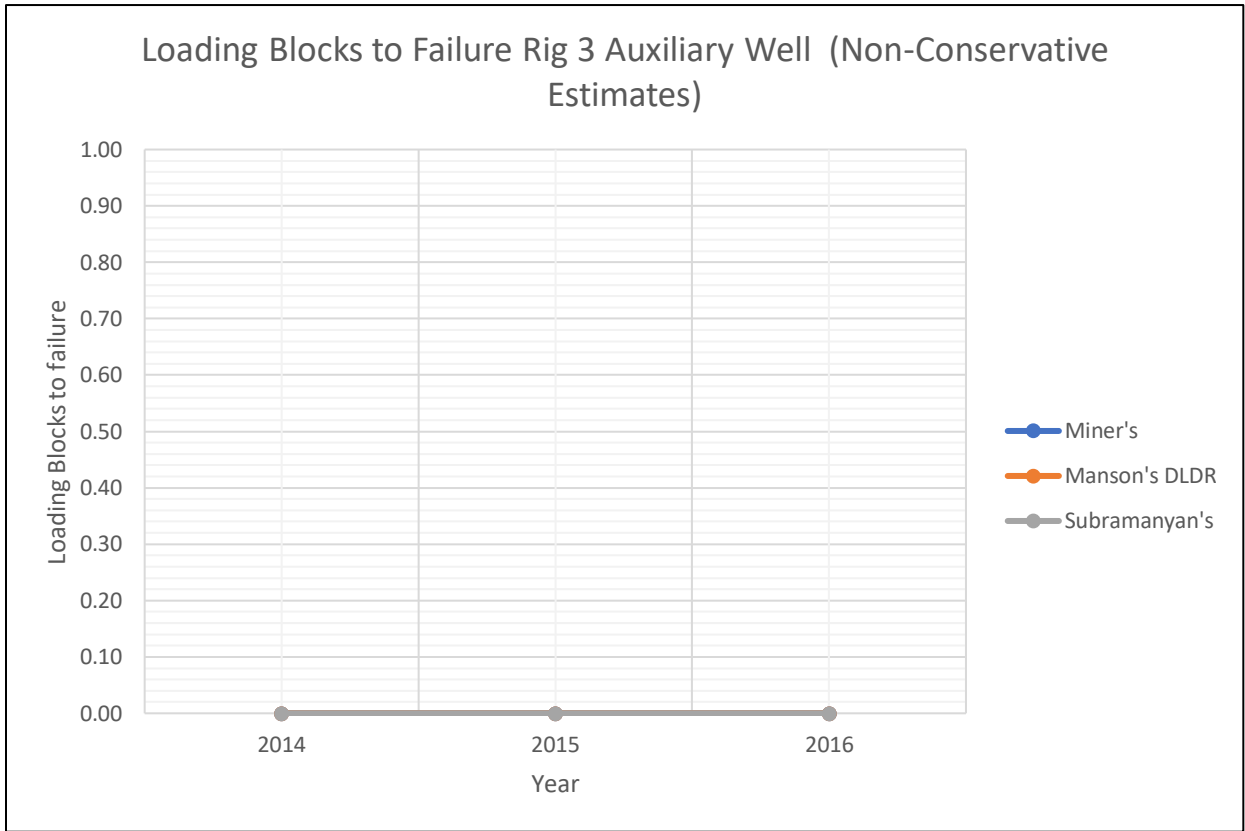


Figure 9-84: Non-conservative estimates of the number of loading blocks until failure from the selected fatigue damage models for Rig 3 Auxiliary Well

Conservative Estimates

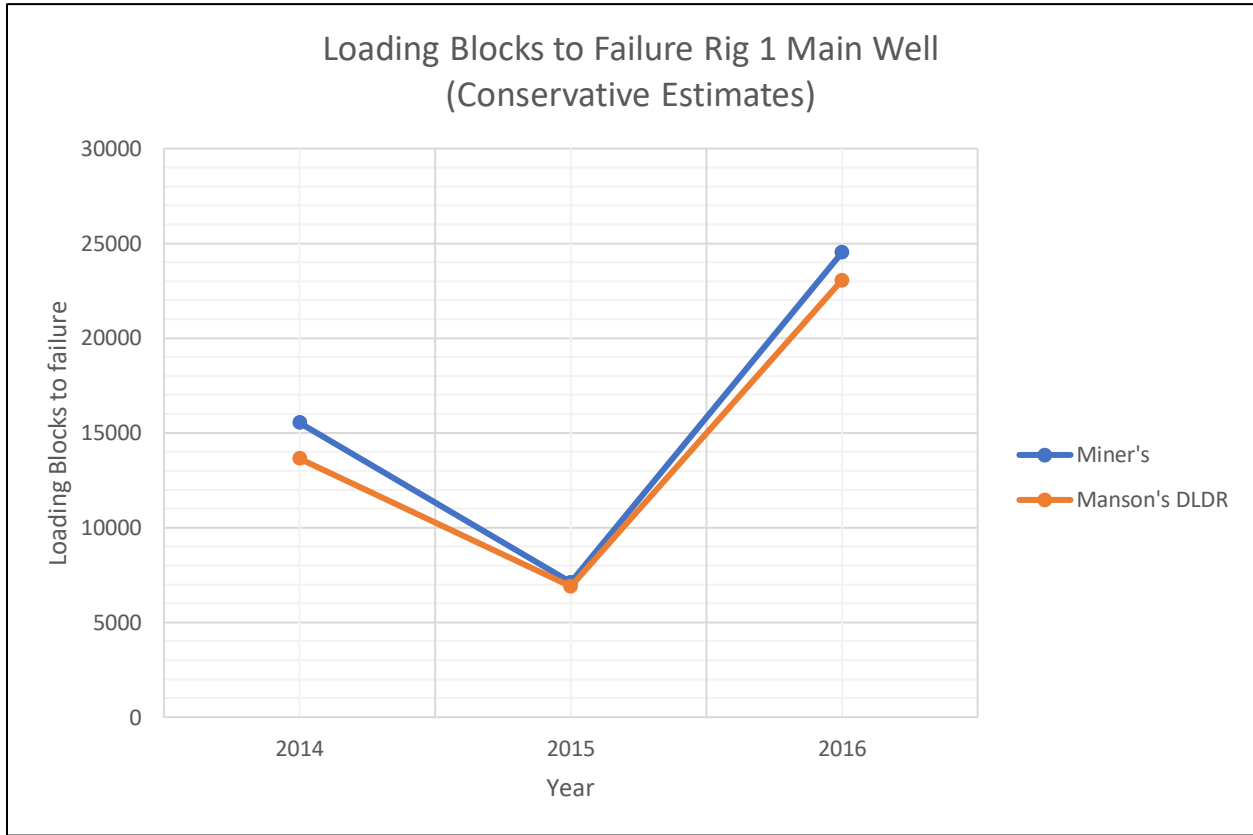


Figure 9-85: Conservative estimates of the number of loading blocks until failure from the selected fatigue damage models for Rig 1 Main Well

Main Well				
Year	Loading Blocks to Failure		Percentage Difference	
	Miner's Linear Damage Rule	Double Linear Damage Rule		
2014	15545.28304	13655.00152	12.15983981	
2015	7116.608943	6898.219818	3.068724528	
2016	24515.87887	23057.10754	5.950312196	

Table 9-19: Conservative estimates of the number of loading blocks until failure from the selected fatigue damage models for Rig 1 Main Well

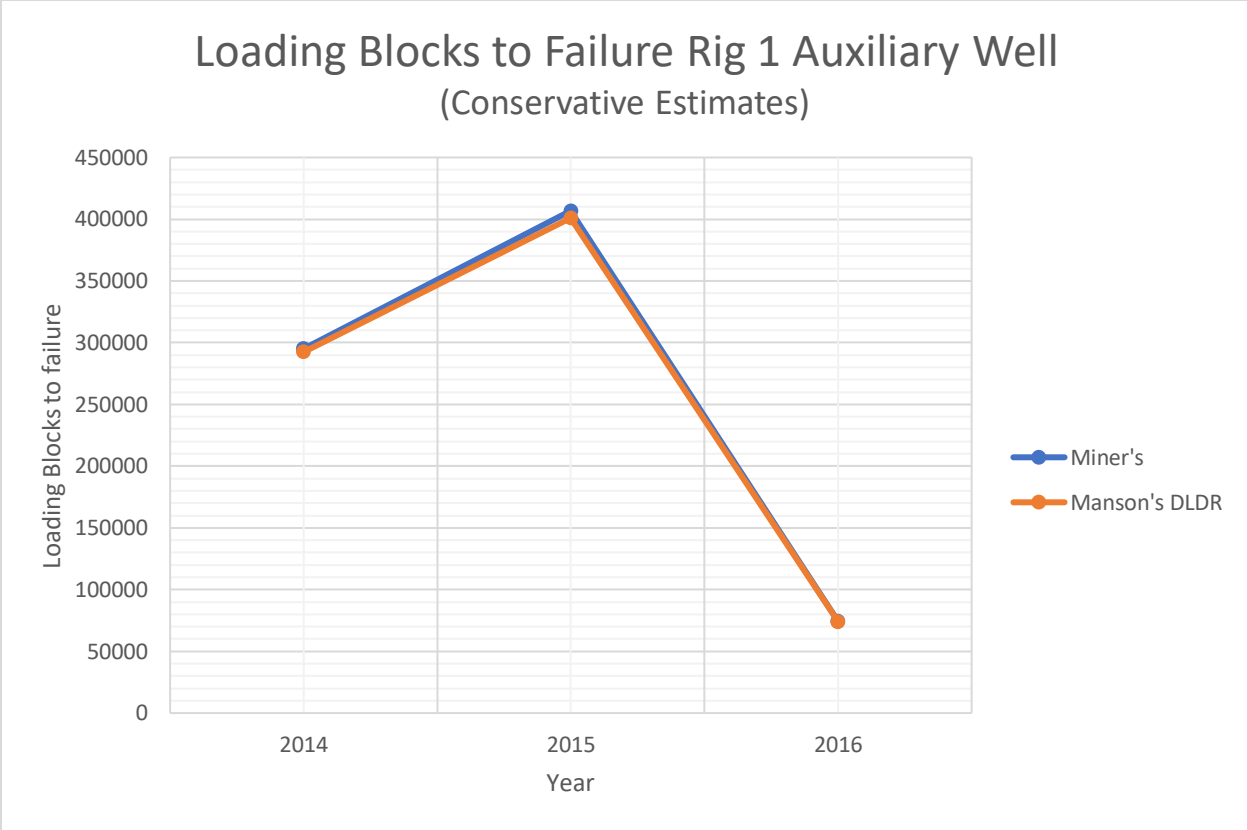


Figure 9-86: Conservative estimates of the number of loading blocks until failure from the selected fatigue damage models for Rig 1 Auxiliary Well

Auxiliary Well			
Year	Loading Blocks to Failure		Percentage Difference
	Miner's Linear Damage Rule	Double Linear Damage Rule	
2014	295260.7235	292487.0861	0.939385847
2015	406772.7963	400986.9686	1.42237331
2016	74366.41212	74149.95719	0.29106544

Table 9-10: Conservative estimates of the number of loading blocks until failure from the selected fatigue damage models for Rig 1 Auxiliary Well

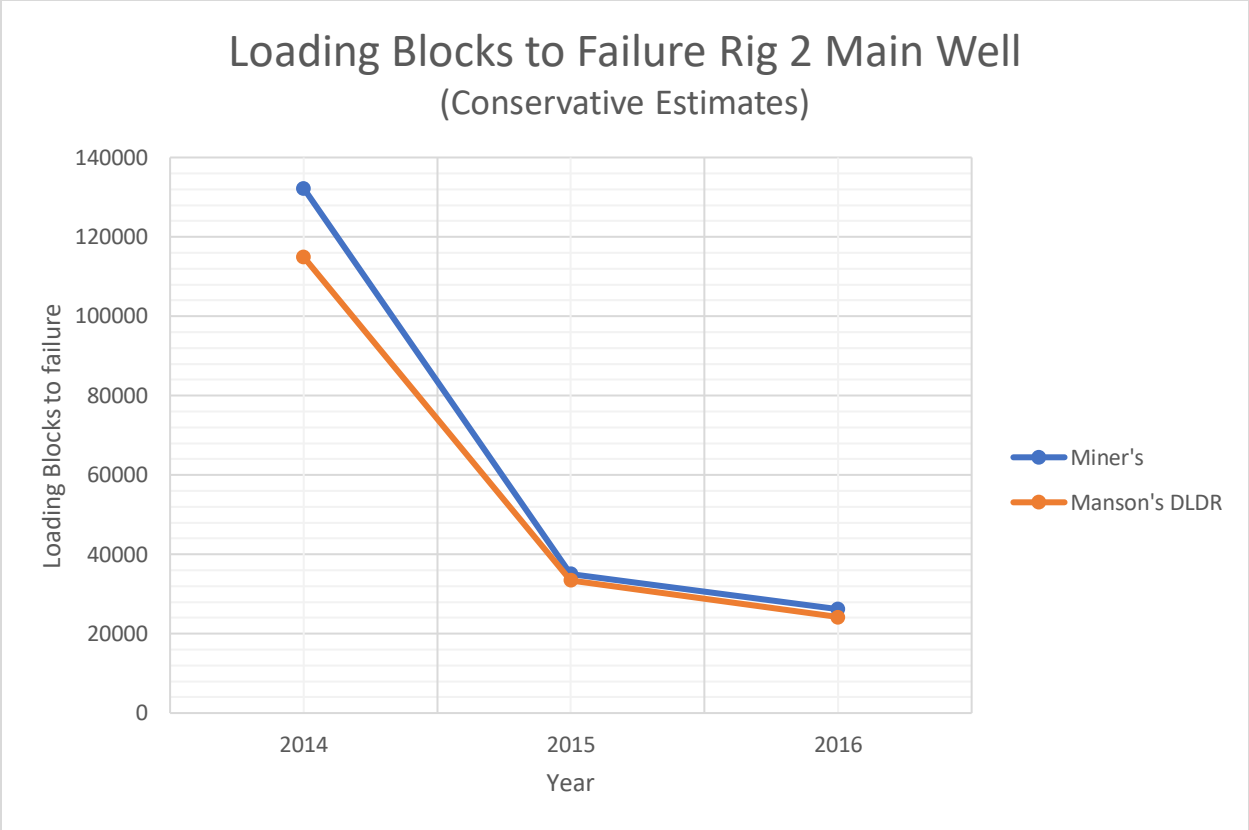


Figure 9-87: Conservative estimates of the number of loading blocks until failure from the selected fatigue damage models for Rig 2 Main Well

Main Well			
Year	Loading Blocks to Failure		Percentage Difference
	Miner's Linear Damage Rule	Double Linear Damage Rule	
2014	132237.5778	114920.4265	13.09548436
2015	35046.61408	33481.42569	4.466018855
2016	26179.18984	24211.43501	7.516484842

Table 9-111: Conservative estimates of the number of loading blocks until failure from the selected fatigue damage models for Rig 2 Main Well

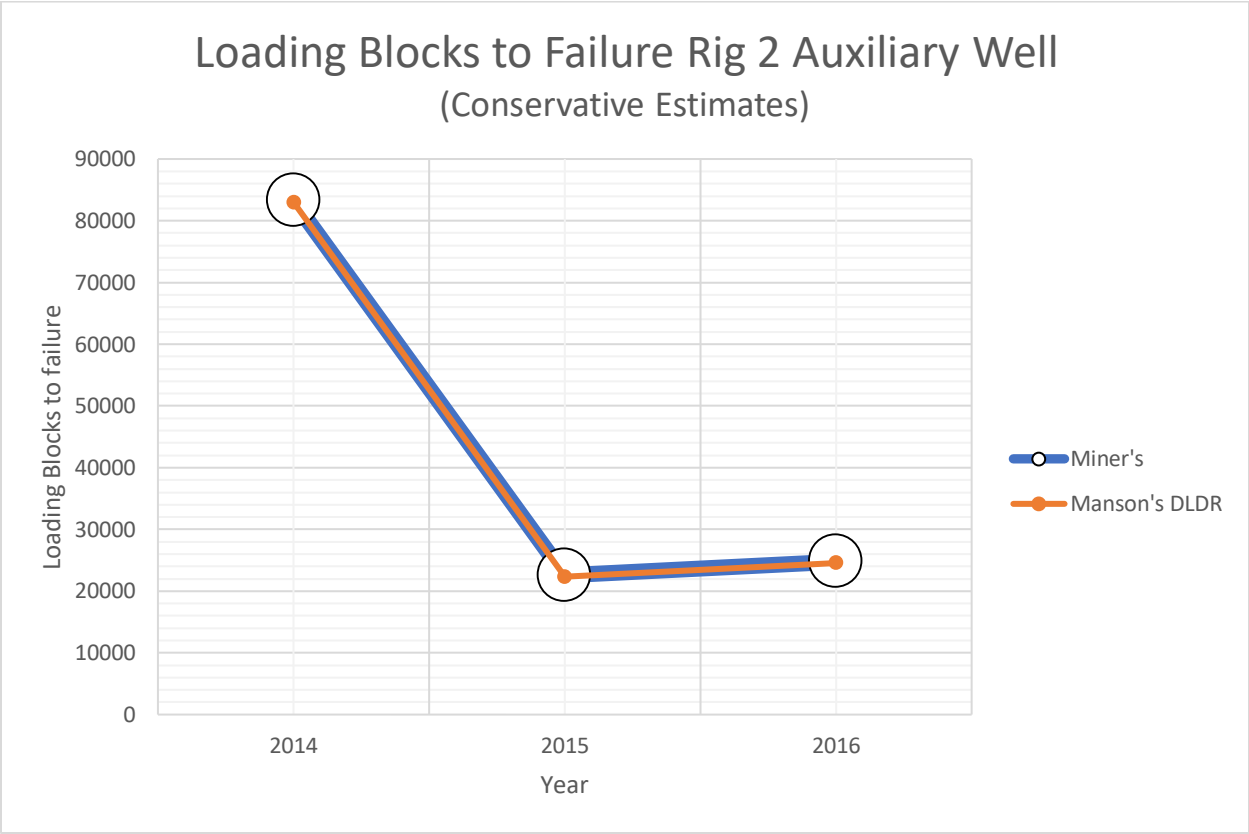


Figure 9-88: Conservative estimates of the number of loading blocks until failure from the selected fatigue damage models for Rig 2 Auxiliary Well

Auxiliary Well			
Year	Loading Blocks to Failure		Percentage Difference
	Miner's Linear Damage Rule	Double Linear Damage Rule	
2014	83229.09254	83002.99927	0.271651721
2015	22559.85834	22340.51577	0.972269282
2016	24795.46176	24592.32712	0.819241193

Table 9-12: Conservative estimates of the number of loading blocks until failure from the selected fatigue damage models for Rig 2 Auxiliary Well

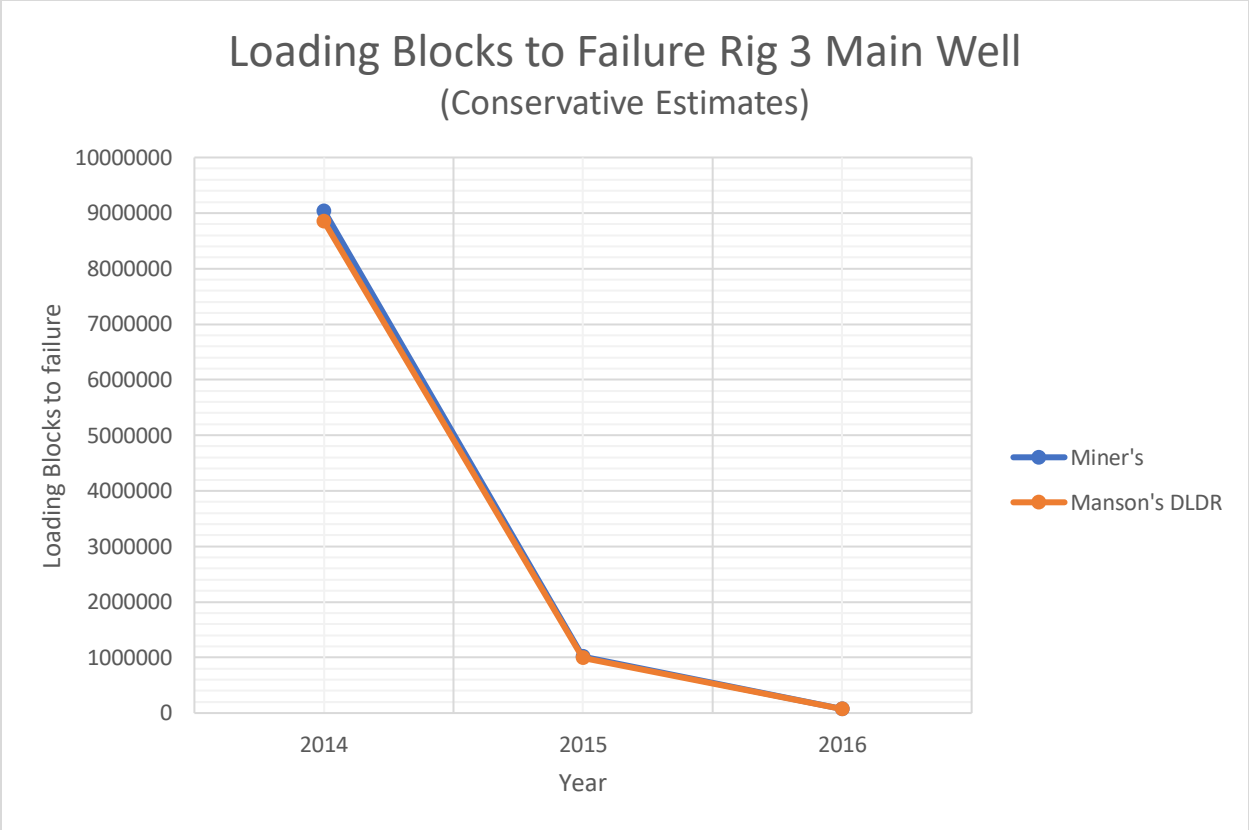


Figure 9-89: Conservative estimates of the number of loading blocks until failure from the selected fatigue damage models for Rig 3 Main Well

Main Well			
Year	Loading Blocks to Failure		Percentage Difference
	Miner's Linear Damage Rule	Double Linear Damage Rule	
2014	9044105.074	8851108.502	2.133948805
2015	1020552.67	998045.1065	2.205428922
2016	73073.04148	72294.91124	1.06486636

Table 9-13: Conservative estimates of the number of loading blocks until failure from the selected fatigue damage models for Rig 3 Main Well

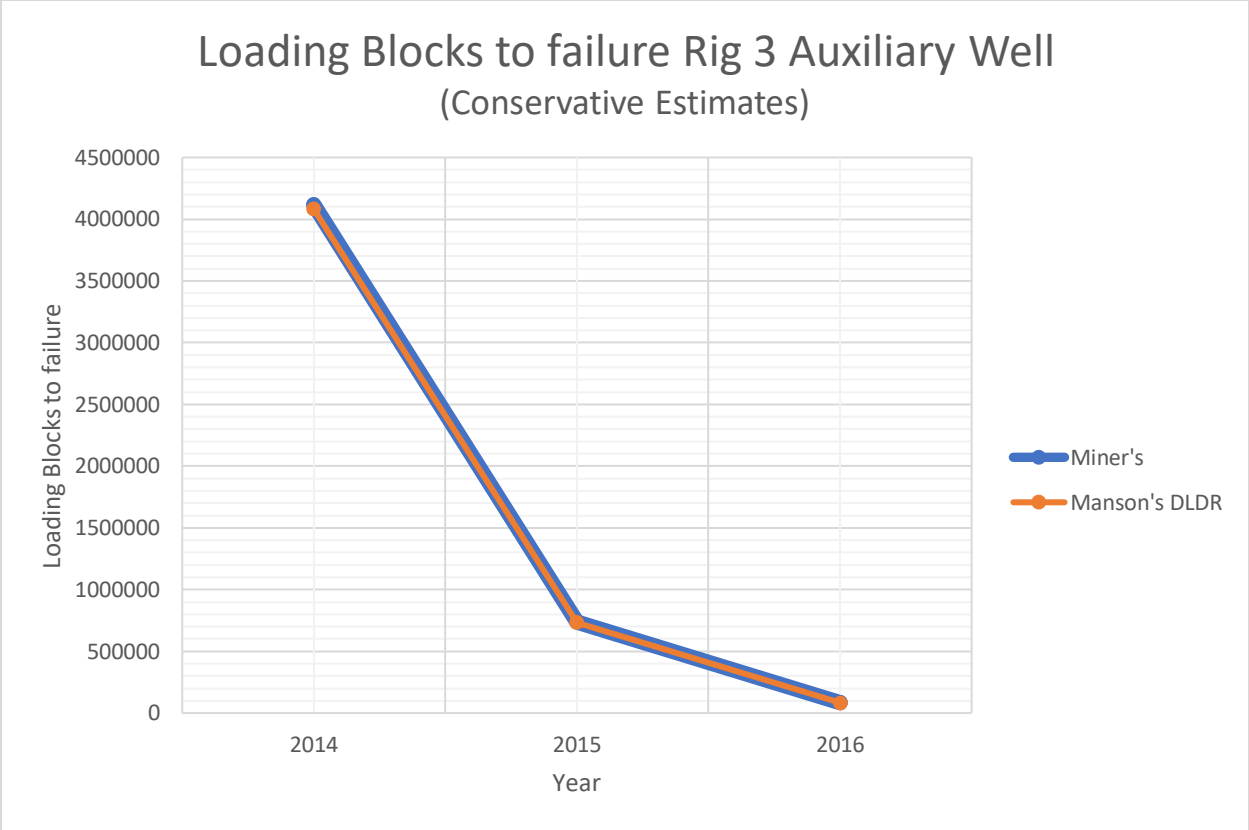


Figure 9-90: Conservative estimates of the number of loading blocks until failure from the selected fatigue damage models for Rig 3 Auxiliary Well

Auxiliary Well			
Year	Loading Blocks to Failure		Percentage Difference
	Miner's Linear Damage Rule	Double Linear Damage Rule	
2014	4117119.601	4082199.887	0.848158853
2015	739490.8565	733934.3048	0.751402353
2016	84165.50807	83565.26153	0.713174026

Table 9-14: Conservative estimates of the number of loading blocks until failure from the selected fatigue damage models for Rig 3 Auxiliary Well

Appendix H: R and Python Codes

R Code

#Loading Libraries

```
library(dplyr)
```

```
library(lubridate)
```

```
library (data. table)
```

```
library(dlookr)
```

Data Diagnosis

```
plot_outlier (Rig_data)
```

```
diagnose_report (Rig_data, output_format = "html")
```

#Importing the datasets Torque Signals and Hook loads for Rigs

#Rig 1 Main Well Torque Signals and Hook loads

Torque Signals and Hook Loads

Part 1

#Torque Signals

```
R1MTSignal_2014p1<- read.csv ('Rig1_TD1_AI_011_01jan14_000000_to_01jul14_000000.txt',  
col. names = c('Tag No','Timestamp', 'TorqueSignal'))
```

```
R1MTSignal_2014p1 <- R1MTSignal_2014p1[, 2:3]
```

```
R1MTSignal_2014p1$Timestamp <- gsub("mai","may",R1MTSignal_2014p1$Timestamp)
```

```
R1MTSignal_2014p1$Timestamp <- dmy_hms(R1MTSignal_2014p1$Timestamp)
```

```
R1MTSignal_2014p1$Timestamp <- ymd_hms(R1MTSignal_2014p1$Timestamp)
```

Full Time Series 1 second interval

Creating standardized time dataset

```
TS <- seq.POSIXt(as.POSIXct('2014-01-01 00:00:00 %Y/%m/%d %HH:%MM:%OS', tz =  
'Europe/Berlin'), as.POSIXct('2014-07-01 00:00:00 %Y/%m/%d %HH:%MM:OS', tz =  
'Europe/Berlin'), by='sec', tz = 'Europe/Berlin')
```

```
TS <- seq.POSIXt(as.POSIXct('2014-01-01 00:00:00 %Y/%m/%d %HH:%MM:%OS', tz =  
'Europe/Berlin'), as.POSIXct('2014-07-01 00:00:00 %Y/%m/%d %HH:%MM:OS', tz =  
'Europe/Berlin'), by='sec', tz = 'Europe/Berlin')
```

```
TS <- seq. POSIXt (as. POSIXlt ('2014-01-01 00:00:00'), as. POSIXlt ('2014-07-01 00:00:00'),  
by='sec')
```

```
format. POSIXct (TS,%Y/%m/%d %H: %M: %OS')
```

```
df<- data. frame (Timestamp=TS)
```

```
df$Timestamp <- ymd_hms(df$Timestamp)
```

```
R1MTSignal_2014p1_fts <- full_join (df, R1MTSignal_2014p1, by="Timestamp")
```

```
R1MTSignal_2014p1_fts[is.na(R1MTSignal_2014p1_fts)] <- 0
```

#Hook Loads

```
R1MHookloads_2014p1
```

```
<- read.csv ('Rig1_DW1_AI_058_01jan14_000000_to_01jul14_000000.txt', col. names = c ('Tag  
No', 'Timestamp', 'Hookloads'))
```

```
R1MHookloads_2014p1 <- R1MHookloads_2014p1[, 2:3]
```

```
R1MHookloads_2014p1$Timestamp <- gsub ("mai", "may",  
R1MHookloads_2014p1$Timestamp)
```

```
R1MHookloads_2014p1$Timestamp <- dmy_hms(R1MHookloads_2014p1$Timestamp)
```

```
R1MHookloads_2014p1$Timestamp <- ymd_hms(R1MHookloads_2014p1$Timestamp)
```

#Full Time Series

```
R1MHookloads_2014p1_fts <- full_join (df, R1MHookloads_2014p1, by="Timestamp")
```

```
R1MHookloads_2014p1_fts[is.na(R1MHookloads_2014p1_fts)] <- 0
```

Stress Calculations

```
#Shear stress
```

```
#Parameters radius = 0.077, polar moment of inertia (Jp) = 5.52183E-05
```

```
R = 0.077
```

Jp = 5.52183E-05

#2014 part 1

```
R1MSigma_xy_14p1 <- data.frame((R1MTSignal_2014p1_fts$TorqueSignal) *  
R)/(Jp*1000000)
```

```
R1MSigma_xy_14p1 <- data.frame (R1MTSignal_2014p1_fts$Timestamp,  
R1MSigma_xy_14p1)
```

```
colnames(R1MSigma_xy_14p1) <- c ("Timestamp", "Sigma_xy")
```

Stress y-direction where we have 2 tie rods g= 9.80665 m/s², thickness = 0.11m, width = 0.32m diameter of hole =0.154m

#2014 part 1

```
R1MSigma_y_14p1
```

```
<-data.frame((R1MHookloads_2014p1_fts$Hookloads) *9.80665)/ (2*1000000*0.11*(0.32-  
0.154))
```

```
R1MSigma_y_14p1<-data.frame (R1MHookloads_2014p1_fts$Timestamp,  
R1MSigma_y_14p1)
```

```
colnames(R1MSigma_y_14p1) <- c ("Timestamp", "Sigma_y")
```

Equivalent Stress

#2014 part 1

```
R1MSigma_eq_14p1<-data.frame(R1MSigma_xy_14p1$Sigma_xy,  
R1MSigma_y_14p1$Sigma_y)
```

```
R1MSigma_eq_14p1 <- rowSums(R1MSigma_eq_14p1)
```

```
R1MSigma_eq_14p1 <- data.frame(R1MSigma_eq_14p1)
```

```
R1MSigma_eq_14p1 <- data.frame(df, R1MSigma_eq_14p1)
```

```
colnames(R1MSigma_eq_14p1) <- c("Timestamp", "Sigma_eq")
```

```
-----  
-----
```

#Extraction

```
R1MSigma_eq_14p1 <- filter(R1MSigma_eq_14p1, Sigma_eq >= 1)
```

```
R1MSigma_eq_14p1$Sigma_eq <- round(R1MSigma_eq_14p1$Sigma_eq,0)
```

```
Sigma_eq_14p1 <- data.frame(R1MSigma_eq_14p1$Sigma_eq)
```

```
colnames(Sigma_eq_14p1) <- c("Sigma_eq")
```

```
fwrite(R1MSigma_eq_14p1, file = "R1MSigma_eq_14p1.csv", dateTimeAs = c("write.csv"))
```

```
fwrite(Sigma_eq_14p1, file = "Sigma_eq_14p1.csv", dateTimeAs = c("write.csv"))
```

```
-----  
-----
```

Part 2

#Torque Signals

```
R1MTSignal_2014p2
```

```
<-read.csv('Rig1_TD1_AI_011_01jul14_000000_to_01jan15_000000.txt', col.names = c('Tag  
No', 'Timestamp', 'TorqueSignal'))
```

```
R1MTSignal_2014p2 <- R1MTSignal_2014p2[, 2:3]
```

```
R1MTSignal_2014p2$Timestamp <- gsub("okt","oct", R1MTSignal_2014p2$Timestamp)
```

```
R1MTSignal_2014p2$Timestamp <- gsub("des","dec", R1MTSignal_2014p2$Timestamp)
```

```
R1MTSignal_2014p2$Timestamp <- dmy_hms(R1MTSignal_2014p2$Timestamp)
```

```
R1MTSignal_2014p2$Timestamp <- ymd_hms(R1MTSignal_2014p2$Timestamp)
```

```
# Full Time Series 1 second interval
```

```
# Creating standardized time dataset
```

```
TS <- seq.POSIXt(as.POSIXct('2014-07-01 00:00:00 %Y/%m/%d %HH:%MM:%OS', tz =  
'Europe/Berlin'), as.POSIXct('2015-01-01 00:00:00 %Y/%m/%d %HH:%MM:%OS', tz =  
'Europe/Berlin'), by='sec', tz = 'Europe/Berlin')
```

```
TS <- seq.POSIXt(as.POSIXct('2014-07-01 00:00:00 %Y/%m/%d %HH:%MM:%OS', tz =  
'Europe/Berlin'), as.POSIXct('2015-01-01 00:00:00 %Y/%m/%d %HH:%MM:%OS', tz =  
'Europe/Berlin'), by='sec', tz = 'Europe/Berlin')
```

```
TS <- seq.POSIXt (as.POSIXlt ('2014-07-01 00:00:00'), as.POSIXlt ('2015-01-01 00:00:00'),  
by='sec')
```

```
format.POSIXct (TS,'%Y/%m/%d %H: %M: %OS')
```

```
df <- data.frame (Timestamp=TS)
```

```
df$Timestamp <- ymd_hms(df$Timestamp)
```

```
R1MTSignal_2014p2_fts <- full_join (df, R1MTSignal_2014p2, by="Timestamp")
```

```
R1MTSignal_2014p2_fts[is.na(R1MTSignal_2014p2_fts)] <- 0
```

```
# Hook Loads
```

```
R1MHookloads_2014p2
```

```
<- read.csv ('Rig1_DW1_AI_058_01jul14_000000_to_01jan15_000000.txt', col.names = c ('Tag  
No', 'Timestamp', 'Hookloads'))
```

```
R1MHookloads_2014p2 <- R1MHookloads_2014p2[, 2:3]
```



```

R1MHookloads_2014p2$Timestamp <- gsub("okt","oct", R1MHookloads_2014p2$Timestamp)
R1MHookloads_2014p2$Timestamp <- gsub("des","dec", R1MHookloads_2014p2$Timestamp)
R1MHookloads_2014p2$Timestamp <- dmy_hms(R1MHookloads_2014p2$Timestamp)
R1MHookloads_2014p2$Timestamp <- ymd_hms(R1MHookloads_2014p2$Timestamp)

```

#Full Time Series

```

R1MHookloads_2014p2_fts <- full_join(df, R1MHookloads_2014p2, by="Timestamp")
R1MHookloads_2014p2_fts[is.na(R1MHookloads_2014p2_fts)] <- 0

```


Stress Calculations

#Shear stress

#Parameters radius = 0.077, polar moment of inertia (Jp) = 5.52183E-05

R = 0.077

Jp = 5.52183E-05

#2014 part 2

```

R1MSigma_xy_14p2 <- data.frame((R1MTSignal_2014p2_fts$TorqueSignal *
R)/(Jp*1000000)

```

```

R1MSigma_xy_14p2 <- data.frame (R1MTSignal_2014p2_fts$Timestamp,
R1MSigma_xy_14p2)

```

```

colnames(R1MSigma_xy_14p2) <- c ("Timestamp", "Sigma_xy")

```

```
# Stress y-direction where we have 2 tie rods g= 9.80665 m/s2, thickness = 0.11m, width = 0.32m diameter of hole =0.154m
```

#2014 part2

```
R1MSigma_y_14p2 <- data.frame((R1MHookloads_2014p2_fts$Hookloads) *9.80665)/  
(2*1000000*0.11*(0.32-0.154))
```

```
R1MSigma_y_14p2<-data.frame(R1MHookloads_2014p2_fts$Timestamp,  
R1MSigma_y_14p2)
```

```
colnames(R1MSigma_y_14p2) <- c ("Timestamp", "Sigma_y")
```

Equivalent Stress

#2014 part 2

```
R1MSigma_eq_14p2<-data.frame(R1MSigma_xy_14p2$Sigma_xy,  
R1MSigma_y_14p2$Sigma_y)
```

```
R1MSigma_eq_14p2 <- rowSums(R1MSigma_eq_14p2)
```

```
R1MSigma_eq_14p2 <- data.frame(R1MSigma_eq_14p2)
```

```
R1MSigma_eq_14p2 <- data.frame(df, R1MSigma_eq_14p2)
```

```
colnames(R1MSigma_eq_14p2) <- c ("Timestamp", "Sigma_eq")
```

```
-----  
-----
```

#Extraction

```
R1MSigma_eq_14p2 <- filter (R1MSigma_eq_14p2, Sigma_eq >= 1)
```

```
R1MSigma_eq_14p2$Sigma_eq <- round(R1MSigma_eq_14p2$Sigma_eq,0)
```

```
Sigma_eq_14p2 <- data.frame(R1MSigma_eq_14p2$Sigma_eq)
```

```
colnames (Sigma_eq_14p2) <- c("Sigma_eq")
```

```
fwrite (R1MSigma_eq_14p2, file = "R1MSigma_eq_14p2.csv", dateTimeAs = c("write.csv"))
```

```
fwrite (Sigma_eq_14p2, file = "Sigma_eq_14p2.csv", dateTimeAs = c("write.csv"))
```

END OF RIG 1 CALCULATIONS FOR 2014

Python Code

```
-----  
# Data processing and Importing the libraries
```

```
-----  
import numpy as np
```

```
import pandas as pd
```

```
import matplotlib.pyplot as plt
```

```
import rainflow as rf
```

```
import wafo as wf
```

```
import bokeh as bk
```

```
import datashader as ds
```

```
-----  
#Importing the Stress Equivalent Time_Series
```

```
-----  
#Rig 1
```

```
# Main Well
```

```
# 2014
```

```
R1MSigma_eq_2014 = pd.read_csv('R1MSigma_eq_14_full.csv')
```

```

R1MSigma_eq_2014 = (R1MSigma_eq_2014.iloc[:, 1]. values)

from collections import defaultdict

counts = defaultdict(float)

for low, high, mult in rainflow. extract_cycles(R1MSigma_eq_2014, left = 'TRUE', right
='TRUE'):

    mean = 0.5 * (high + low)

    rng = high - low

    counts [(mean, rng)] += mult

RFC_MW2014 = pd. DataFrame([(k[0], k[1], v) for k, v in counts.items()], columns = ['Mean',
'Range', 'Cycle'])

RFC_MW2014.to_excel ("RFC_MW2014.xlsx", sheet_name = "ext")

```

2015

```

R1MSigma_eq_2015 = pd. read_csv ('R1MSigma_eq_15_full.csv')

R1MSigma_eq_2015 = (R1MSigma_eq_2015.iloc[:, 1]. values)

from collections import defaultdict

counts = defaultdict(float)

for low, high, mult in rainflow. extract_cycles (R1MSigma_eq_2015, left = 'TRUE', right
='TRUE'):

    mean = 0.5 * (high + low)

```

```
rng = high - low
```

```
counts [(mean, rng)] += mult
```

```
RFC_MW2015 = pd. DataFrame([(k[0], k[1], v) for k, v in counts.items()], columns = ['Mean',  
'Range', 'Cycle'])
```

```
RFC_MW2015.to_excel ("RFC_MW2015.xlsx", sheet_name = "ext")
```

#2016

```
R1MSigma_eq_2016 = pd. read_csv ('R1MSigma_eq_16p1.csv')
```

```
R1MSigma_eq_2016 = (R1MSigma_eq_2016.iloc[:, 1]. values)
```

```
from collections import defaultdict
```

```
counts = defaultdict(float)
```

```
for low, high, mult in rainflow. extract_cycles(R1MSigma_eq_2016, left = 'TRUE', right  
='TRUE'):
```

```
mean = 0.5 * (high + low)
```

```
rng = high - low
```

```
counts [(mean, rng)] += mult
```

```
RFC_MW2016 = pd. DataFrame([(k[0], k[1], v) for k, v in counts.items()], columns = ['Mean',  
'Range', 'Cycle'])
```

```
RFC_MW2016.to_excel ("RFC_MW2016.xlsx", sheet_name = "ext")
```